



PALACKÝ UNIVERSITY  
FACULTY OF MEDICINE AND DENTISTRY

Program DSP: Pediatrics

**ANTICANCER AND NEUROPROTECTIVE ACTIVITY  
OF NUCLEOSIDES, MICROTUBULE-TARGETING**

Hrubá Lenka, Dr.

**Supervising department:**

Institute of Molecular and Translational Medicine,  
Faculty of Medicine and Dentistry,  
Palacký University in Olomouc

**Supervisor:**

Džubák Petr, M.D., Ph.D.

Olomouc 2023

I declare that this thesis has been written solely by myself and that all the sources used in this publication are cited and included in the reference part. The research was done in the Laboratory of Experimental Medicine, Institute of Molecular and Translational Medicine, Faculty of Medicine and Dentistry, Palacký University in Olomouc.

In Olomouc  
August 2023

.....  
Lenka Hrubá, Dr.

## Acknowledgments

I would like to thank my supervisor, Petr Džubák, M.D., Ph.D., for his leadership and advice, which helped me during my Ph.D. study. I would also like to thank IMTM's director, Marián Hajdúch, M.D., Ph.D., for the opportunity to work on my Ph.D. thesis in IMTM and for his advice. My thanks also go to colleagues from IMTM for creating a pleasant working environment and their cooperation on projects.

A big thanks also goes to my family, especially to my husband and parents, who made it possible for me to study and always supported me.

The work was supported by the Czech Ministry of Education, Youth and Sports projects CZ-OPENSREEN (LM2018130), EATRIS-CZ (LM2018133), Grant Agency of Czech Republic (19-08124S), an internal grant of Palacky University (IGA\_LF\_2018\_031, IGA\_LF\_2019\_018, IGA\_LF\_2020\_019, IGA\_LF\_2021\_038) and by the European Regional Development Fund project ENOCH (No. CZ.02.1.01/0.0/0.0/16\_019/0000868). The study was supported by project nr. LX22NPO5107 (MEYS): Financed by EU – Next Generation EU and partially supported by the Ministry of Education, Youth and Sports of the Czech Republic through the e-INFRA CZ (ID:90140).

In Olomouc

August 2023

.....

Lenka Hrubá, Dr.

## Bibliography identification

Author's name and surname:	Lenka Hrubá
Title:	Anticancer and neuroprotective activity of nucleosides, microtubule-targeting
Type of thesis:	Dissertation
Department:	Institute of Molecular and Translational Medicine, Faculty of Medicine and Dentistry, Palacký University in Olomouc
Supervisor:	Petr Džubák, MD., Ph.D.
The year of presentation:	2023
Keywords:	Nucleosides, drug repurposing, neurodegenerative diseases, cancer, drug development, drug resistance, leukemia
Language:	English

## Abstract

Nucleosides are biologically active compounds, structurally very similar to nucleotides, of which nucleic acids are composed. In clinics, nucleosides are used as antiviral or anticancer drugs. However, the possibilities of their further application have been explored in recent years. In this dissertation thesis, we focused mainly on the anticancer activity of nucleosides and mechanisms of their drug resistance in leukemia cells (acute lymphoblastic and chronic myelogenous leukemia), which were exposed to nucleoside-based drugs to develop resistant cellular models. Developed *in vitro* models were used for the study of nucleoside drug resistance, and they were also used in the screening of new potential anticancer drugs that can overcome their resistant phenotype.

In the second part of this thesis, we studied the neuroprotective activity of nucleosides. We specifically investigated their activity as inhibitors of kinases, which are responsible for pathological phosphorylation of tau protein, leading to neuronal cytoskeleton destabilization and the development of dementia.

Similarly to the cytoskeleton targeting in neurodegenerative diseases, we have utilized our know-how to address the anticancer activity of a novel class of drugs known as steroid dimers. These compounds are promising because of their potential to destabilize tubulin and kill the proliferating cancer cells.

## Bibliografická identifikace

Jméno a příjmení autora:	Lenka Hrubá
Název práce:	Protinádorová a neuroprotektivní aktivita nukleosidů, léčba cílená na mikrotubuly
Typ práce:	Disertační
Pracoviště:	Ústav molekulární a translační medicíny, Lékařská fakulta Univerzity Palackého v Olomouci
Školitel:	MUDr. Petr Džubák, Ph.D.
Rok obhajoby:	2023
Klíčová slova:	Nukleosidy, neurodegenerativní onemocnění, rakovina, leukémie, vývoj léčiv, lékové rezistence
Jazyk:	Angličtina

## Abstrakt

Nukleosidy jsou biologicky aktivní látky, strukturně velmi podobné nukleotidům, které jsou základními stavebními kameny nukleových kyselin. V klinické praxi nacházejí nukleosidy uplatnění jako antivirotika a protinádorová léčiva, nicméně v posledních letech se objevují další možnosti jejich klinického uplatnění. V této práci jsme se zaměřili na protinádorové účinky nukleosidů a mechanismy vzniku rezistence vůči léčivům s nukleosidovou strukturou u leukemických buněk. Tyto buňky byly cíleně selektovány a vytvořené rezistentní *in vitro* buněčné modely byly následně využity ke studiu mechanismů lékové rezistence a ve screeningu nových potenciálních léčiv schopných překonávat daný rezistentní fenotyp.

V druhé části práce byla zkoumána neuroprotektivní aktivita nukleosidů. Zaměřovali jsme se konkrétně na nalezení látek působících jako inhibitory kináz způsobujících patologickou fosforylaci tau proteinu, a tím destabilizaci cytoskeletu neuron vedoucí k rozvoji demence.

Podobně jako v případě cílení na cytoskelet u neurodegenerativních onemocnění jsme využili naše know-how pro identifikaci protinádorové aktivity nové třídy léčiv známých jako steroidní dimery. Tyto sloučeniny jsou slibné díky svému potenciálu destabilizovat tubulin a zabít proliferující nádorové buňky.

# TABLE OF CONTENTS

1 INTRODUCTION – NUCLEOSIDES.....	1
1.1 Nucleosides in the cancer treatment.....	3
1.1.1 Nucleoside-based drugs resistance .....	4
1.1.1.1 Active uptake via nucleoside transporters (ENTs, CNTs).....	5
1.1.1.2 Proteins connected with multidrug resistance development.....	7
1.1.1.3 Nucleoside-based drugs: metabolism and the mechanism of resistance .....	9
1.1.2 Current strategies for overcoming the MDR .....	16
1.1.2.1 Combinatory therapy .....	16
1.1.2.2 Efflux pump inhibitors.....	16
1.1.2.3 Targeted therapy.....	17
1.2 Neuroprotective activity of nucleosides and microtubule-targeting drugs.....	18
1.2.1 Microtubules dynamics as a therapeutic target.....	18
1.2.2 Tauopathies.....	19
1.2.2.1 Tau protein phosphorylation.....	21
1.2.2.2 MARK4 inhibitors.....	23
1.2.2.3 Cdk5 inhibitors .....	24
1.2.2.4 LKB1 inhibitors.....	24
1.2.2.5 GSK-3 $\beta$ inhibitors .....	24
1.2.3 CNS drug design.....	25
2 EXPERIMENTAL PART .....	27
2.1 Aims .....	28
2.2 Nucleoside-based drugs resistance .....	29
2.2.1 Materials and Methods .....	29
2.2.1.1 Development of resistant cancer cell lines .....	29
2.2.1.2 MTS cytotoxicity assay .....	29
2.2.1.3 Expression of membrane transporters .....	30
2.2.1.4 Expression of proteins involved in the nucleoside metabolism.....	30
2.2.2 Results .....	32
2.2.2.1 Development of resistant cancer cell lines .....	32
2.2.2.2 Resistant cellular models in the screening of new drugs.....	33
2.2.2.3 Expression of MDR proteins .....	34
2.2.2.4 Expression of nucleoside transporters (ENTs, CNTs).....	37
2.2.2.5 Expression of proteins involved in nucleosides metabolism .....	39
2.2.3 Discussion.....	45
2.2.3.1 Cytarabine, gemcitabine, fludarabine cross-resistance.....	46

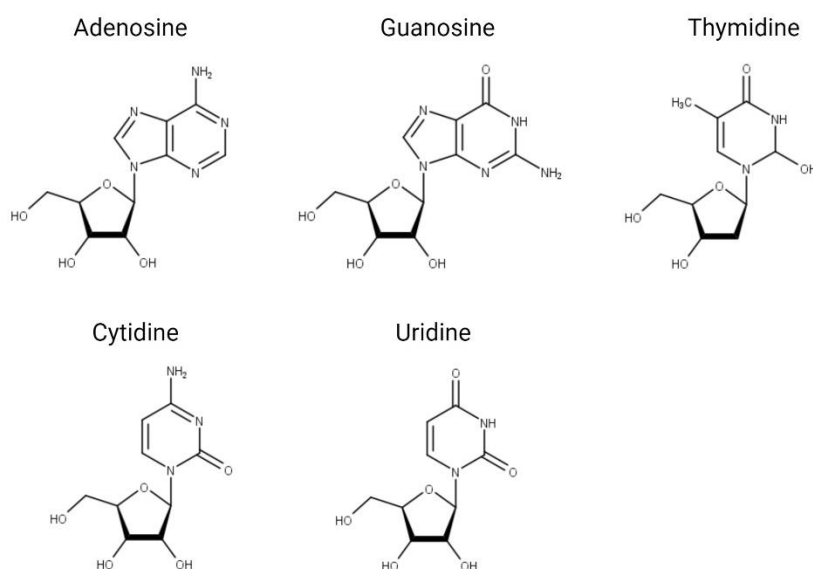
2.2.3.2 6-thioguanine and 6-mercaptopurine cross-resistance.....	47
2.2.3.3 Involvement of mTOR pathway in nucleoside-based drug resistance .....	48
2.3 Neuroprotective effect of nucleosides .....	50
2.3.1 Materials and Methods .....	50
2.3.1.1 Kinase assay .....	50
2.3.1.2 <i>In vitro</i> pharmacology .....	51
2.3.1.3 MARK4-tau co-transfection and compound treatment .....	51
2.3.2 Results .....	52
2.3.2.1 MARK kinase assay .....	52
2.3.2.2 Screening of MARK4 inhibitors.....	55
2.3.2.3 MARK1-3 inhibitory activity .....	60
2.3.2.4 Cytotoxicity of MARK inhibitors.....	60
2.3.2.5 <i>In vitro</i> pharmacological parameters .....	61
2.3.2.6 Physiochemical parameters .....	64
2.3.2.7 Selectivity of MARK4 inhibitors.....	64
2.3.2.8 GSK-3 $\beta$ kinase assay .....	66
2.3.2.9 Inhibition of MARK4-mediated tau phosphorylation .....	67
2.3.2.10 Compounds inhibit MARK4-mediated tau phosphorylation in cells .....	69
2.3.3 Discussion.....	72
2.3.3.1 MALDI-TOF kinase assay .....	72
2.3.3.2 Screening of MARK4 inhibitors.....	72
2.3.3.3 Analysis of the most active MARK4 inhibitors .....	73
3 Summary.....	76
4 Souhrn .....	77
5 Supplementary .....	78
6 Abbreviations .....	87
7 References .....	90
8 Bibliography .....	112
8.1 Original articles and reviews .....	112
8.2 Book chapters .....	112
8.3 Oral and poster presentations .....	112
9 Appendix – Full text publications related to the thesis.....	114
9.1 Nucleoside-based anticancer drugs: Mechanism of action and drug resistance.....	114
9.2 Triazole-based estradiol dimers prepared via CuAAC from 17 $\alpha$ -ethinyl estradiol with five-atom linkers causing G2/M arrest and tubulin inhibition.....	130
9.3 An identification of MARK inhibitors using high throughput MALDI-TOF mass spectrometry .....	144
9.4 Laboratory techniques in cellular and molecular medicine .....	155

# **1 INTRODUCTION – NUCLEOSIDES**



Nucleosides are organic molecules consisting of nucleobase (purine or pyrimidine) and five-carbon sugar. They occur naturally in the human body, mainly as DNA and RNA synthesis precursors. Because of their biological functions, they have been intensively studied for years as starting structures for drug development. New active molecules, which can be derived from known molecules, can have broad spectra of applications.<sup>1</sup> Until now, around 30 molecules with nucleoside structures are approved for treating viral, bacterial, or fungal infections and cancer, but much more of them are in ongoing preclinical and clinical trials.<sup>2-4</sup>

There are many naturally occurring nucleosides, but the most common ones in the human body are adenosine, guanosine, thymidine, cytidine, and uridine (Fig. 1).<sup>4</sup> These molecules are often used as structures from which new molecules are derived. This way of finding new biologically active compounds, called rational drug design, is much more effective than trial-and-error drug development using *de novo* synthesis and extensive screenings of random compounds, because a slight change in the structure of natural nucleosides can have a significant biological effect. These compounds act as substrates or inhibitors of enzymes involved in natural nucleoside metabolism. They can bind to membrane transporters, incorporate into DNA, and inhibit the synthesis of DNA in human and bacteria cells and even in viruses, in which they interact with DNA polymerase and/or cause DNA chain termination.<sup>5,6</sup> It makes nucleoside analogs promising candidates for antiviral, antibacterial, and also anticancer drugs.



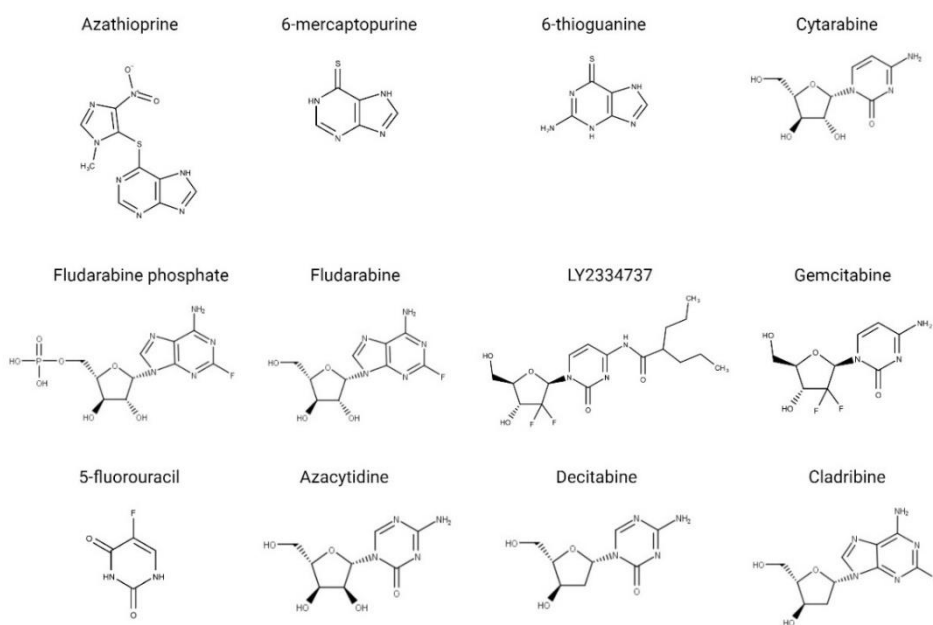
**Figure 1.** Chemical structure of the five most common natural nucleosides: adenosine, guanosine, thymidine, cytidine, and uridine.

## 1.1 Nucleosides in the cancer treatment

Nucleosides were first studied as antimetabolites that interfere with natural biological pathways. One of the first clinically used nucleosides was 6-mercaptopurine (6-MP) (Fig. 2), synthesized in 1950 by Nobel prize winners G. Elion and G. H. Hitchings and applied in treating acute leukemia in pediatric patients.<sup>7</sup> Since that, this compound is used to treat leukemia, and unfortunately, some less or more severe side effects have been described. A common side effect of 6-MP treatment is tiredness, diarrhea, decreased appetite, or throwing up. A more severe complication is hepatotoxicity, which is caused by the accumulation of 6-methyl-mercaptopurine (6-MMPT) metabolite in some patients depending on the expression of NUD15 (nudix hydrolase 15), TPMT (thiopurine-S-methyltransferase), and ITPA (inosine triphosphatase) proteins, which can be used as prognostic markers of 6-MP treatment.<sup>8,9</sup>

Between 1949 and 1951, another purine analog, 6-thioguanine (6-TG), was synthesized. This compound is structurally similar to the 6-MP (Fig. 2) and belongs to 6-MP metabolites. The activity of 6-TG is higher than 6-MP, but there is also a higher risk of toxicity in the long-term continuing treatment, for which 6-MP remains a more suitable drug. 6-TG is mainly used for short intensive treatment of leukemia patients.<sup>10</sup>

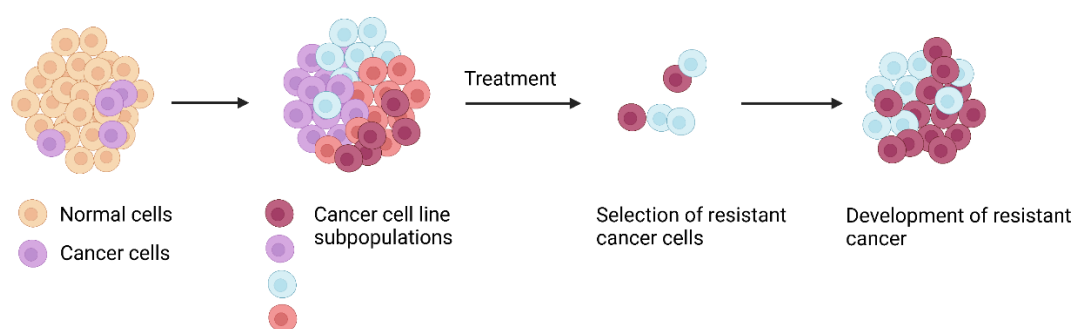
In 1957, a 6-mercaptopurine prodrug, azathioprine, was synthesized to produce higher concentrations of active 6-MP metabolites in the human body and make 6-MP treatment more effective.<sup>11,12</sup> Other nucleoside-based drugs, such as cytarabine, gemcitabine, fludarabine, 5-fluorouracil, azacytidine, decitabine, cladribine (Fig. 2), etc., gradually followed.



**Figure 2.** Chemical structure of nucleoside-based drugs and their prodrugs: azathioprine, 6-mercaptopurine, 6-thioguanine, cytarabine, fludarabine phosphate, fludarabine, LY2334737, gemcitabine, 5-fluorouracil, azacytidine, decitabine, and cladribine.<sup>13</sup>

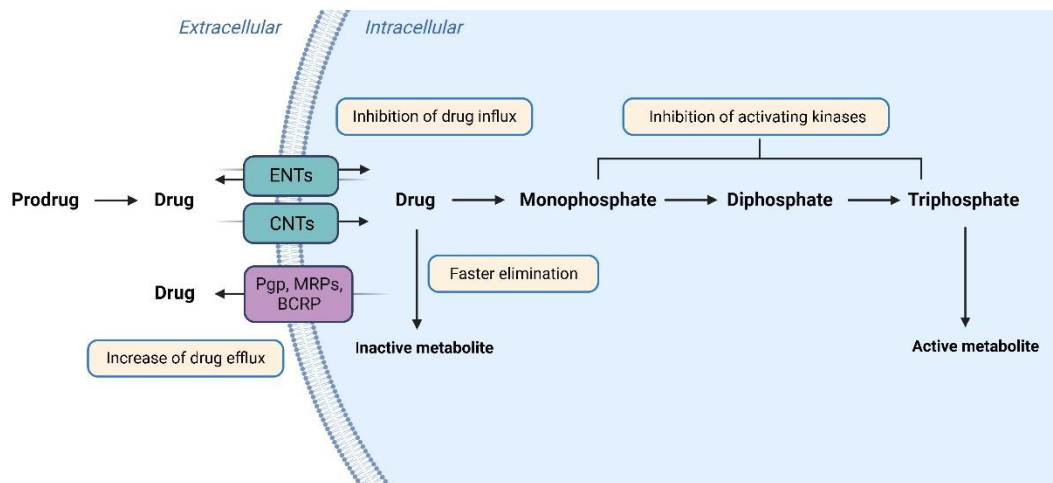
### 1.1.1 Nucleoside-based drugs resistance

A serious problem, which decreases the success of oncology treatment, except for drugs side effects, is drug resistance development. Drug resistance can occur in the first administration of the drug (primary resistance) or during the treatment due to the selection of insensitive cellular subpopulations (secondary resistance). Based on clonal expansion theory, cancer tissue is not a homogenous cluster of cells. But it consists of numerous subpopulations which can be genetically altered.<sup>14</sup> Cancer cells are characterized, among other things, by damaged DNA repair mechanisms, unregulated proliferation, and inhibited apoptosis. This leads to the production of many cells, whereas each cell cycle potentially gives rise to new genetic mutations.<sup>15</sup> This intra-tumor heterogeneity can cause non-equal sensitivity of the tumor to the treatment, and resistant subpopulations can be naturally selected. (Fig. 3) Dividing these insensitive cells creates insensitive cancer cell populations, and changes in the treatment are needed.<sup>16</sup> In patients, this condition is manifested by improved health status during primary treatment, followed by clinical relapse caused by the proliferation of resistant subpopulations. This state is called minimal residual disease.<sup>17</sup>



**Figure 3.** Clonal expansion of the cancer cells and selection of the resistant subpopulations.

In general, there are several mechanisms of chemoresistance (MOC). The first one is the reduction of drug uptake, which is mediated mainly via nucleoside transporters (MOC-1a), or increase in drug efflux (MOC-1b), which can be done by ABC transporters family (P-glycoprotein, Multidrug resistance-associated proteins, breast cancer resistance protein). Another mechanism can be connected with the alteration of drug metabolism: reduced expression of activating enzymes (MOC-2a) or faster elimination (MOC-2b). (Fig. 4) There can also be other mechanisms, such as molecular changes in the cellular drug targets (MOC-3), enhanced DNA damaged repair mechanisms (MOC-4), reduction of pro-apoptotic factors (MOC-5a), and/ or increased activity of anti-apoptotic factors (MOC-5b). There can also be changes in the tumor microenvironment (MOC-6), such as hypoxia, acidity, or epithelial-mesenchymal transition (MOC-7).<sup>18,19</sup>



**Figure 4.** General mechanisms of nucleoside-based drug resistance. ENTs: equilibrative nucleoside transporters, CNTs: concentrative nucleoside transporters, Pgp: P-glycoprotein, MRPs: multidrug resistance-associated proteins, BCRP: breast cancer resistance protein.<sup>13</sup>

### 1.1.1.1 Active uptake via nucleoside transporters (ENTs, CNTs)

Nucleoside transporters ensure the transport of purine and pyrimidine nucleosides across the cytoplasmic membrane and are thus significantly involved in their biological activity. In the case of nucleoside-based drugs, these transporters' expression can affect the treatment's effectiveness. Nucleoside transporters can be divided into two groups: equilibrative (ENTs) and concentrative (CNTs) transporters encoded by the solute-carrier (SLC) gene superfamily.<sup>20</sup>

ENT transporters (SLC29) consist of four members, ENT1 (SLC29A1), ENT2 (SLC29A2), ENT3 (SLC29A3), and ENT4 (SLC29A4), which are transmembrane proteins mediating the transport of nucleosides, nucleobases, and their analogs.<sup>21</sup>

ENT1 transporter is a glycoprotein localized in the plasma and mitochondrial membranes. It is usually expressed in broad spectra of human tissues, such as the brain, gastrointestinal tract, endocrine tissues, liver, kidneys, heart, testis, ovarium, or pancreas, and its function is the transport of endogenous purine and pyrimidine nucleosides.<sup>22,23</sup> Its substrates also include exogenous nucleoside-based drugs, for example, 5-fluorouracil, 6-mercaptopurine, azacytidine, cladribine, cytarabine, decitabine, fludarabine, and gemcitabine.<sup>24–28</sup>

ENT2 has similar substrate specificity as ENT1. It is also able to transport purine and pyrimidine nucleosides, and moreover, it can transport nucleobases, which cannot be transported by ENT1 (adenine, hypoxanthine, guanine, thymine, cytosine, uracil).<sup>29</sup> ENT2 is ubiquitously expressed in the human body. It can be found in the brain, liver, kidneys, placenta, heart, pancreas, and gastrointestinal tract, but the highest expression of ENT2 mRNA was confirmed in the skeletal muscles.<sup>29–31</sup> In addition to endogenous substrates, some drugs can be

transported by the ENT2, such as 5-fluorouracil, 6-mercaptopurine, 6-thioguanine, cytarabine, azacytidine, etc.<sup>24,27,28,32,33</sup>

ENT3 has broad substrate specificity, and it is able to transport nucleosides and nucleobases. ENT1 and 2 are localized in the plasma membrane, whereas ENT3 is expressed in the endosomal, lysosomal, and mitochondrial membranes.<sup>34,35</sup> It is a pH-dependent transporter responsible for nucleoside homeostasis in lysosomes and mitochondria.<sup>36,37</sup> This transporter has a low tissue specificity. It is usually expressed across the human body, for example, in connective tissue, pancreas, placenta, liver, and kidneys.<sup>21</sup> It has been found that ENT3 is highly expressed in peripheral T cells, supporting their proliferation and homeostasis via the normal function of lysosomes<sup>38</sup> and in  $\beta$ -cells of islets of Langerhans, where they participate in the correct function of mitochondria. Depletion of ENT3 leads to mitochondria dysfunction, induces apoptosis of  $\beta$ -cells, and it may contribute to the development of juvenile diabetes.<sup>39</sup> Drugs, which are ENT3 substrates, include, for example, cladribine, clofarabine, fludarabine, or gemcitabine.<sup>40,41</sup>

ENT4 transporter is expressed mainly in the brain tissue, and its natural substrates are monoamine neurotransmitters, such as serotonin and dopamine.<sup>42</sup> Exogenous substrates of ENT4 are, for example, azacytidine and cladribine.<sup>28,43</sup>

Concentrative nucleoside transporters (SLC28) include CNT1 (SLC28A1), CNT2 (SLC28A2) and CNT3 (SLC28A3). These are Na<sup>+</sup>-dependent transporters ensuring the influx of purine and pyridine nucleosides and their analogs to target tissues in the human body.<sup>44</sup>

CNT1 transporter has pyrimidine specificity and is naturally expressed in epithelia tissue, the liver, the gastrointestinal tract, and kidneys.<sup>45</sup> CNT1 also mediates the influx of pyrimidine-analogs, including clinically used as antiviral and anticancer drugs, such as ribavirin, zidovudine, cytarabine, gemcitabine, and zalcitabine.<sup>46-49</sup>

CNT2 is a transmembrane protein with mainly affinity to purines but can also transport pyrimidines. It is expressed across the human body, especially in the gastrointestinal tract, kidneys, liver, and testis.<sup>50</sup> Drugs that are CNT2 substrates include, for example, 5-fluorouracil, azacytidine, and decitabine.<sup>27,28,51</sup>

CNT3 is able to transport purine and also pyrimidine nucleosides and their analogs, including anticancer drugs such as 6-mercaptopurine, 6-thioguanine, cytarabine, fludarabine, gemcitabine.<sup>24,52</sup> It can be found in the brain, breast, gastrointestinal tract, kidneys, pancreas, placenta, and testis.<sup>51</sup>

### 1.1.1.2 Proteins connected with multidrug resistance development

Drug resistance can arise between drugs with a similar structure and/ or mechanism of action (cross-resistance), but also between completely different substances (multidrug resistance, MDR). Cross-resistance is quite common in nucleoside-based drugs, for example, between structurally similar 6-thioguanine and 6-mercaptopurine.<sup>53</sup> Multidrug resistance does not depend on the similarities of individual drugs, only on their ability to serve as substrates of ATP-binding cassette (ABC) transporters that actively transport them from the intracellular space and decrease their biological activity.

The first protein identified in association with multidrug resistance is P-glycoprotein (Pgp/ ABCB1), which is the best-known ABC transporter. Pgp is typically expressed in the brain (especially in the blood-brain barrier, BBB), liver, kidneys, gastrointestinal tract, placenta or testis (blood-testis barrier). Its natural function is protection against potentially toxic compounds.<sup>54-56</sup> However, increased expression of this transporter can significantly affect the effectiveness of drugs, which are its substrates.<sup>57</sup> More than 480 compounds were identified as Pgp substrates, and this number is still rising.<sup>58</sup> Endogenous substrates of Pgp include for example, testosterone, androstenedione, endorphin, or glutamate.<sup>59,60</sup> It has been found that Pgp can also transport  $\beta$ -amyloid, whose accumulation is one of the factors involved in neurodegeneration, which is typical for illnesses such as Alzheimer's disease (AD).<sup>61</sup>

Exogenous Pgp substrates include various drugs, for example, anti-cancer, anti-epileptic, immunosuppressive drugs, human immunodeficiency virus (HIV) protease inhibitors, steroids, antibiotics, and others.<sup>62-64</sup> Nucleoside-based drugs, which are Pgp substrates, include 6-mercaptopurine, cladribine, or decitabine.<sup>65,66</sup> Drug identification as a Pgp substrate is an essential prognostic marker of treatment efficacy.

Another group of proteins connected with MDR is the multidrug resistance-associated proteins family (MRPs, ABCC), and until now, 9 MRP isoforms have been described. MRP proteins are also members of the ABC transporter family, and their function is an efflux of endogenous and exogenous compounds from human tissues. Naturally, MRP proteins are expressed across the human body, especially in the gastrointestinal tract, kidneys, adrenal glands, and the blood-brain barrier.<sup>67-69</sup> MRPs transport mainly organic anions, but MRP1 (ABCC1), MRP2 (ABCC2), and MRP3 (ABCC3) are able to transport also neutral molecules if they are conjugated to acidic ligands, such as glutathione (GSH), glucuronate or sulfate.<sup>70,71</sup>

MRP1 (ABCC1) was isolated from multidrug-resistant human lung cancer cells in 1992, and the discovery of other MRP isoforms generally followed.<sup>72</sup> MRP1 is present mainly in tissue barriers, such as blood-brain barrier or blood-testis barrier mediating transport of

endogenous and exogenous compounds including several drugs, such as doxorubicin, vincristine or methotrexate.<sup>56,73,74</sup>

MRP2 (ABCC2) is also part of the blood-brain barrier and regulates the transport of compounds into brain tissue.<sup>75</sup> In addition to the brain, we can also find this transporter in the gastrointestinal tract and kidney, acting as an ATP-dependent efflux pump.<sup>76,77</sup> Substrates of MRP2 can be endogenous molecules, such as conjugates of glutathione or bilirubin and heavy metals, but also antibiotics and anticancer and antiepileptic drugs.<sup>75,78</sup>

MRP3 (ABCC3) is expressed mainly in the liver, but its overexpression was also detected in ovarian carcinoma and acute lymphoblastic (ALL) and acute myeloid leukemia (AML) cells.<sup>79–81</sup> Substrates of MRP3 are for example etoposide, teniposide and methotrexate.<sup>82</sup>

MRP4 (ABCC4) can be found in broad spectra of tissues, such as kidneys, lungs, thymus, pancreas, testis, ovarium, gastrointestinal tract, and skeletal muscles.<sup>83,84</sup> MRP4 transports organic anionic molecules, including cyclic nucleotides and their analogs, nucleoside monophosphate analogs, conjugated steroids, urate, and eicosanoids. Substrates of MRP4 are also antibiotics, antiviral, cardiovascular, and anticancer drugs.<sup>85,86</sup>

MRP5 (ABCC5) was identified as a homolog of MRP1, which can transport cyclic adenosine and guanosine monophosphate (cAMP, cGMP) and also thiopurine drugs, 6-mercaptopurine, and 6-thioguanine.<sup>85,87</sup>

MRP6 (ABCC6), another homolog of MRP1, is expressed mainly in the liver and kidney, but it can also be found in other tissues, such as the connective tissue, where its deficiency leads to the development of Pseudoxanthoma elasticum (PXE).<sup>88,89</sup> Substrates of MRP6 are conjugated glutathione anions and also some anticancer drugs, such as daunorubicin, doxorubicin, etoposide or teniposide.<sup>90</sup>

MRP7 (ABCC10) transporter was identified in 2001, and its expression has been proved in the testis, gastrointestinal tract, epithelial tissue, and pancreas.<sup>91</sup> Physiological substrates of MRP7 are glucuronide conjugates, but it is able to transport broad spectra of exogenous compounds, including drugs such as docetaxel, paclitaxel, vinblastine or vincristine.<sup>92,93</sup>

MRP8 (ABCC11) transports purine and pyrimidine analogues. Endogenous substrates of MRP8 are, for example, cAMP or cGMP. Exogenous substrates include fluoropyrimidines, such as 5-fluorouracil.<sup>94</sup> MRP8 is generally expressed in axons of neuronal cells of central and peripheral neuronal systems (CNS, PNS), but it can also be found in the breast and lungs.<sup>95–97</sup>

MRP9 (ABCC12) is the latest described protein from the MRP protein family. It is expressed throughout the human body, and it can be found, for example, in the liver, ovary, testis, breast, skeletal muscles, kidneys, or lungs, but its substrate specificity is still unknown.<sup>98</sup>

The third member of the ABC protein family is breast cancer resistance protein (BCRP, ABCG2), also known as mitoxantrone resistance-associated protein (MXR), which was discovered in 1998 in multidrug-resistant breast cancer cell lines.<sup>99,100</sup> BCRP protein is expressed mainly in the placenta, where it regulates the administration of endogenous and exogenous compounds to the fetus, suggesting its role in protecting against potentially harmful substances.<sup>101</sup> Endogenous substrates of BCRP are, for example, uric acid,  $\beta$ -D-glucuronide and estrone-3-sulfate, and exogenous substrates include several drugs, such as 5-fluorouracil, mitoxantrone, flavopiridol, and lamivudine.<sup>100</sup> Identifying drugs as BCRP substrates is a prognostic factor of treatment efficacy.

Outside the ABC transporter family, there is another protein associated with the development of MDR, lung resistance-related protein (LRP).<sup>102</sup> LRP was identified as a major vault protein, which is the central part of the multimeric vault particles.<sup>103</sup> It acts as an efflux pump, but its specific function is not entirely understood. LRP was identified in lung cancer cells, but its expression was also confirmed in acute myeloid leukemia cells and brain tumors such as glioblastomas, meningiomas, neurofibromas, etc.<sup>103,104</sup>

### **1.1.1.3 Nucleoside-based drugs: metabolism and the mechanism of resistance**

In this chapter, the metabolism of clinically used nucleoside-based drugs is summarized, supplemented with information about the mechanisms of drug resistance.

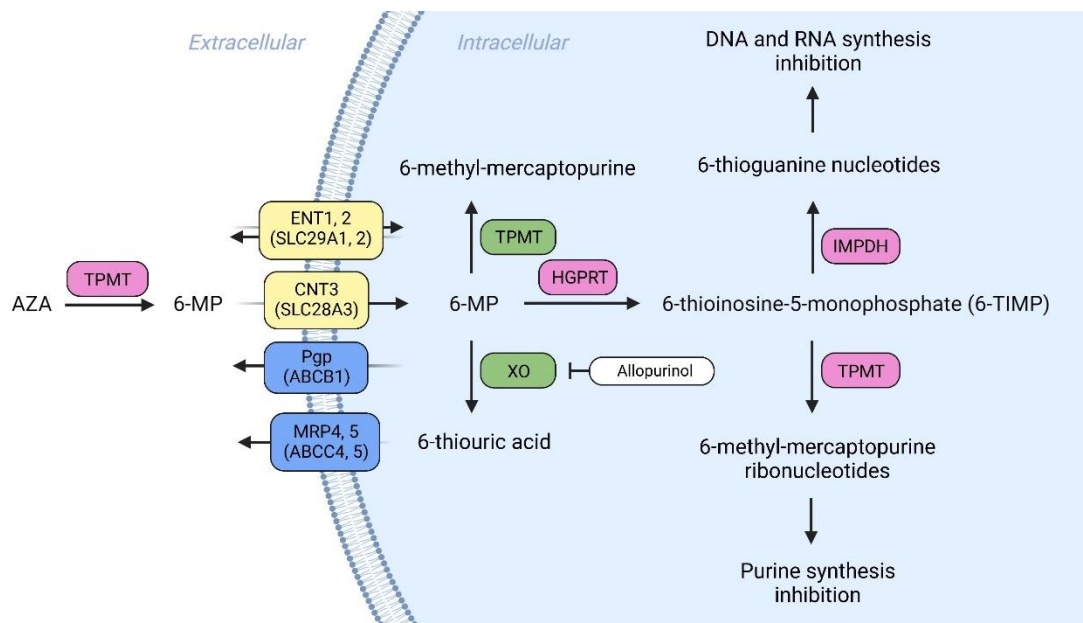
#### **6-mercaptopurine (6-MP)**

6-mercaptopurine (Fig. 2) is a purine analog clinically used to treat acute lymphoblastic leukemia and autoimmune diseases (Crohn's disease, rheumatoid arthritis, ulcerative colitis).<sup>105,106</sup> 6-MP is mainly used as a prodrug, azathioprine (Fig. 2), which is extracellularly metabolized by thiopurine S-methyl transferase (TPMT) into 6-mercaptopurine.<sup>107,108</sup> Transport of 6-MP across the cellular membrane is mediated via ENT1, 2, and CNT3, and expression of these transporters can affect its bioavailability and the associated effectiveness of the treatment.<sup>24</sup>

Several enzymes control the intracellular metabolism of 6-mercaptopurine. TPMT converts 6-mercaptopurine into 6-methyl-mercaptopurine, which is responsible for hepatotoxicity in some patients.<sup>109,110</sup> Activation of 6-mercaptopurine to 6-thioinosine-5-monophosphate (6-TIMP) is done by hypoxanthine-guanine phosphoribosyltransferase (HGPRT). 6-TIMP can be metabolized by a) inosine-5-monophosphate dehydrogenase



(IMPDH) into 6-thioguanine nucleotides, which interact with DNA and RNA leading to inhibition of their synthesis or by b) TPMT into 6-methyl-mercaptopurine ribonucleotides, which inhibit purine synthesis.<sup>111</sup> Elimination of 6-MP is mediated via xanthine oxidase (XO), which can be inhibited by allopurinol.<sup>112</sup> (Fig. 5)



**Figure 5.** Metabolism of azathioprine (AZA) and 6-mercaptopurine (6-MP). ENT: equilibrative nucleoside transporter, CNT: concentrative nucleoside transporter, Pgp: P-glycoprotein, MRP: multidrug resistance-associated protein, TPMT: thiopurine S-methyl transferase, XO: xanthine oxidase, HGPRT: hypoxanthine-guanine phosphoribosyltransferase, IMPDH: inosine-5-monophosphate dehydrogenase.<sup>13</sup>

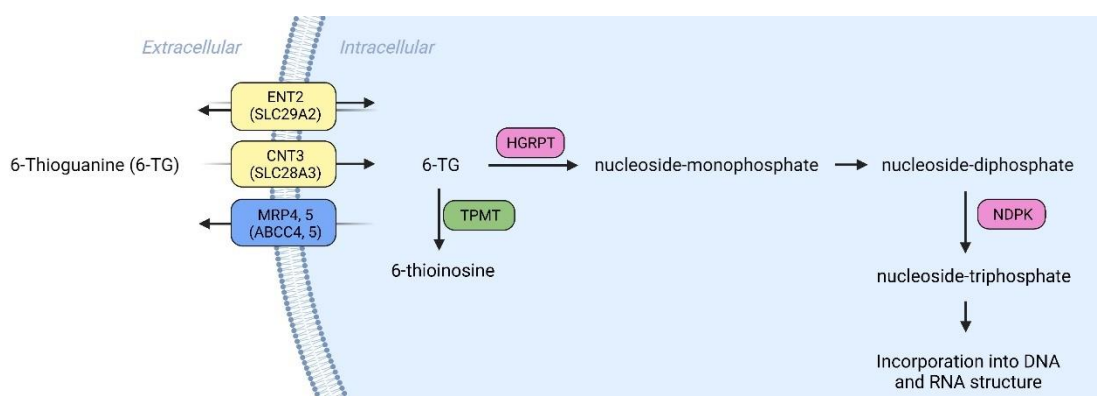
General mechanisms of 6-MP resistance are connected with the expression of MDR efflux pumps, Pgp, MRP4, and MRP5. Higher expression of these transporters can negatively affect 6-MP treatment efficacy.<sup>66,113–115</sup>

Changes in the expression of enzymes involved in the 6-MP metabolism were also described as a risk factor for resistance development. One of the first enzymes described in this connection was inosinic and guanylic acid pyrophosphorylase, which facilitate the formation of active metabolites, mercaptopurine ribonucleotides, in human cancer tissues.<sup>116</sup> Another enzyme is NT5C2 (cytosolic 5-nucleotidase II), which inactivates HGPRT and reduces the number of active metabolites in the cells.<sup>117</sup> Recent studies also show the connection between mTOR (mammalian target of rapamycin) pathway activity and 6-MP resistance in acute leukemia patients. Inhibition of mTOR complex 1 decreases the toxicity of 6-mercaptopurine. This protective effect is attributed to a reduction in cellular proliferation.<sup>118</sup>

## 6-thioguanine (6-TG)

6-thioguanine (Fig. 2) is a compound structurally very similar to 6-mercaptopurine. In fact, 6-TG is one of the 6-MP active metabolites. This purine analog is used in the treatment of chronic and acute myelogenous leukemia in mono and also in the combinatory therapy with cytarabine, daunorubicin, etoposide, prednisone, cyclophosphamide or oncovin to achieve better treatment efficacy.<sup>119–123</sup>

6-TG is administered orally and transported into cells via ENT2 and CNT3.<sup>32</sup> Intracellularly 6-TG is metabolized by HGPRT into nucleoside monophosphate, which is phosphorylated into diphosphate (TGDP) and triphosphate form (TGTP), which is the active metabolite of 6-TG.<sup>124,125</sup> TGTP incorporates into the structure of DNA and RNA and blocks their replication.<sup>126</sup> Elimination of 6-TG is mediated mainly by TPMT, which metabolizes 6-TG into an inactive form, 6-thioinosine.<sup>127</sup> (Fig. 6) TPMT expression level can significantly affect 6-TG biological activity, and cancer tissues expressing a low amount of TPMT (for example, pancreatic ductal adenocarcinoma cells, PDACs) are naturally more sensitive to 6-TG treatment.<sup>128</sup>



**Figure 6.** Metabolism of 6-thioguanine (6-TG). ENT: equilibrative nucleoside transporter, CNT: concentrative nucleoside transporter, MRP: multidrug resistance-associated protein, TPMT: thiopurine S-methyl transferase, HGPRT: hypoxanthine-guanine phosphoribosyltransferase, NDPK: nucleoside diphosphate kinase.<sup>13</sup>

Resistance to 6-TG is often connected with the expression and activity of HGPRT, a key enzyme in the 6-TG activation. Mutations in the *HGPRT* gene can significantly decrease the amount of HGPRT protein and thereby reduce the number of active metabolites of 6-TG. Mutations in this gene were found, for example, in circulating human lymphocytes, and the number of these cells was proportional to the age of patients.<sup>129,130</sup>

*In vitro* experiments also showed the connection between 6-TG resistance and DNA repair mechanisms. It has been found that 6-TG resistant cancer cell lines express approximately three times more MGMT (methylguanine-DNA methyltransferase), which is an enzyme

involved in DNA repair, which is associated with higher efficiency of tumor cell defense against treatment and reduced 6-TG activity. MGMT inhibitors were able to restore cell sensitivity.<sup>131</sup>

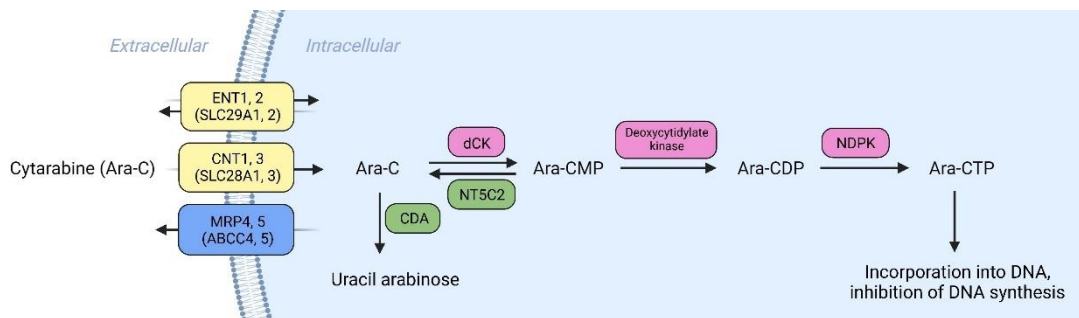
The expression level of membrane transporters also influences the biological activity of 6-thioguanine. Specifically, ENT2 and CNT3 mediate mainly the uptake of 6-TG and enable its intracellular activation and MRP4 and 5, which actively transport 6-TG to the extracellular spaces and thus reduce its activity.<sup>32,132</sup> 6-TG resistance is associated with lower expression of ENT2 and CNT3 and higher expression of MRP4 and 5. 6-TG is not a substrate of P-glycoprotein and can, therefore, be used in treating cancers typically associated with higher expression of Pgp, such as BRCA1-positive breast and ovarian cancers.<sup>133</sup>

### **Cytarabine (Ara-C)**

Cytarabine (Fig. 2) is a pyrimidine analog that is mainly used in the treatment of hematological malignancies, such as acute lymphoblastic leukemia (ALL), acute myeloid leukemia (AML), chronic myelogenous leukemia (AML) or acute non-lymphocytic leukemia (ANLL).<sup>134-136</sup> Cytarabine is used in monotherapy since 1969, and in the 1990s FDA also approved its combinations with other drugs, for example, with clofarabine, decitabine, sorafenib, or idarubicin to make cytarabine treatment more efficient.<sup>137-141</sup> Recently, a combination of low-dose cytarabine and venetoclax was tested in adult AML patients, resulting in complete remission in 60-80 % of patients.<sup>142</sup>

Cytarabine can be administered orally, but this is less effective than intravenous application due to its high first-pass metabolism. GIT (gastrointestinal tract) absorption undergoes less than 20 % of the applied dosage. The primary metabolism of cytarabine is mediated by cytidine deaminase (CDA), which converts cytarabine into its inactive form, uracil arabinose (Ara-U).<sup>143,144</sup> CDA expression is significantly related to the development of cytarabine resistance, and lower levels of CDA connected with severe or lethal toxicity of cytarabine have been described in the clinics.<sup>143</sup> Making CDA a valuable predictive marker of cytarabine treatment efficacy and potential toxicity.

Cytarabine is transported into cells mainly via ENT1, but it is also a substrate of ENT2, CNT1, and 3.<sup>25,33,45</sup> Intracellularly, cytarabine is phosphorylated by deoxycytidine kinase (dCK) into cytarabine monophosphate (Ara-CMP). Ara-CMP is phosphorylated by deoxycytidylate kinase into cytarabine diphosphate (Ara-CDP), which is phosphorylated into triphosphate form (Ara-CTP) by nucleoside diphosphate kinase (NDPK). Ara-CTP is the active metabolite of cytarabine, which is incorporated into DNA, and this incorporation leads to the inhibition of DNA replication.<sup>145,146</sup> (Fig. 7)



**Figure 7.** Metabolism of cytarabine (Ara-C). ENT: equilibrative nucleoside transporter, CNT: concentrative nucleoside transporter, MRP: multidrug resistance-associated protein, dCK: deoxycytidine kinase, CDA: cytidine deaminase, NT5C2: cytosolic 5-nucleotidase II, NDPK: nucleoside diphosphate kinase.<sup>13</sup>

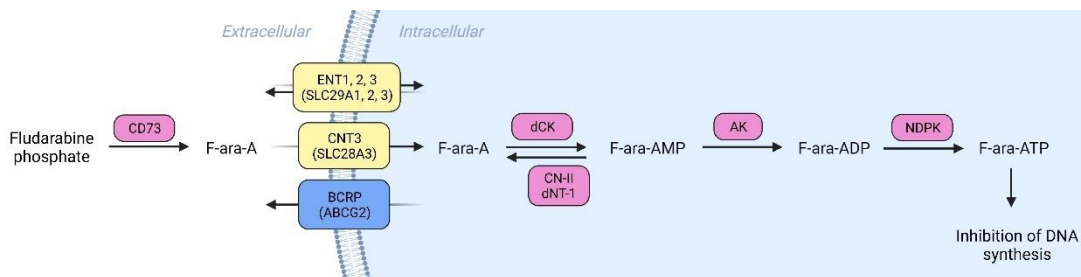
Cytarabine resistance can be connected with faster elimination via CDA or by cytosolic 5-nucleotidase II (NT5C2), which dephosphorylates Ara-CMP.<sup>147</sup> Cytarabine inactivation can also be done by dephosphorylation of Ara-CTP, mediated by SAMHD1 (SAM and HD domain-containing protein 1).<sup>148</sup> The effectiveness of the treatment can be restored by the use of SAMHD1 inhibitors that prevent the reduction of the active metabolites, Ara-CTP.<sup>149</sup>

Another mechanism of cytarabine resistance is reduced activation due to lower expression/ activation of dCK, which is the crucial enzyme in the cytarabine metabolism, or faster efflux mediated by MRP4 and 5.<sup>145,150,151</sup>

### Fludarabine (F-ara-A)

Fludarabine (Fig. 2) is a purine analog clinically used to treat chronic lymphocytic leukemia (CLL) and other lymphoproliferative malignancies.<sup>141,152</sup> As previously described nucleoside-based drugs, fludarabine can be used in mono and combinatory therapy. Combinations of fludarabine and cytarabine, cyclophosphamide, idarubicin, clofarabine, rituximab, bortezomib, and ibrutinib are clinically used.<sup>153–155</sup>

Fludarabine is usually administered as a phosphorylated prodrug (fludarabine phosphate, Fig. 2), which is extracellularly dephosphorylated by ectoenzyme CD73 (ecto-5-nucleotidase, S-NT) into F-ara-A.<sup>156</sup> F-ara-A is transported into cells via ENT1, 2, 3 and CNT3. Intracellularly, F-ara-A is phosphorylated by dCK into monophosphate (F-ara-AMP). F-ara-AMP is phosphorylated into diphosphate (F-ara-ADP) by adenylate kinase (AK), and third phosphorylation is done by NDPK forming fludarabine active metabolite, F-ara-ATP, which interacts with DNA and inhibits its replication.<sup>156,157</sup> (Fig. 8)



**Figure 8.** Metabolism of fludarabine (F-ara-A) and its prodrug (fludarabine phosphate). CD73: ecto-5-nucleotidase, ENT: equilibrative nucleoside transporter, CNT: concentrative nucleoside transporter, BCRP: breast cancer resistance protein, dCK: deoxycytidine kinase, CN-II: 5-nucleotidase, dNT-1: deoxynucleotidase-1, AK: adenylate kinase, NDPK: nucleoside diphosphate kinase.<sup>13</sup>

Resistance to fludarabine can be significantly connected with the expression of ENT1, 2, and 3 and CNT3, which affects its bioavailability.<sup>156</sup> Fludarabine is a non-MDR drug, but its resistance has been reported in cases with overexpression of Pgp, MRP1, and LRP.<sup>158</sup> Fludarabine has been described as a substrate of BCRP transporter, and its higher expression can negatively affect the treatment and increase risk of patient relapse.<sup>159</sup>

Many mechanisms affecting fludarabine activity have been described. For example, the involvement of glucosylceramide synthase (GSC) in CLL patients. Higher expression of GSC leads to the accumulation of glucosylceramide, which promotes cell proliferation and helps the development of fludarabine resistance. This resistance can be overcome using GSC inhibitors, such as PDMP (1-phenyl-2-decanoylamino-3-morpholino-1-propanol).<sup>160</sup>

CLL cells resistant to fludarabine are also five-time more sensitive to PEITC ( $\beta$ -phenethyl isothiocyanate), which is the anticancer and chemopreventive agent. PEITC exposure leads to ROS (reactive oxygen species) accumulation in CLL cells, followed by glutathione depletion and the oxidation of mitochondrial cardiolipin, leading to apoptosis.<sup>161</sup>

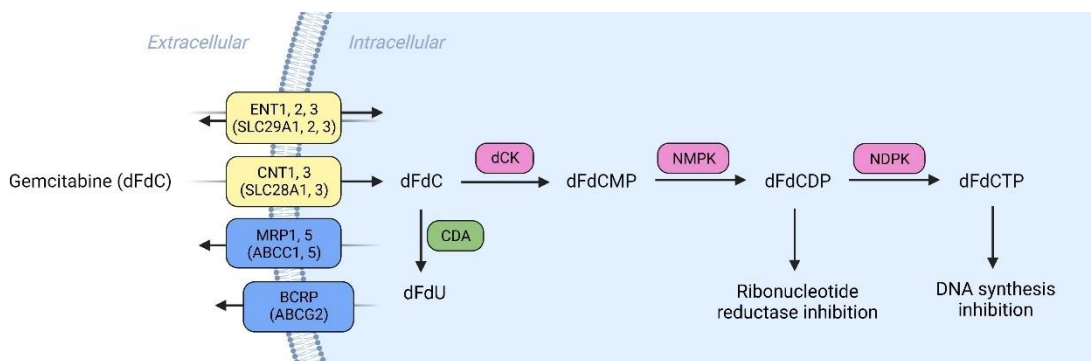
Another mechanism of fludarabine resistance is linked to the mTOR pathway. Especially with higher phosphorylation of ribosomal protein S6 kinase (p-70S6K) leading to higher phosphorylation of ribosomal S6 protein and induction of photosynthesis.<sup>162</sup>

### **Gemcitabine (GEM, dFdC)**

Gemcitabine (Fig. 2) is a pyrimidine analog, which is similar to cytarabine due to its structure and metabolism. This similarity may account for the frequent occurrence of cross-resistance between cytarabine and gemcitabine.<sup>163</sup> In contrast to cytarabine, gemcitabine is used mainly in treating solid tumors, such as breast, pancreatic, ovarian, bladder, or non-small cell lung cancers.<sup>164-166</sup>

Gemcitabine is administered intravenously as gemcitabine itself or by prodrug LY2334737 (Fig. 2). Active uptake of gemcitabine is mediated mainly via ENT1 and CNT3,

but it is also the substrate for ENT2, 3, and CNT1. Intracellularly, gemcitabine is phosphorylated into monophosphate (dFdCMP) by dCK, into diphosphate (dFdCDP) by nucleotide monophosphate kinase (NMPK), and into triphosphate (dFdCTP) by NDPK.<sup>167</sup> Gemcitabine diphosphate (dFdCDP) acts as an inhibitor of ribonucleotide reductase (RR), a key enzyme in deoxyribonucleotide synthesis. Gemcitabine triphosphate (dFdCTP) interacts with DNA and causes inhibition of DNA synthesis.<sup>168,169</sup> (Fig. 9)



**Figure 9.** Metabolism of gemcitabine (GEM, dFdC). ENT: equilibrative nucleoside transporter, CNT: concentrative nucleoside transporter, MRP: multidrug resistance-associated protein, BCRP: breast cancer resistance protein, dCK: deoxycytidine kinase, CDA: cytidine deaminase, NMPK: nucleotide monophosphate kinase, NDPK: nucleoside diphosphate kinase.<sup>13</sup>

The development of gemcitabine resistance can be due to the reduction of ENT1, 2, 3 and CNT1, 3 expressions, which negatively influence the bioavailability of active gemcitabine metabolites. Also, lower expression/ activation of dCK or higher expression of CDA, which mediates gemcitabine elimination, can negatively affect gemcitabine activity and contribute to the development of a resistant phenotype.<sup>170</sup> Gemcitabine is also a substrate for MDR efflux pumps, MRP1 and 5, and BCRP, which effectively reduce the intracellular concentration of gemcitabine and thus increase the resistance of tumor cells.<sup>171</sup>

Recent studies show the connection between the alteration of many cellular pathways, such as the Hedgehog pathway (HH), extracellular signal-regulated kinase (ERK)/ Protein kinase B (Akt)/ Signal transducer and activator of transcription 3 (STAT3), Wnt or neurogenic locus notch homolog protein (Notch) pathways, and gemcitabine resistance.<sup>172,173</sup>

In patients with urothelial carcinoma, Gli2-dependent activation of the HH pathway was observed after gemcitabine induction. This pathway fosters cellular migration and invasion and supports the development of resistant phenotype.<sup>174</sup>

The involvement of the Wnt pathway was studied in pancreatic carcinoma. It has been found that patients with lower levels of  $\beta$ -catenin, which is a key protein in the Wnt cascade, were more sensitive to gemcitabine treatment and with longer disease-free time periods and also higher overall survival, compared to patients who express high levels of  $\beta$ -catenin.<sup>175</sup>

ERK/ Akt/ STAT3 is involved in cellular proliferation and improves cancer cells' survival, thereby reducing the effectiveness of gemcitabine treatment.<sup>173</sup>

## **1.1.2 Current strategies for overcoming the MDR**

### **1.1.2.1 Combinatory therapy**

One of the most common ways to increase anticancer drug efficacy is by combining two or more drugs in the treatment. These drugs can hit different targets, and their synergistic effect can reduce risk or resistant clone selection.<sup>176</sup> Drug combination is also effective when monotherapy no longer has such clinical impact as needed.<sup>177,178</sup>

Combinatory therapy is also commonly used in nucleoside-based drug treatment. Several combinations have been used. For example, cytarabine has been combined with fludarabine in the treatment of relapsed/ refractory acute AML, 6-thioguanine has been used with disulfiram/Cu, leading to significantly reduced proliferation of triple-negative breast cancer cells, fludarabine combined with alemtuzumab have been successfully used in the treatment of patients with relapsed/ refractory CLL, etc.<sup>179-181</sup>

### **1.1.2.2 Efflux pump inhibitors**

Since proteins connected with the MDR phenotype have been described, they have become an attractive therapeutic target to increase cancer cells' sensitivity to therapy. The most intensively studied was P-glycoprotein, which was the first described efflux pump connected with MDR development. Until now, four generations of Pgp inhibitors have been described and synthesized. First and second-generation Pgp inhibitors (verapamil, dexverapamil, dextiguldipine) showed many off-target interactions (for example, inhibition of cytochrome P450), too high serum concentration, and potential toxicity.<sup>182-184</sup> Third and fourth generation Pgp inhibitors used besides natural products should be less toxic and more specific.<sup>185</sup> However, none of the Pgp inhibitors make significant improvements in anticancer therapy, and non of them have passed clinical trials.

One of the reasons for the failure of Pgp inhibitors may be that MDR transporters are often co-expressed, and inhibition of only one of them will not cause the expected clinical effect. Broad spectra of compounds with dual inhibitory activity have been described. For example, schisandrin B (Sch B), quinazolinones, and glycyrrhetic acid were described as dual Pgp/ MRP1 inhibitors.<sup>186-188</sup> Elacridar, azepine scaffold and alkoxy biphenyl derivatives, bifendate-chalcone hybrids, and propafenone analogs have described dual Pgp/BCRP activity.<sup>189-192</sup> Dual inhibitors appear to be an attractive therapeutic tool that could help reduce the impact of MDR proteins on anticancer therapy and reverse the multidrug resistance phenotype.

### 1.1.2.3 Targeted therapy

Target therapy is A more specific way to overcome drug resistance in cancer. Identification of cellular or molecular targets, which are responsible for treatment failure, is a crucial step toward the development of new therapeutic approaches. Prognostic biomarkers of anticancer treatment can be found on genomic or proteomic levels, and they can be heterogeneous among patients. Personalized medicine allows the identification of these differences and adapts the treatment to the needs of the current patient.<sup>193</sup>

Based on these findings, small molecules of monoclonal antibodies, antibiotics, and small drug molecules are synthesized. At the forefront of interest are mainly monoclonal antibodies conjugated with anticancer drugs or with radionuclides, which allow target therapy into tumor tissue without off-target interactions, reducing the risk of severe side effects.<sup>194,195</sup>

Although drug-conjugated antibodies (ADCs) offer a wide range of new therapeutic options, finding a compatible drug-antibody pair that exhibits the correct biological activity is not easy. Until now, around 11 ADCs have been approved by the FDA. For example, gemtuzumab ozogamicin (AML), ado-trastuzumab emtansine (breast cancer), brentuximab vedotin (Hodgkin lymphoma), inotuzumab ozogamicin (ALL).<sup>196-199</sup>

Also, nucleoside-based drugs have been studied in the form of conjugates. Aptamer-drug conjugates (ApDCs) using nucleic acids instead of monoclonal antibodies were prepared for several nucleoside-based drugs, such as gemcitabine and 5-fluorouracil, which were conjugated with RNA, and these ApDCs were used for the treatment of gemcitabine-resistant pancreatic cells resulting in significantly inhibited proliferation.<sup>200</sup> Recently, new drug-constituted DNA-like oligomers (drugtamers) have been synthesized for nucleoside-based drugs, such as gemcitabine, clofarabine, ara-guanosine, and floxuridine. Compared to ApDCs, drugtamers should have a higher loading ratio, better active release controlled by enzymes, and active targeting capability.<sup>201</sup>



## **1.2 Neuroprotective activity of nucleosides and microtubule-targeting drugs**

Nucleosides are mainly used as anticancer and antiviral drugs for treating pathological states all over the human body, and also their CNS activity was also described. Boron-containing nucleosides seem to be promising candidates for the treatment of brain tumors; adenosine, guanosine, inosine, and uridine are endogenous antiepileptogenic modulators, suggesting nucleosides and their analogs are potential antiepileptic drugs and anti-HIV nucleoside based drugs (nucleoside reverse transcriptase inhibitors) can prevent the development of HIV-associated dementia.<sup>202–205</sup>

Unfortunately, anti-HIV nucleoside-based drugs facilitate lower uptake into CNS or fast elimination due to several factors, such as the activity of metabolic enzymes or the activity of membrane transporters, including ABC and SLC superfamilies. Modifications of drug delivery techniques, such as nano-carriers (liposomes, micelles, dendrimers, nanoparticles, etc.), are currently being studied to enhance CNS uptake and treatment efficacy.<sup>206–208</sup> Wide spectra of nanoparticles (NPs) have been synthesized, and the results are promising. For example, nanoparticles conjugated to trans-activating transcriptor (TAT) peptide or NPs of poly(lactic-co-glycolic) acid (PLGA) seem to be potential carriers for effective drug penetration into CNS.<sup>209,210</sup>

This thesis explores microtubules as a molecular target in the treatment of neurodegenerative diseases via stabilization of their structure or in cancer treatment, where the targeted therapy causes their depolymerization, leading to cellular death. The thesis is mainly focused on pathological phosphorylation of tau protein, which is typical for AD.’

### **1.2.1 Microtubules dynamics as a therapeutic target**

Microtubules are an essential part of the cellular cytoskeleton and participate in many processes, such as cell division, intracellular transport, localization of organelles, etc., and thus disruption of its structure leads to cellular death.<sup>211,212</sup> Microtubules consist of tubulin, a heterodimeric protein with  $\alpha$  and  $\beta$  subunits.<sup>213</sup> They are very dynamic, with growing and dissociating parts. These processes are regulated via a GTP-cap located in the plus end of microtubules. This GTP-cap consists of GTP-liganded  $\beta$ -tubulin and allows microtubules to grow. Once GTP is hydrolyzed into GDP, polymer binding is weaker, and microtubules start to dissociate.<sup>214</sup> Stabilization of microtubule structure is done by microtubule-associated proteins (MAPs). Several MAPs have been investigated, including MAP1-7 or tau protein.<sup>215</sup>

Since microtubules are essential for cellular viability, they became potential therapeutic targets, and microtubule-regulating drugs have been investigated. Regulation of microtubule

dynamics can be done in positive and negative ways. Disruption of microtubule dynamics and structure can be used in anticancer treatment, including solid tumors and hematological malignancies.<sup>216</sup> Several microtubule-targeted drugs are clinically used, such as vinca alkaloids or paclitaxel. Historically, microtubule-targeted drugs have been used as inhibitors of mitosis, but it has been found that the activity is more complex, and these drugs also affect non-dividing cells via inhibition of signaling pathways.<sup>217</sup> For example, paclitaxel or vinorelbine inhibits the STAT3 pathway, which is constitutively activated in approximately 70 % of cancers and causes disruption of STAT3-tubulin interaction in breast cancer. A similar effect was observed in the case of ovarian and prostate cancer cells.<sup>218</sup> Overactivated STAT3 inhibits the expression of immune regulators and promotes the expression of immunosuppressive factors, so its inhibition can be an effective way to increase the efficacy of anticancer therapy.<sup>219</sup> Other STAT3 inhibitors have been investigated, and several compounds are currently in clinical trials.<sup>220</sup>

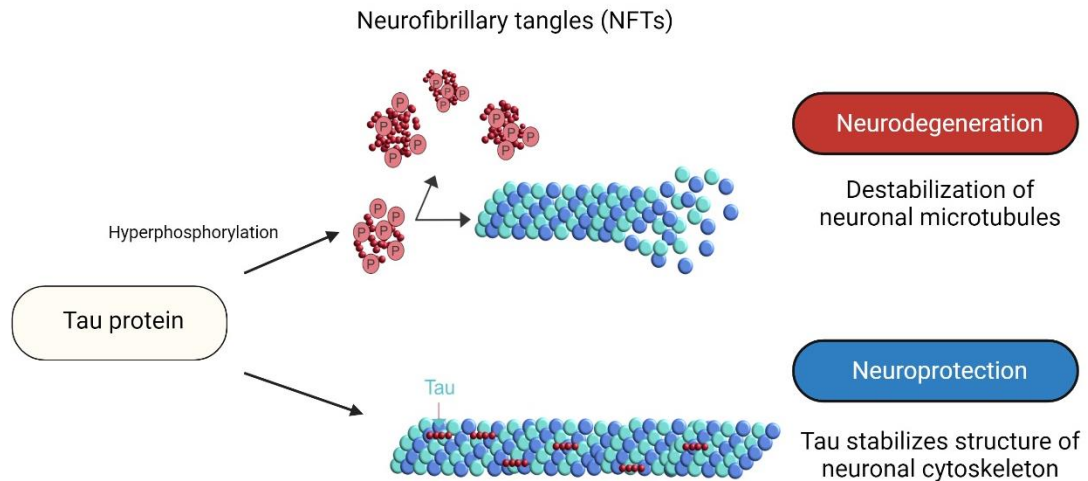
It has also been found that microtubule-targeted drugs inhibit the expression of vascular endothelial growth factor receptor 2 (VEGFR-2), which is essential in angiogenesis.<sup>221</sup>

In our work, we studied triazole-based estradiol dimers with five-atom linkers consisting of carbon, oxygen, or nitrogen in their center. Nitrogen dimers were modified by a benzyl group with methoxy or hydroxy substituents, and in one case, the length of the linker was extended. Our tested compounds significantly interacted with microtubules, and their ability to cause G2/M arrest suggests their application as mitosis inhibitors.<sup>216</sup>

In the other way, stabilization of microtubule structure can improve cognitive functions of patients with neurogenerative diseases, such as tauopathies, and decrease the progression of dementia associated with the loss of neuronal cells.<sup>222</sup>

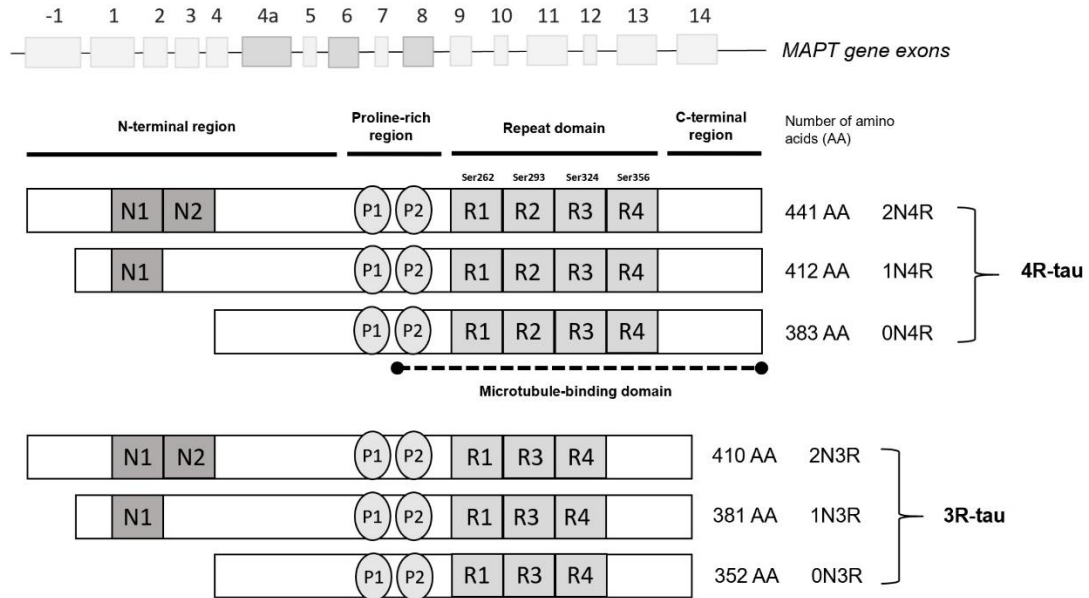
### **1.2.2 Tauopathies**

Tauopathies are a class of more than twenty neurogenerative diseases characterized by the accumulation of abnormal tau protein in the CNS.<sup>223</sup> The most common tauopathy is Alzheimer's disease, but pathological tau protein aggregation has also been found in patients with Pick's disease (frontotemporal dementia), progressive supranuclear palsy (PSP), corticobasal degeneration (CBD), post-encephalitic parkinsonism, etc.<sup>224,225</sup> Tau is a microtubule-associated protein that stabilizes neuronal microtubules (Fig. 10).<sup>211,212</sup> Tau protein can be mainly found in the neurons of the CNS (primarily in their axons), with abundant expression in the cerebral cortex.<sup>226</sup> Lower expression has been found in the oligodendrocytes and astrocytes.<sup>227</sup>



**Figure 10.** Tau protein naturally stabilizes microtubule structure. Once tau is hyperphosphorylated, it releases from binding to microtubules, and free tau forms aggregates, leading to neurofibrillary tangles (NFTs) forming. Microtubules become unstable, leading to their depolymerization and neuronal death, typical in AD brains.

Tau protein is encoded by *MAPT* (microtubule-associated protein tau) gene localized on the locus 17q21 in the human genome. Alternative splicing of *MAPT* gene exons 2, 3, and 10 results in the synthesis of six tau protein isoforms, which differ in the number of N-terminal inserts (0N, 1N or 2N) and repeat domains (3R or 4R) (Fig. 11), whereas in normal brain tissue R3: R4 ratio is approximately 1: 1.<sup>228,229</sup> All six tau isoforms are able to form pathological aggregates and form neurofibrillary tangles, but some diseases are characterized by the presence of specific tau isoform. For example, Pick's disease contains only 3R tau isoforms, PSP contains mainly 4R isoforms, and Alzheimer's disease is characterized by the presence of 3R and 4R isoforms.<sup>230–232</sup>



**Figure 11.** Tau protein isoforms according to alternative splicing of *MAPT* gene: 2N4R, 1N4R, 0N4R, 2N3R, 1N3R, and 0N3R

There are different domains in the structure of the tau protein: the N-terminal region, the microtubule-binding domain, and the C-terminal region. (Fig. 11) Interaction with microtubules is mediated via microtubule-binding domain, including proline-rich region, repeat domains, and C-terminal region.<sup>233</sup> The Physiological function of tau protein is not completely clear, but it has been found that tau protein decreases tubulin depolymerization, which stabilizes microtubules and the structure of neuronal cytoskeleton.<sup>234</sup>

### 1.2.2.1 Tau protein phosphorylation

Under physiological conditions, tau protein is phosphorylated in multiple sites, mainly in the microtubule-binding domain. Hyperphosphorylated tau protein starts forming aggregates with itself instead of interacting with microtubules, leading to destabilization of the axonal cytoskeleton and neuronal death. Accumulation of tau aggregates and creating structures called neurofibrillary tangles are one of the main hallmarks of AD.<sup>235,236</sup>

Until now, approximately 45 phosphorylating sites of tau protein have been identified. Clinically relevant are mainly S262, Ser324, and Ser356, which are associated with pathological tau phosphorylation in AD.<sup>237–239</sup> Several kinases have been found to phosphorylate tau protein. Still, hyperphosphorylation of tau protein and the development of AD have been connected mainly with the MARK (microtubule-affinity regulating kinase) kinase family and GSK-3 $\beta$  (glycogen synthase kinase 3 $\beta$ ).<sup>240,241</sup> (Fig. 12)

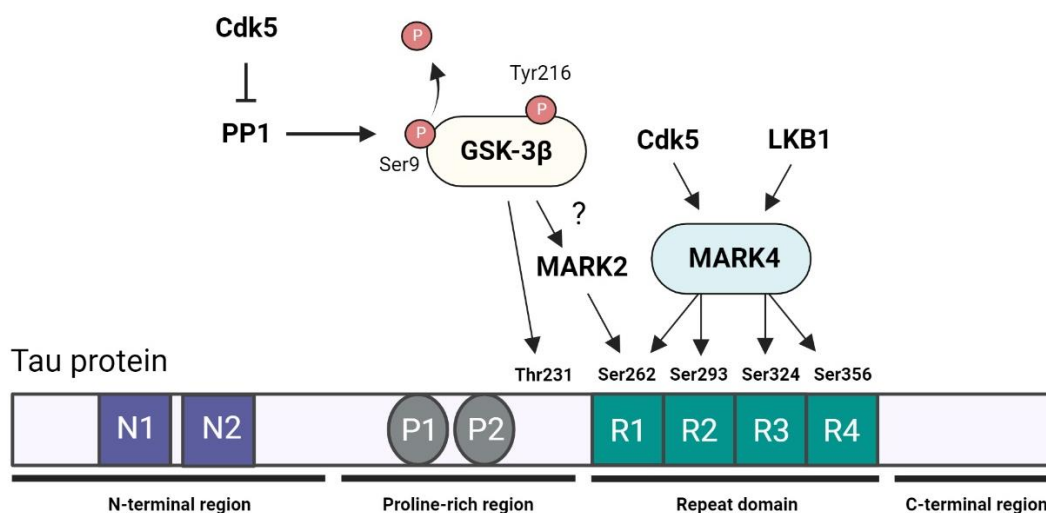
MARK is a Ser/Thr kinases family, including four different isoforms. These kinases are expressed predominantly in the brain tissue, but they can also be found in the kidneys, heart, skeletal muscles, and spleen.<sup>242</sup> But not all of these isoforms have been identified in connection with pathological tau hyperphosphorylation.

MARK1 localizes in the plasmatic membrane and cytoplasm and is involved mainly in intracellular signal transduction and cellular migration.<sup>243</sup> MARK3 contributes to cell cycle regulation and cellular differentiation, and its low expression was found in the hippocampus of AD patients.<sup>240</sup>

The activity of MARK2 and mainly of MARK4 is essential for the pathological phosphorylation of the tau protein.<sup>244</sup> MARK2 mediates cellular transport and microtubule dynamics and plays a role in the tau protein phosphorylation at Ser262 of tau protein.<sup>245</sup> Overexpression of MARK4 was detected in the brain tissue of AD patients, and it has been found that this kinase has a prominent role in the tau protein hyperphosphorylation and neurodegeneration, which is typical for AD.<sup>240</sup> This kinase is implicated in the early phosphorylation of tau at Ser262, leading to the detachment of tau protein from microtubules. Unbound, free tau is more susceptible to phosphorylation by other kinases, leading to tau aggregates and neurofibrillary tangles forming.<sup>246</sup> MARK4 phosphorylates tau protein also at Ser356 (this phosphorylation is essential for tau accumulation and toxicity) and with lower affinity at Ser324 and Ser293.<sup>246-248</sup>

MARK4 is, in its active form, highly phosphorylated. Cyclin-dependent kinase 5 (Cdk5) phosphorylates MARK4 in the spacer domain, and the second activating kinase, liver kinase 1 (LKB1), phosphorylates the activation loop of MARK4. Both kinases were described to be connected with increased MARK4 activity in AD.<sup>249,250</sup>

There is a close relationship between Cdk5 and other kinases involved in the tau hyperphosphorylation, GSK-3 $\beta$ .<sup>249,251,252</sup> Cdk5 is indirect regulator of GSK-3 $\beta$  activity. Cdk5 phosphorylates PP1 (phosphatase 1), leading to its inactivation.<sup>253</sup> In its active form, PP1 dephosphorylates GSK-3 $\beta$  at Ser9, leading to increase of autophosphorylation at Tyr216 and increase in its activity.<sup>254</sup> GSK-3 $\beta$  then phosphorylates tau protein in multiple sites, but phosphorylation at Ser262 and Thr231 has been found to be most important for AD development.<sup>255</sup> There is no direct phosphorylation of GSK-3 $\beta$  at Ser262. Kosuga *et al.* identified the involvement of GSK-3 $\beta$  in MARK2 activation via phosphorylation at Ser212 and MARK2, then mediate phosphorylation of tau at Ser262,<sup>256</sup> but several studies identified this phosphorylation as an inhibitory and described activation of MARK2 via phosphorylation at Thr208.<sup>257,258</sup> Thus, the exact mechanism is not completely clear. (Fig. 12)



**Figure 12.** Kinases involved in AD's pathological hyperphosphorylation of tau protein (MARK2, MARK4, GSK-3 $\beta$ , Cdk5, and LKB1).

Extracellular signal-regulated kinase 2 (ERK2) has also been identified to participate in tau hyperphosphorylation, but not under physiological conditions. ERK2 – tau interactions were observed after paclitaxel induction during anticancer treatment.<sup>259</sup>

### 1.2.2.2 MARK4 inhibitors

Since MARK4 was identified to be connected with the development of several pathological states, such as neurodegenerative diseases, cancer (glioma), diabetes, and obesity, broad spectra of its inhibitors have been synthesized and tested, including *N*-substituted acridones, morpholine-based hydroxylamine analogs, and isatin-triazole hydrazones.<sup>260–262</sup> *In vitro* experiments using recombinant MARK4 enzyme also proved MARK4 inhibition by serotonin, which is naturally present in the CNS.<sup>263</sup> *In silico* experiments using molecular docking analysis identified 5 pyrazolopyrimidine analogs to be MARK4 inhibitors (PubChem IDs: 90794095, 91145515, 91895678, 91895692, and 91895679).<sup>264</sup> However, none of these compounds are currently approved for use in clinical practice.

Nevertheless, some clinically used drugs have also been identified as MARK4 inhibitors. For example, sunitinib malate, which is used for the treatment of gastrointestinal tumors, inhibits MARK4 with nanomolar activity, and acetylcholinesterase (AChE) inhibitors (donepezil and rivastigmine tartrate), which are used in the symptomatic cure of AD inhibit MARK4 with IC<sub>50</sub> values of 5.3  $\mu$ M (donepezil) and 6.74  $\mu$ M (rivastigmine tartrate).<sup>265,266</sup>

MARK4 activity can also be inhibited indirectly via inhibition of its activating kinases Cdk5 and LKB1.

### 1.2.2.3 Cdk5 inhibitors

Cdk5 is an essential enzyme involved in neuronal signal transduction, and its activity has been connected with several neurodegenerative states, such as depression, AD, Parkinson's disease, anxiety, or stress.<sup>267</sup> Although Cdk5 mainly regulates neuronal cells, its activity has also been detected in tumor cells (brain tumors, breast, colon, lung, pancreatic, or breast cancer).<sup>268</sup> Therefore, Cdk5 inhibitors are being tested as neuroprotective and also antitumor drugs.

Constitutive Cdk5 gene knockout has been found to be lethal, but conditional knockout of Cdk5 improves cognition and exhibits a neuroprotective effect.<sup>269</sup> Several Cdk5 inhibitors were identified, such as amino pyrazole-based analogs, olomoucine, roscovitine, and GFB-12811, but the number of BBB penetrating compounds is limited.<sup>270–272</sup> Until now, no Cdk5 inhibitor has been approved for the treatment of neurodegenerative diseases.

### 1.2.2.4 LKB1 inhibitors

LKB1 (liver kinase B1) is involved in several cellular processes, such as growth, polarity, and metabolism, but it also acts as a tumor suppressor.<sup>250</sup> Hereditary inactivation of LKB1 is associated with Peutz-Jeghers syndrome (PJS), and somatic mutations were found in patients with non-small cell lung cancer, cervical cancer, and melanoma.<sup>273–276</sup> LKB1 also has an important role in the neuronal tissue, and it is one of the critical enzymes involved in neuronal polarization and axon development.<sup>277</sup>

LKB1 kinase is targeted mainly as a tumor suppressor, but due to its ability to activate the MARK4 enzyme, it has the potential to become also the neuroprotective target.<sup>250,273</sup> Only a limited number of LKB1 inhibitors were described, such as radicicol, which is an antimalarial and antifungal antibiotic, but none of them is clinically used in treating neurodegenerative diseases.<sup>278</sup>

### 1.2.2.5 GSK-3 $\beta$ inhibitors

GSK-3 $\beta$  is an enzyme involved in multiple cellular processes, such as protein and glycogen synthesis, inflammation, differentiation, cell cycle, proliferation, and apoptosis.<sup>279</sup> Activity of GSK-3 $\beta$  was also connected with the development of several pathological states, including tau hyperphosphorylation in neurodegenerative diseases or cancer, where it aids the metastatic process and is also involved in the resistance development.<sup>280</sup> In cancer, GSK-3 $\beta$  inhibitors reduce cellular growth and metastasis, and in neurodegenerative diseases, inhibition of GSK-3 $\beta$  can help reduce the number of tau aggregates and stabilize the structure of the neuronal cytoskeleton.<sup>281</sup> GSK-3 $\beta$  inhibitors can be, therefore, used as neuroprotective and also anticancer agents.

GSK-3 $\beta$  inhibitors have been intensively studied, and many of them have been identified. For example, SAR502250, SB-216763, SB-415286, donepezil, and lithium have been described with neuroprotective effects.<sup>282–285</sup> Donepezil is a clinically used drug prescribed for AD treatment as an acetylcholinesterase inhibitor. Its ability to also inhibit GSK-3 $\beta$  can enhance its neuroprotective effect.<sup>286</sup> Lithium was also clinically used to treat bipolar affective disorder. Still, long-term treatment led to build-up toxicity, a severe side effect that greatly outweighed the benefits of the treatment.<sup>287,288</sup>

Inhibitors 9-ING-41 and 9-ING-87 have been found to be effective in decreasing the viability of breast cancer cells, and 9-ING-41 was also able to increase the efficacy of irinotecan treatment *in vitro*.<sup>289</sup> Another anticancer GSK-3 $\beta$  inhibitor is, for example, pinosylvin, which is a naturally occurring *trans*-stilbenoid able to reduce the proliferation of colorectal cancer cells *in vitro*.<sup>290</sup>

### 1.2.3 CNS drug design

The human brain is a unique organ that is key to the function of the human body. For this reason, a sophisticated defense system (blood-brain barrier, BBB; blood-cerebrospinal fluid barrier, BCB; arachnoid barrier) has been developed to protect the brain against potentially toxic compounds.<sup>291</sup> BBB has a specific structure (tight junctions, limited pinocytosis, absence of fenestrations, and close contact between astrocyte protrusion), which limits the uptake of endogenous and exogenous compounds.<sup>266,292</sup> There are also membrane transporters, which ensure active efflux of their substrate compounds. These transporters include members of the ABC protein family, especially Pgp, which can transport broad spectra of lipophilic drugs. Identification of the drug as a Pgp substrate can significantly decrease its CNS activity.<sup>293</sup>

Based on these facts, only a few substances can successfully pass into the brain tissue or achieve the concentration needed for the therapeutic effect. CNS drug design examines the similarities between these compounds and, based on them, tries to design and synthesize new molecules that will not only pass through the brain barrier but also have the desired biological activity without adverse side effects and off-target interactions.<sup>294</sup>

Drug design (primarily focused on orally administered drugs) uses Lipinski's rule of five: the molecular weight of the compound should not be greater than 500 Da, the number of hydrogen bond donors should not be greater than 5, and the number of acceptors should be lower than 10, octanol-water partition coefficient (logP) lower than 5 and number of rotational bonds should be lower than 10.<sup>295</sup>

The induction of high-throughput screenings led to the modification of the original rules, which were modified for the needs of CNS drug design. Optimized parameters suggest



that CNS active compounds, which successfully pass through BBB, should have molecular weight lower than 400 Da, logP should be 3-5, number of rotatable bonds should be 5 or lower, number of hydrogen bond donors should be lower than 3 and number of acceptors lower than 10.<sup>296-299</sup> There is also additional parameter, topological polar surface area (TPSA), which is the summary of the surfaces of nitrogen or oxygen atoms and hydrogen atoms, which are attached to them.<sup>300</sup> In the case of CNS active compounds, TPSA should be lower than 60-90 Å<sup>2</sup>.<sup>301</sup>

## **2 EXPERIMENTAL PART**

## 2.1 Aims

The experimental part aims to show nucleosides' biological activity and their potential application as antitumor and neuroprotective drugs.

In the first part, cellular models of cancer cells resistant to nucleoside-based drugs will be developed. Resistant clones will be selected by clinically used drugs: cytarabine, fludarabine, and 6-thioguanine. Cross and multidrug resistance will be verified by MTS cytotoxicity assay. Successfully developed resistant cell lines will be used to study nucleoside-based drug resistance (expression of ABC transporters, nucleoside-based transporters, and proteins connected with nucleoside metabolism).

The second part will develop a kinase assay for detecting enzyme activity. The method will be optimized for the detection activity of MARK kinases and GSK-3 $\beta$ . Optimized methods will be used for screening MARK4 and GSK-3 $\beta$  inhibitors. The most active and selective inhibitors will be verified for their ability to act as neuroprotective drugs and improve AD treatment.

## 2.2 Nucleoside-based drugs resistance

### 2.2.1 Materials and Methods

#### 2.2.1.1 Development of resistant cancer cell lines

CCRF-CEM and K562 cell lines were purchased from ATCC and cultivated in RPMI (CCRF-CEM) and Icove's media (K562) containing 10 % heat-inactivated fetal bovine serum, penicillin, streptomycin. Cells were incubated at 37°C and 5 % CO<sub>2</sub>. The selection of resistant clones was made by incubation in the presence of the drug (cytarabine, 6-thioguanine, and fludarabine, respectively), whereas the drug concentration was slowly increased depending on cell viability (Tab. 1). Drug concentration was increased when cellular viability was higher than 90 %. Cytarabine, 6-thioguanine, and fludarabine were purchased from Merck.

**Table 1.** Scheme for the selection of resistant clones.

Cell line	The final concentration of the drug in the culture media [μM]												
	Cycles of selection												
	1	2	3	4	5	6	7	8	9	10	11	12	13
CCRF-CEM: cytarabine selection	2	4	6	8	10	12	14	16	20	24	28	32	41
CCRF-CEM: 6-thioguanine selection	0.5	2	4	8	10	12	14	16	20	24	28	32	36
CCRF-CEM: fludarabine selection	2	4	6	8	10	12	14	16	20	24	28	32	36
K562: cytarabine selection	2	4	6	8	10	12	14	16	20	24	28	32	41
K562: 6-thioguanine selection	0.5	2	4	8	10	12	14	16	20	24	28	32	36
K562: fludarabine selection	6	8	10	12	24	36	40	50	60	70	80	90	100

After 13 cycles of increasing drug concentration (Tab. 1), the degree of drug resistance was analyzed by the MTS cytotoxicity test. Results were compared to the control (parental cells CCRF-CEM or K562 without treatment). Data were processed by Dotmatics software.

#### 2.2.1.2 MTS cytotoxicity assay

MTS cytotoxicity test was performed using a 384well plate (Corning). Each well was applied 30 μl of cellular suspension, except background control (30 μl media without cells). Cells were diluted and seeded (MultiDrop Combi, Thermo Fisher Scientific) according to the particular cell type at concentrations of 500 to 4000 cells/ well, incubated for 24 hours at 37°C

in a 5% CO<sub>2</sub> atmosphere, and then treated by drugs (Echo 550, Labcyte) for 72 hours. Compounds were tested in four replicates and nine concentration spots. The concentration range tested was 0,78 μM to 200 μM (2-times dilution) for fludarabine-treated K562 cell lines and 0,76 nM to 50 μM (4-times dilution) for the other cases. MTS (Promega) was added after 72 hours of incubation with drugs. Viability was assessed based on the color change of the MTS reagent and measured spectrophotometrically at 490 nm wavelength (Envision) after 1-4 hours. IC<sub>50</sub> was calculated by Dotmatics software.

### **2.2.1.3 Expression of membrane transporters**

Expression of membrane transporters (MDR proteins, ENTs, CNTs) was done by RNA extraction (phenol-chloroform extraction), reverse transcription, and real-time PCR (polymerase chain reaction). The quantity and purity of isolated RNA were evaluated spectrophotometrically by Spectrophotometer ND-1000 (NanoDrop). Total isolated RNA was used for the preparation of cDNA using a Peltier Thermal Cycler (PTC-100, MJ Research). The reaction mixture contained 3 μg of isolated RNA, 0.3 μg of hexamers, water, and a master mix (reverse transcriptase buffer, dNTP, RNasin) with a total reaction volume of 30 μl. The reaction was incubated for 60 minutes at 42°C and then 10 minutes at 70°C.

TaqMan Gene Expression Assay kits (Thermo Fisher Scientific) were used for real-time PCR for each transporter (Pgp, BCRP, MRP1-6, ENT1-4, CNT1-3). Real-time PCR was done using a Cobas cycler and 96well plates (ThermoFisher Scientific) with a reaction volume of 10 μl. Reaction consisted of 1 μl of cDNA and 9 μl of master mix (LightCycler 480 Probes Master), including 1x TaqMan Gene Expression assay solution. The number of cycles was set to 50, and the results were normalized to GAPDH (glyceraldehyde-3-phosphate dehydrogenase). DEPC water was used as a negative control.

### **2.2.1.4 Expression of proteins involved in the nucleoside metabolism**

Protein expression in nucleoside metabolism was evaluated by protein isolation (RIPA buffer treated with protease and phosphatase inhibitors), electrophoresis, and western blotting analysis. Electrophoresis was done using TGX Stain-Free FastCast Acrylamide kits 7,5 and 12% (BioRad). Voltage was set to 80 V, and separation took around 120 minutes. Multicolor Broad Range Protein Ladder (Thermo Fisher Scientific) was used as a molecular weight marker.

Western blotting was done using semi-dry transfer into nitrocellulose membrane (BioRad). Membranes were blocked by 5% BSA in TBST buffer for 60 minutes and then incubated with primary antibody overnight at 4°C in the dark. Primary antibodies were purchased from CellSignaling () and Thermo Fisher Scientific (). Membranes were washed three times for 6 minutes using TBST buffer and then incubated with secondary antibodies (Thermo

Fisher Scientific) for 90 minutes at room temperature. Unbound secondary antibody was washed out using TBST buffer (washing three times for 6 minutes), and HRP substrate (Millipore) was used for visualization done by BioRad ChemiDoc Imaging System. Results were normalized to beta actin, which was used as a protein loading control.

## 2.2.2 Results

### 2.2.2.1 Development of resistant cancer cell lines

Human leukemia cell lines (CCRF-CEM and K562) were used for the selection of cell lines resistant to nucleoside-based drugs. This part follows the rigorous thesis (L. Hrubá, 2023) in which the selection of resistant clones and their basic characterization were made. Compared to this work, we continued in the selection using higher concentrations of drugs (Tab. 1), while the resulting phenotype was similar to the previous case (Tab. 2 and 3). The level of resistance was verified using the MTS test and evaluated using Dotmatics software.

Cytarabine selection led to the development of cross-resistance between cytarabine, gemcitabine, and fludarabine in both the CCRF-CEM and the K562 cell line. Fludarabine selection was more successful in the CCRF-CEM cell line, which is naturally more sensitive to this drug than K562. The selection of CCRF-CEM cells by fludarabine led to cross-resistance development among fludarabine, cytarabine, and gemcitabine, which is similar to the case of cytarabine selection. The K562 cell line selected by fludarabine did not develop such a strong resistance as the CCRF-CEM cell line. We detected a slight increase in resistance to fludarabine, cytarabine, 6-mercaptopurine, and paclitaxel. Selection by 6-thioguanine developed cross-resistance between 6-thioguanine and 6-mercaptopurine, which are structurally very similar compounds, and this resistant phenotype occurred in the CCRF-CEM and K562 cell lines.

**Table 2.** Cytotoxicity of selected nucleoside-based drugs to CCRF-CEM cell line and its derived resistant clones. Data are mean (n= 4) and sd (standard deviation). Increase/ decrease of resistance is compared to control cells without selection. Data were processed, and IC<sub>50</sub> values were calculated using Dotmatics software.

Compound	CCRF-CEM		CCRF-CEM: cytarabine selection			CCRF-CEM: 6-thioguanine selection			CCRF-CEM: fludarabine selection		
	Mean IC <sub>50</sub> [μM]	sd	Mean IC <sub>50</sub> [μM]	sd	x-fold	Mean IC <sub>50</sub> [μM]	sd	x-fold	Mean IC <sub>50</sub> [μM]	sd	x-fold
6-thioguanine	0.97	0.042	0.36	0.059	0.37	> 50	0	> 51.29	0.56	0.065	0.58
6-mercaptopurine	9.47	0.57	2.13	0.44	0.23	> 50	0	> 5.28	1.57	0.20	0.16
Cytarabine	0.023	0.0037	> 50	0	> 2155.17	0.013	0.0019	0.54	0.43	0.060	18.52
Gemcitabine	0.020	0.0023	17.17	2.72	876.97	0.0096	0.0021	0.49	0.15	0.017	7.87
Fludarabine	2.76	0.13	> 50	0	> 18.14	2.09	0.13	0.76	> 50	0	> 18.14
5-fluorouracil	12.83	2.08	11.56	1.44	0.90	5.92	1.08	0.46	9.50	1.38	0.74
Roscovitine	19.26	0.27	16.39	0.68	0.85	7.38	0.53	0.38	12.11	0.19	0.63
Daunorubicine	0.0077	0.00051	0.0080	0.0013	1.04	0.014	0.0011	1.83	0.020	0.0017	2.57
Paclitaxel	0.0014	0.00017	0.0011	0.00017	0.77	0.0018	0.00043	1.28	0.0018	0.000071	1.23

> 50	> 10	> 2
Resistance increased (x-fold)		

**Table 3.** Cytotoxicity of selected nucleoside-based drugs to K562 cell line and its derived resistant clones. Data are mean (n= 4) and sd (standard deviation). Increase/ decrease of resistance is compared to control cells without selection. Data were processed, and IC<sub>50</sub> values were calculated using Dotmatics software.

Compound	K562		K562: cytarabine selection			K562: 6-thioguanine selection			K562: fludarabine selection		
	Mean IC <sub>50</sub> [μM]	sd	Mean IC <sub>50</sub> [μM]	sd	x-fold	Mean IC <sub>50</sub> [μM]	sd	x-fold	Mean IC <sub>50</sub> [μM]	sd	x-fold
6-thioguanine	0.67	0.076	0.59	0.061	0.88	> 50	0	> 74.57	0.94	0.13	1.40
6-mercaptopurine	0.54	0.14	0.52	0.077	0.96	> 50	0	> 92.86	1.26	0.090	2.34
Cytarabine	0.17	0.034	> 50	0	> 291.89	0.18	0.024	1.05	0.81	0.14	4.72
Gemcitabine	0.078	0.029	> 50	0	> 640.20	0.033	0.0036	0.43	0.11	0.016	1.43
Fludarabine	36.63	2.97	147.72	8.96	4.03	19.88	2.58	0.54	100.30	3.77	2.74
5-fluorouracil	10.62	0.87	8.25	1.20	0.78	5.69	1.21	0.54	6.19	0.75	0.58
Roscovitine	49.73	0.54	33.31	5.78	0.67	19.01	0.94	0.38	21.96	2.50	0.44
Daunorubicine	0.022	0.0034	0.043	0.0019	1.96	0.031	0.0023	1.39	0.034	0.0050	1.55
Paclitaxel	0.0012	0.00014	0.0012	0.000058	0.96	0.0019	0.00057	1.58	0.011	0.0013	9.02

> 50	> 10	> 2
Resistance increased (x-fold)		

### 2.2.2.2 Resistant cellular models in the screening of new drugs

Our developed resistant cell lines were used to screen new compounds to overcome nucleoside-based drug resistance. Eight compounds synthesized in the Institute of Organic Chemistry and Biochemistry (IOCB) of the CAS were tested. (Tab. 4 and 5) We identified five compounds (LEM 10888, 10889, 10892, 11465, and 12791), which were able to overcome cytarabine, gemcitabine, fludarabine, 6-thioguanine and 6-mercaptopurine resistance in K562 cells and two compounds (LEM 11465 and 13267), which were active in all resistant CCRF-CEM cell lines. LEM 11465 overcame all developed resistant phenotypes and can be an interesting structure for another analysis.

**Table 4.** Screening of new potential anticancer drugs synthesized in IOCB Prague using K562 cross-resistant cell lines. The results are mean (n = 4) and standard deviation (sd). Increase/ decrease of resistance is compared to control cells without selection. Data were processed, and IC<sub>50</sub> values were calculated using Dotmatics software.

LEM code	K562		K562: cytarabine selection			K562: 6-thioguanine selection			K562: fludarabine selection		
	Mean IC <sub>50</sub> [μM]	sd	Mean IC <sub>50</sub> [μM]	sd	x-fold	Mean IC <sub>50</sub> [μM]	sd	x-fold	Mean IC <sub>50</sub> [μM]	sd	x-fold
10870	33.26	1.91	> 50	0	> 1.50	> 50	0	> 1.50	> 50	0	> 1.50
10873	30.64	3.04	> 50	0	> 1.63	> 50	0	> 1.63	> 50	0	> 1.63
10888	10.07	1.91	0.44	0.40	0.044	1.08	0.12	0.11	1.01	0.11	0.10
10889	0.99	0.11	0.17	0.020	0.17	0.46	0.030	0.46	0.49	0.010	0.49
10892	0.27	0.015	0.050	0.010	0.19	0.11	0.020	0.41	0.10	0.020	0.37
11465	0.88	0.15	0.23	0.17	0.26	0.82	0.060	0.93	0.88	0.20	1.00
12791	1.53	0.22	0.16	0.0020	0.10	0.50	0.050	0.33	0.53	0.050	0.35
13267	18.87	2.98	15.97	2.00	0.85	44.02	12.99	2.33	31.46	2.83	1.67

> 50	> 10	> 2
Resistance increased (x-fold)		



**Table 5.** Screening of new potential anticancer drugs synthesized in IOCB Prague using CCRF-CEM cross-resistant cell lines. The results are mean (n = 4) and standard deviation (sd). Increase/ decrease of resistance is compared to control cells without selection. Data were processed, and IC<sub>50</sub> values were calculated using Dotmatics software.

LEM code	CCRF-CEM		CCRF-CEM: cytarabine selection			CCRF-CEM: 6-thioguanine selection			CCRF-CEM: fludarabine selection		
	Mean IC <sub>50</sub> [μM]	sd	Mean IC <sub>50</sub> [μM]	sd	x-fold	Mean IC <sub>50</sub> [μM]	sd	x-fold	Mean IC <sub>50</sub> [μM]	sd	x-fold
10870	4.76	0.93	30.28	3.10	6.36	34.22	5.36	7.19	> 50	1.58	> 10.50
10873	0.57	0.084	8.59	0.35	15.07	0.29	0.010	0.51	1.30	0.010	2.28
10888	0.79	0.25	1.41	0.71	1.78	0.63	0.070	0.80	> 50	0	> 63.29
10889	0.56	0.099	10.18	0.51	18.18	0.40	0.020	0.71	1.28	0.19	2.29
10892	0.27	0.087	13.56	0.23	50.22	0.12	0.010	0.44	1.11	0.14	4.11
11465	0.70	0.19	1.07	0.10	1.53	0.42	0.010	0.60	1.12	0.060	1.60
12791	0.40	0.065	0.25	0.02	0.63	0.20	0.010	0.50	0.86	0.19	2.15
13267	7.38	1.80	6.53	0.61	0.88	7.53	1.00	1.02	6.61	2.80	0.90

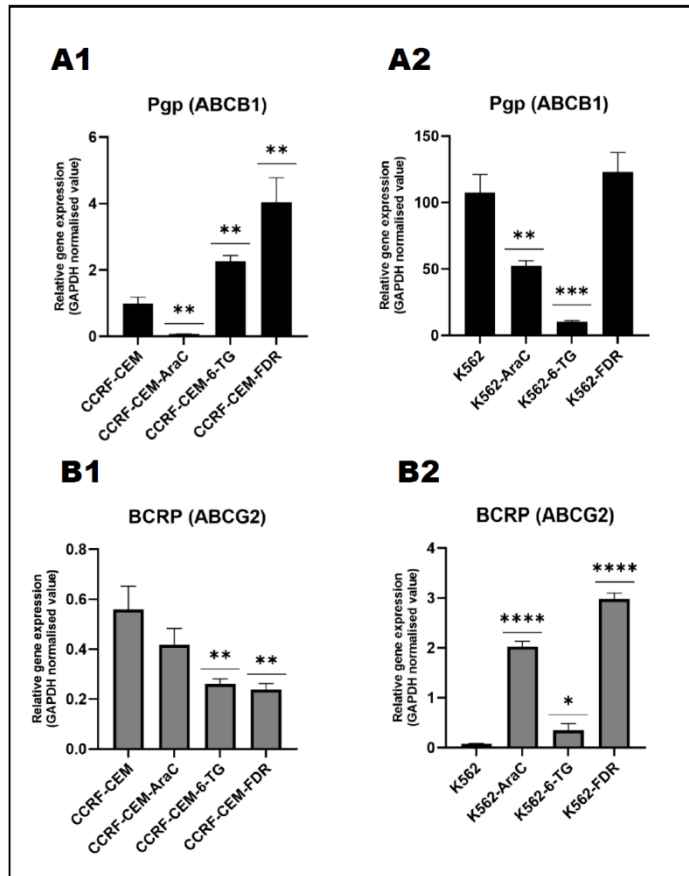
> 50	> 10	> 2
Resistance increased (x-fold)		

### 2.2.2.3 Expression of MDR proteins

To evaluate the involvement of MDR proteins in rising drug resistance, we analyzed expression levels of Pgp (Fig. 13A1, 2), BCRP (Fig. 13B1, 2), and MRP proteins (Fig. 14), the most common proteins connected with multidrug resistance. Expression was analyzed on mRNA levels using RNA isolation, reverse transcription, and real-time PCR detection. Results were done in three replicates and normalized to GAPDH (glyceraldehyde-3-phosphate dehydrogenase).

Pgp levels in non-treated control cells K562 were much higher compared to the CCRF-CEM cell line, and expression profile after treatment differed between these two cell lines. K562 cells selected by cytarabine and 6-thioguanine showed decreased Pgp expression, while fludarabine selection did not affect the Pgp expression. In the CCRF-CEM cell line, cytarabine selection led to the same phenotype, a decrease of Pgp expression, but in the case of 6-thioguanine and fludarabine selection, there was an increase in its expression levels. (Fig. 13A1, A2).

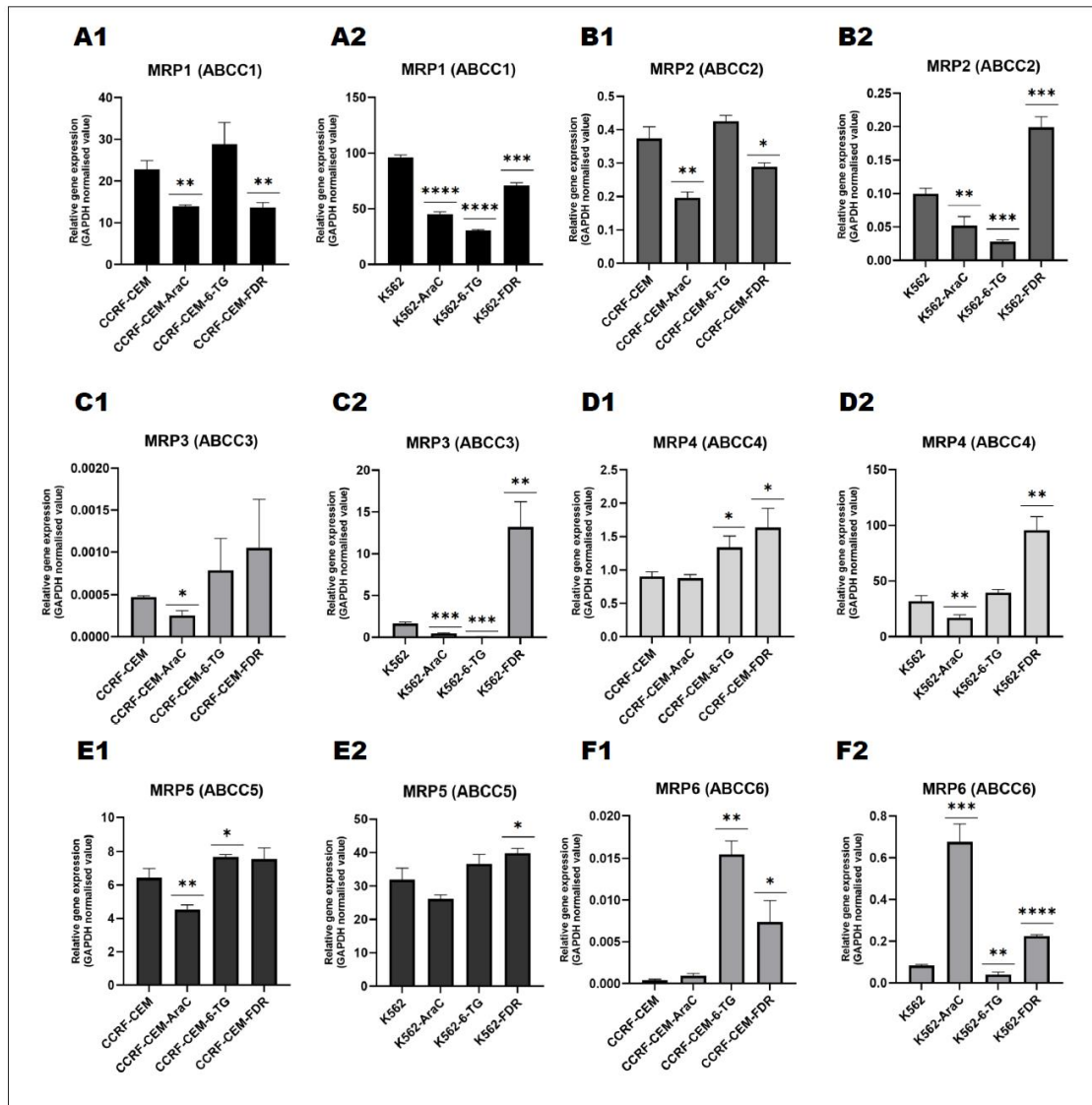
The expression profile was also different in the case of protein BCRP. There was almost no difference after cytarabine selection, but selection by 6-thioguanine and fludarabine decreased BCRP levels. Compared to this, the selection of K562 cells led to increased BCRP expression in all three cases, most prominently in the case of cytarabine and fludarabine selection. (Fig. 13B1, B2)



**Figure 13.** Expression of P-glycoprotein (Pgp) (A1) and breast cancer resistance protein (BCRP) (B1) in CCRF-CEM cell line and its derived resistant clones, and Pgp (A2) and BCRP (B2) K562 cell line and its derived resistant clones. The data are mean ( $n=3$ )  $\pm$  sd and normalized to GAPDH. Statistical analysis was performed with an unpaired t-test: selected cell lines were compared to the parental line (CCRF-CEM or K562) at  $p < 0.05$  using the GraphPad Prism 9.5.1 software program. We represent the level of statistical significance in this figure as follows: \*\*\*\* p-value  $< 0.0001$ , \*\*\* p-value  $< 0.001$ , \*\* p-value  $< 0.01$ , \* p-value  $< 0.05$ . For a p-value  $> 0.05$ , we consider the differences to be not significant (ns).

MRP expression was tested for isoforms 1-6, and there were differences between cell line CCRF-CEM and K562. MRP1 expression was decreased in all selected cell lines, except CCRF-CEM selected by 6-thioguanine, where the expression level was similar to the control cell line. (Fig. 14A1, A2) MRP2 expression was increased only after selecting the K562 cell line with fludarabine. The rest showed decreased MRP2 levels, and CCRF-CEM selected by 6-thioguanine had a similar expression level of MRP2 as the control. (Fig. 14B1, B2) MRP3 levels were decreased in CCRF-CEM cells after cytarabine selection and K562 after cytarabine and 6-thioguanine selection. In contrast, selecting K562 cells with fludarabine led to a significant increase in MRP3 expression. (Fig. 14C1, C2) Expression of MRP4 was decreased after 6-thioguanine selection of CCRF-CEM cells and by fludarabine selection in both CCRF-CEM and K562 cells. Cytarabine selection of K562 led to a decrease in MRP4 expression. (Fig. 14D1, D2) Levels of MRP5 protein expression were quite similar in all tested cell lines, except CCRF-CEM selected by cytarabine, which showed a slight decrease in expression of this protein, and in K562 selected by fludarabine, where the MRP5 expression was quite a higher compared to

control. (Fig. 14E1, E2) There was a big difference between MRP6 levels after cytarabine selection. In the CCRF-CEM cell line, cytarabine selection didn't affect MRP6 expression, but K562 cells selected by cytarabine expressed significantly more MRP6 than the control cell line. An increase in the MRP6 levels was also detected after fludarabine selection; this was similar in CCRF-CEM and K562 cells. 6-thioguanine selection led to a strong increase in MRP6 expression in CCRF-CEM, but the same selection led to an MRP6 decrease in the K562 cell line. (Fig. 14F1, F2).

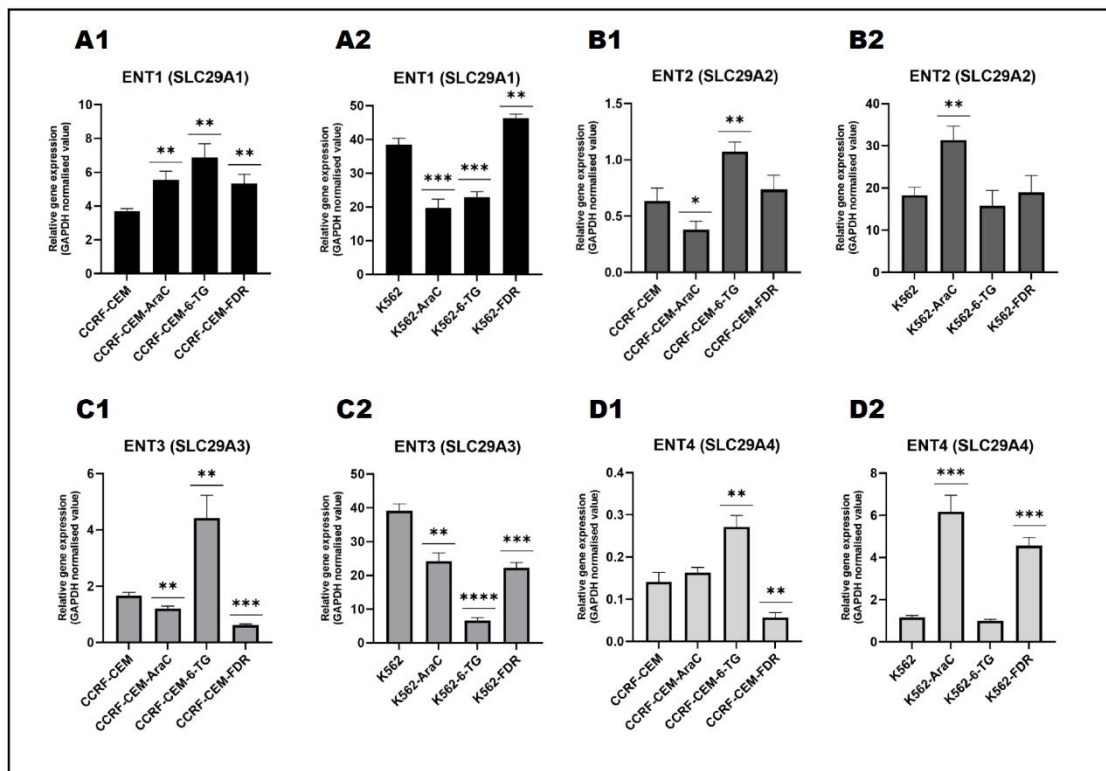


**Figure 14.** Expression of multidrug resistance-associated proteins (MRPs) in the CCRF-CEM cell line and its derived resistant clones (A1, B1, C1, D1, E1, F1), and K562 cell line and its derived resistant clones (A2, B2, C2, D2, E2, F2). The data are mean (n= 3)  $\pm$  sd and normalized to GAPDH. Statistical analysis was performed with an unpaired t-test: selected cell lines were compared to the parental line (CCRF-CEM or K562) at  $p < 0.05$  using the GraphPad Prism 9.5.1 software program. We represent the level of statistical significance in this figure as follows: \*\*\*\* p-value < 0.0001, \*\*\* p-value < 0.001, \*\* p-value < 0.01, \* p-value < 0.05. For a p-value > 0.05, we consider the differences to be not significant (ns).

### 2.2.2.4 Expression of nucleoside transporters (ENTs, CNTs)

The transport of nucleoside-based drugs across the cellular membrane is mediated mainly by the nucleoside transporters, which are divided into two groups: a) ENTs (SLC29s) and b) CNTs (SLC28s). We analyzed the expression of all ENT and CNT isoforms using RNA isolation, reverse transcription, and real-time PCR. Results were done in the three replicates and normalized to GAPDH.

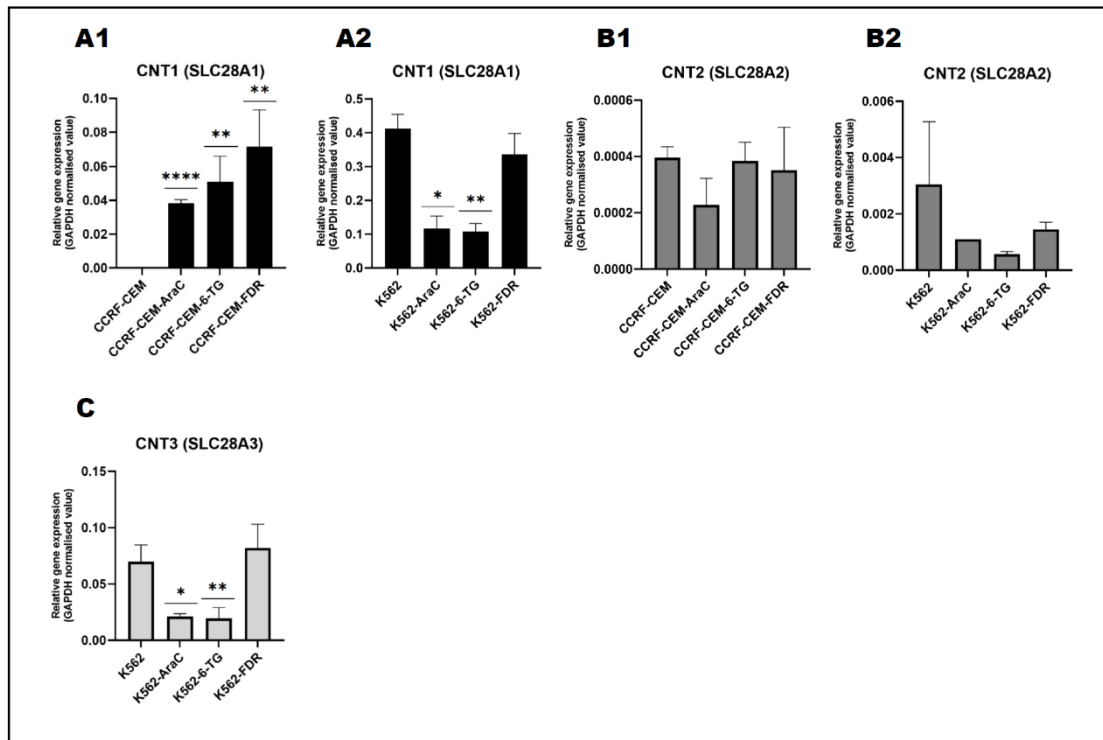
Selection of CCRF-CEM cells by cytarabine, 6-thioguanine, and fludarabine led to an increase in the ENT1 expression. (Fig. 15A1) Compared to the K562 cells, where only fludarabine selection caused an increase in the ENT1 expression. Cytarabine and 6-thioguanine selection led to a decrease in ENT1 levels. (Fig. 15A2). ENT2 expression was mainly affected by cytarabine and 6-thioguanine selection. There was a decrease of ENT2 in CCRF-CEM cells, an increase in its expression in K562 after cytarabine selection, and a significant rise in ENT2 expression in CCRF-CEM cells after 6-thioguanine selection. (Fig. 15B1, B2) ENT3 expression levels were decreased in all cases, mostly in K562 cells selected by 6-thioguanine. (Fig. 15C3) Only the 6-thioguanine selection of the CCRF-CEM cell line led to a significant increase in ENT3 expression. (Fig. 15C1) ENT4 expression was increased after the 6-thioguanine selection of the CCRF-CEM cell line (Fig. 15D1) and after the cytarabine and fludarabine selection of K562 cells. (Fig. 15D2) The other selections didn't affect the levels of ENT4.



**Figure 15.** Expression of equilibrative nucleoside transporters (ENT/ SLC29) proteins in CCRF-CEM cell line and its derived resistant clones (A1, B1, C1, D1), and K562 cell line and its derived resistant clones

(A2, B2, C2, D). The data are mean ( $n=3$ )  $\pm$  sd and normalized to GAPDH. Statistical analysis was performed with an unpaired t-test: selected cell lines were compared to the parental line (CCRF-CEM or K562) at  $p < 0,05$  using the GraphPad Prism 9.5.1 software program. We represent the level of statistical significance in this figure as follows: \*\*\*\* p-value  $< 0.0001$ , \*\*\* p-value  $< 0.001$ , \*\* p-value  $< 0.01$ , \* p-value  $< 0.05$ . For a p-value  $> 0.05$ , we consider the differences to be not significant (ns).

The selection of CCRF-CEM with all three tested compounds (cytarabine, fludarabine, and 6-thioguanine) caused an increase in CNT1 expression. (Fig. 16A1) In contrast to cytarabine and 6-thioguanine selection in the K562 cell line, the treatment caused a decrease in CNT1 levels. Fludarabine selection of K562 didn't affect CNT1 expression. (Fig. 16A2) CCRF-CEM-resistant cell lines showed no significant difference in CNT2 expression compared to the control (Fig. 16B1) as well as the K562-resistant cells. (Fig. 16B2) CNT3 expression was decreased in K562 cells after selection with cytarabine and 6-thioguanine. Fludarabine selection didn't lead to a change in the CNT3 expression. (Fig. 16C) CNT3 was not expressed in the CCRF-CEM cell line.

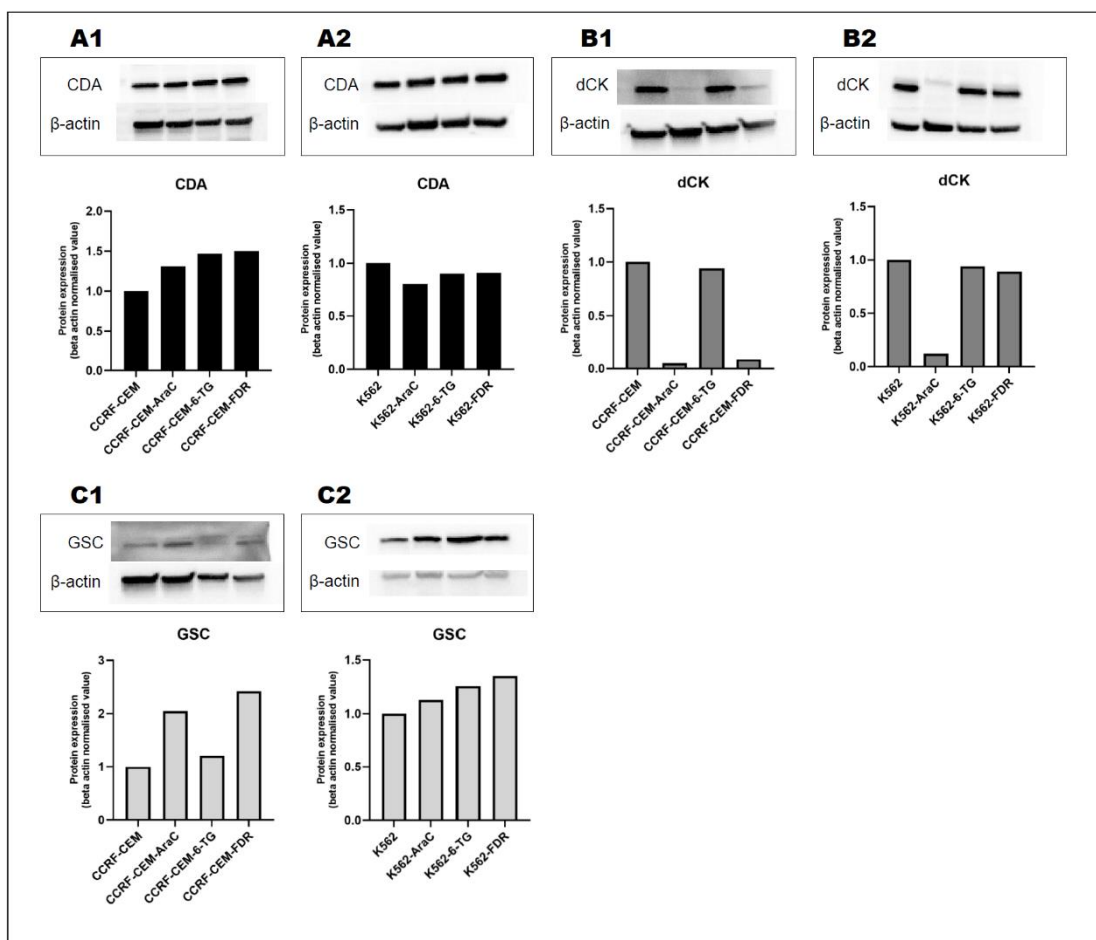


**Figure 16.** Expression of concentrative nucleoside transporters (CNT/ SLC28) proteins in CCRF-CEM cell line and its derived resistant clones (A1, B1), and K562 cell line and its derived resistant clones (A2, B2, C). CNT3 transporter was not expressed in the CCRF-CEM cell line. The data are mean ( $n=3$ )  $\pm$  sd and normalized to GAPDH. Statistical analysis was performed with an unpaired t-test: selected cell lines were compared to the parental line (CCRF-CEM or K562) at  $p < 0,05$  using the GraphPad Prism 9.5.1 software program. We represent the level of statistical significance in this figure as follows: \*\*\*\* p-value  $< 0.0001$ , \*\*\* p-value  $< 0.001$ , \*\* p-value  $< 0.01$ , \* p-value  $< 0.05$ . For a p-value  $> 0.05$ , we consider the differences to be not significant (ns).

#### **2.2.2.5 Expression of proteins involved in nucleosides metabolism**

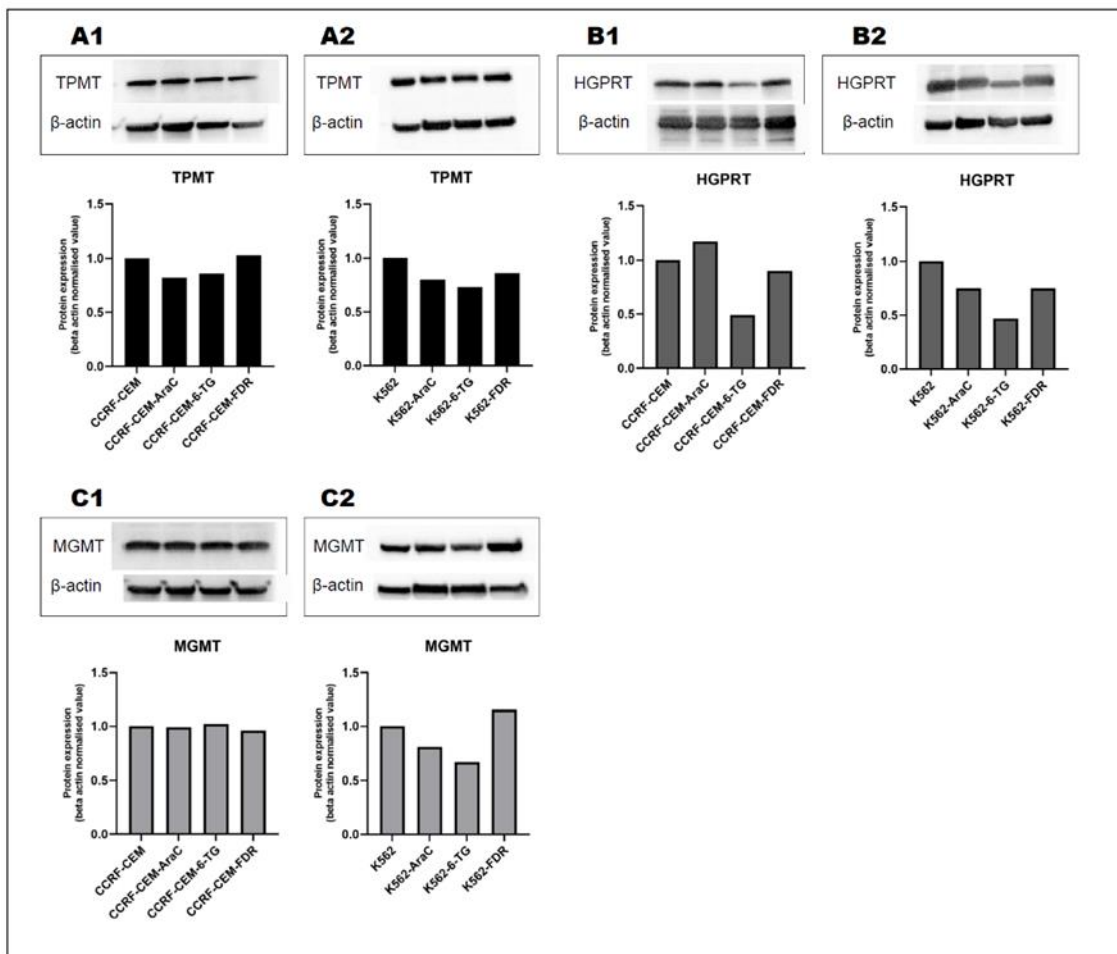
To evaluate the background of developed drug resistance, we analyzed the expression of proteins involved in their metabolism. They were mainly activating kinases or kinases, which mediate the elimination of these drugs. Analyses were done by western blotting, and results were normalized to beta-actin. In addition to enzymes involved in nucleoside metabolism, the mTOR pathway influencing protein synthesis was also tested.

In the first group of analyses, the expression of proteins involved in the metabolism of cytarabine and fludarabine was tested. CDA levels slightly increased after the cytarabine, 6-thioguanine, and fludarabine selection of the CCRF-CEM cell line. (Fig. 17A1) K562-resistant cells showed similar CDA expression as the control. (Fig. 17A2) dCK expression significantly decreased after the cytarabine and fludarabine selection of CCRF-CEM cells. (Fig. 17B1) Cytarabine selection also caused a decrease in the dCK expression in the K562 cells, but the selection with 6-thioguanine and fludarabine didn't affect the dCK expression. (Fig. 17B2) GSC protein expression was affected only after cytarabine and fludarabine selection of CCRF-CEM cells. The other cell lines had a similar expression as the controls. (Fig. 17C1, C2)



**Figure 17.** Expression of proteins involved in the activation/ elimination of cytarabine and fludarabine in CCRF-CEM cell line (A1, B1, C1), K562 (A2, B2, C2), and its derived resistant clones. Data were normalized to beta-actin and processed using GraphPad Prism 9.5.1 software program. CDA: cytidine deaminase, dCK: deoxycytidine kinase, GSC: glycosylceramide synthase.

Another set of analyses focused on the expression of the proteins involved in expressing 6-thioguanine and 6-mercaptopurine. TPMT levels were comparable among resistant cell lines and the controls. (Fig. 18A1, A2) HGPRT expression was decreased in all resistant K562 cell lines (Fig. 18B2) and in the case of 6-thioguanine and fludarabine-resistant CCRF-CEM cell lines. (Fig. 18B1) Cytarabine selection didn't affect the expression of HGPRT in CCRF-CEM cells. MGMT protein expression was similar to control in CCRF-CEM resistant cell lines. (Fig. 18C1) Cytarabine and 6-thioguanine selection caused a decrease in MGMT expression in K562 cells, but fludarabine caused a slight increase in this protein's expression. (Fig. 18C2)



**Figure 18.** Expression of proteins involved in the activation/ elimination of 6-thioguanine in CCRF-CEM cell line (A1, B1, C1), K562 (A2, B2, C2), and its derived resistant clones. Data were normalized to beta actin and processed using GraphPad Prism 9.5.1 software program. TPMT: thiopurine-S-methyltransferase, HGPRT: hypoxanthine-guanine phosphoribosyltransferase, MGMT: methylguanine-DNA methyltransferase.

mTOR pathway analysis included verification of the expression of mTOR protein and its phosphorylated form. (Fig. 19A1, A2, B1, B2) In the case of CCRF-CEM cell lines, mTOR expression was not significantly affected, and the levels were comparable to the control. K562-resistant cell lines showed increased levels of this protein. mTOR phosphorylation was shown as a conversion of mTOR protein into its phosphorylated form. This conversion was reduced in all resistant cell lines (CCRF-CEM and K562), except CCRF-CEM was selected with cytarabine. (Fig. 19B1, B2)

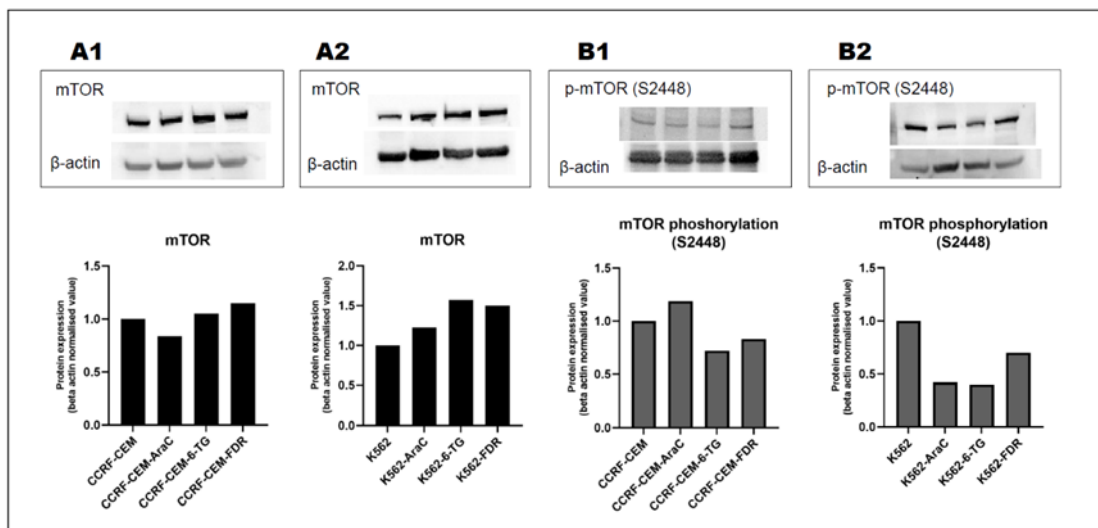
Other proteins analyzed as a part of the mTOR pathway were p70 S6 kinase and S6 protein and their phosphorylated forms. (Fig. 20 and 21) Expression of p70 S6 kinase was unified in all K562 cell lines. (Fig. 20A2) CCRF-CEM selected with fludarabine showed a decrease in the p70 S6 kinase expression. In contrast, the other resistant cells showed an increase in its expression. (Fig. 20A1) Phosphorylation of p70 S6 kinase was analyzed in two



phosphorylated sites: T421/S424 and S371. Phosphorylation was analyzed as a conversion of p70 S6 kinase into its phosphorylated form. There was a conversion of T421/S424 phosphorylation of p70 S6 kinase in all resistant cell lines, except for CCRF-CEM cells selected by fludarabine. (Fig. 20B1, B2) S371 phosphorylation of p70 S6 kinase was not significantly affected, except for CCRF-CEM selected with fludarabine, which had an increase in this phosphorylation (Fig. 20C1) and K562 also selected by fludarabine, but with a different result. In this case, we detected a reduction of the S371 phosphorylation. (Fig. 20C2)

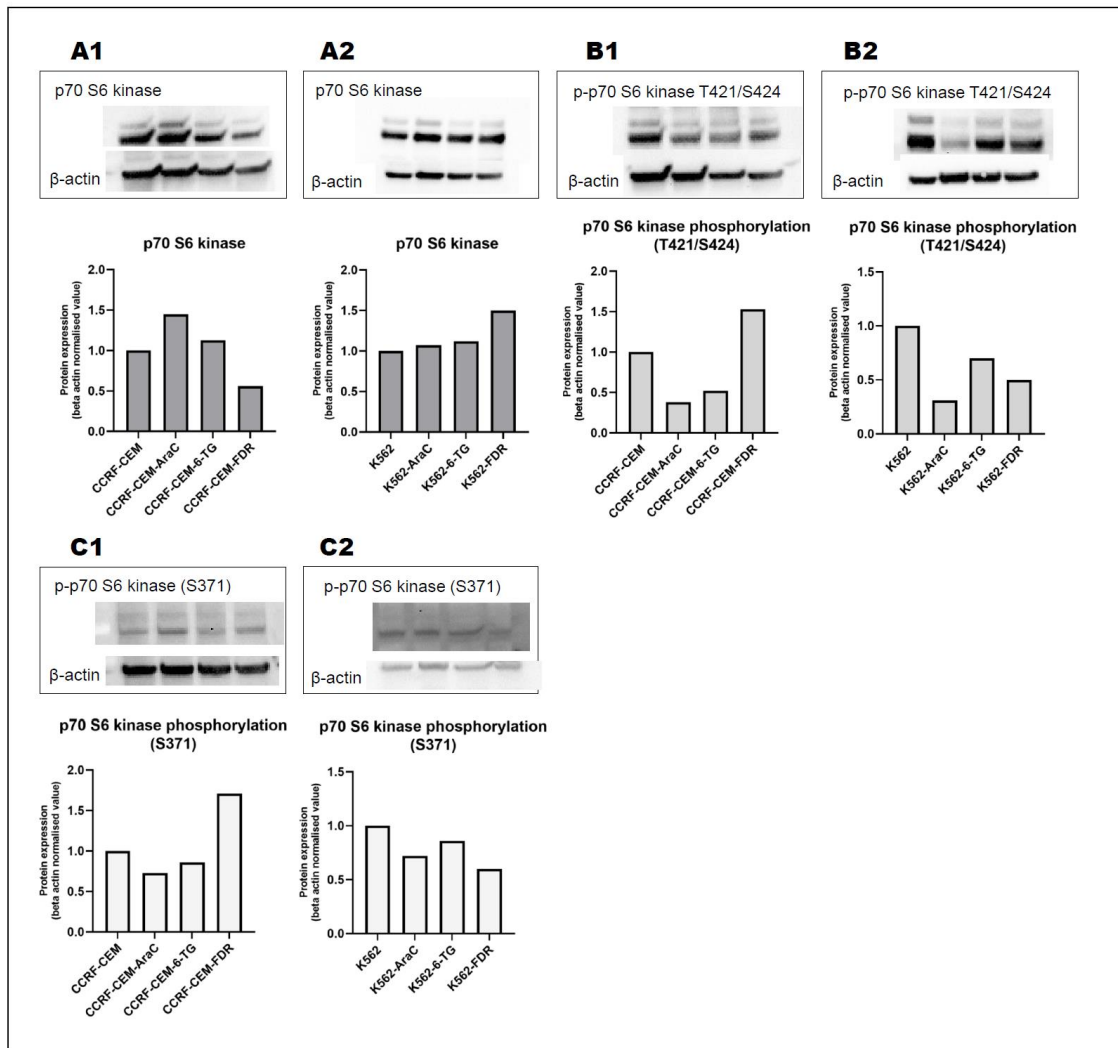
Levels of S6 ribosomal proteins were uniform in all CCRF-CEM cell lines (Fig. 21A1), and all selected K562 had decreased expression of this protein compared to the controls. (Fig. 21A2) Phosphorylation of S6 ribosomal protein was analyzed in the S235/236, S240/244, and 244/247 phosphorylation sites. There was no S235/236 phosphorylation in all CCRF-CEM resistant cell lines (Fig. 21B1), and these cells also had a substantial decrease in the S244/247 phosphorylation. (Fig. 21D1) Phosphorylation of S240/244 was more robust than the previous two phosphorylations, but there was still a decrease compared to the control cells. (Fig. 21C1)

The most significant decrease of S6 ribosomal protein phosphorylation in the K562 cells was S235/236 phosphorylation after selection with cytarabine. (Fig. 21B2) This phosphorylation was also decreased after the 6-thioguanine and fludarabine. There was also a decrease in the S244/247 phosphorylation in the K562-resistant cells (Fig. 21D2), but not as strong as in the CCRF-CEM cells. S240/S244 phosphorylation was not affected by cytarabine selection in K562 cells and increased after 6-thioguanine and fludarabine selection of these cells. (Fig. 21C2)

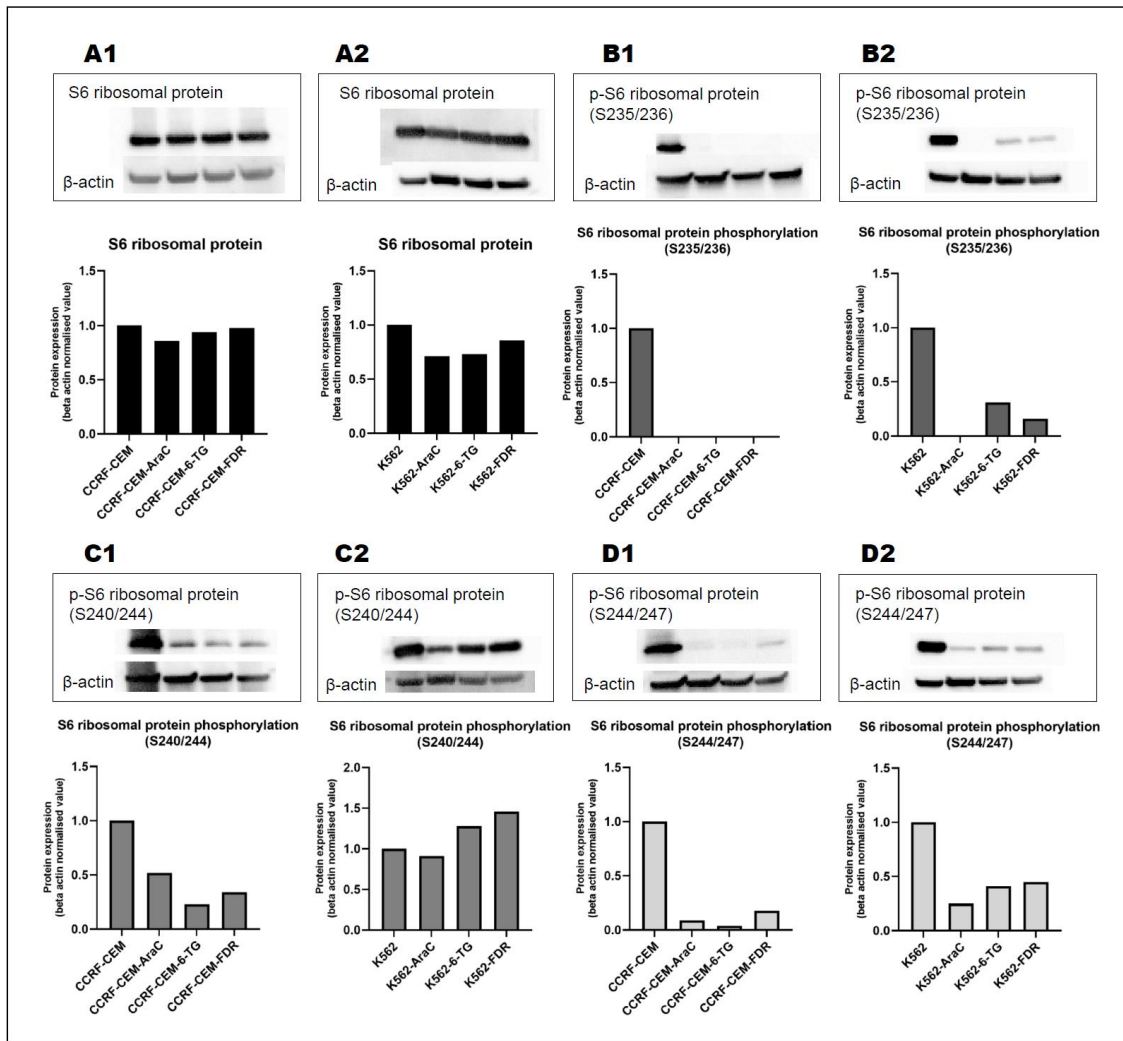


**Figure 19.** Expression of mTOR protein (CCRF-CEM and its derived resistant cell lines: A1; K562 and its derived resistant cell lines: A2) and its phosphorylated form, p-mTOR S448 (CCRF-CEM and its derived resistant cell lines: B1; K562 and its derived resistant cell lines: B2). mTOR phosphorylation was

expressed as a ratio of conversion of mTOR protein into its phosphorylated form. Data were normalized to beta actin and processed using GraphPad Prism 9.5.1 software program.



**Figure 20.** Expression of p70 S6 kinase (CCRF-CEM and its derived resistant cell lines: A1; K562 and its derived resistant cell lines: A2) and its phosphorylated form, p-p70 S6 kinase T421/S424 and S371 (CCRF-CEM and its derived resistant cell lines: B1, C1; K562 and its derived resistant cell lines: B2, C2). p70 S6 kinase phosphorylation was expressed as a ratio of conversion of p70 S6 kinase into its phosphorylated form. Data were normalized to beta actin and processed using GraphPad Prism 9.5.1 software program.



**Figure 21.** Expression of S6 ribosomal protein (CCRF-CEM and its derived resistant cell lines: A1; K562 and its derived resistant cell lines: A2) and its phosphorylated form, p-S6 ribosomal protein S235/236, S240/244 and S244/247 (CCRF-CEM and its derived resistant cell lines: B1, C1, D1; K562 and its derived resistant cell lines: B2, C2, D2). S6 ribosomal protein phosphorylation was expressed as a ratio of conversion of S6 ribosomal protein into its phosphorylated form. Data were normalized to beta actin and processed using GraphPad Prism 9.5.1 software program.

### 2.2.3 Discussion

In the first part of this thesis, resistant leukemia cell lines have been successfully developed. Cytarabine selection led to the development of similar cross-resistant phenotypes among cytarabine, gemcitabine, and fludarabine in the CCRF-CEM and K562 cell lines. Fludarabine selection of the CCRF-CEM cell line increased resistance to fludarabine, cytarabine, and gemcitabine, which is similar to cytarabine selection. There was also a slight increase in resistance to daunorubicin. In contrast, the K562 cell line, which is naturally less sensitive to fludarabine than CCRF-CEM cells, did not show such a significant development of resistance. We observed only a slight increase in resistance among fludarabine, 6-mercaptopurine, cytarabine, and paclitaxel.

Also, 6-thioguanine selection resulted in a similar resistant profile in both cell lines, cross-resistance between 6-thioguanine and 6-mercaptopurine.

Cellular models of drug resistance can be useful tools in the identification of effective treatment using known drugs for the new application. Drug repurposing is a method that can significantly shorten the time needed to apply drugs into clinical practice compared to finding completely new structures.<sup>302</sup> Known drugs, which have been clinically used for years, have proven safety, specified dosage that is not toxic, verified possible side effects, etc., and their approval for a new application is much faster. Identifying drugs that can overcome cancer drug resistance may be an important step to improving anticancer treatment and a possible way to increase the number of patients who achieve complete clinical remission.

We screened eight clinically used drugs and one experimental compound (roscovitine) for their ability to overcome developed drug resistance in CCRF-CEM and K562 cell lines. Fludarabine, cytarabine, and gemcitabine cross-resistance were overcome by 6-thioguanine, 6-mercaptopurine, 5-fluorouracil and paclitaxel in the CCRF-CEM cell line. Suggesting possible application of these compounds in the treatment of acute lymphoblastic leukemia insensitive to fludarabine, cytarabine, and gemcitabine.

6-thioguanine, 5-fluorouracil, and daunorubicin overcame cytarabine, gemcitabine, and fludarabine cross-resistance in the K562 cell line. These drugs can be potentially applied in treating acute myeloid leukemia cells non-responding to cytarabine, fludarabine or gemcitabine treatment.

5-thioguanine and 6-mercaptopurine cross-resistance was overcome by all tested compounds (cytarabine, gemcitabine, fludarabine, 5-fluorouracil, roscovitine, daunorubicin, and paclitaxel) in both cell lines.

Our developed resistant cell lines were also used in the screenings of new compounds synthesized by the Institute of Organic Chemistry and Biochemistry of the CAS. We identified five compounds (LEM 10888, 10889, 10892, 11465, and 12791) that were able to overcome all resistant phenotypes (resistance to cytarabine, gemcitabine, fludarabine, gemcitabine, 6-thioguanine, and 6-mercaptopurine) in K562 cell lines, and two compounds, LEM 11465 and 13267, were able to overcome drug resistance also in the resistant CCRF-CEM cell lines. Identifying these compounds can bring information about highly active chemical structures (most of these compounds were more active in the resistant cell lines than the control) in the resistant cancer cells. These compounds can potentially become new anticancer drugs or start structures in synthesizing new highly active compounds.

### **2.2.3.1 Cytarabine, gemcitabine, fludarabine cross-resistance**

To explain the emergence of the observed cross-resistance among cytarabine, gemcitabine, and fludarabine, we verified the level of expression of membrane transporters (ENTs, CNTs, ABC transporters), as well as enzymes involved in the metabolism of these drugs.

Cellular uptake of cytarabine, gemcitabine, and fludarabine is mediated mainly via ENT1, 2, and CNT1. There was a significant decrease in ENT1 expression in K562 cells selected by cytarabine. These cells also showed decreased expression of ENT2 and CNT1, which may contribute to the development of the observed resistant phenotype. Interestingly, CCRF-CEM cells selected by cytarabine had increased ENT1 and CNT1 levels. There was only a decrease in the ENT2 expression. CCRF-CEM cells selected by fludarabine had similar or higher expression of ENT1, 2, and CNT1 expression compared to control. Suggesting that the observed resistance of CCRF-CEM cells is not associated with the nucleoside transporters' expression level.

Efflux of cytarabine is mediated via MRP4, 5, fludarabine via BCRP, and gemcitabine via BCRP, MRP1, and 5. K562-cells selected by cytarabine showed a significant decrease of MRP1, MRP4, and BCRP, leading to more intensive efflux of cytarabine, gemcitabine, and fludarabine and decreased intracellularly of active metabolites. CCRF-CEM cells selected by cytarabine and fludarabine had decreased MRP1 and 5 levels. MRP4 and BCRP levels were not altered after selection. CCRF-CEM cells selected by fludarabine also showed a decrease in MRP1 expression, MRP5, and BCRP expression were not altered, and only MRP4 expression was increased, which may have contributed to the development of the observed resistant phenotype.

The results show that the K562 cell line (chronic myeloid leukemia) has its resistant phenotype much more associated with the expression of membrane transporters, including both

influx and efflux pumps. The resistant phenotype of CCRF-CEM cells seems to be independent of the expression of membrane transporters.

An explanation of observed cross-resistance in the CCRF-CEM cells has been found in the expression of the dCK kinase, which mediates the first intracellular phosphorylation of cytarabine, gemcitabine, and fludarabine. Both cell lines, CCRF-CEM selected by cytarabine and fludarabine, had significantly decreased expression of dCK and, at the same time, also increased expression of CDA, which is responsible for the elimination of gemcitabine and cytarabine. A decrease in dCK expression was also detected in K562 cells selected by cytarabine, suggesting a strong connection between cytarabine, gemcitabine, and fludarabine cross-resistance and decreased expression of dCK. This finding is in connection with the current literature.

GSC is a new potential prognostic marker of fludarabine treatment efficacy, and its higher expression has been described in connection with fludarabine resistance. We detected a significant increase in GSC expression after fludarabine and also cytarabine treatment. The connection between GSC expression and cytarabine resistance has not been described yet.

### **2.2.3.2 6-thioguanine and 6-mercaptopurine cross-resistance**

Selection of CCRF-CEM and K562 cells by 6-thioguanine resulted in the same phenotype in both cell lines – cross-resistance between 6-thioguanine and 6-mercaptopurine. This cross-resistance has been previously described *in vitro*, but in the clinics, 6-thioguanine remains an alternative drug for patients resistant or intolerant to 6-mercaptopurine.<sup>53,303</sup>

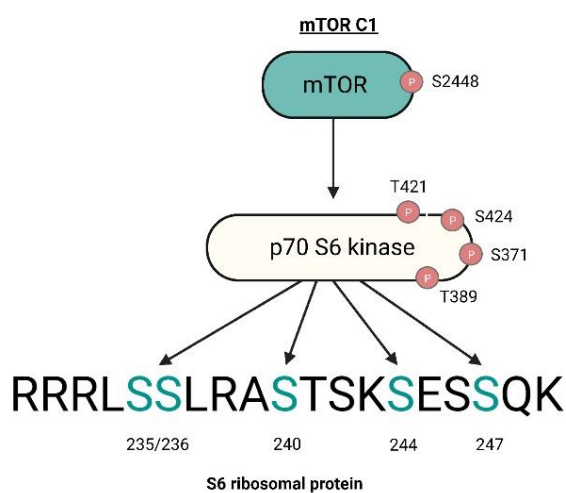
Both 6-TG and 6-MP are transported into cells via ENT2 and CNT3 nucleoside transporters. Our results show no significant connection between ENT2 and CNT3 expression and developed cross-resistance to 6-TG and 6-MP, except for a decrease of CNT3 expression in K562 6-TG resistant cells. Expression of the other transporters was equal or higher compared to the control, and yet there was the development of a resistant phenotype in CCRF-CEM and K562 cells. This suggests that the resistance mechanism will be independent of the expression of nucleoside transporters.

The effect of MDR efflux pumps could explain the resistance development in the CCRF-CEM cell line, where there were elevated levels of Pgp, MRP4, and MRP5. However, no such increase occurred in the K562 line. A common feature was a decrease in the HGPRT expression, which is a key enzyme in the activation of both 6-TG and 6-MP. Lower levels of HGPRT were connected with thiopurines insensitivity and a worse therapeutic prognosis, including shorter overall survival time in *in vitro* experiments and also in the clinics,<sup>304,305</sup> which makes HGPRT a valuable prognostic marker of thiopurine treatment.

### 2.2.3.3 Involvement of mTOR pathway in nucleoside-based drug resistance

Analysis of the mTOR pathway (Fig. 22) showed that all resistant cell lines (except fludarabine-selected K562 cells, which did not develop highly resistant phenotype) had reduced phosphorylation of S6 ribosomal protein (rpS6) in Ser235/236 and Ser244/247. Resistant CCRF-CEM cells also reduced the phosphorylation of S6 ribosomal protein in Ser240/244.

The main kinase responsible for rpS6 phosphorylation is p70 S6 kinase, which phosphorylates all five phosphorylating sites of rpS6. The expression of this kinase was not significantly affected after the selection of resistant clones, but a decrease in its phosphorylation at the Thr421/Ser424 position was detected. The exception was fludarabine-selected CCRF-CEM cells, which had no reduction in Thr421/Ser424 phosphorylation, yet rpS6 was not phosphorylated. There is the possible involvement of protein phosphatase 1 (PP1), which dephosphorylates rpS6.<sup>306</sup>



**Figure 22.** mTOR C1 complex pathway.

S6 ribosomal protein is a downstream effector of the mTOR pathway, but its physiological activity is not entirely understood. In vivo experiments using mice models showed the involvement of rpS6 in the regulation of cellular size, but not in all cell types, and glucose homeostasis.<sup>307,308</sup> The primary phosphorylation site of rpS6 is Ser2, suggesting that inhibition of this phosphorylation will significantly affect the function of rpS6 protein.<sup>309</sup>

The connection between S6 ribosomal protein phosphorylation and drug resistance development has been previously described, but there was always an increase in rpS6 phosphorylation, leading to improved cancer cell viability. For example, increased phosphorylation of rpS6 is related to resistance to PARP inhibitors in BRCA1-deficient cells.<sup>310</sup>

Our results show a significant connection between nucleoside-based drug resistance and rpS6 dephosphorylation. However, the mechanism of involvement in the inhibition of the rpS6 protein in drug resistance has to be further investigated and is beyond the goals of this thesis.



## 2.3 Neuroprotective effect of nucleosides

### 2.3.1 Materials and Methods

#### 2.3.1.1 Kinase assay

The kinase assay was based on direct detection of peptide substrate and its phosphorylated form. CHKtide peptide (m/z 2701; KKKVSRSGLYRSPSPENLNRPR) was used as a substrate for MARK kinases, and GSK peptide substrate (m/z 3028; YRRAAVPPSPSLSRHSSPHQ(pS)EDEEE) was used as a substrate for GSK-3 $\beta$  kinase. Each phosphorylation creates a shift in the molecular mass of the peptide about 80 kDa. Peptide detection was done by MALDI-TOF mass spectrometry (ultraflexXtreme, Bruker Daltonik GmbH), whereas the voltage of ion source 1 was 25.11 kV, ion source 2 22.46 kV, the lens 8.02 kV, reflector 1 26.5 kV, and reflector 2 13.7 kV.

MARK1-4 and GSK-3 $\beta$  kinases were purchased from Carna Biosciences and stored at -80°C. Peptide substrates for all kinases were obtained from SignalChem (aliquoted and stored at -20°C). The assay buffer for MARK kinases consisted of 1 mM HEPES (pH 7,5), 1 mM DTT, and 1 mM MgCl<sub>2</sub>. GSK-3 $\beta$  assay buffer consisted of 2 mM HEPES (pH 7,2), 1 mM DTT, and 4 mM MgCl<sub>2</sub>.

Kinase activity was measured as a conversion of peptide substrate to its phosphorylated form. The inhibition effect was detected as a decrease in this conversion. Staurosporine was used as a control inhibitor. Experimental MARK inhibitors were obtained from ÚOCHB. All compounds were diluted in DMSO (the final concentration of DMSO in the reaction was 0.5 %). Control samples (without inhibition) were treated with DMSO at a final concentration 0.5 %. MALDI-TOF data were processed by flexAnalysis 3.4 software (Bruker Daltonik GmbH), exported by flexAnalysis Batch Process, and analyzed by GraphPad Prism 9 software.

The percentage of kinase activity was calculated as a ratio of phosphorylated peptide (product) peak intensity ( $I_P$ ) to the peptide (substrate) peak intensity ( $I_S$ ), as described below:

$$\text{Enzyme activity [\%]} = 100 \times (I_P/I_S)$$

In the case of multiple phosphorylation, phosphorylated peak intensities added up and compared to substrate peak intensity as previously described.

The percentage of inhibition was calculated as a decrease in the conversion of substrate to the product in the presence of an inhibitor compared to the control reaction without inhibitors. According to dose-response inhibition analysis, IC<sub>50</sub> values were calculated by GraphPad Prism 9.

$$\text{Inhibition [\%]} = 100 - [(I_{\text{Pi}}/I_{\text{Si}})/(I_{\text{Pc}}/I_{\text{Sc}}) \times 100]$$

$I_{\text{Pi}}$  is the product's peak intensity, and  $I_{\text{Si}}$  is the intensity of the substrate peak in the reaction with the inhibitor present.  $I_{\text{Pc}}$  is the intensity of the product peak, and  $I_{\text{Sc}}$  is the intensity of the substrate peak in the control reaction without an inhibitor.

The method for detection activity of MARK kinases was published in Hrubá et al. (2022).<sup>266</sup>

### **2.3.1.2 *In vitro* pharmacology**

The pharmacological properties of the compounds were measured as described previously.<sup>311,312</sup>

### **2.3.1.3 MARK4-tau co-transfection and compound treatment**

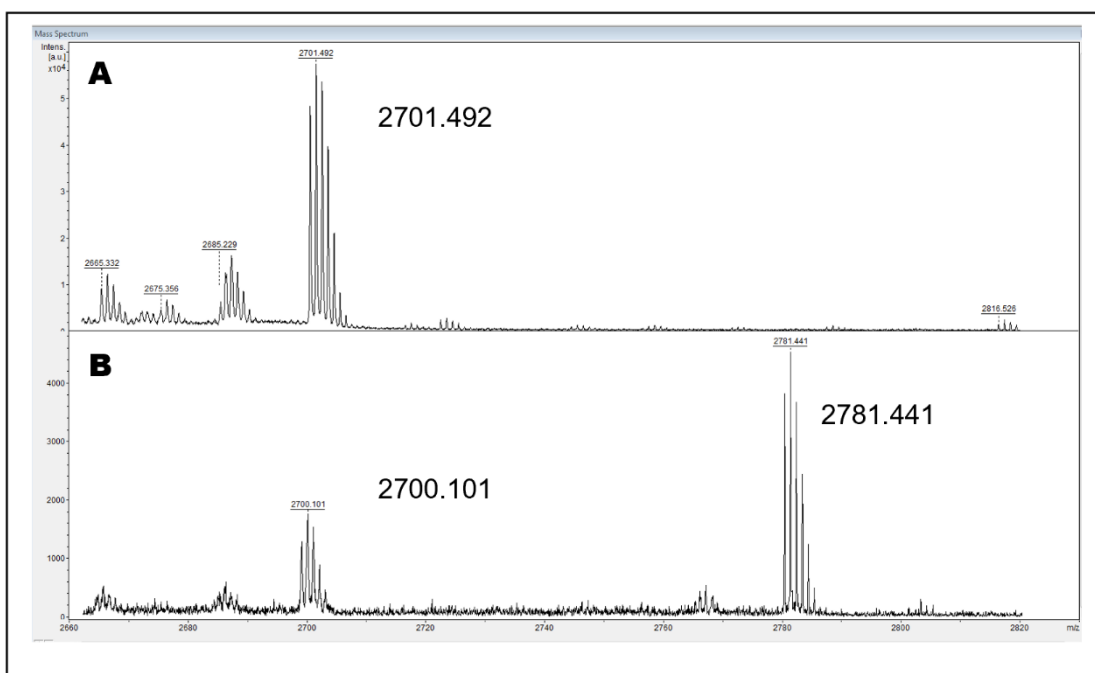
HEK293 cells were transfected with human GFP-MARK4 wildtype (Cat. # DU2288, MRC PPU Reagents and Services, Dundee, Scotland, UK), and pRK5-EGFP-Tau was a gift from Karen Ashe (Addgene plasmid # 46904; RRID: Addgene\_46904).<sup>313</sup> Before the transfection, the cells were plated at the density of  $0.5 \times 10^6$  cells/ mL in a 6-well plate and incubated in a CO<sub>2</sub> incubator overnight. The cells were either transfected with 1 µg MARK4 and 1 µg tau plasmids alone or co-transfected with MARK4 and tau at a 1:1 (1 µg MARK4:1 µg tau), 1:2 (500 ng MARK4:1 µg tau) and 2:1 (1 µg MARK4:500 ng tau) ratios diluted in jetPRIME® Buffer supplemented with jetPRIME® reagent (Cat. # 101000046, Polyplus-transfection®, Illkirch-Graffenstaden, France) following the manufacturer's protocol for 24 h. The total plasmid concentration per well was always  $\leq 2$  µg. using jetPRIME® reagent. The expression of proteins was verified by Western blotting as described below.

For compounds treatment, the cells were first washed with  $1 \times$  PBS 24 h post-transfection and then treated with the compounds at 10, 50, and 75 µM concentrations for 4 hours. After the treatment, the cells were collected and processed for Western blotting, as described below.

## 2.3.2 Results

### 2.3.2.1 MARK kinase assay

MARK kinase assay is based on the direct detection of a peptide substrate (CHKtide,  $m/z$  2701) and its phosphorylated form ( $m/z$  2781) by MALDI-TOF mass spectrometry (Fig. 23).

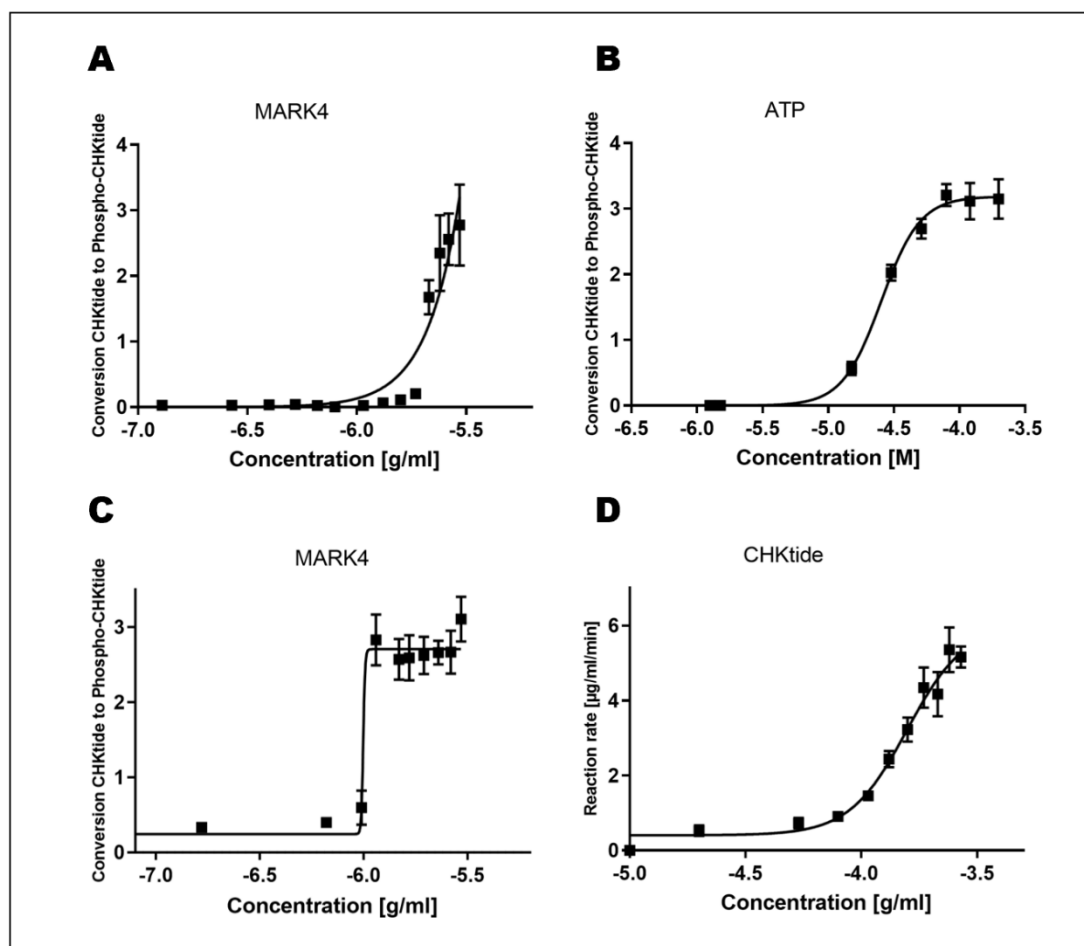


**Figure 23.** (A) Detection of CHKtide peptide substrate ( $m/z$  2701) in the assay buffer by MALDI-TOF mass spectrometry. (B) Detection of a peptide substrate (CHKtide) and its phosphorylated form ( $m/z$  2781) in the presence of MARK4 enzyme in the assay buffer after 60 minutes of incubation. Mass spectra were analyzed by flexAnalysis software (Bruker Daltonik GmbH).<sup>266</sup>

Method development was done using the MARK4 enzyme and then optimized for other MARK isoforms. The method was optimized in four steps. The first one was the optimization of MARK4 concentration (Fig. 24A), which was tested in the 0.05- 2.95  $\mu\text{g/ml}$  range using an initial concentration of 100  $\mu\text{M}$  ATP and 0.13 mg/ml of CHKtide peptide substrate. We chose the optimal conversion ratio of substrate to product (phosphorylated CHKtide) 1:2, obtained by using 2.25  $\mu\text{g/ml}$  of MARK4 in the reaction. This concentration was used to optimize ATP concentration (Fig. 24B), which was tested in the range of 1.85 – 200  $\mu\text{M}$  using 0.13 mg/ml of the peptide substrate. The optimal ATP concentration was 46.4  $\mu\text{M}$ , which was used for reevaluation of MARK4 concentration (Fig. 24C) in the same concentrations as in step one. In optimized ATP conditions, phosphorylation was more effective, and optimal MARK4 concentration decreased to 1.19  $\mu\text{g/ml}$ . This concentration and the optimized concentration of ATP were used for the dose-dependent analysis of CHKtide optimal concentration. (Fig. 24D).

CHKtide was tested in the 0.020 to 0.267 mg/ml range, and  $K_M$  was calculated. The optimal CHKtide concentration was 0.12 mg/ml, corresponding to the  $K_M$ .

The final conditions for MARK4 kinase assay were 1.19  $\mu\text{g/ml}$  of MARK4, 46.4  $\mu\text{M}$  of ATP, and 0.12 mg/ml of CHKtide.

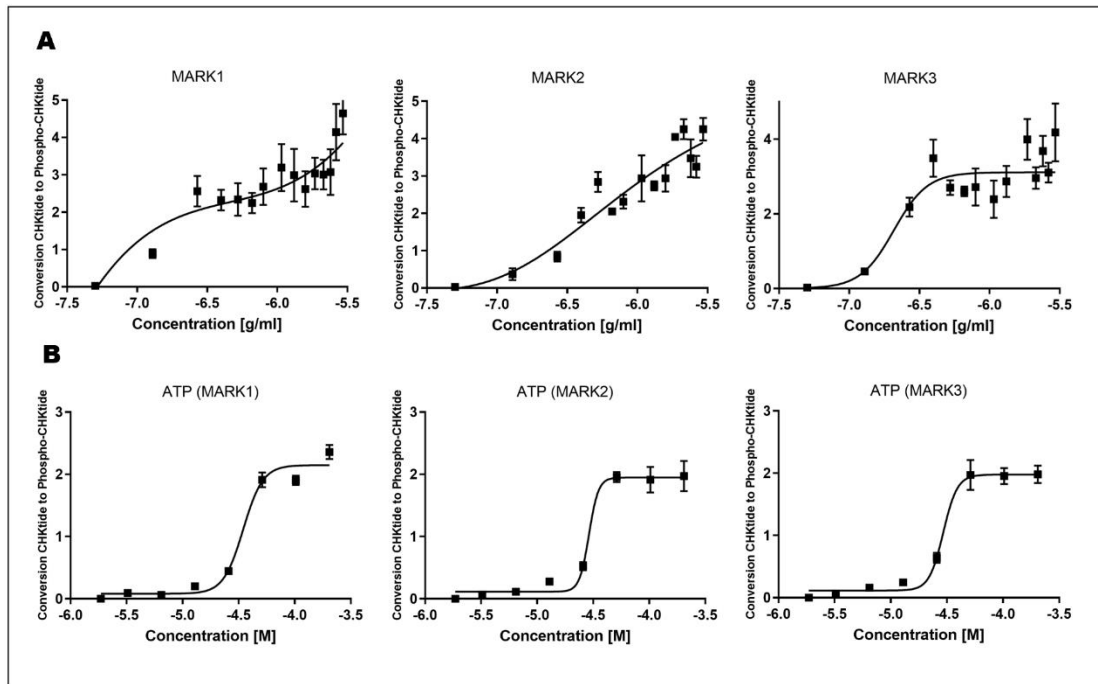


**Figure 24.** (A) Optimization of MARK4 concentration in the range of 0.05 to 2.95  $\mu\text{g/ml}$  at initial concentrations of ATP (100  $\mu\text{M}$ ) and CHKtide (0.13 mg/ml). The optimal MARK4 concentration was 2.25  $\mu\text{g/ml}$ . (B) Optimization of ATP concentration in the range of 1.85 to 200  $\mu\text{M}$  at the optimized concentrations of MARK4 of 2.25  $\mu\text{g/ml}$  and CHKtide of 0.13 mg/ml. The selected concentration of ATP was 46.4  $\mu\text{M}$ . (C) Reevaluation of MARK4 concentration under optimized conditions (46.4  $\mu\text{M}$  ATP and 0.13 mg/ml CHKtide). (D) Optimization of CHKtide concentration under optimized conditions (1.19  $\mu\text{g/ml}$  MARK4, 46.5  $\mu\text{M}$ , 0.13 mg/ml CHKtide) in the range of 0.020 to 0.267 mg/ml. The optimal CHKtide concentration was 0.12 mg/ml. The reaction rate was calculated as the conversion of substrate to the product over time. Data are mean  $\pm$  SD,  $n = 3$ , and were processed using the GraphPad Prism 9.5.1 software program.<sup>266</sup>

Since the method was optimized for the MARK4 enzyme, we also optimized conditions for other MARK isoforms (MARK1-3). First of all, we optimized enzyme concentration (range 0.05 to 2.92  $\mu\text{g/ml}$  in MARK4 optimized ATP (46.4  $\mu\text{M}$ ) and CHKtide concentration (0.12 mg/ml) (Fig. 25A). Optimal enzyme concentration was corresponding to peptide to phospho-peptide conversion ratio 1:2. Optimal MARK1 concentration was 0.31  $\mu\text{g/ml}$ , MARK2 0.55

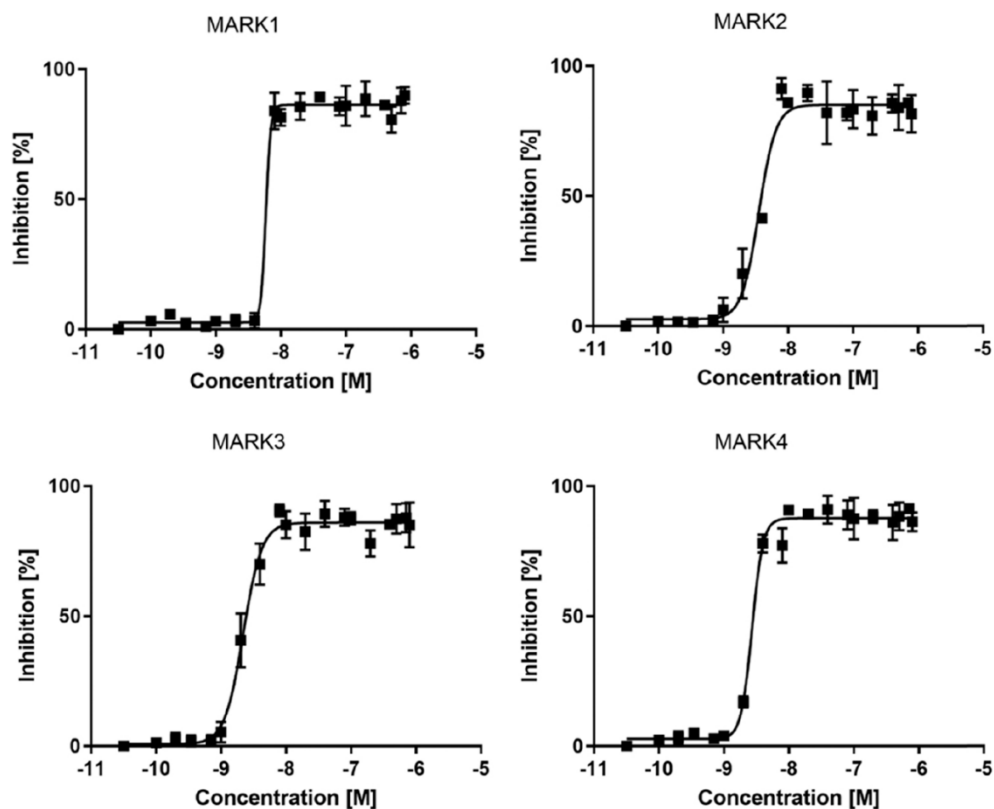
$\mu\text{g/ml}$ , and MARK3  $0.40 \mu\text{g/ml}$ . In the second step, ATP concentration was optimized using a range of  $3.21$  to  $205 \mu\text{M}$  with a CHKtide concentration of  $0.12 \text{ mg/ml}$ . (Fig. 25B) The optimal ATP concentration was similar to the MARK4 method,  $46.4 \mu\text{M}$ , so reevaluation of enzyme concentration was not needed.

The final condition was  $46.4 \mu\text{M}$  of ATP,  $0.12 \text{ mg/ml}$  of CHKtide peptide substrate,  $0.31 \mu\text{g/ml}$  of MARK1,  $0.55 \mu\text{g/ml}$  of MARK2, and  $0.40 \mu\text{g/ml}$ .



**Figure 25.** (A) Optimization of MARK1-3 concentration in the range of  $0.05$  to  $2.92 \mu\text{g/ml}$  with initial ATP ( $46.4 \mu\text{M}$ ) and substrate concentration ( $0.12 \text{ mg/ml}$  CHKtide). The optimal concentration of MARK1 was  $0.31 \mu\text{g/ml}$ , MARK2  $0.55 \mu\text{g/ml}$ , and MARK3  $0.40 \mu\text{g/ml}$ . (B) Optimization of ATP concentration (range from  $3.21$  to  $205 \mu\text{M}$ ) in the presence of MARK1, 2, or 3, respectively, and  $0.12 \text{ mg/ml}$  of CHKtide peptide substrate. The optimal concentration for all MARK isoforms was  $46.4 \mu\text{M}$ . Data are mean  $\pm$  sd,  $n \geq 3$ , and were processed using the GraphPad Prism 9.5.1 software program.<sup>266</sup>

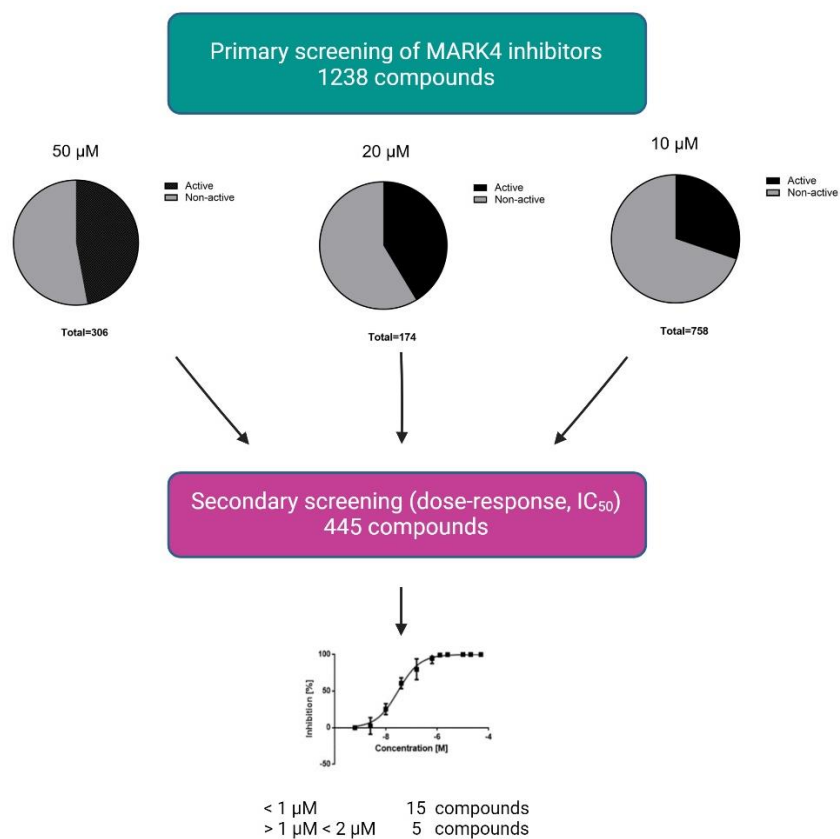
Inhibition of MARK1-4 activity was tested using kinase inhibitor, staurosporine, with  $\text{IC}_{50}$   $9.46 \text{ nM} \pm 0.13$  (MARK1),  $5.82 \text{ nM} \pm 0.12$  (MARK2),  $3.79 \text{ nM} \pm 0.12$  (MARK3) and  $4.6 \text{ nM} \pm 0.12$  (MARK4). (Fig. 26)



**Figure 26.** Staurosporine inhibition of MARK1-4 kinases with  $IC_{50}$  values:  $9.46 \text{ nM} \pm 0.13$  (MARK1),  $5.82 \text{ nM} \pm 0.12$  (MARK2),  $3.79 \text{ nM} \pm 0.12$  (MARK3) and  $4.6 \text{ nM} \pm 0.12$  (MARK4). Data are mean  $\pm$  sd,  $n \geq 3$ . Data were processed, and  $IC_{50}$  values were calculated using the GraphPad Prism 9.5.1 software program.<sup>266</sup>

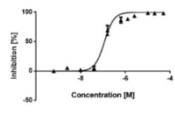
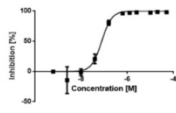
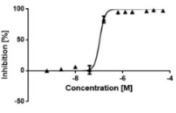
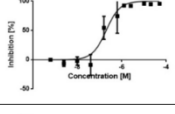
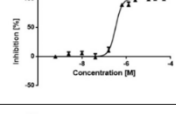
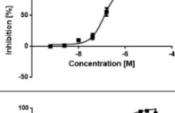
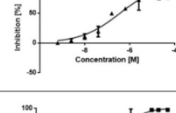
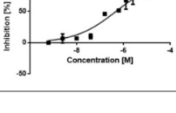
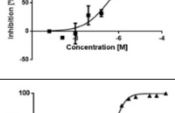
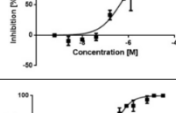
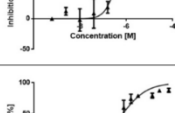
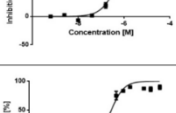
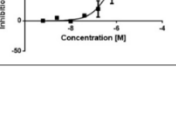
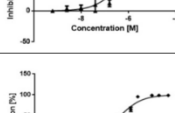
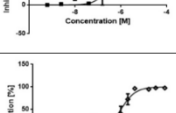
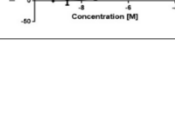
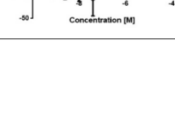
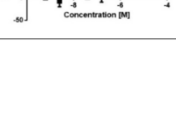
### 2.3.2.2 Screening of MARK4 inhibitors

The screening of MARK4 inhibitors was divided into two parts. Part one included the primary screening of testing MARK4 inhibitory activity of analyzed compounds in one concentration and at least three replicates. The first group of tested compounds consisted of 306 compounds, and their activity was tested at  $50 \mu\text{M}$ . 144 compounds were identified as MARK4 inhibitors in this group and were selected for secondary screening. Since the initial concentration of  $50 \mu\text{M}$  resulted in a high number of positive compounds, the concentration was decreased to  $20 \mu\text{M}$  for the second batch of compounds (174 analyzed compounds and 72 positive MARK4 inhibitors) and to  $10 \mu\text{M}$  for the third batch (758 tested compounds and 229 positive MARK4 inhibitors). We analyzed 1238 compounds, and 445 compounds were tested in the secondary screening. The secondary screening was the dose-response analysis of the inhibitory activity in concentration from  $2,44 \text{ nM}$  to  $50 \mu\text{M}$ . Based on this data, the  $IC_{50}$  value was calculated. We identified 15 compounds with  $IC_{50}$  lower than  $1 \mu\text{M}$  and 5 compounds with  $IC_{50}$  between  $1 \mu\text{M}$  and  $2 \mu\text{M}$  (Fig. 27). These 20 compounds were used for further analyses. Dose-response curves are summarized in Tab. 6A, B and C.



**Figure 27.** MARK4 screening. The primary screening included 1238 compounds divided into three groups tested in concentrations 50, 20, and 10  $\mu$ M. 445 compounds were analyzed in the dose-response secondary screening. Data were evaluated, and the IC<sub>50</sub> value was calculated by GraphPad Prism 9.5.1 software program.

**Table 6A.** Dose-response analyses of the most active MARK4 inhibitors. Each graph is mean  $IC_{50} \pm$  standard deviation ( $n \geq 2$ ). Data were processed, and  $IC_{50}$  was calculated using the GraphPad Prism 9.5.1 software program.

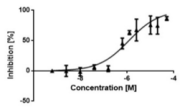
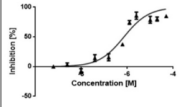
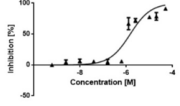
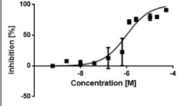
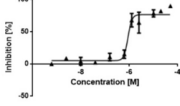
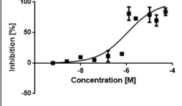
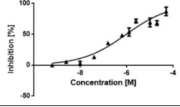
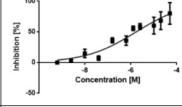
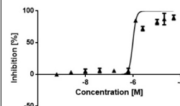
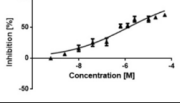
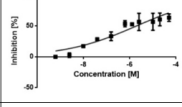
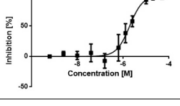
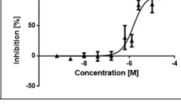
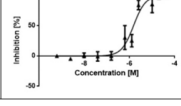
LEM code	MARK4 inhibition						Mean	sd
	$IC_{50}$ [ $\mu$ M]	$IC_{50}$ [ $\mu$ M]	$IC_{50}$ [ $\mu$ M]	$IC_{50}$ [ $\mu$ M]	$IC_{50}$ [ $\mu$ M]			
2999		0.11		0.08		0.11	0.10	0.02
2998		0.19		0.32			0.26	0.09
21033		0.12		0.36		0.47	0.32	0.18
2997		0.30		0.42			0.36	0.08
2994		0.32		0.43		0.50	0.42	0.09
11482		0.56		0.38			0.47	0.13
2695		0.42		0.63		0.41	0.49	0.12



**Table 6B.** Dose-response analyses of the most active MARK4 inhibitors. Each graph is mean  $IC_{50} \pm$  standard deviation ( $n \geq 2$ ). Data were processed, and  $IC_{50}$  was calculated using the GraphPad Prism 9.5.1 software program.

LEM code	MARK4 Inhibition							
		$IC_{50}$ [ $\mu$ M]		$IC_{50}$ [ $\mu$ M]		$IC_{50}$ [ $\mu$ M]	Mean	sd
20776		0.82		0.44		0.25	0.50	0.29
2990		0.71		0.45			0.58	0.18
11480		0.53		0.65			0.59	0.08
12737		0.62		0.58			0.60	0.03
2993		0.51		0.85			0.68	0.24
1223		0.91		0.74			0.83	0.12
11134		0.91		0.80			0.85	0.07

**Table 6C.** Dose-response analyses of the most active MARK4 inhibitors. Each graph is mean  $IC_{50} \pm$  standard deviation ( $n \geq 2$ ). Data were processed, and  $IC_{50}$  was calculated using the GraphPad Prism 9.5.1 software program.

LEM code	MARK4 inhibition							
		$IC_{50}$ [ $\mu$ M]		$IC_{50}$ [ $\mu$ M]		$IC_{50}$ [ $\mu$ M]	Mean	sd
2989		1.18		0.72			0.95	0.33
11133		1.48		0.95			1.22	0.37
20967		1.57		1.08		1.23	1.30	0.25
11152		0.94		1.68			1.31	0.52
2387		1.32		1.94			1.63	0.44
10893		1.92		1.50			1.71	0.3

### 2.3.2.3 MARK1-3 inhibitory activity

20 compounds selected from MARK4 screening were tested for their ability to inhibit other MARK isoforms (MARK1, 2, and 3). Compounds that were active MARK1-3 inhibitors (LEM 2999, 2998, 2997, 2994, 2695, 2990, 12737, 2993, and 10983) were removed from the tested group, and further experiments were done only for selective MARK4 inhibitors. Results are summarized in Tab. 7. Dose-response curves are provided in Supplementary Table 1, 2, and 3 (A-C).

**Table 7.** IC<sub>50</sub> values for the most active compounds from the MARK4 screening (IC<sub>50</sub> < 2 μM). Compounds were also tested for their activity against other MARK isoforms (1-3). Data shows mean IC<sub>50</sub> values and standard deviation (sd). n ≥ 6. Data were processed using the GraphPad Prism 9.5.1 software program.

LEM code	IC <sub>50</sub> [μM]							
	MARK 4	sd	MARK 1	sd	MARK 2	sd	MARK 3	sd
2999	0.10	0.02	5.48	1.42	0.39	0.12	0.29	0.17
2998	0.26	0.09	3.67	1.19	1.42	0.53	1.04	0.03
21033	0.32	0.18	>50	0	20.87	5.58	>50	0
2997	0.36	0.08	2.23	2.08	1.65	0.88	1.02	0.84
2994	0.42	0.09	7.57	2.41	42.16	3.21	1.75	1.41
11482	0.47	0.13	>50	0	>50	0	>50	0
2695	0.49	0.12	15.39	2.79	19.94	6.56	0.17	0.05
20776	0.50	0.29	>50	0	>50	0	>50	0
2990	0.58	0.18	0.48	0.14	0.31	0.22	0.38	0.35
11480	0.59	0.08	>50	0	>50	0	38.8	18.86
12737	0.60	0.03	11.62	4.2	0.13	0.02	0.34	0.53
2993	0.68	0.24	0.98	0.34	0.11	0.08	0.11	0.04
1223	0.83	0.12	43.12	9.4	33.46	3.27	40.87	15.81
11134	0.85	0.07	>50	0	>50	0	>50	0
2989	0.95	0.33	>50	0	>50	0	>50	0
11133	1.22	0.37	>50	0	46.21	5.2	>50	0
20967	1.30	0.25	>50	0	>50	0	>50	0
11152	1.31	0.52	>50	0	>50	0	>50	0
2387	1.63	0.44	>50	0	>50	0	>50	0
10983	1.71	0.30	5.35	1.57	0.24	0.06	0.11	0.01

### 2.3.2.4 Cytotoxicity of MARK inhibitors

Tab. 8 summarizes the cytotoxicity of the selective MARK4 inhibitors using human cancer and non-cancer cell lines. Cytotoxicity was evaluated by the MTS test. The data were obtained from the IMTM MedChemBio portal (data were done by Dr. S. Gurská, IMTM).

All of the tested compounds, except LEM 20776, were not toxic for non-tumor cell lines (BJ, MRC-5). LEM 20776 and LEM 11133 were highly toxic for all tested cancer cell lines, and the other compounds were slightly or non-active.

**Table 8.** IC<sub>50</sub> values of selective MARK4 inhibitors using human cancer (CCRF-CEM, CEM-DNR, K562, K562-TAX, A549, HCT 116, HCT 116 p53-/-, U-2 OS) and non-cancer cell lines (BJ, MRC-5, HEK-293 MARK4). Data are mean ± standard deviation (sd), n ≥ 4. Nt – not tested

LEM code	IC <sub>50</sub> [μM]										
	BJ	MRC-5	HEK293 MARK4	CCRF-CEM	CEM-DNR	K562	K562-TAX	A549	HCT 116	HCT 116 p53-/-	U-2 OS
21033	> 50	> 50	Nt	> 50	> 50	> 50	> 50	> 50	> 50	> 50	> 50
11482	> 50	> 50	> 50	> 50	> 50	> 50	> 50	> 50	> 50	> 50	> 50
20776	3.99 (± 1.1)	4.73 (± 0.9)	Nt	1.75 (± 0.3)	1.48 (± 0.08)	0.68 (± 0.08)	1.37 (± 0.2)	0.64 (± 0.04)	0.62 (± 0.04)	0.92 (± 0.04)	0.66 (± 0.07)
11480	> 50	> 50	> 50	> 50	> 50	> 50	> 50	> 50	> 50	> 50	> 50
1223	> 50	> 50	> 50	36.37 (± 5.2)	> 50	> 50	> 50	> 50	49.66 (± 3.8)	39.27 (± 4.8)	Nt
11134	> 50	> 50	> 50	> 50	> 50	> 50	> 50	> 50	> 50	> 50	> 50
2989	> 50	> 50	47,3	> 50	> 50	> 50	12.86 (± 4.3)	> 50	> 50	> 50	> 50
11133	> 50	> 50	Nt	1.03 (± 0.1)	1.34 (± 0.1)	0.36 (± 0.04)	0.54 (± 0.05)	0.48 (± 0.05)	0.47 (± 0.03)	0.53 (± 0.05)	0.49 (± 0.04)
20967	> 50	> 50	Nt	27.55 (± 2.2)	42.4 (± 6.9)	47.7 (± 6.1)	33.39 (± 4.9)	> 50	33.95 (± 2.9)	48.17 (± 2.6)	> 50
11152	> 50	> 50	Nt	33.91 (± 4.9)	> 50	> 50	> 50	> 50	48.87 (± 1.8)	48.1 (± 3.8)	> 50
2387	44.28 (± 6.2)	43.03 (± 10.9)	Nt	3.85 (± 0.9)	28.92 (± 0.9)	31.95 (± 2.7)	28.54 (± 0.8)	37.59 (± 2.6)	32.24 (± 4.2)	24.8 (± 3.1)	19.69 (± 1.7)

### 2.3.2.5 *In vitro* pharmacological parameters

*In vitro* pharmacological parameters were analyzed to predict the behavior of selected compounds in the human body. *In vitro* metabolism, binding to plasma proteins, and active transport across the blood-brain barrier (BBB) were tested (Tab. 9). The data were obtained from the IMTM MedChemBio portal (data were done by Dr. B. Lišková, IMTM).

Stability in the solution is a fundamental property of successful drug candidates, and most of our tested compounds demonstrated quite a high chemical stability in the phosphate-buffered saline (PBS pH 7,4) after 120 minutes at 37 °C. The compounds 11482, 20776, and 11134 showed a lack of stability that may be due to non-enzymatic processes (less than 70% presence in PBS after 120 min). The synthesized compounds were incubated with human plasma *in vitro* for fast determination if they maintained acceptable concentration and half-life to achieve desirable pharmacological effects.<sup>314</sup> Compounds were found to be stable in plasma (all compounds showed more than 80% presence in plasma after 120 min). The exception is compound 20776, which is potentially labile to the plasma enzymes.

The binding of studied molecules to plasma proteins can impact their stability in plasma, distribution, and efficacy. The measurement of plasma protein binding was performed using a

Rapid Equilibrium Dialysis device, and studied compounds reported a percent of fraction bound in the range of 40 - 95%. The intrinsic clearance calculated from the microsomal stability assay indicated a high category, except for the derivatives 2989, and 2387, which reported a medium sort of intrinsic clearance.

The derivatives 20967, 11152, and 2387 had the medium ability ( $-\log P_{app}$  4.9 - 6 cm/s) to diffuse passively through an artificial cellular membrane in the Parallel artificial membrane permeability assay (PAMPA) for the remaining studied compounds, another alternative mechanism of intracellular transport may be necessary. It can be concluded that studied molecules could be divided into three groups.

First, 11152 and 2387 showed the best permeability properties based on cell assays from the studied compounds. Molecules 11152 and 2387 showed high and moderate ( $P_{appAB}$  5-20 $\times 10^{-6}$  cm/s; moderate category) probability of intestinal absorption and cross blood-brain barriers ( $P_{appAB} > 10 \times 10^{-6}$  cm/s; CNS +). We assessed rates of transport across Caco-2 and MDCK-MDR1 monolayers in both directions (apical to basolateral (A-B) and basolateral to apical (B-A)) across the cell monolayer, which enables us to determine the efflux ratio and shows if the compound undergoes active efflux. Studied derivatives 11152 and 2387 were actively exported from the cells in both barrier models as indicated by efflux ratios  $> 2$ . Still, values of efflux ratio were very close to the limit of active and passive efflux that the compounds could not be clearly identified as substrates of the MDR1 (Pgp) efflux pump present in both cell types.

The second group, studied compounds reported better permeability in the intestinal barrier model than in the blood-brain barrier model, including 11133 (not actively exported from the cells in both barrier models as indicated by efflux ratios  $< 2$ ) and other 2989, 1223, and 20967 (actively exported from the cells in both barrier models as indicated by efflux ratios  $> 2$ ).

The third group, the other studied compounds 21033, 11482, and 20776, manifested a low category of permeability in both cell assays and were actively exported from the cells in both barrier models.

**Table 9.** *In vitro* pharmacological parameters for selected MARK4 inhibitors. Data were analyzed using a Rapid Equilibrium Dialysis device.

LEM code	Compound	Metabolism							Plasma protein binding	Permeability				
		in vitro							in vitro	in vitro		in vivo		
		Chemical stability		Plasma stability		Microsomal stability			Rapid Equilibrium dialysis	PAMPA		Caco-2	MDR1-MDCK	
Time (min)	% compound remaining	Time (min)	% compound remaining	Time (min)	% compound remaining	Intrinsic clearance	The fraction bound (%)	log Pe	Category	Category	CNS negative/positive			
21033	YC122	0	100	0	100	0	100	Medium	78.76	-8.03	Low	Low	CNS negative	
		15	93	15	100	15	99					Papp (x10e-6): 1.23	Papp (x10e-6): 0.11	
		30	103	30	97	30	76					Efflux ratio: 8.59	Efflux ratio: 8.00	
		60	86	60	86	60	70					Active efflux: yes	Active efflux: yes	
		120	80	120	84	ND	ND					% recovery: 41.67	% recovery: 41.88	
11482	IK-1032-I	0	100	0	100	0	100	Medium	83.98	-8.05	Low	Low	CNS negative	
		15	93	15	97	15	99					Papp (x10e-6): 1.25	Papp (x10e-6): 0.53	
		30	84	30	92	30	85					Efflux ratio: 3.01	Efflux ratio: 7.41	
		60	79	60	89	60	58					Active efflux: yes	Active efflux: yes	
		120	54	120	87	ND	ND					% recovery: 45.67	% recovery: 96.52	
20776	MIT891	0	100	0	100	0	100	Medium	38.71	-6.97	Low	Low	CNS negative	
		15	96	15	105	15	79					Papp (x10e-6): 0.063	Papp (x10e-6): 1.36	
		30	106	30	86	30	80					Efflux ratio: 4.33	Efflux ratio: 1.44	
		60	89	60	64	60	47					Active efflux: yes	Active efflux: no	
		120	60	120	46	ND	ND					% recovery: 65.47	% recovery: 47.28	
11480	IK-1029-I	Nt												
1223	PNH760	0	100	0	100	0	100	Low	89.87	-7.08	Low	Moderate	CNS negative	
		15	97	15	99	15	95					Papp (x10e-6): 10.30	Papp (x10e-6): 2.31	
		30	98	30	105	30	89					Efflux ratio: 5.78	Efflux ratio: 19.01	
		60	103	60	98	60	82					Active efflux: yes	Active efflux: yes	
		120	92	120	98	ND	ND					% recovery: 68.43	% recovery: 96.14	
11134	IK-886-I	0	100	0	100	0	100	Low	95.42	-7.39	Low	Low	CNS negative	
		15	77	15	103	15	98					Papp (x10e-6): 3.45	Papp (x10e-6): 4.61	
		30	67	30	100	30	97					Efflux ratio: 1.00	Efflux ratio: 1.67	
		60	65	60	94	60	89					Active efflux: no	Active efflux: no	
		120	49	120	105	ND	ND					% recovery: 59.02	% recovery: 87.77	
2989	SPS25	0	100	0	100	0	100	High	96.74	-6.94	Low	Moderate	CNS negative	
		15	100	15	98	15	71					Papp (x10e-6): 12.06	Papp (x10e-6): 2.61	
		30	96	30	97	30	57					Efflux ratio: 2.47	Efflux ratio: 3.37	
		60	96	60	102	60	16					Active efflux: yes	Active efflux: yes	
		120	84	120	100	ND	ND					% recovery: 48.74	% recovery: 92.88	
11133	IK-888-I	0	100	0	100	0	100	Medium	78.45	-7.68	Low	Moderate	CNS negative	
		15	99	15	93	15	72					Papp (x10e-6): 6.13	Papp (x10e-6): 2.83	
		30	93	30	95	30	50					Efflux ratio: 0.97	Efflux ratio: 1.36	
		60	85	60	93	60	27					Active efflux: no	Active efflux: no	
		120	88	120	87	ND	ND					% recovery: 64.17	% recovery: 86.26	
20967	MFC170	0	100	0	100	0	100	Medium	79.81	-5.84	Medium	Moderate	CNS negative	
		15	92	15	92	15	91					Papp (x10e-6): 9.01	Papp (x10e-6): 9.56	
		30	95	30	91	30	81					Efflux ratio: 10.21	Efflux ratio: 6.99	
		60	95	60	90	60	68					Active efflux: yes	Active efflux: yes	
		120	100	120	78							% recovery: 108.22	% recovery: 94.75	
11152	IK-963-I	0	100	0	100	0	100	Medium	68.14	-4.95	Medium	High	CNS positive	
		15	104	15	104	15	86					Papp (x10e-6): 36.98	Papp (x10e-6): 15.80	
		30	102	30	88	30	75					Efflux ratio: 2.00	Efflux ratio: 3.66	
		60	106	60	82	60	64					Active efflux: no	Active efflux: yes	
		120	102	120	80	ND	ND					% recovery: 54.47	% recovery: 109.28	
2387	IK725	0	100	0	100	0	100	High	87.79	-5.89	Medium	Moderate	CNS positive	
		15	95	15	105	15	75					Papp (x10e-6): 18.52	Papp (x10e-6): 13.93	

		30	102	30	101	30	52					Efflux ratio: 2.64	Efflux ratio: 2.84
		60	103	60	97	60	18					Active efflux: yes	Active efflux: yes
		120	103	120	88	ND	ND					% recovery: 92.47	% recovery: 77.75

### 2.3.2.6 Physicochemical parameters

Compounds selected in the MARK screening were also analyzed for their physicochemical parameters, which affect their ability to cross the BBB, such as their molecular mass, lipophilicity (Log  $P_{o/w}$ ), number of H-bond donors and acceptors, number of rotatable bonds and polar surface area (TPSA). All parameters were analyzed according to the structure of tested compounds using the SwissADME service (Swiss Institute of Bioinformatics) and summarized in Tab. 10.

According to physicochemical parameters, only compounds 2989 and 11133 should be able to passively cross the BBB. Compound 11133 is also the substrate for P-glycoprotein (Pgp), which is an efflux pump reducing the concentration of potentially toxic compounds in the brain tissue, which may decrease the activity of this compound. 2989 was not identified as a Pgp substrate.

**Table 10.** Physicochemical parameters of most active MARK4 inhibitors. Molecular mass (Mw), lipophilicity (Log  $P_{o/w}$ ), number of H-bond donors and acceptors, number of rotatable bonds, and total polar surface area (TPSA). The SwissADME service was used to analyze these parameters, and accordingly, a prediction of their ability to cross the BBB was made. Based on their structure, there was also a prediction of being a substrate of P-glycoprotein (Pgp) for those compounds.

LEM code	Mw	Log $P_{o/w}$	H-bond donors	H-bond acceptors	Rotatable bonds	TPSA [Å]	Ability to cross the BBB	Pgp substrate
21033	473.50	2.95	3	7	3	142.01	No	No
11482	409.44	4.11	1	6	5	85.81	No	Yes
20776	405.50	3.97	1	5	4	131.09	No	Yes
11480	423.42	4.09	1	7	4	98.95	No	Yes
1223	383.35	0.50	4	7	3	133.74	No	No
11134	276.29	2.42	2	3	2	80.73	No	Yes
2989	265.27	2.80	1	4	2	63.94	Yes	No
11133	286.33	3.16	2	2	2	67.59	Yes	Yes
20967	421.41	0.77	3	8	3	131.59	No	No
11152	325.25	2.44	1	9	4	85.81	No	Yes
2387	231.27	2.48	1	3	2	79.04	No	No

### 2.3.2.7 Selectivity of MARK4 inhibitors

Based on previous analyses, we selected compounds LEM 2989, 11133, 11152, and 2387 for additional tests. To investigate the selectivity of our selected compounds, inhibitory activity against 50 kinases was analyzed. Analysis was done by Carna Sciences, Inc. (Japan). Inhibitory activity was tested in a single concentration 5  $\mu$ M and two replicates. Results are

summarized in Tab. 11. All compounds showed high inhibitory activity to at least one of the tested kinases. The most selective compound was LEM 11152, which highly inhibited just Cdk2/CycA2 and GSK-3 $\beta$ .

**Table 11.** Inhibitory activity of compounds LEM 2989, 11133, 11152, and 2387 in concentration 5  $\mu$ M against a panel of 50 kinases. Data are mean (n = 2).

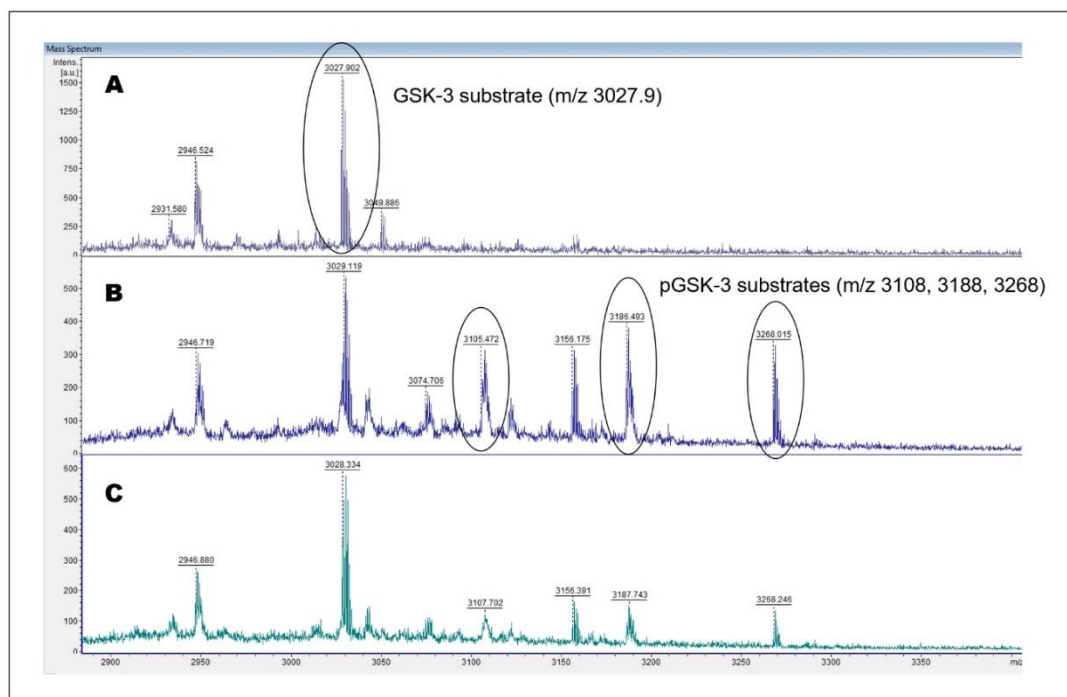
Kinase	% Inhibition			
	2989	11133	11152	2387
ABL	5.9	88.3	2.6	97.0
CSK	0.9	53.3	-1.9	43.0
EGFR	6.1	62.6	3.2	24.1
EPHA2	0.1	89.4	-1.6	83.5
EPHB4	2.0	83.9	-1.3	82.6
FGFR1	2.8	29.9	-4.2	16.9
FLT3	31.2	92.3	-4.4	85.8
IGF1R	3.1	2.8	-1.2	15.7
ITK	7.9	52.5	-2.3	61.9
JAK3	45.6	71.9	0.6	48.9
KDR	11.3	61.9	-2.2	59.2
LCK	2.3	66.6	-3.8	67.7
MET	-0.5	9.8	-5.7	18.8
PDGFR $\alpha$	18.0	103.7	-5.9	93.9
PYK2	51	33.4	-1.1	31.0
SRC	11.1	86.0	-0.8	89.8
SYK	-17.8	59.5	-18.6	55.4
TIE2	1.9	16.5	-2.6	20.3
TRKA	35.8	81.4	0.5	77.9
TYRO3	6.8	70.5	1.7	58.0
AKT1	-7.0	-11.1	-12.3	-11.2
AMPK $\alpha$ 1/ $\beta$ 1/ $\gamma$ 1	-1.3	-3.6	-10.6	-6.0
AurA	9.1	64.9	-2.4	63.5
CaMK4	1.6	1.9	-0.1	3.0
Cdk2/CycA2	8.3	72.7	66.9	67.9

Kinase	% Inhibition			
	2989	11133	11152	2387
CHK1	30.5	53.0	10.4	39.7
CK1 $\epsilon$	72.7	31.9	-1.1	17.4
DAPK1	39.8	6.2	0.8	18.5
DYRK1B	41.0	54.9	5.5	5.9
ERK2	-9.2	-6.3	-6.9	-6.5
GSK-3 $\beta$	28.1	92.8	61.7	69.0
HGK	99.9	96.3	3.6	78.6
IKK $\beta$	17.8	1.5	-4.0	2.1
IRAK4	13.8	17.0	0.1	15.6
JNK2	-1.3	1.9	-0.6	15.6
MAPKAPK2	-10.1	-14.4	-8.1	-11.1
MST1	70.0	18.1	-1.5	7.4
NEK2	-3.1	29.7	0.8	9.2
p38 $\alpha$	-7.2	1.0	-5.0	-3.9
p70S6K	70.5	18.2	0.3	18.6
PAK2	-11.7	-12.7	-15.7	-9.8
PBK	4.5	-1.1	15.1	1.1
PDK1	16.4	11.5	-2.3	13.6
PIM1	10.6	-7.7	1.6	-2.6
PKAC $\alpha$	40.6	-4.2	-7.1	-14.9
PKC $\alpha$	11.5	7.7	0.1	-1.8
PKD2	5.0	-9.1	-16.4	-10.1
ROCK1	23.2	-2.5	-1.6	1.3
SGK	36.7	8.4	1.0	6.0
TSSK1	9.3	1.3	-0.5	6.3



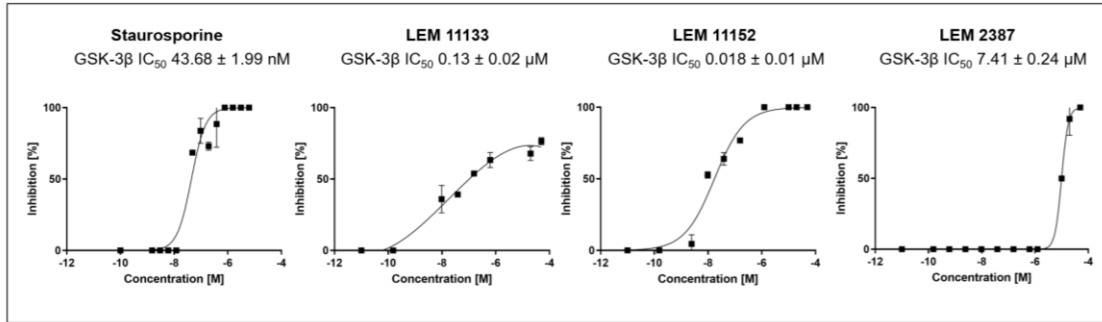
### 2.3.2.8 GSK-3 $\beta$ kinase assay

Since GSK-3 $\beta$  is a kinase, which is, together with MAKR4, involved in pathological tau hyperphosphorylation, we optimized the kinase assay for detecting GSK-3 $\beta$  activity. GSK-3 $\beta$  phosphorylates substrate (GSK-3 peptide; m/z 3028) (Fig. 28A) in three phosphorylation sites, where one phosphorylation exists naturally. So we detected twice, three, and four times phosphorylated GSK-3 substrates with m/z 3108, 3188, and 3268. (Fig. 28B) Staurosporine was used as a control inhibitor of GSK-3 $\beta$  activity. (Fig. 28C)



**Figure 28.** (A) GSK-3 peptide substrate detected by MALDI-TOF in the GSK-3 assay buffer. (B) GSK-3 substrate and its phosphorylated forms (m/z 3108, 3188, and 3268) after two hours of incubation with the GSK-3 $\beta$  enzyme (concentration 4  $\mu$ g/ml) in the assay buffer. (C) Decrease of GSK-3 peptide phosphorylation in the presence of staurosporine (100 nM).

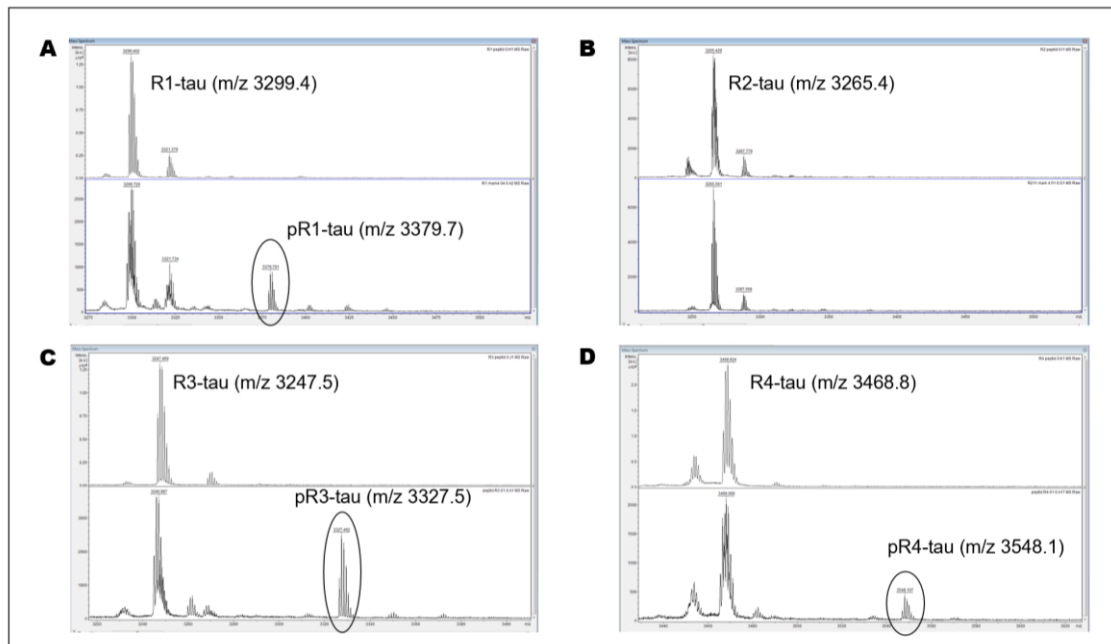
GSK-3 $\beta$  kinase dose-response analysis was done for compounds LEM 11133, 11152, and 2387, which showed activity higher than 50 % at a concentration 5  $\mu$ M. LEM 11133 and 11152 had a nanomolar inhibitory activity against GSK-3 $\beta$  (LEM 11133 IC<sub>50</sub> 130 nM, LEM 11152 IC<sub>50</sub> 18 nM), which is higher than their activity against MARK4. LEM 2387 was the less active, with IC<sub>50</sub> 7.41  $\mu$ M. Staurosporine was used as a control GSK-3 $\beta$  inhibitor with an IC<sub>50</sub> value of 43.68 nM. (Fig. 29)



**Figure 29.** Dose-response curves of staurosporine, 11133, 11152, and 2387 against GSK-3 $\beta$ . Data are mean  $\pm$  sd,  $n \geq 3$ . Data were processed using the GraphPad Prism 9.5.1 software program.

### 2.3.2.9 Inhibition of MARK4-mediated tau phosphorylation

Tau peptides (R1, R2, R3, and R4) were used for the evaluation of MARK4 phosphorylation of tau protein and its inhibition. Phosphorylation was detected only for R1, R3, and R4 peptides (Fig. 30) corresponding to tau phosphorylating sites Ser262 (R1), Ser324 (R3), and Ser356 (R4).



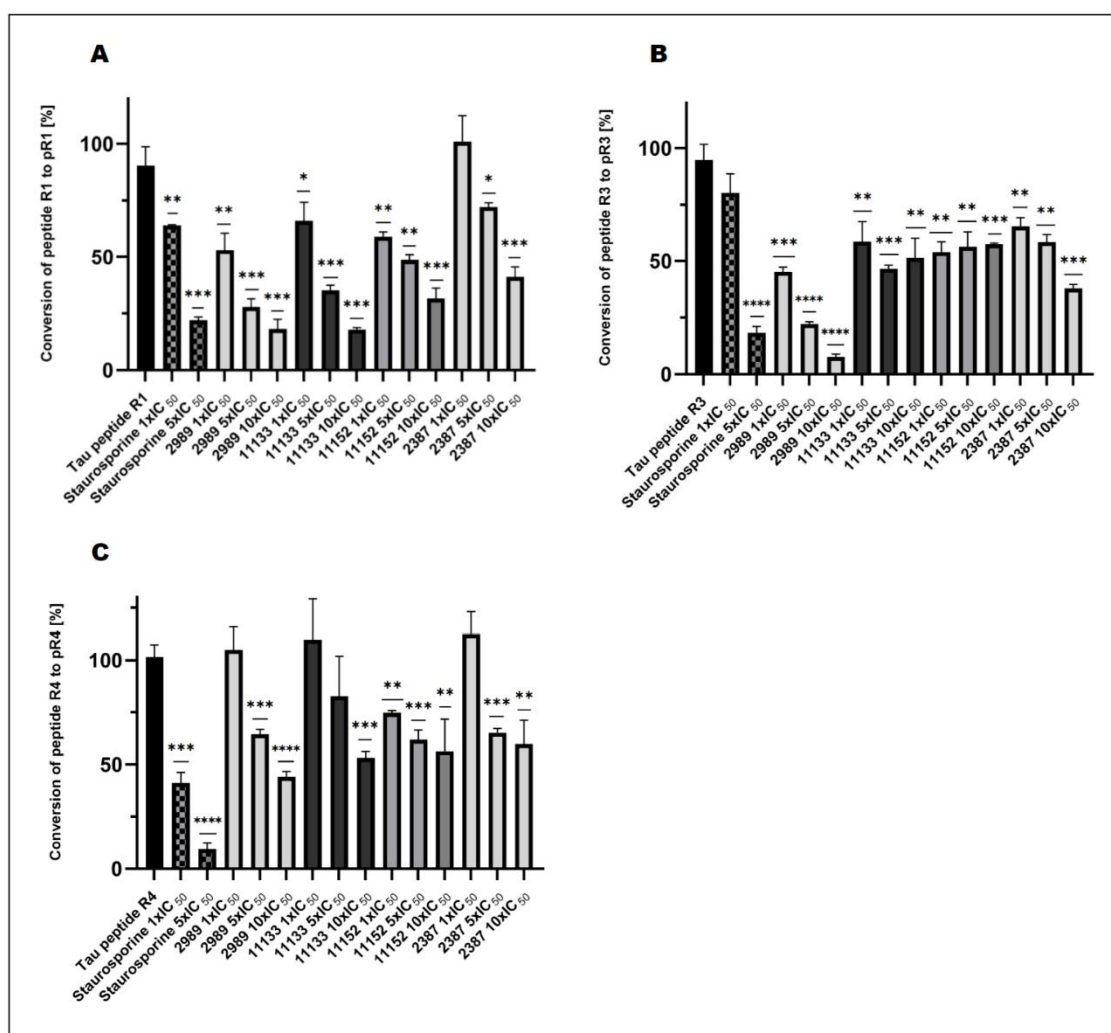
**Figure 30.** (A) Tau peptide R1 (m/z 3299,4) was detected in the assay buffer without the presence of the MARK4 enzyme and after 2 hours of incubation with MARK4. After two hours, we detected the R1 peptide and its phosphorylated form (m/z 3379,7). (B) Tau peptide R2 (m/z 3265,4) was detected in the assay buffer. There was no phosphorylated form after incubation with MARK4 for the R2-tau peptide. (C) Tau peptide R3 (m/z 3247,5) was detected in the assay buffer and its phosphorylated form (m/z 3327,5) after two hours of incubation with the MARK4 enzyme. (D) Tau peptide R4 (m/z 3468,8) was detected in the assay buffer and its phosphorylated form (m/z 3548,1) after 2 hours of incubation with the MARK4 enzyme. Data were obtained using MALDI-TOF mass spectrometry.

Since MARK4 phosphorylation was detected only for R1, R3, and R4 tau peptides, the R2 peptide was not used for inhibition experiments. Inhibitors were tested in the three concentrations corresponding to 1x, 5x, and 10x MARK4 IC<sub>50</sub>. LEM 2989 was tested in concentrations 0.95 μM, 4.75 μM, and 9.5 μM, LEM 11133 in concentrations 1.22 μM, 6.1 μM, and 12.2 μM, LEM 11152 in concentrations 1.31 μM, 6.55 μM, and 13.1 μM, and LEM 2387 in concentrations 1.63 μM, 8.15 μM, and 16.3 μM. Staurosporine was used as a control inhibitor and was tested in concentrations of 4.6 nM and 23 nM.

All four tested compounds inhibited R1-tau peptide phosphorylation, whereas compound LEM 2989 had similar inhibitory activity as staurosporine. The other compounds also showed dose-dependent inhibitory activity and inhibited MARK4-mediated R1-tau peptide phosphorylation (Fig. 31).

R3-tau peptide showed the highest conversion to a phosphorylated form among all the tested tau peptides. This phosphorylation was strongly inhibited by staurosporine and LEM 2989. Dose-dependent inhibition was also observed for 2387, but the inhibitory activity was lower than inhibition by LEM 2989 and control. LEM 11133 and 11152 also decreased the conversion of R3-tau peptide to its phosphorylated form (around 50% inhibition), but increasing the concentration did not enhance the inhibitory effect (Fig. 31).

R4-tau peptide was strongly inhibited by staurosporine, and all four tested compounds showed dose-dependent inhibitory activity. In the case of compounds LEM 2989 and 11133, there was a significant increase in their activity regarding increasing concentration. Compounds LEM 11152 and 2387 also showed inhibitory activity against R4 peptide phosphorylation, but there was no significant difference between their activity in concentration 5x and 10x IC<sub>50</sub>. (Fig. 31).



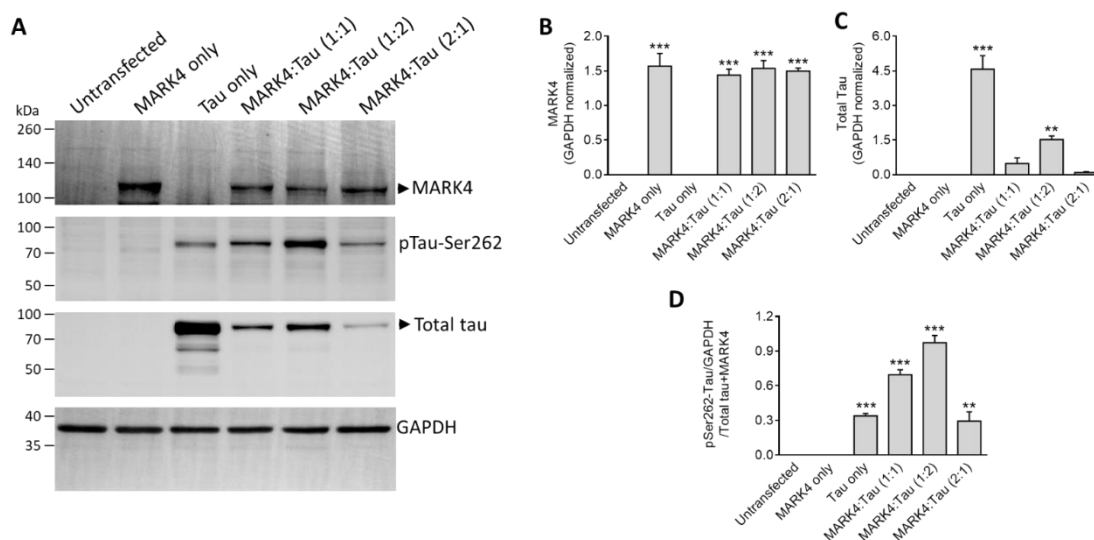
**Figure 31.** Conversion of tau peptides (A: R1 peptide; B: R3 peptide; C: R4 peptide) to their phosphorylated forms by MARK4 in the absence/presence of inhibitors (staurosporine, LEM 2989, 11133, 11152, and 2387). Results were normalized to a positive control (tau peptide without inhibitors), and graphs show mean values (n = 3) and standard deviation. Staurosporine was used as a control inhibitor. Statistical analysis was performed with an unpaired t-test: selected cell lines were compared to the parental line (CCRF-CEM or K562) at p < 0.05 using the GraphPad Prism 9.5.1 software program. We represent the level of statistical significance in this figure as follows: \*\*\*\* p-value < 0.0001, \*\*\* p-value < 0.001, \*\* p-value < 0.01, \* p-value < 0.05. For a p-value > 0.05, we consider the differences to be not significant (ns).

### 2.3.2.10 Compounds inhibit MARK4-mediated tau phosphorylation in cells

To evaluate the activity of our MARK4/GSK-3 $\beta$  inhibitors in the more complex system, we used a dual-gene expressing (MARK4 and tau) cellular model. We selected four BBB-penetrating compounds to determine if they inhibit MARK4-mediated Ser262 phosphorylation of tau protein. This evaluation was done by Dr. V. Das and Dr. N. Annadurai.

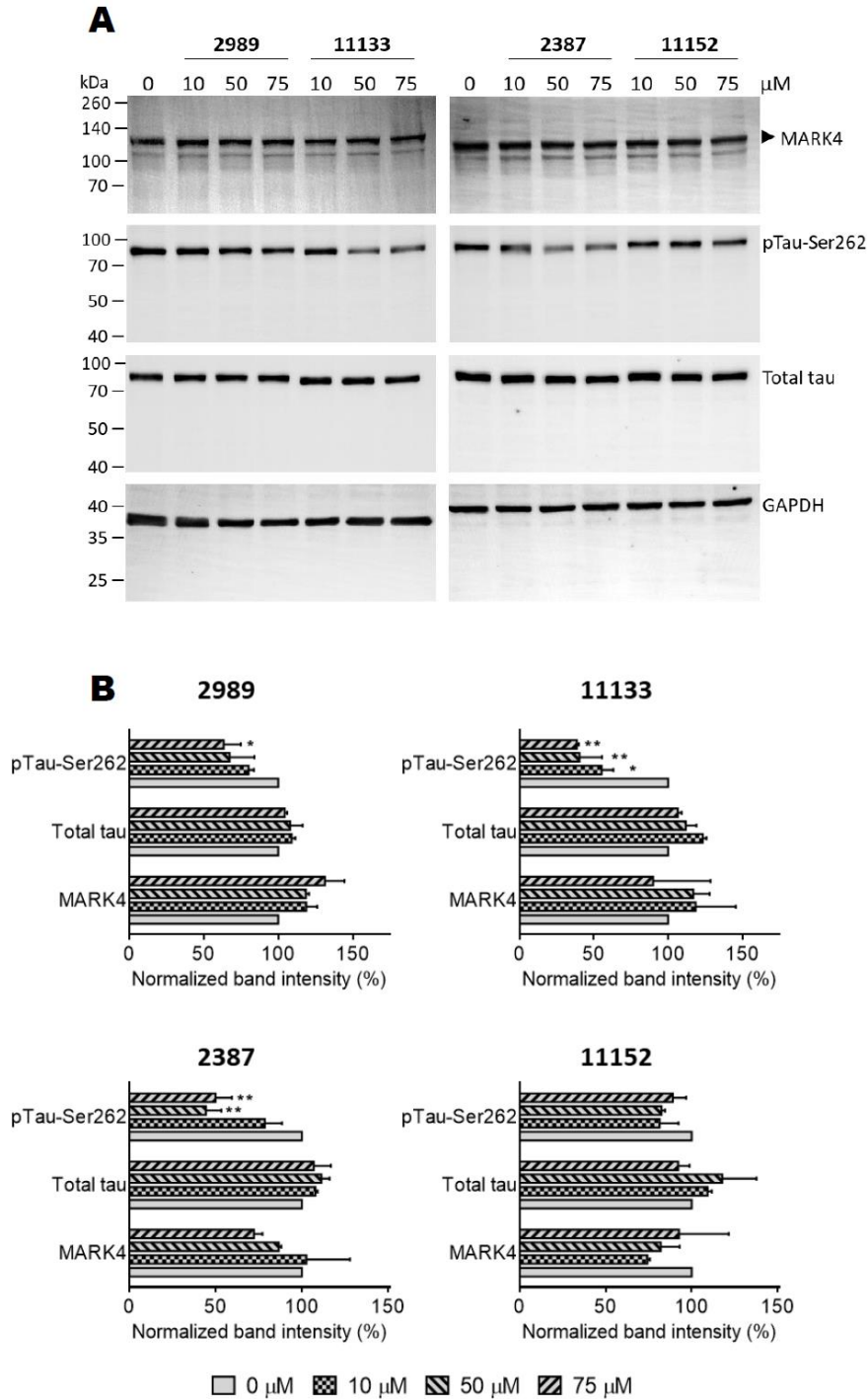
Compounds LEM 2989 and 11133 were identified as BBB-positive using the SwissADME service, whereas LEM 2387 and 11152 were identified by *in vitro* pharmacological studies. To generate the cell model, MARK4 and tau protein were

overexpressed in HEK293 cells after co-transfecting with MARK and tau protein at different ratios. Tau expression was detected in cells only when transfected with tau plasmid (Fig. 32). Although a low level of pTau-Ser262 in cells in the absence of MARK4 co-transfection was noted, this possibly resulted from the activity of the endogenous MARK4. However, pTau-Ser262 levels increased when the cells were co-transfected with MARK4 or when tau was overexpressed (Fig. X). Based on these findings, a ratio of 1:2 for MARK4 and tau co-transfection was used to study compounds' effect on pTau-Ser262 levels.



**Figure 32.** Validation of MARK4 and tau expression levels after transfection of HEK293 cells. (A) Representative immunoblots showing changes in protein levels in untransfected cells and cells transfected with 1  $\mu$ g MARK4 only, 1  $\mu$ g tau only, and co-transfected with MARK4 and Tau at 1:1 (1  $\mu$ g:1  $\mu$ g), 1:2 (500 ng:1  $\mu$ g) and 2:1 (1  $\mu$ g:500 ng) ratios. Total plasmid concentration was always  $\leq$  2  $\mu$ g. GAPDH was used as a loading control. n = 3. (B-D) Graphs showing the quantification of MARK4 (B), total tau (C), and pTau-Ser262 (D) protein levels. MARK4 and total tau band intensities were normalized to GAPDH, whereas pTau-Ser262 band intensities were first normalized to GAPDH, followed by normalizing to the normalized values of total tau + MARK4 according to the method described elsewhere.<sup>315</sup> Results are mean  $\pm$  SEM, n = 3 independent experiments. \*\*\* p-value < 0.001, \*\* p-value < 0.01, \* p-value < 0.05; One-way ANOVA, Dunnett's multiple comparisons test.

Next, cells were treated with three concentrations (10, 50, and 75  $\mu$ M) of the selected compounds for 4 hours (Fig. 33). A similar shorter treatment time has been previously reported to be effective for cell line studies.<sup>316,317</sup> While LEM 2989 reduced pTau-Ser262 levels only at the highest tested, LEM 11133 reduced pTau-Ser262 levels dose-dependently. Likewise, compound LEM 2387 effect on the level of pTau-Ser262 was evident at 50 and 75  $\mu$ M. Although LEM 11152 reduced pTau-Ser262 levels compared to the untreated controls, the effect was insignificant. None of the compounds had statistically significant impacts on MARK4 and total tau levels.



**Figure 33.** Effect of drug treatment on MARK4-mediated tau phosphorylation. (A) Representative immunoblots showing the changes in MARK4, total tau, and p-Tau-Ser262 levels following treatment of cells co-transfected with MARK4 and tau plasmids at a ratio of 1:2 with LEM 2989, 11133, 2387, and 11152 at the indicated concentrations. GAPDH was used as a loading control. The final plasmid concentration was always  $< 2 \mu\text{g}$ .  $n = 2$ . (B) Graphs showing the quantification of MARK4, total tau, and pTau-Ser262 band intensities after treatment with LEM 2989, 11133, 2387, and 11152. MARK4 and total tau band intensities were normalized to GAPDH, whereas pTau-Ser262 bands were normalized to total tau. Data are mean  $\pm$  SD,  $n = 2$ . \*\* p-value  $< 0.01$ , \* p-value  $< 0.05$ . One-way ANOVA, Dunnet's multiple comparisons test.

### 2.3.3 Discussion

#### 2.3.3.1 MALDI-TOF kinase assay

We successfully developed and optimized a new method for the detection of enzyme activity. Originally, the method was developed for MARK4 enzyme, then optimized for MARK1-3 isoforms and additionally optimized also for other kinases (polo-like kinases, PLK; aurora kinases, Aur; glycogen synthase kinase-3 alfa and beta, GSK- $\alpha$ , and  $\beta$ ). In this thesis, we used MARK1-3 and GSK-3 $\beta$  methodology. Our method combines the automatic transfer of assay components (assay buffer and ATP solution via Multidrop Combi Dispenser, enzyme, peptide, and analyzed compounds via Echo 550 acoustic dispenser), which makes the processes more precise and faster (we are able to analyze more than 1536 data points in 3-4 hours) and allows us to use low reaction volume, compare to other methods used for enzyme detection. Our reaction volume is only 2.593  $\mu$ l. The automatic transfer also decreases the risk of sample cross-contamination.

Another advantage of our method is its simplicity. Due to detection using a MALDI-TOF mass spectrometer, it was necessary to reduce the composition of the reaction buffer to the necessary minimum, at which the enzymatic reaction would still occur. The reaction comprises an assay buffer, enzyme, peptide substrate, and ATP. Due to the small reaction volume, the reaction is incubated at room temperature to avoid sample evaporation. Conversion of peptide substrate to its phosphorylated product for all tested enzymes took around 1-2 hours. Higher volume usage allows to heat the samples and thus speed up the reaction.

Using mass spectrometry for detecting enzyme activity was previously described, which confirms the suitability of using mass spectrometry for this application.<sup>318-321</sup> However, MARK4 activity was not previously tested in this way. The activity of the MARK4 enzyme is usually tested by colorimetric assays (ATPase enzyme assays).<sup>260,322</sup> Compared to these assays, mass spectrometry has a lower limit of detection, which allows the usage of lower concentrations of reagents.

#### 2.3.3.2 Screening of MARK4 inhibitors

Our developed kinase assays are standardly used for the screening of kinase inhibitors at the Institute of Molecular and Translational Medicine (IMTM) at Palacky University. In this thesis, we screened 1 238 nucleoside/ nucleobases-based analogs synthesized from 2018 to 2020 at the Institute of Organic Chemistry and Biochemistry (IOCB) of the CAS. Since compounds were screened for three years, they were divided into separate groups. Initially, a high concentration (50  $\mu$ M) was used for the primary screening to ensure we don't miss any MARK4 inhibitors. However, the dose-response analysis revealed relatively high IC<sub>50</sub> values for these

compounds, and we gradually reduced the concentration for primary screening to 20 and 10  $\mu\text{M}$ , respectively.

In total, we analyzed 1238 compounds in the primary and 445 compounds in the secondary screening, but only 20 of them had MARK4  $\text{IC}_{50}$  under 2  $\mu\text{M}$ . These compounds were further characterized for their potential toxicity, selectivity, and their ability to inhibit tau phosphorylation *in vitro*.

### **2.3.3.3 Analysis of the most active MARK4 inhibitors**

All 20 selected compounds were tested for their ability to inhibit MARK1-3. Nine of them have been identified as active inhibitors of these MARK isoforms. Since we wanted to find selective MARK4 inhibitors, these compounds were removed from the tested group, and only 11 compounds passed to the other phase of analyses (LEM 21033, 11482, 20776, 11480, 1223, 11134, 2989, 11133, 20967, 11152, 2387).

Another important parameter that was checked for these compounds was their toxicity. All compounds, except LEM 20776, were non-toxic for physiological cell lines (BJ and MRC-5). This compound also had high activity against analyzed cancer cells. The high anti-cancer activity also had compound 11133, suggesting the potential application of LEM 20776 and 11133 in both anti-cancer and neuroprotective applications.

This dual activity, neuroprotective and anti-cancer, has been previously described for many anti-cancer drugs. For example, 5-fluorouracil, which is clinically used for the treatment of solid tumors (breast, colon, pancreas, etc.) protects neuronal tissue by improving motor activities in amyotrophic lateral sclerosis.<sup>323–325</sup> Another anticancer drug, cladribine, which is used for the treatment of hematologic malignancies, has been identified to reduce demyelination in multiple sclerosis.<sup>326–328</sup> Others could be named, such as bexarotene, carmustine, dactolisib, dasatinib, paclitaxel, or lonafarnib with potential neuroprotective effect in Alzheimer's disease, erlotinib in the amyotrophic lateral sclerosis or mitoxantrone and methotrexate in multiple sclerosis.<sup>329–335</sup>

Since our MARK4 inhibitors should be used as CNS drugs, their ability to penetrate the blood-brain barrier is essential for their biological activity in the human body. We used two different approaches to analyze their potential ability to cross the BBB. The first was an analysis of *in vitro* pharmacological parameters, such as *in vitro* metabolism (chemical, plasma, and microsomal stability), binding to plasma proteins, and their *in vitro* and *in vivo* permeability using cell monolayer. In this case, the prediction of their ability to cross the BBB was based on the experimental evaluation, and only actively transporter compounds were identified as CNS positive, in this case compounds LEM 11152 and 2387.



The second approach was based on the chemical structure of the analyzed compounds. The prediction was made by the SwissADME service, which evaluates the molecular mass of compounds, their lipophilicity, TPSA, logP, number of H-bond donors and acceptors, and number of rotatable bonds and based on this data, LEM 2989 and 11133 should be able to passively pass the BBB. LEM 11133 was also identified as a potential substrate of the Pgp efflux pump, which may decrease its CNS activity. However, this should be evaluated experimentally, so this compound was not removed from the tested group.

We combined results from both approaches, and all four compounds (LEM 11152, 2387, 2989, and 11133) were tested by Carna Sciences for their ability to inhibit a panel of 50 kinases. These results showed a lot of off-targets in the case of LEM 11133 and 2387. LEM 2989 had high activity only against CK1 $\epsilon$  (casein kinase 1) and HGK (hepatocyte progenitor kinase-like/germinal center kinase-like kinase), but the best results were obtained for LEM 11152, which was identified, and GSK-3 $\beta$  and Cdk2/CycA2 inhibitor.

Based on this data, compound LEM 11152 becomes the most promising candidate. Its ability to act as a dual MARK4-GSK-3 $\beta$  may enhance its neuroprotective effect.

Since also compounds LEM 11133 and 2387 were identified to be GSK-3 $\beta$  inhibitors, we evaluated their IC<sub>50</sub> values. The highest activity (IC<sub>50</sub> 18 nM) was detected for LEM 11152, LEM 11133 was approximately 10 times less active, and LEM 2387 had IC<sub>50</sub> 7.41  $\mu$ M. This compound was the least active.

All these kinase experiments were done using commercial peptides, which suppliers recommend. To evaluate the ability of our inhibitors to reduce tau protein phosphorylation, we used tau peptides corresponding to the repeat domain (R1-R4). Each peptide included one phosphorylation site: R1-Ser262, R2-Ser293, R3-Ser324, and R4-Ser356. We optimized our MARK4 kinase assay to detect tau peptides phosphorylation, and we detected MARK4-induced phosphorylation of R1, R3, and R4 tau peptides.

Experiments with inhibitors (LEM 2989, 11133, 11152, and 2387) showed dose-dependent reduction of MARK4 phosphorylation of R1 and R4 tau peptides, whereas this trend was most significant in the case of peptide R1, which corresponds to phosphorylation at Ser262. This phosphorylation has been identified as one of the most important to AD development, and its effective inhibition can reduce pathological aggregation of the tau protein and improve neuronal viability. In the case of the R3 tau peptide, which corresponds to the phosphorylation site Ser324, which was also identified to be connected with AD development, there was strong inhibition by LEM 2989. The other compounds reduce MARK4 phosphorylation, but this inhibition was not dose-dependent, and even the highest concentration didn't increase their inhibitory effect.

Since then, all kinase experiments have been done *in vitro* using very simple reactions consisting of assay buffer, ATP, enzymes, and peptides. Evaluation of inhibitors' activity in the more complex system was needed. We used double-transfected (MARK4 and tau) cell lines and tested the inhibitory activity of Ser262 MARK4 phosphorylation in the cellular system. The highest inhibition was detected using LEM2387 and 11133. There was also a slight decrease in phosphorylation using LEM 2989. In the case of LEM 11152, there was also a decrease of Ser262 phosphorylation, but the effect was insignificant. Results can be evaluated using a longer time of incubation with inhibitors from the recent 4 hours to longer time points, such as 12, 24, 48, or 72 hours.

Based on the cellular data, LEM 2989 seems to be the most promising candidate with a low number of off-targets and good activity in all *in vitro* experiments. Due to the excellent properties of LEM 11152, its activity in the cellular system should be evaluated in longer time points, and in the case of unsatisfactory results, this compound can serve as a basis for the synthesis of new inhibitors that could show higher activity.

### 3 Summary

The aim of this dissertation was to verify the biological activity of nucleoside derivatives and confirm their applicability in antitumor and neuroprotective treatment using microtubules as a molecular drug target.

In the first part of the work, cancer cell lines resistant to well-known nucleoside-based drugs, namely cytarabine, fludarabine, and 6-thioguanine, were successfully developed. These cell lines were subsequently used to test the emergence of possible cross-resistance to other clinically used anticancer drugs and also to screen new compounds with the potential to overcome the resistant phenotype. These resistant cell lines were used as an *in vitro* model of nucleoside-based drug resistance. Some known mechanisms of resistance were confirmed, but also some new mechanisms were outlined. These mechanisms will be further investigated and verified.

In the second part of the work, the neuroprotective activity of nucleoside-based derivatives was investigated. Specifically, inhibition of enzymes involved in the pathological phosphorylation of the tau protein (MARK4, GSK-3 $\beta$ ) leads to the degeneration of microtubules in the neuronal cells, typical for Alzheimer's disease. In this work, 4 highly active MARK4 inhibitors (LEM 2989, 2387, 11133, and 11152) were identified, whereas two of these compounds (LEM 11133 and 11152) were also GSK-3 $\beta$  inhibitors with submicromolar IC<sub>50</sub> values. The activity of these compounds was verified using commercially recommended substrates and tau peptides, and inhibition of MARK4-tau phosphorylation at Ser262 was also analyzed in the cellular system. All tested compounds reduced this phosphorylation, while the highest inhibitory effect was observed for the compounds LEM 2387 and 11133. However, based on the obtained results, the most interesting compound was LEM 11152, which did not show toxicity on tumor and non-tumor cell lines, had only one detected off-target interaction (inhibition of Cdk2/CycA2), and was a dual inhibitor of MARK4 and GSK-3 $\beta$ . In the cellular experiments, it did not show such activity as the LEM 2387 and 11133, but it can be verified again using a more extended time period. Even in the case of negative results, LEM 11152 can be an interesting structure for the development of other dual MARK4-GSK-3 $\beta$  inhibitors.

## 4 Souhrn

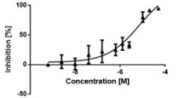
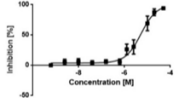
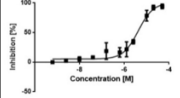
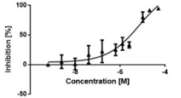
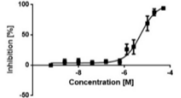
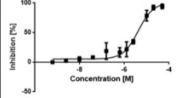
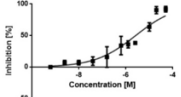
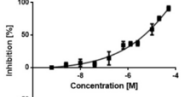
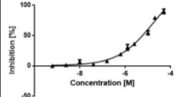
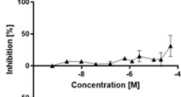
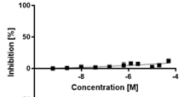
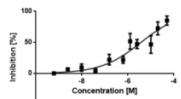
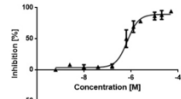
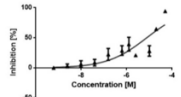
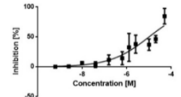
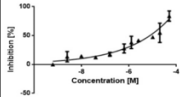
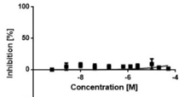
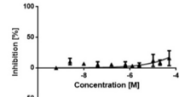
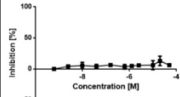
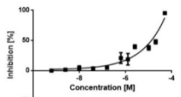
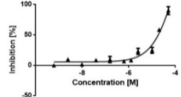
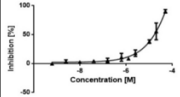
Cílem disertační práce bylo ověřit biologickou aktivitu nukleosidových derivátů, ověřit jejich aplikovatelnost do protinádorové a neuroprotektivní léčby s využitím mikrotubulů jako molekulárních cílů.

V první části práce byly úspěšně vytvořeny nádorové buněčné linie rezistentní vůči vybraným cytostatikům s nukleosidovou strukturou (cytarabin, fludarabin a 6-thioguanin). Tyto linie byly následně využity pro testování vzniku případných zkřížených rezistencí vůči dalším klinicky užívaným protinádorovým léčivům a také pro screening nových látek s potenciálem překonávat vzniklý rezistentní fenotyp. U rezistentních buněčných linií byly potvrzeny některé známé mechanismy vzniku rezistence pro konkrétní léčiva, ale byly nastíněny také některé další mechanismy, které budou dále zkoumány.

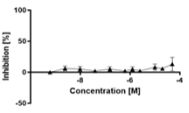
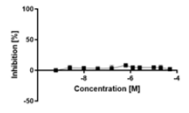

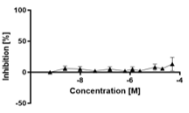
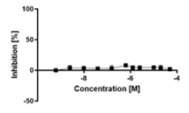

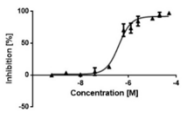
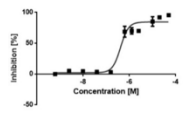
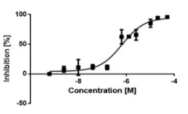
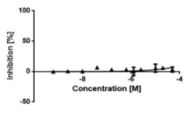
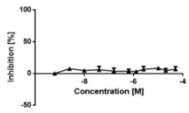
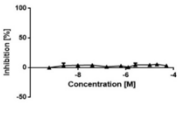
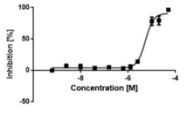
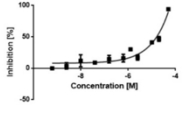
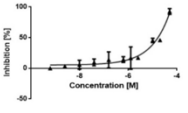
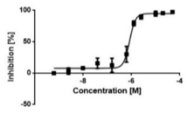
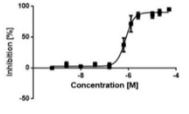
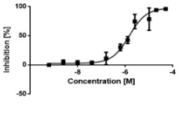
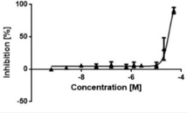
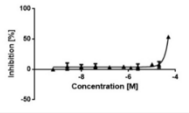
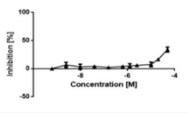
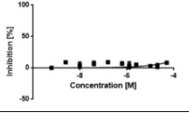
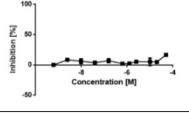
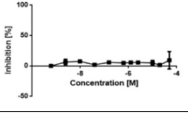
V druhé části práce byla nastíněna neuroprotektivní aktivita látek s nukleosidovou strukturou. Konkrétně v podobě inhibice enzymů zapojených do patologické fosforylace tau proteinu vedoucí k degeneraci mikrotubulů nervových buněk, například u Alzheimerovy choroby. Konkrétně se jednalo o enzymy MARK4 a GSK-3 $\beta$ . V rámci této práce byly nalezeny 4 vysoce aktivní MARK4 inhibitory (LEM 2989, 2387, 11133 a 11152), přičemž dvě z těchto látek (LEM 11133 a 11152) byly také GSK-3 $\beta$  inhibitory se submikromolární hodnotou IC<sub>50</sub>. Aktivita těchto látek byla ověřena *in vitro* s použitím komerčně doporučených substrátů, tau peptide a také v buněčném systému, kde byla ověřena fosforylace tau protein v pozici Ser262 pomocí MARK4 kinázy. Všechny testované látky snižovaly tuto fosforylaci, přičemž nejvyšší efekt byl pozorován pro látky LEM 2387 a 11133. Nejzajímavější látkou, na základě získaných výsledků, byla ovšem látka LEM 11152, která nevykazovala toxicitu na nádorových a nenádorových buněčných liniích, měla pouze jednu detekovanou of-target interakci (inhibici Cdk2/CycA2) a byla duálním inhibitorem MARK4 i GSK-3 $\beta$ . V buněčných experimentech nevykazovala takovou aktivitu jako zmíněné látky LEM 2387 a 11133, ovšem aktivita by mohla být znovu ověřena při působení v delším časovém úseku. I v případě negativních výsledků by mohla být látka LEM 11152 zajímavou vedoucí strukturou pro odvození dalších derivátů, které by mohly sloužit jako duální inhibitory MARK4 a GSK-3 $\beta$ .

## 5 Supplementary

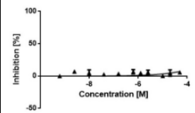
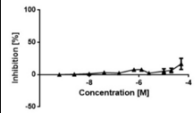
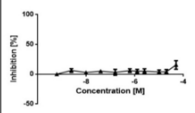
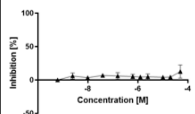
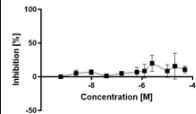
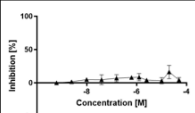
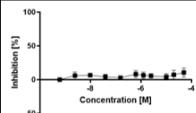
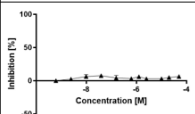
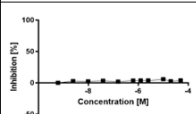
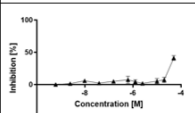
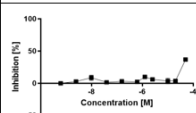
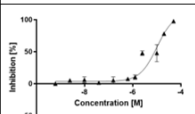
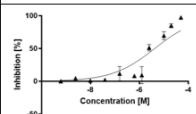
**Table 1A.** Dose-response analyses of the MARK1 inhibition. Each graph is mean  $IC_{50} \pm$  standard deviation ( $n \geq 2$ ). Data were processed, and  $IC_{50}$  was calculated using the GraphPad Prism 9.5.1 software program.

LEM code	MARK1 inhibition						Mean	sd
		$IC_{50}$ [ $\mu$ M]		$IC_{50}$ [ $\mu$ M]		$IC_{50}$ [ $\mu$ M]		
2999		7.00		5.26		4.18	5.48	1.42
2988		2.61		3.47		4.95	3.67	1.19
21033		> 50		> 50			> 50	0
2997		3.71		0.76			2.23	2.08
2994		7.63		9.95		5.13	7.57	2.41
11482		> 50		> 50		> 50	> 50	0
2695		12.32		17.78		16.08	15.39	2.79

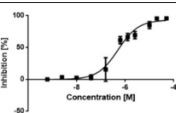
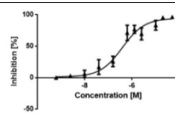
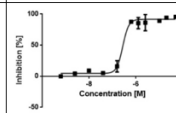
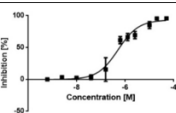
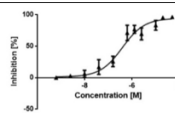
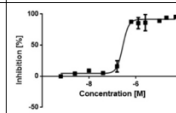
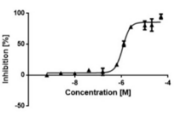
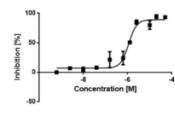
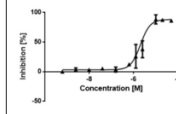
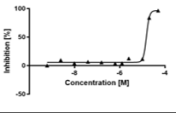
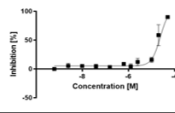
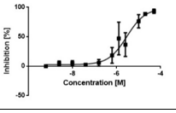
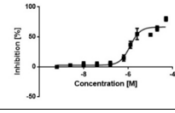
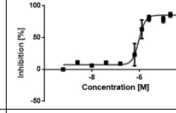
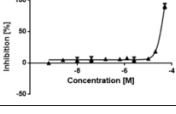
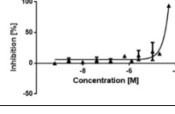
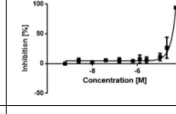
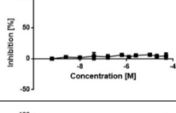
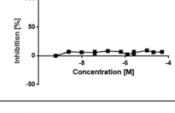
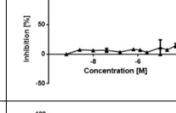
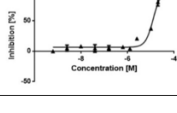
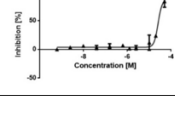
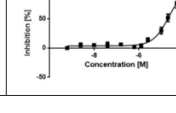
**Table 1B.** Dose-response analyses of the MARK1 inhibition. Each graph is mean  $IC_{50} \pm$  standard deviation ( $n \geq 2$ ). Data were processed, and  $IC_{50}$  was calculated using the GraphPad Prism 9.5.1 software program.

LEM code	MARK1 inhibition						Mean	sd
		$IC_{50}$ [ $\mu$ M]		$IC_{50}$ [ $\mu$ M]		$IC_{50}$ [ $\mu$ M]		
20776		> 50		> 50		> 50	0	
2990		0.39		0.41		0.65	0.48	0.14
11480		> 50		> 50		> 50	> 50	0
12737		7.08		15.38		12.41	11.62	4.20
2993		0.84		0.74		1.37	0.98	0.34
1223		32.41		46.95		> 50	43.12	9.40
11134		> 50		> 50		> 50	> 50	0

**Table 1C.** Dose-response analyses of the MARK1 inhibition. Each graph is mean  $IC_{50} \pm$  standard deviation ( $n \geq 2$ ). Data were processed, and  $IC_{50}$  was calculated using the GraphPad Prism 9.5.1 software program.

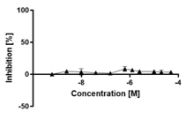
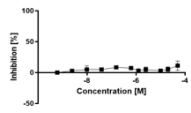
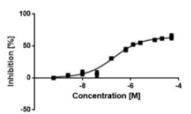
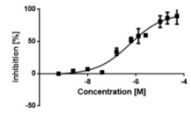
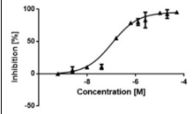
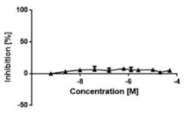
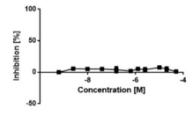
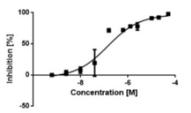
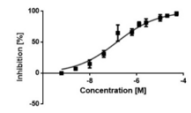
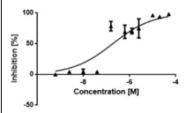
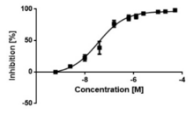
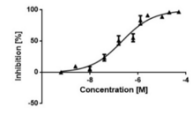
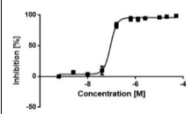
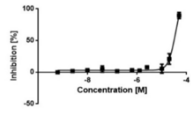
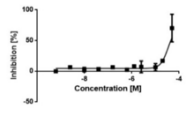
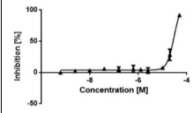
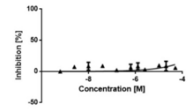
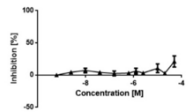
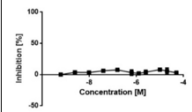
LEM code	MARK1 inhibition						Mean	sd
	$IC_{50}$ [ $\mu$ M]	$IC_{50}$ [ $\mu$ M]	$IC_{50}$ [ $\mu$ M]	$IC_{50}$ [ $\mu$ M]	$IC_{50}$ [ $\mu$ M]	$IC_{50}$ [ $\mu$ M]		
2989		> 50		> 50		> 50	> 50	0
11133		> 50		> 50			> 50	0
20967		> 50		> 50			> 50	0
11152		> 50		> 50			> 50	0
2387		> 50		> 50			> 50	0
10893		6.46		4.24			5.35	1.57

**Table 2A.** Dose-response analyses of the MARK2 inhibition. Each graph is mean  $IC_{50} \pm$  standard deviation ( $n \geq 2$ ). Data were processed, and  $IC_{50}$  was calculated using the GraphPad Prism 9.5.1 software program.

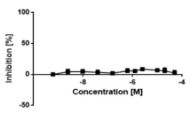
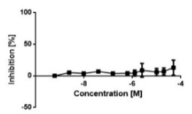
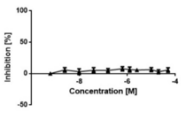
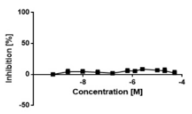
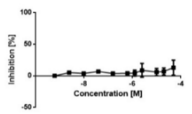
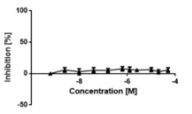
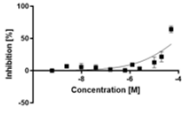
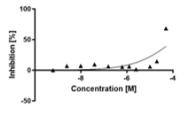
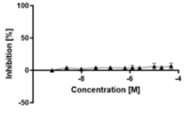
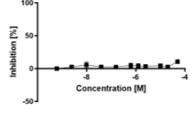
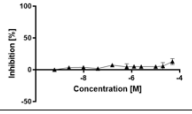
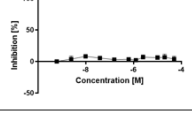
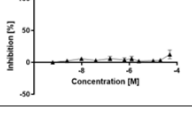
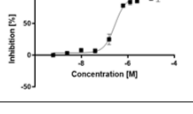
LEM code	MARK2 inhibition						Mean	sd
		$IC_{50}$ [ $\mu$ M]		$IC_{50}$ [ $\mu$ M]		$IC_{50}$ [ $\mu$ M]		
2999		0.51		0.39		0.27	0.39	0.12
2998		1.20		1.11		2.03	1.42	0.53
21033		15.14		16.92			20.87	5.58
2997		2.92		1.21		0.95	1.65	0.88
2994		42.63		38.74		45.10	42.16	3.21
11482		> 50		> 50		> 50	> 50	0
2695		12.63		25.32		21.86	19.94	6.56



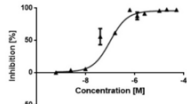
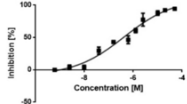
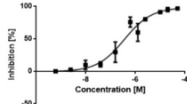
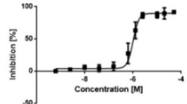
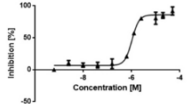
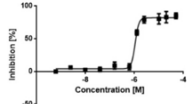
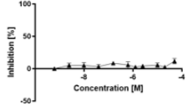
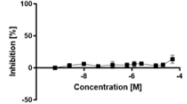
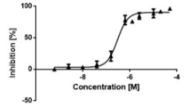
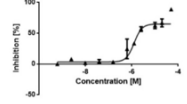
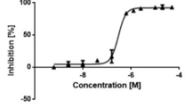
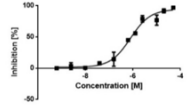
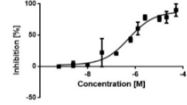
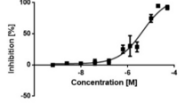
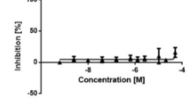
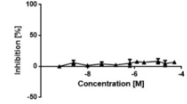
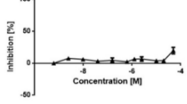
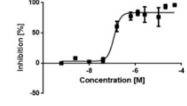
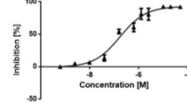
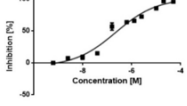
**Table 2B.** Dose-response analyses of the MARK2 inhibition. Each graph is mean  $IC_{50} \pm$  standard deviation ( $n \geq 2$ ). Data were processed, and  $IC_{50}$  was calculated using the GraphPad Prism 9.5.1 software program.

LEM code	MARK2 inhibition						Mean	sd
	$IC_{50}$ [ $\mu$ M]	$IC_{50}$ [ $\mu$ M]	$IC_{50}$ [ $\mu$ M]	$IC_{50}$ [ $\mu$ M]	$IC_{50}$ [ $\mu$ M]			
20776		> 50		> 50		> 50	0	
2990		0.20		0.56		0.17	0.31	0.22
11480		> 50		> 50		> 50	0	
12737		0.14		0.14		0.11	0.13	0.02
2993		0.05		0.20		0.088	0.11	0.08
1223		36.24		34.28		29.85	33.46	3.27
11134		> 50		> 50		> 50	> 50	0

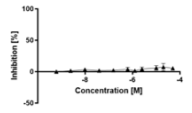
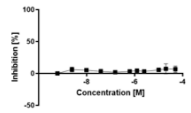
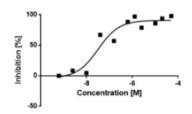
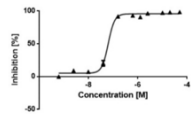
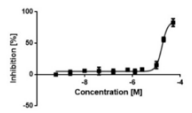
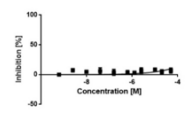
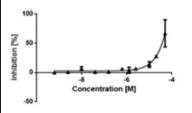
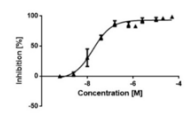
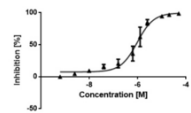
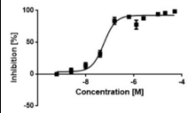
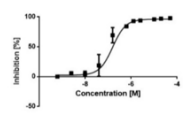
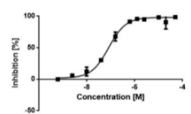
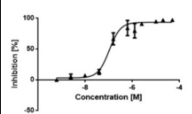
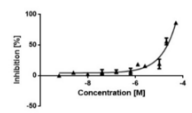
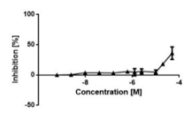
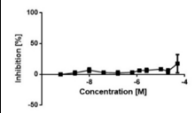
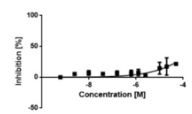
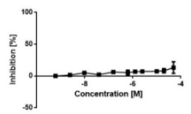
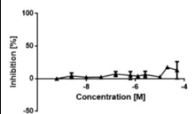
**Table 2C.** Dose-response analyses of the MARK2 inhibition. Each graph is mean  $IC_{50} \pm$  standard deviation ( $n \geq 2$ ). Data were processed, and  $IC_{50}$  was calculated using the GraphPad Prism 9.5.1 software program.

LEM code	MARK2 inhibition							
		$IC_{50}$ [ $\mu$ M]		$IC_{50}$ [ $\mu$ M]		$IC_{50}$ [ $\mu$ M]	Mean	sd
2989		> 50		> 50		> 50	> 50	0
11133		49.89		42.53			46.21	5.2
20967		> 50		> 50			> 50	0
11152		> 50		> 50			> 50	0
2387		> 50					> 50	0
10893		0.28		0.20			0.24	0.06

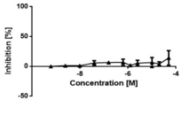
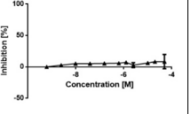
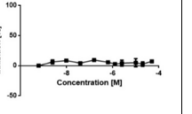
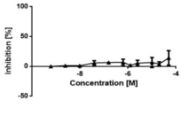
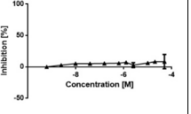
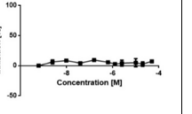
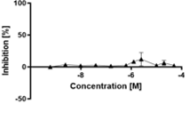
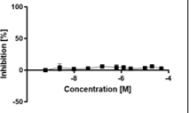
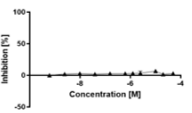
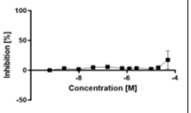
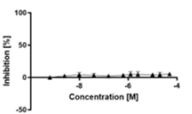
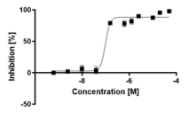
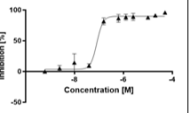
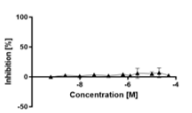
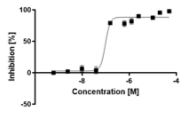
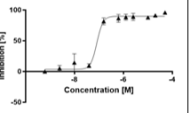
**Table 3A.** Dose-response analyses of the MARK3 inhibition. Each graph is mean  $IC_{50} \pm$  standard deviation ( $n \geq 2$ ). Data were processed, and  $IC_{50}$  was calculated using the GraphPad Prism 9.5.1 software program.

LEM code	MARK3 inhibition						Mean	sd
	$IC_{50}$ [ $\mu$ M]	$IC_{50}$ [ $\mu$ M]	$IC_{50}$ [ $\mu$ M]	$IC_{50}$ [ $\mu$ M]	$IC_{50}$ [ $\mu$ M]			
2999		0.10		0.42		0.36	0.29	0.17
2998		1.01		1.04		1.07	1.04	0.03
21033		> 50		> 50			> 50	0
2997		0.42		1.26		0.29	1.02	0.84
2994		0.78		0.53		2.07	1.75	1.41
11482		> 50		> 50		> 50	> 50	0
2695		0.12		0.16		0.22	0.17	0.05

**Table 3B.** Dose-response analyses of the MARK3 inhibition. Each graph is mean  $IC_{50} \pm$  standard deviation ( $n \geq 2$ ). Data were processed, and  $IC_{50}$  was calculated using the GraphPad Prism 9.5.1 software program.

LEM code	MARK3 inhibition						Mean	sd
	$IC_{50}$ [ $\mu$ M]	$IC_{50}$ [ $\mu$ M]	$IC_{50}$ [ $\mu$ M]	$IC_{50}$ [ $\mu$ M]	$IC_{50}$ [ $\mu$ M]			
20776		> 50		> 50		> 50	0	
2990		0.13		0.63		0.38	0.35	
11480		17.02		> 50		49.38	38.80	18.86
12737		0.02		0.95		0.06	0.34	0.53
2993		0.16		0.08		0.10	0.11	0.04
1223		22.61		> 50		> 50	40.87	15.81
11134		> 50		> 50		> 50	> 50	0

**Table 3C.** Dose-response analyses of the MARK3 inhibition. Each graph is mean  $IC_{50} \pm$  standard deviation ( $n \geq 2$ ). Data were processed, and  $IC_{50}$  was calculated using the GraphPad Prism 9.5.1 software program.

LEM code	MARK3 inhibition							
		$IC_{50}$ [ $\mu$ M]		$IC_{50}$ [ $\mu$ M]		$IC_{50}$ [ $\mu$ M]	Mean	sd
2989		> 50		> 50		> 50	> 50	0
11133		> 50		> 50			> 50	0
20967		> 50		> 50			> 50	0
11152		> 50		0.10		0.11	0.11	001
2387		> 50					> 50	0
10893		0.10		0.11			0.11	001

## 6 Abbreviations

6-MMPT	6-methyl-mercaptopurine
6-MP	6-mercaptopurine
6-TG	6-thioguanine
6-TIMP	6-thioinosine-5-monophosphate
ABC	ATP-binding cassette
AD	Alzheimer's disease
ADCs	Drug-conjugated antibodies
AChE	Acetylcholinesterase
AK	Adenylate kinase
Akt	Protein kinase B
ALL	Acute lymphoblastic leukemia
AML	Acute myeloid leukemia
ANLL	Acute non-lymphocytic leukemia
ApDCs	Aptamer-drug conjugates
Ara-C	Cytarabine
Ara-CDP	Cytarabine diphosphate
Ara-CMP	Cytarabine monophosphate
Ara-CTP	Cytarabine triphosphate
Ara-U	Uracil arabinose
ATP	Adenosine triphosphate
AZA	Azathioprine
BBB	Blood-brain barrier
BCB	Blood-cerebrospinal fluid barrier
BCRP	Breast cancer resistance protein
BRCA	Breast cancer gene
cAMP	Cyclic adenosine monophosphate
CBD	Corticobasal degeneration
CD73	Ecto-5-nucleotidase, S-NT
CDA	Cytidine deaminase
Cdk2	Cyclin-dependent kinase 2
Cdk5	Cyclin-dependent kinase 5
cGMP	Cyclic guanosine monophosphate
CK1 $\epsilon$	Casein kinase 1
CLL	Chronic lymphocytic leukemia
CN-II	5-nucleotidase
CNS	Central neuronal system
CNT	Concentrative nucleoside transporter
dCK	Deoxycytidine kinase
dFdC	Gemcitabine
dFdCDP	Gemcitabine diphosphate
dFdCMP	Gemcitabine monophosphate
dFdCTP	Gemcitabine triphosphate
DMSO	Dimethyl sulfoxide
DNA	Deoxyribonucleic acid
dNT-1	Deoxynucleotidase-1
ENT	Equilibrative nucleoside transporter

Erk	Extracellular signal-regulated kinase
ERK2	Extracellular signal-regulated kinase 2
F-ara-ADP	Fludarabine diphosphate
F-ara-AMP	Fludarabine monophosphate
F-ara-ATP	Fludarabine triphosphate
FDA	U.S. Food and Drug Administration
GAPDH	Glyceraldehyde-3-phosphate dehydrogenase
GIT	Gastrointestinal tract
GSC	Glucosylceramide synthase
GSH	Glutathione
GSK-3 $\beta$	Glycogen synthase kinase 3 $\beta$
HGK	Hepatocyte progenitor kinase-like/ germinal center kinase-like kinase
HGPRT	Hypoxanthine-guanine phosphoribosyltransferase
HH	Hedgehog pathway
HIV	Human immunodeficiency virus
HRP	Horseradish peroxidase
IC <sub>50</sub>	Half maximal inhibitory concentration
IMPDH	Inosine-5-monophosphate dehydrogenase
IMTM	Institute of Molecular and Translational Medicine at Palacky University
IOCB	Institute of Organic Chemistry and Biochemistry
ITPA	Inosine triphosphatase
LKB1	Liver kinase 1
logP	Octanol-water partition coefficient
LRP	Lung resistance-related protein
MAP	Microtubule-associated protein
MAPT	Microtubule-associated protein tau
MARK	Microtubule-affinity regulating kinase
MDR	Multidrug resistance
MGMT	Methylguanine-DNA methyltransferase
MOC	Mechanisms of chemoresistance
MRP	Multidrug resistance-associated protein
mTOR	Mammalian target of rapamycin
MTS	3-(4,5-dimethylthiazol-2-yl)-5-(3-carboxymethoxyphenyl)-2-(4-sulfophenyl)-2h-tetrazolium
MXR	Mitoxantrone resistance-associated protein
NDPK	Nucleotide diphosphate kinase
NMPK	Nucleotide monophosphate kinase
Notch1	Neurogenic locus notch homolog protein 1
NPs	Nanoparticles
NT5C2	Cytosolic-5-nucleotidase II
NUD15	Nudix hydrolase 15
p-70S6K	Ribosomal protein S6 kinase
PAMPA	Parallel artificial membrane permeability assay
PARP	Poly (ADP-ribose) polymerase
PCR	Polymerase chain reaction
PDACs	Pancreatic ductal adenocarcinoma cells
PDMP	1-phenyl-2-decanoylamino-3-morpholino-1-propanol
PEITC	$\beta$ -phenetyl isothiocyanate
Pgp	P-glycoprotein

PJS	Peutz-Jeghers syndrome
PLGA	Poly(lactic-co-glycolic) acid
PNS	Peripheral neuronal system
PP1	Phosphatase 1
PSP	Progressive supranuclear palsy
PXE	Pseudoxanthoma elasticum
RNA	Ribonucleic acid
ROS	Reactive oxygen species
rpS6	S6 ribosomal protein
SAMHD1	SAM and HD domain-containing protein 1
SLC	Solute-carrier
STAT3	Signal transducer and activator of transcription 3
TAT	Trans-activating transcription factor
TBST	Tris-buffered saline with Tween 20
TGDP	6-thioguanine diphosphate
TGTP	6-thioguanine triphosphate
TPMT	Thiopurine-S-methyltransferase
TPSA	Topological polar surface area
VEGFR	Vascular endothelial growth factor receptor
Wnt	Wingless-related integration site
XO	Xanthine oxidase



## 7 References

1. Saenger, W. Structure and function of nucleosides and nucleotides. *Angew Chem Int Ed Engl* **12**, 591–601 (1973).
2. Kataev, V. E. & Garifullin, B. F. Antiviral nucleoside analogs. *Chem Heterocycl Compd (N Y)* **57**, 326–341 (2021).
3. Jordheim, L. P., Durantel, D., Zoulim, F. & Dumontet, C. Advances in the development of nucleoside and nucleotide analogues for cancer and viral diseases. *Nat Rev Drug Discov* **12**, 447–464 (2013).
4. Herdewijn, P. Biologically Active Nucleosides. *Curr Protoc Nucleic Acid Chem* **28**, 1401 (2007).
5. Elion, G. B. An overview of the role of nucleosides in chemotherapy. *Adv Enzyme Regul* **24**, 323–334 (1985).
6. Deval, J., Symons, J. A. & Beigelman, L. Inhibition of viral RNA polymerases by nucleoside and nucleotide analogs: therapeutic applications against positive-strand RNA viruses beyond hepatitis C virus. *Curr Opin Virol* **9**, 1 (2014).
7. Raju, T. N. The Nobel chronicles. 1988: James Whyte Black, (b 1924), Gertrude Elion (1918-99), and George H Hitchings (1905-98). *Lancet* **355**, 1022 (2000).
8. Adam de Beaumais, T. *et al.* Determinants of mercaptopurine toxicity in paediatric acute lymphoblastic leukemia maintenance therapy. *Br J Clin Pharmacol* **71**, 575 (2011).
9. Zgheib, N. K. *et al.* NUDT15 and TPMT genetic polymorphisms are related to 6-mercaptopurine intolerance in children treated for acute lymphoblastic leukemia at the Children’s Cancer Center of Lebanon. *Pediatr Blood Cancer* **64**, 146–150 (2017).
10. Vora, A. *et al.* Toxicity and efficacy of 6-thioguanine versus 6-mercaptopurine in childhood lymphoblastic leukaemia: a randomised trial. *Lancet* **368**, 1339–1348 (2006).
11. ELION, G. B. The George Hitchings and Gertrude Elion Lecture. The pharmacology of azathioprine. *Ann N Y Acad Sci* **685**, 401–407 (1993).
12. Van Scoik, K. G., Johnson, C. A. & Porter, W. R. The pharmacology and metabolism of the thiopurine drugs 6-mercaptopurine and azathioprine. *Drug Metab Rev* **16**, 157–174 (1985).
13. Hrubá, L., Das, V., Hajdúch, M. & Dzubak, P. Nucleoside-based anticancer drugs: mechanism of action and drug resistance. *Biochem Pharmacol* **215**, 115741 (2023).
14. Greaves, M. & Maley, C. C. CLONAL EVOLUTION IN CANCER. *Nature* **481**, 306 (2012).
15. Torgovnick, A. & Schumacher, B. DNA repair mechanisms in cancer development and therapy. *Front Genet* **6**, (2015).
16. Wang, W. *et al.* Dynamics between Cancer Cell Subpopulations Reveals a Model Coordinating with Both Hierarchical and Stochastic Concepts. *PLoS One* **9**, (2014).
17. Tie, J. *et al.* Circulating tumor DNA analysis detects minimal residual disease and predicts recurrence in patients with stage II colon cancer. *Sci Transl Med* **8**, (2016).

18. Marin, J. J. G. *et al.* Molecular bases of drug resistance in hepatocellular carcinoma. *Cancers (Basel)* **12**, 1–26 (2020).
19. Zheng, H. C. The molecular mechanisms of chemoresistance in cancers. *Oncotarget* **8**, 59950 (2017).
20. Pastor-Anglada, M. & Pérez-Torras, S. Emerging Roles of Nucleoside Transporters. *Front Pharmacol* **9**, (2018).
21. Baldwin, S. A. *et al.* The equilibrative nucleoside transporter family, SLC29. *Pflugers Archiv European Journal of Physiology* vol. 447 735–743 Preprint at <https://doi.org/10.1007/s00424-003-1103-2> (2004).
22. Jennings, L. L. *et al.* Distinct regional distribution of human equilibrative nucleoside transporter proteins 1 and 2 (hENT1 and hENT2) in the central nervous system. *Neuropharmacology* **40**, 722–731 (2001).
23. Griffiths, M. *et al.* Cloning of a human nucleoside transporter implicated in the cellular uptake of adenosine and chemotherapeutic drugs. *Nat Med* **3**, 89–93 (1997).
24. Conklin, L. S. *et al.* 6-mercaptopurine transport in human lymphocytes: Correlation with drug-induced cytotoxicity. *J Dig Dis* **13**, 82 (2012).
25. Macanas-Pirard, P. *et al.* Resistance of leukemia cells to cytarabine chemotherapy is mediated by bone marrow stroma, involves cell-surface equilibrative nucleoside transporter-1 removal and correlates with patient outcome. *Oncotarget* **8**, 23073 (2017).
26. Molina-Arcas, M. *et al.* Fludarabine uptake mechanisms in B-cell chronic lymphocytic leukemia. *Blood* **101**, 2328–2334 (2003).
27. Naes, S. M., Ab-Rahim, S., Mazlan, M. & Rahman, A. A. Equilibrative Nucleoside Transporter 2: Properties and Physiological Roles. *Biomed Res Int* **2020**, (2020).
28. Damaraju, V. L. *et al.* Role of human nucleoside transporters in the uptake and cytotoxicity of azacitidine and decitabine. *Nucleosides Nucleotides Nucleic Acids* **31**, 236–255 (2012).
29. Ward, J. L., Sherali, A., Mo, Z. P. & Tse, C. M. Kinetic and pharmacological properties of cloned human equilibrative nucleoside transporters, ENT1 and ENT2, stably expressed in nucleoside transporter-deficient PK15 cells. Ent2 exhibits a low affinity for guanosine and cytidine but a high affinity for inosine. *J Biol Chem* **275**, 8375–8381 (2000).
30. Govindarajan, R. *et al.* In situ hybridization and immunolocalization of concentrative and equilibrative nucleoside transporters in the human intestine, liver, kidneys, and placenta. *Am J Physiol Regul Integr Comp Physiol* **293**, (2007).
31. Senyavina, N. V., Gerasimenko, T. N., Fomicheva, K. A., Tonevitskaya, S. A. & Kaprin, A. D. Localization and Expression of Nucleoside Transporters ENT1 and ENT2 in Polar Cells of Intestinal Epithelium. *Bull Exp Biol Med* **160**, 771–774 (2016).
32. Fotoohi, A. K., Lindqvist, M., Peterson, C. & Albertioni, F. Involvement of the concentrative nucleoside transporter 3 and equilibrative nucleoside transporter 2 in the resistance of T-lymphoblastic cell lines to thiopurines. *Biochem Biophys Res Commun* **343**, 208–215 (2006).

33. Gray, J. H., Owen, R. P. & Giacomini, K. M. The concentrative nucleoside transporter family, SLC28. *Pflugers Arch* **447**, 728–734 (2004).
34. Govindarajan, R. *et al.* Facilitated mitochondrial import of antiviral and anticancer nucleoside drugs by human equilibrative nucleoside transporter-3. *Am J Physiol Gastrointest Liver Physiol* **296**, (2009).
35. Baldwin, S. A. *et al.* Functional characterization of novel human and mouse equilibrative nucleoside transporters (hENT3 and mENT3) located in intracellular membranes. *J Biol Chem* **280**, 15880–15887 (2005).
36. Govindarajan, R. *et al.* Facilitated mitochondrial import of antiviral and anticancer nucleoside drugs by human equilibrative nucleoside transporter-3. *Am J Physiol Gastrointest Liver Physiol* **296**, (2009).
37. Hsu, C. L. *et al.* Equilibrative nucleoside transporter 3 deficiency perturbs lysosome function and macrophage homeostasis. *Science* **335**, 89–92 (2012).
38. Wei, C. W. *et al.* Equilibrative Nucleoside Transporter 3 Regulates T Cell Homeostasis by Coordinating Lysosomal Function with Nucleoside Availability. *Cell Rep* **23**, 2330–2341 (2018).
39. Liu, B. *et al.* Equilibrative nucleoside transporter 3 depletion in  $\beta$ -cells impairs mitochondrial function and promotes apoptosis: Relationship to pigmented hypertrichotic dermatosis with insulin-dependent diabetes. *Biochimica et Biophysica Acta (BBA) - Molecular Basis of Disease* **1852**, 2086–2095 (2015).
40. Young, J. D., Yao, S. Y. M., Baldwin, J. M., Cass, C. E. & Baldwin, S. A. The human concentrative and equilibrative nucleoside transporter families, SLC28 and SLC29. *Mol Aspects Med* **34**, 529–547 (2013).
41. E. Parkinson, F. *et al.* Molecular biology of nucleoside transporters and their distributions and functions in the brain. *Curr Top Med Chem* **11**, 948–972 (2011).
42. Zhu, S. *et al.* Luteolin shows antidepressant-like effect by inhibiting and downregulating plasma membrane monoamine transporter (PMAT, Slc29a4). *J Funct Foods* **54**, 440–448 (2019).
43. Hermann, R. *et al.* Review of Transporter Substrate, Inhibitor, and Inducer Characteristics of Cladribine. *Clin Pharmacokinet* **60**, 1509–1535 (2021).
44. Wright, N. J. & Lee, S. Y. Toward a Molecular Basis of Cellular Nucleoside Transport in Humans. *Chem Rev* **121**, 5336 (2021).
45. Gray, J. H. *et al.* Functional and genetic diversity in the concentrative nucleoside transporter, CNT1, in human populations. *Mol Pharmacol* **65**, 512–519 (2004).
46. Choi, M. K., Kim, M. H., Maeng, H. J. & Song, I. S. Contribution of CNT1 and ENT1 to ribavirin uptake in human hepatocytes. *Arch Pharm Res* **38**, 904–913 (2015).
47. Ashraf, T., Kao, A. & Bendayan, R. Functional Expression of Drug Transporters in Glial Cells: Potential Role on Drug Delivery to the CNS. *Adv Pharmacol* **71**, 45–111 (2014).
48. Persaud, A. K. *et al.* Increased renal elimination of endogenous and synthetic pyrimidine nucleosides in concentrative nucleoside transporter 1 deficient mice. *Nature Communications* **2023 14:1** **14**, 1–19 (2023).

49. Minami, K. *et al.* Ribonucleotide reductase is an effective target to overcome gemcitabine resistance in gemcitabine-resistant pancreatic cancer cells with dual resistant factors. *J Pharmacol Sci* **127**, 319–325 (2015).
50. Huber-Ruano, I., Pinilla-Macua, I., Torres, G., Casado, F. J. & Pastor-Anglada, M. Link between high-affinity adenosine concentrative nucleoside transporter-2 (CNT2) and energy metabolism in intestinal and liver parenchymal cells. *J Cell Physiol* **225**, 620–630 (2010).
51. Cass, C. E., Baldwin, S. A. & Young, J. CNT2, concentrative nucleoside transporter 2. *xPharm: The Comprehensive Pharmacology Reference* 1–4 (2007) doi:10.1016/B978-008055232-3.60462-3.
52. Errasti-murugarren, E., Pastor-Anglada, M. & Casado, F. J. Role of CNT3 in the transepithelial flux of nucleosides and nucleoside-derived drugs. *Journal of Physiology* **582**, 1249–1260 (2007).
53. Sartorelli, A. C., LePage, G. A. & Moore, E. C. Metabolic Effects of 6-Thioguanine: I. Studies on Thioguanine-resistant and sensitive Ehrlich Ascites Cells. *Cancer Res* **18**, 1232–1239 (1958).
54. Ahmed Juvale, I. I., Abdul Hamid, A. A., Abd Halim, K. B. & Che Has, A. T. P-glycoprotein: new insights into structure, physiological function, regulation and alterations in disease. *Heliyon* **8**, e09777 (2022).
55. Aryal, M. *et al.* Effects on P-Glycoprotein Expression after Blood-Brain Barrier Disruption Using Focused Ultrasound and Microbubbles. *PLoS One* **12**, e0166061 (2017).
56. Bart, J. *et al.* The distribution of drug-efflux pumps, P-gp, BCRP, MRP1 and MRP2, in the normal blood-testis barrier and in primary testicular tumours. *Eur J Cancer* **40**, 2064–2070 (2004).
57. Prachayasittikul, V. & Prachayasittikul, V. P-glycoprotein transporter in drug development. *EXCLI J* **15**, 113–118 (2016).
58. Zhou, S. F. Structure, function and regulation of P-glycoprotein and its clinical relevance in drug disposition. *Xenobiotica* **38**, 802–832 (2008).
59. Liu, X. D. & Liu, G. Q. P glycoprotein regulated transport of glutamate at blood brain barrier. *Acta Pharmacol Sin* **22**, 111–116 (2001).
60. Yano, K., Seto, S., Kamioka, H., Mizoi, K. & Ogihara, T. Testosterone and androstenedione are endogenous substrates of P-glycoprotein. *Biochem Biophys Res Commun* **520**, 166–170 (2019).
61. McCormick, J. W., Ammerman, L., Chen, G., Vogel, P. D. & Wise, J. G. Transport of Alzheimer's associated amyloid- $\beta$  catalyzed by P-glycoprotein. *PLoS One* **16**, (2021).
62. Pawarode, A. *et al.* Differential effects of the immunosuppressive agents cyclosporin A, tacrolimus and sirolimus on drug transport by multidrug resistance proteins. *Cancer Chemother Pharmacol* **60**, 179–188 (2007).
63. Jiang, B., Yan, L. J. & Wu, Q. ABCB1 (C1236T) Polymorphism Affects P-Glycoprotein-Mediated Transport of Methotrexate, Doxorubicin, Actinomycin D, and Etoposide. *DNA Cell Biol* **38**, 485–490 (2019).

64. Luna-Tortós, C., Fedrowitz, M. & Löscher, W. Several major antiepileptic drugs are substrates for human P-glycoprotein. *Neuropharmacology* **55**, 1364–1375 (2008).
65. Hermann, R. *et al.* The Clinical Pharmacology of Cladribine Tablets for the Treatment of Relapsing Multiple Sclerosis. *Clin Pharmacokinet* **58**, 283–297 (2019).
66. Chen, Y. *et al.* Discovery of novel multidrug resistance protein 4 (MRP4) inhibitors as active agents reducing resistance to anticancer drug 6-Mercaptopurine (6-MP) by structure and ligand-based virtual screening. *PLoS One* **13**, e0205175 (2018).
67. Flens, M. J. *et al.* Tissue Distribution of the Multidrug Resistance Protein. *American Journal of Pathology* **148**, (1996).
68. Sodani, K., Patel, A., Kathawala, R. J. & Chen, Z. S. Multidrug resistance associated proteins in multidrug resistance. *Chin J Cancer* **31**, 58 (2012).
69. Lingineni, K., Belekar, V., Tangadpalliwar, S. R. & Garg, P. The role of multidrug resistance protein (MRP-1) as an active efflux transporter on blood-brain barrier (BBB) permeability. *Mol Divers* **21**, 355–365 (2017).
70. Jedlitschky, G. *et al.* Transport of glutathione, glucuronate, and sulfate conjugates by the MRP gene-encoded conjugate export pump. *Cancer Res* (1996).
71. Zaman, G. J. R., Cnubben, N. H. P., Van Bladeren, P. J., Evers, R. & Borst, P. Transport of the glutathione conjugate of ethacrynic acid by the human multidrug resistance protein MRP. *FEBS Lett* **391**, 126130–17327 (1996).
72. Cole, S. P. C. *et al.* Overexpression of a transporter gene in a multidrug-resistant human lung cancer cell line. *Science* **258**, 1650–1654 (1992).
73. Zhang, W., Clair, D. S., Butterfield, A. & Vore, M. Loss of Mrp1 Potentiates Doxorubicin-Induced Cytotoxicity in Neonatal Mouse Cardiomyocytes and Cardiac Fibroblasts. *Toxicological Sciences* **151**, 44 (2016).
74. Zeng, H., Chen, Z. S., Belinsky, M., Rea, P. A. & Kruh, G. Transport of methotrexate (MTX) and folates by multidrug resistance protein (MRP) 3 and MRP1: effect of polyglutamylation on MTX transport. *Cancer Res* (2001).
75. Potschka, H., Fedrowitz, M. & Löscher, W. Multidrug resistance protein MRP2 contributes to blood-brain barrier function and restricts antiepileptic drug activity. *J Pharmacol Exp Ther* **306**, 124–131 (2003).
76. Dahan, A. & Amidon, G. L. Small intestinal efflux mediated by MRP2 and BCRP shifts sulfasalazine intestinal permeability from high to low, enabling its colonic targeting. *Am J Physiol Gastrointest Liver Physiol* **297**, (2009).
77. Notenboom, S. *et al.* Increased apical insertion of the multidrug resistance protein 2 (MRP2/ABCC2) in renal proximal tubules following gentamicin exposure. *J Pharmacol Exp Ther* **318**, 1194–1202 (2006).
78. Hagenbuch, B. MRP2, multiple drug resistance protein 2. *xPharm: The Comprehensive Pharmacology Reference* 1–5 (2007) doi:10.1016/B978-008055232-3.60470-2.
79. König, J., Rost, D., Cui, Y. & Keppler, D. Characterization of the human multidrug resistance protein isoform MRP3 localized to the basolateral hepatocyte membrane. *Hepatology* **29**, 1156–1163 (1999).

80. Sedláková, I. *et al.* Clinical significance of the resistance proteins LRP, Pgp, MRP1, MRP3, and MRP5 in epithelial ovarian cancer. *International Journal of Gynecological Cancer* **25**, 236–243 (2015).
81. Benderra, Z. *et al.* MRP3, BCRP, and P-glycoprotein activities are prognostic factors in adult acute myeloid leukemia. *Clin Cancer Res* **11**, 7764–7772 (2005).
82. Kool, M. *et al.* MRP3, an organic anion transporter able to transport anti-cancer drugs. *Proc Natl Acad Sci U S A* **96**, 6914–6919 (1999).
83. Robertson, S., Penzak, S. R. & Huang, S. M. Drug Interactions. *Principles of Clinical Pharmacology, Third Edition* 239–257 (2012) doi:10.1016/B978-0-12-385471-1.00015-5.
84. Hagenbuch, B. MRP4, multiple drug resistance protein 4. *xPharm: The Comprehensive Pharmacology Reference* 1–3 (2007) doi:10.1016/B978-008055232-3.60472-6.
85. Reid, G. *et al.* Characterization of the transport of nucleoside analog drugs by the human multidrug resistance proteins MRP4 and MRP5. *Mol Pharmacol* **63**, 1094–1103 (2003).
86. Russel, F. G. M., Koenderink, J. B. & Masereeuw, R. Multidrug resistance protein 4 (MRP4/ABCC4): a versatile efflux transporter for drugs and signalling molecules. *Trends Pharmacol Sci* **29**, 200–207 (2008).
87. Sampath, J. *et al.* Role of MRP4 and MRP5 in biology and chemotherapy. *AAPS PharmSci* **4**, (2002).
88. Boraldi, F. *et al.* Multidrug resistance protein-6 (MRP6) in human dermal fibroblasts. Comparison between cells from normal subjects and from Pseudoxanthoma elasticum patients. *Matrix Biology* **22**, 491–500 (2003).
89. Kool, M., Linden, M., Haas, M., Baas, F. & Borst, P. Expression of human MRP6, a homologue of the multidrug resistance protein gene MRP1, in tissues and cancer cells. *Cancer Res* (1999).
90. Zhou, S.-F. *et al.* Substrates and inhibitors of human multidrug resistance associated proteins and the implications in drug development. *Curr Med Chem* **15**, 1981–2039 (2008).
91. Hopper, E. *et al.* Analysis of the structure and expression pattern of MRP7 (ABCC10), a new member of the MRP subfamily. *Cancer Lett* **162**, 181–191 (2001).
92. Oguri, T. *et al.* MRP7/ABCC10 expression is a predictive biomarker for the resistance to paclitaxel in non-small cell lung cancer. *Mol Cancer Ther* **7**, 1150–1155 (2008).
93. Hopper-Borge, E., Chen, Z. S., Shchaveleva, I., Belinsky, M. G. & Kruh, G. D. Analysis of the drug resistance profile of multidrug resistance protein 7 (ABCC10): resistance to docetaxel. *Cancer Res* **64**, 4927–4930 (2004).
94. Guo, Y. *et al.* MRP8, ATP-binding cassette C11 (ABCC11), is a cyclic nucleotide efflux pump and a resistance factor for fluoropyrimidines 2',3'-dideoxycytidine and 9'-(2'-phosphonylmethoxyethyl)adenine. *J Biol Chem* **278**, 29509–29514 (2003).
95. Uemura, T. *et al.* ABCC11/MRP8 confers pemetrexed resistance in lung cancer. *Cancer Sci* **101**, 2404–2410 (2010).

96. Honorat, M. *et al.* ABCC11 expression is regulated by estrogen in MCF7 cells, correlated with estrogen receptor  $\alpha$  expression in postmenopausal breast tumors and overexpressed in tamoxifen-resistant breast cancer cells. *Endocr Relat Cancer* **15**, 125–138 (2008).
97. Bortfeld, M. *et al.* Human multidrug resistance protein 8 (MRP8/ABCC11), an apical efflux pump for steroid sulfates, is an axonal protein of the CNS and peripheral nervous system. *Neuroscience* **137**, 1247–1257 (2006).
98. Yabuuchi, H., Shimizu, H., Takayanagi, S. ichiro & Ishikawa, T. Multiple splicing variants of two new human ATP-binding cassette transporters, ABCC11 and ABCC12. *Biochem Biophys Res Commun* **288**, 933–939 (2001).
99. Robey, R. W. *et al.* A functional assay for detection of the mitoxantrone resistance protein, MXR (ABCG2). *Biochimica et Biophysica Acta (BBA) - Biomembranes* **1512**, 171–182 (2001).
100. Mao, Q. & Unadkat, J. D. Role of the Breast Cancer Resistance Protein (BCRP/ABCG2) in Drug Transport—an Update. *AAPS J* **17**, 65 (2015).
101. Francois, L. N. *et al.* Down-regulation of the placental BCRP/ABCG2 transporter in response to hypoxia signaling. *Placenta* **51**, 57–63 (2017).
102. Scheffer, G. L. *et al.* The drug resistance-related protein LRP is the human major vault protein. *Nat Med* **1**, 578–582 (1995).
103. Sasaki, T., Hankins, G. R. & Helm, G. A. Major vault protein/lung resistance-related protein (MVP/LRP) expression in nervous system tumors. *Brain Tumor Pathol* **19**, 59–62 (2002).
104. Kulsoom, B., Shamsi, T. S. & Afsar, N. A. Lung resistance-related protein (LRP) predicts favorable therapeutic outcome in Acute Myeloid Leukemia. *Scientific Reports* **2019 9:1 9**, 1–11 (2019).
105. Mercaptopurine. *LiverTox: Clinical and Research Information on Drug-Induced Liver Injury* (2017).
106. Schmiegelow, K., Nielsen, S. N., Frandsen, T. L. & Nersting, J. Mercaptopurine/methotrexate maintenance therapy of childhood acute lymphoblastic leukemia: Clinical facts and fiction. *J Pediatr Hematol Oncol* **36**, 503–517 (2014).
107. Yeo, N. K., Park, W. J., Eom, D. W., Oh, M. Y. & Lee, J. H. Effects of azathioprine and its metabolites on inflammatory cytokines in human nasal polyp organ cultures. *Int Forum Allergy Rhinol* **9**, 648–655 (2019).
108. Cuffari, C. A Physician’s Guide to Azathioprine Metabolite Testing. *Gastroenterol Hepatol (N Y)* **2**, 58 (2006).
109. Nygaard, U., Toft, N. & Schmiegelow, K. Methylated Metabolites of 6-mercaptopurine are Associated with Hepatotoxicity. *Clin Pharmacol Ther* **75**, 274–281 (2004).
110. Björnsson, E. S. *et al.* Azathioprine and 6-Mercaptopurine Induced Liver Injury: Clinical Features and Outcomes. *J Clin Gastroenterol* **51**, 63 (2017).
111. Chan, G. L. C., Erdmann, G. R., Gruber, S. A., Matas, A. J. & Canafax, D. M. Azathioprine Metabolism: Pharmacokinetics of 6-Mercaptopurine, 6-Thiouric Acid and 6-Thioguanine Nucleotides in Renal Transplant Patients. *The Journal of Clinical Pharmacology* **30**, 358–363 (1990).

112. Conneely, S. E., Cooper, S. L. & Rau, R. E. Use of Allopurinol to Mitigate 6-Mercaptopurine Associated Gastrointestinal Toxicity in Acute Lymphoblastic Leukemia. *Front Oncol* **10**, 1129 (2020).
113. Peng, X. X. *et al.* Up-regulation of P-glycoprotein confers acquired resistance to 6-mercaptopurine in human chronic myeloid leukemia cells. *Oncol Lett* **2**, 549 (2011).
114. Wijnholds, J. *et al.* Multidrug-resistance protein 5 is a multispecific organic anion transporter able to transport nucleotide analogs. *Proceedings of the National Academy of Sciences* **97**, 7476–7481 (2000).
115. Zeng, H., Lin, Z. P. & Sartorelli, A. C. Resistance to purine and pyrimidine nucleoside and nucleobase analogs by the human MDR1 transfected murine leukemia cell line L1210/VMDRC.06. *Biochem Pharmacol* **68**, 911–921 (2004).
116. Brockman, R. W. BIOCHEMICAL ASPECTS OF MERCAPTOPYRINE INHIBITION AND RESISTANCE - PubMed. *Cancer Res.* **23**, 1191–1201 (1963).
117. Tzoneva, G. *et al.* Activating mutations in the NT5C2 nucleotidase gene drive chemotherapy resistance in relapsed ALL. *Nat Med* **19**, 368–371 (2013).
118. Vo, T. T. T. *et al.* mTORC1 Inhibition Induces Resistance to Methotrexate and 6-Mercaptopurine in Ph<sup>+</sup> and Ph-like B-ALL. *Mol Cancer Ther* **16**, 1942–1953 (2017).
119. Chen, L., Yan, H. X., Liu, X. W. & Chen, W. X. Clinical efficacy and safety of 6-thioguanine in the treatment of childhood acute lymphoblastic leukemia: A protocol for systematic review and meta-analysis. *Medicine* **99**, E20082 (2020).
120. Ruutu, T. & Elonen, E. Etoposide, 6-thioguanine and idarubicin, an oral combination regimen (ETI) for the induction treatment of acute leukemia. *Hematol Oncol* **9**, 87–92 (1991).
121. Arthur, C. *et al.* Prolonged administration of low-dose cytarabine and thioguanine in elderly patients with acute myeloid leukaemia (AML) achieves high complete remission rates and prolonged survival. *Leuk Lymphoma* **61**, 831–839 (2020).
122. Amadori, S., Papa, G., Meloni, G., Pacilli, L. & Mandelli, F. Daunorubicin, cytosine arabinoside and 6-thioguanine (DAT) combination chemotherapy for the treatment of acute non-lymphocytic leukemia. *Leuk Res* **3**, 147–152 (1979).
123. Chard, R. L. *et al.* Increased survival in childhood acute nonlymphocytic leukemia after treatment with prednisone, cytosine arabinoside, 6-thioguanine, cyclophosphamide, and oncovin (PATCO) combination chemotherapy. *Med Pediatr Oncol* **4**, 263–273 (1978).
124. Karner, S. *et al.* Determination of 6-thioguanosine diphosphate and triphosphate and nucleoside diphosphate kinase activity in erythrocytes: novel targets for thiopurine therapy? *Ther Drug Monit* **32**, 119–128 (2010).
125. Zhang, L., Hinz, D. J., Kiruba, G. S. M., Ding, X. & Lee, J. K. Gas-phase experimental and computational studies of human hypoxanthine-guanine phosphoribosyltransferase substrates: Intrinsic properties and biological implications. *J Phys Org Chem* **35**, e4343 (2022).
126. Ding, L. *et al.* Hypoxanthine guanine phosphoribosyltransferase activity is related to 6-thioguanine nucleotide concentrations and thiopurine-induced leukopenia in the treatment of inflammatory bowel disease. *Inflamm Bowel Dis* **18**, 63–73 (2012).



127. Dean, L. Thioguanine Therapy and TPMT and NUDT15 Genotype. *Medical Genetics Summaries* (2020).
128. Kim, I. *et al.* A drug-repositioning screen for primary pancreatic ductal adenocarcinoma cells identifies 6-thioguanine as an effective therapeutic agent for TPMT-low cancer cells. *Mol Oncol* **12**, 1526–1539 (2018).
129. Morley, A. A., Cox, S. & Holliday, R. Human lymphocytes resistant to 6-thioguanine increase with age. *Mech Ageing Dev* **19**, 21–26 (1982).
130. Glaab, W. E. *et al.* Resistance to 6-thioguanine in mismatch repair-deficient human cancer cell lines correlates with an increase in induced mutations at the HPRT locus. *Carcinogenesis* **19**, 1931–1937 (1998).
131. Gefen, N. *et al.* Acquired resistance to 6-thioguanine in melanoma cells involves the repair enzyme O 6-methylguanine-DNA methyltransferase (MGMT). *Cancer Biol Ther* **49**, 49–55 (2010).
132. Wielinga, P. R. *et al.* Thiopurine metabolism and identification of the thiopurine metabolites transported by MRP4 and MRP5 overexpressed in human embryonic kidney cells. *Mol Pharmacol* **62**, 1321–1331 (2002).
133. Issaeva, N. *et al.* 6-thioguanine selectively kills BRCA2-defective tumors and overcomes PARP inhibitor resistance. *Cancer Res* **70**, 6268–6276 (2010).
134. Möllgård, L. *et al.* High single dose of mitoxantrone and cytarabine in acute non-lymphocytic leukemia: A pharmacokinetic and clinical study. *Ther Drug Monit* **20**, 640–645 (1998).
135. Cortes, J. E. *et al.* Glasdegib in combination with cytarabine and daunorubicin in patients with AML or high-risk MDS: Phase 2 study results. *Am J Hematol* **93**, 1301–1310 (2018).
136. Hehlmann, R. *et al.* Assessment of imatinib as first-line treatment of chronic myeloid leukemia: 10-year survival results of the randomized CML study IV and impact of non-CML determinants. *Leukemia* 2017 31:11 **31**, 2398–2406 (2017).
137. Faderl, S. *et al.* Clofarabine and cytarabine combination as induction therapy for acute myeloid leukemia (AML) in patients 50 years of age or older. *Blood* **108**, 45–51 (2006).
138. Ravandi, F. *et al.* Final Report of Phase II Study of Sorafenib, Cytarabine, and Idarubicin for Initial Therapy in Younger Patients with Acute Myeloid Leukemia. *Leukemia* **28**, 1543 (2014).
139. Hong, M. *et al.* Decitabine in combination with low-dose cytarabine, aclarubicin and G-CSF tends to improve prognosis in elderly patients with high-risk AML. *Ageing (Albany NY)* **12**, 5792 (2020).
140. Halpern, A. B. *et al.* Addition of Sorafenib to Cladribine, High-Dose Cytarabine, G-CSF, and Mitoxantrone (CLAG-M) in Adults with Newly-Diagnosed Acute Myeloid Leukemia (AML) and High-Grade Myeloid Neoplasms Independent of FLT3-Mutation Status: Final Results of a Phase 1/2 Study. *Blood* **140**, 8999–9001 (2022).
141. Borthakur, G. *et al.* Retrospective comparison of survival and responses to Fludarabine, Cytarabine, GCSF (FLAG) in combination with gemtuzumab ozogamicin (GO) or Idarubicin (IDA) in patients with newly diagnosed core binding factor (CBF) acute

- myelogenous leukemia: MD Anderson experience in 174 patients. *Am J Hematol* **97**, 1427–1434 (2022).
142. Dillon, R. *et al.* Venetoclax combined with low dose cytarabine compared to standard of care intensive chemotherapy for the treatment of favourable risk adult acute myeloid leukaemia (VICTOR): Study protocol for an international, open-label, multicentre, molecularly-guided randomised, phase II trial. *BMC Cancer* **22**, 1–13 (2022).
  143. Fanciullino, R. *et al.* CDA as a predictive marker for life-threatening toxicities in patients with AML treated with cytarabine. *Blood Adv* **2**, 462–469 (2018).
  144. Malani, D. *et al.* Enhanced sensitivity to glucocorticoids in cytarabine-resistant AML. *Leukemia* **31**, 1187–1195 (2016).
  145. Song, J. H. *et al.* Defective expression of deoxycytidine kinase in cytarabine-resistant acute myeloid leukemia cells. *Int J Oncol* **34**, 1165–1171 (2009).
  146. Li, Z. *et al.* Exploring the Antitumor Mechanism of High-Dose Cytarabine through the Metabolic Perturbations of Ribonucleotide and Deoxyribonucleotide in Human Promyelocytic Leukemia HL-60 Cells. *Molecules* **22**, (2017).
  147. Mitra, A. K. *et al.* Genetic variants in cytosolic 5'-nucleotidase II are associated with its expression and cytarabine sensitivity in HapMap cell lines and in patients with acute myeloid leukemia. *J Pharmacol Exp Ther* **339**, 9–23 (2011).
  148. Schneider, C. *et al.* SAMHD1 is a biomarker for cytarabine response and a therapeutic target in acute myeloid leukemia. *Nature Medicine* **23**, 250–255 (2016).
  149. Rudd, S. G. *et al.* Ribonucleotide reductase inhibitors suppress SAMHD1 ara-CTPase activity enhancing cytarabine efficacy. *EMBO Mol Med* **12**, e10419 (2020).
  150. Adema, A. D. *et al.* Overexpression of MRP4 (ABCC4) and MRP5 (ABCC5) confer resistance to the nucleoside analogs cytarabine and troxacitabine, but not gemcitabine. *Springerplus* **3**, 1–11 (2014).
  151. Jaramillo, A. C. *et al.* Ex vivo resistance in childhood acute lymphoblastic leukemia: Correlations between BCRP, MRP1, MRP4 and MRP5 ABC transporter expression and intracellular methotrexate polyglutamate accumulation. *Leuk Res* **79**, 45–51 (2019).
  152. Keating, M. J. *et al.* Fludarabine: A new agent with marked cytoreductive activity in untreated chronic lymphocytic leukemia. *Journal of Clinical Oncology* **9**, 44–49 (1991).
  153. Davids, M. S. *et al.* Ibrutinib plus fludarabine, cyclophosphamide, and rituximab as initial treatment for younger patients with chronic lymphocytic leukaemia: a single-arm, multicentre, phase 2 trial. *Lancet Haematol* **6**, e419–e428 (2019).
  154. Smolej, L. *et al.* Low-dose fludarabine and cyclophosphamide combined with rituximab in the first-line treatment of elderly/comorbid patients with chronic lymphocytic leukaemia/small lymphocytic lymphoma (CLL/SLL): long-term results of project Q-lite by the Czech CLL Study Group. *Br J Haematol* **193**, 769–778 (2021).
  155. Wang, X. X. *et al.* Bortezomib in combination with fludarabine plus cyclophosphamide for patients with relapsed or refractory mantle-cell lymphoma: results of the LYM-4003 study. *Ann Hematol* **100**, 2961–2968 (2021).
  156. Gandhi, V. & Plunkett, W. Cellular and clinical pharmacology of fludarabine. *Clin Pharmacokinet* **41**, 93–103 (2002).

157. Gorzkiewicz, M. *et al.* Glycodendrimer Nanocarriers for Direct Delivery of Fludarabine Triphosphate to Leukemic Cells: Improved Pharmacokinetics and Pharmacodynamics of Fludarabine. *Biomacromolecules* **19**, 531–543 (2018).
158. Candoni, A. *et al.* Flai (fludarabine, cytarabine, idarubicin) plus low-dose Gemtuzumab Ozogamicin as induction therapy in CD33-positive AML: Final results and long term outcome of a phase II multicenter clinical trial. *Am J Hematol* **93**, 655–663 (2018).
159. Damiani, D. *et al.* Fludarabine-based induction therapy does not overcome the negative effect of ABCG2 (BCRP) over-expression in adult acute myeloid leukemia patients. *Leuk Res* **34**, 942–945 (2010).
160. Huang, C., Tu, Y. & Freter, C. E. Fludarabine-resistance associates with ceramide metabolism and leukemia stem cell development in chronic lymphocytic leukemia. *Oncotarget* **9**, 33124 (2018).
161. Trachootham, D. *et al.* Effective elimination of fludarabine-resistant CLL cells by PEITC through a redox-mediated mechanism. *Blood* **112**, 1912–1922 (2008).
162. Sharma, A. *et al.* Targeting mTORC1-mediated metabolic addiction overcomes fludarabine resistance in malignant B cells. *Molecular Cancer Research* **12**, 1205–1215 (2014).
163. Schirmer, M., Stegmann, A. P. A., Geisen, F. & Konwalinka, G. Lack of cross-resistance with gemcitabine and cytarabine in cladribine-resistant HL60 cells with elevated 5'-nucleotidase activity. *Exp Hematol* **26**, 1223–1228 (1998).
164. Toschi, L., Finocchiaro, G., Bartolini, S., Gioia, V. & Cappuzzo, F. Role of gemcitabine in cancer therapy. *Future Oncol* **1**, 7–17 (2005).
165. Conroy, T. *et al.* FOLFIRINOX or Gemcitabine as Adjuvant Therapy for Pancreatic Cancer. *New England Journal of Medicine* **379**, 2395–2406 (2018).
166. Yardley, D. A. *et al.* nab-Paclitaxel plus carboplatin or gemcitabine versus gemcitabine plus carboplatin as first-line treatment of patients with triple-negative metastatic breast cancer: results from the tnAcity trial. *Annals of Oncology* **29**, 1763–1770 (2018).
167. Ciccolini, J., Serdjebi, C., Peters, G. J. & Giovannetti, E. Pharmacokinetics and pharmacogenetics of Gemcitabine as a mainstay in adult and pediatric oncology: an EORTC-PAMM perspective. *Cancer Chemother Pharmacol* **78**, 1 (2016).
168. Xu, H., Faber, C., Uchiki, T., Racca, J. & Dealwis, C. Structures of eukaryotic ribonucleotide reductase I define gemcitabine diphosphate binding and subunit assembly. *Proc Natl Acad Sci U S A* **103**, 4028–4033 (2006).
169. Plunkett, W., Huang, P. & Gandhi, V. Preclinical characteristics of gemcitabine. *Anticancer Drugs* **6 Suppl 6**, 7–13 (1995).
170. Bjånes, T. K. *et al.* Intracellular Cytidine Deaminase Regulates Gemcitabine Metabolism in Pancreatic Cancer Cell Lines s. *DRUG METABOLISM AND DISPOSITION Drug Metab Dispos* **48**, 153–158 (2020).
171. Hagmann, W., Jesnowski, R. & Löhr, J. M. Interdependence of Gemcitabine Treatment, Transporter Expression, and Resistance in Human Pancreatic Carcinoma Cells. *Neoplasia* **12**, 740 (2010).

172. Jia, Y. & Xie, J. Promising molecular mechanisms responsible for gemcitabine resistance in cancer. *Genes Dis* **2**, 299–306 (2015).
173. Yang, H. *et al.* Genome-Wide CRISPR Screening Identifies DCK and CCNL1 as Genes That Contribute to Gemcitabine Resistance in Pancreatic Cancer. *Cancers (Basel)* **14**, (2022).
174. Chang, Y. H., Tam, H. L., Lu, M. C. & Huang, H. S. Gemcitabine-induced Gli-dependent activation of hedgehog pathway resists to the treatment of urothelial carcinoma cells. *PLoS One* **16**, (2021).
175. Zhang, Q. *et al.* The Wnt/ $\beta$ -catenin signaling pathway mechanism for pancreatic cancer chemoresistance in a three-dimensional cancer microenvironment. *Am J Transl Res* **8**, 4490 (2016).
176. Mokhtari, R. B. *et al.* Combination therapy in combating cancer. *Oncotarget* **8**, 38022 (2017).
177. S, A., Chakraborty, A. & Patnaik, S. Clonal evolution and expansion associated with therapy resistance and relapse of colorectal cancer. *Mutation Research/Reviews in Mutation Research* **790**, 108445 (2022).
178. Alexander, T. B. *et al.* Phase I study of selinexor, a selective inhibitor of nuclear export, in combination with fludarabine and cytarabine, in pediatric relapsed or refractory acute leukemia. *Journal of Clinical Oncology* **34**, 4094–4101 (2016).
179. Jabbour, E. *et al.* Twice-daily fludarabine and cytarabine combination with or without gentuzumab ozogamicin is effective in patients with relapsed/refractory acute myeloid leukemia, high-risk myelodysplastic syndrome, and blast- phase chronic myeloid leukemia. *Clin Lymphoma Myeloma Leuk* **12**, 244–251 (2012).
180. Chu, M. *et al.* Combination of the 6-thioguanine and disulfiram/Cu synergistically inhibits proliferation of triple-negative breast cancer cells by enhancing DNA damage and disrupting DNA damage checkpoint. *Biochimica et Biophysica Acta (BBA) - Molecular Cell Research* **1869**, 119169 (2022).
181. Elter, T. *et al.* Fludarabine in combination with alemtuzumab is effective and feasible in patients with relapsed or refractory B-cell chronic lymphocytic leukemia: results of a phase II trial. *J Clin Oncol* **23**, 7024–7031 (2005).
182. Wang, L. & Sun, Y. Efflux mechanism and pathway of verapamil pumping by human P-glycoprotein. *Arch Biochem Biophys* **696**, 108675 (2020).
183. Summers, M. A., Moore, J. L. & McAuley, J. W. Use of verapamil as a potential P-glycoprotein inhibitor in a patient with refractory epilepsy. *Ann Pharmacother* **38**, 1631–1634 (2004).
184. Lehnert, M. *et al.* Phase II trial of dexverapamil and epirubicin in patients with non-responsive metastatic breast cancer. *Br J Cancer* **77**, 1155–1163 (1998).
185. Karthikeyan, S. & Hoti, S. Development of Fourth Generation ABC Inhibitors from Natural Products: A Novel Approach to Overcome Cancer Multidrug Resistance. *Anticancer Agents Med Chem* **15**, 605–615 (2015).
186. Sun, M., Xu, X., Lu, Q., Pan, Q. & Hu, X. Schisandrin B: a dual inhibitor of P-glycoprotein and multidrug resistance-associated protein 1. *Cancer Lett* **246**, 300–307 (2007).

187. Andresen, G., Gundersen, L. L., Nissen-Meyer, J., Rise, F. & Spilsberg, B. Studies on Quinazolinones as Dual Inhibitors of Pgp and MRP1 in Multidrug Resistance. *Bioorg Med Chem Lett* **12**, 571–574 (2002).
188. Nabekura, T., Yamaki, T., Ueno, K. & Kitagawa, S. Inhibition of P-glycoprotein and multidrug resistance protein 1 by dietary phytochemicals. *Cancer Chemother Pharmacol* **62**, 867–873 (2008).
189. Sato, H. *et al.* Elacridar enhances the cytotoxic effects of sunitinib and prevents multidrug resistance in renal carcinoma cells. *Eur J Pharmacol* **746**, 258–266 (2015).
190. Gu, X. *et al.* Discovery of alkoxy biphenyl derivatives bearing dibenzo[c,e]azepine scaffold as potential dual inhibitors of P-glycoprotein and breast cancer resistance protein. *Bioorg Med Chem Lett* **24**, 3419–3421 (2014).
191. Gu, X., Ren, Z., Peng, H., Peng, S. & Zhang, Y. Bifendate-chalcone hybrids: A new class of potential dual inhibitors of P-glycoprotein and breast cancer resistance protein. *Biochem Biophys Res Commun* **455**, 318–322 (2014).
192. Schwarz, T. *et al.* Subtle Structural Differences Trigger Inhibitory Activity of Propafenone Analogues at the Two Polyspecific ABC Transporters: P-Glycoprotein (P-gp) and Breast Cancer Resistance Protein (BCRP). *ChemMedChem* **11**, 1380–1394 (2016).
193. Sechidis, K. *et al.* Distinguishing prognostic and predictive biomarkers: an information theoretic approach. *Bioinformatics* **34**, 3365–3376 (2018).
194. Lambert, J. M. Drug-conjugated antibodies for the treatment of cancer. *Br J Clin Pharmacol* **76**, 248 (2013).
195. Buchegger, F. *et al.* Radiolabeled fragments of monoclonal antibodies against carcinoembryonic antigen for localization of human colon carcinoma grafted into nude mice. *Journal of Experimental Medicine* **158**, 413–427 (1983).
196. Dahl, J., Marx, K. & Jabbour, E. Inotuzumab ozogamicin in the treatment of acute lymphoblastic leukemia. *Expert Rev Hematol* **9**, 329–334 (2016).
197. Hitzler, J. & Estey, E. Gemtuzumab ozogamicin in acute myeloid leukemia: act 2, with perhaps more to come. *Haematologica* **104**, 7 (2019).
198. Van De Donk, N. W. C. J. & Dhimolea, E. Brentuximab vedotin. *MAbs* **4**, 458 (2012).
199. Peddi, P. F. & Hurvitz, S. A. Ado-trastuzumab emtansine (T-DM1) in human epidermal growth factor receptor 2 (HER2)-positive metastatic breast cancer: latest evidence and clinical potential. *Ther Adv Med Oncol* **6**, 202 (2014).
200. Yoon, S. *et al.* Aptamer-Drug Conjugates of Active Metabolites of Nucleoside Analogs and Cytotoxic Agents Inhibit Pancreatic Tumor Cell Growth. *Mol Ther Nucleic Acids* **6**, 80–88 (2017).
201. Zhu, L., Yang, J., Ma, Y., Zhu, X. & Zhang, C. Aptamers Entirely Built from Therapeutic Nucleoside Analogues for Targeted Cancer Therapy. *J Am Chem Soc* **144**, 1493–1497 (2022).
202. Kovacs, Z. *et al.* Effects of nucleosides on glia - neuron interactions open up new vistas in the development of more effective antiepileptic drugs. *Curr Med Chem* **22**, 1500–1514 (2015).

203. Price, R. W. & Brew, B. J. The AIDS Dementia Complex. *J Infect Dis* **158**, 1079–1083 (1988).
204. Bourdais, J. *et al.* Cellular Phosphorylation of Anti-HIV Nucleosides. *Journal of Biological Chemistry* **271**, 7887–7890 (1996).
205. Barth, R. F. *et al.* Boron-Containing Nucleosides as Potential Delivery Agents for Neutron Capture Therapy of Brain Tumors. *Cancer Res* **64**, 6287–6295 (2004).
206. Gallo, J. M. Delivery of anti-HIV nucleosides to the central nervous system. *Adv Drug Deliv Rev* **14**, 199–209 (1994).
207. Varatharajan, L. & Thomas, S. A. The transport of anti-HIV drugs across blood–CNS interfaces: Summary of current knowledge and recommendations for further research. *Antiviral Res* **82**, A99 (2009).
208. Chhikara, B. S. *et al.* Nanotherapeutics and HIV: Four decades of infection canvass the quest for drug development using nanomedical technologies. *Applied NanoMedicine* **2**, 354–354 (2022).
209. Martins, C. *et al.* Using microfluidic platforms to develop CNS-targeted polymeric nanoparticles for HIV therapy. *European Journal of Pharmaceutics and Biopharmaceutics* **138**, 111–124 (2019).
210. Rao, K. S., Reddy, M. K., Horning, J. L. & Labhasetwar, V. TAT-conjugated nanoparticles for the CNS delivery of anti-HIV drugs. *Biomaterials* **29**, 4429–4438 (2008).
211. Mollinedo, F. & Gajate, C. Microtubules, microtubule-interfering agents and apoptosis. *Apoptosis* **8**, 413–450 (2003).
212. Quraishe, S., Cowan, C. M. & Mudher, A. Tau-Centric Therapies for Treating Alzheimer’s Disease. *Neuroprotection in Alzheimer’s Disease* 73–96 (2017) doi:10.1016/B978-0-12-803690-7.00005-3.
213. Bera, A. & Gupta, M. L. Microtubules in Microorganisms: How Tubulin Isoforms Contribute to Diverse Cytoskeletal Functions. *Front Cell Dev Biol* **10**, 913809 (2022).
214. Roostalu, J. *et al.* The speed of GTP hydrolysis determines GTP cap size and controls microtubule stability. *Elife* **9**, (2020).
215. Drewes, G., Ebnet, A. & Mandelkow, E. M. MAPs, MARKs and microtubule dynamics. *Trends Biochem Sci* **23**, 307–311 (1998).
216. Jurášek, M. *et al.* Triazole-based estradiol dimers prepared via CuAAC from 17 $\alpha$ -ethinyl estradiol with five-atom linkers causing G2/M arrest and tubulin inhibition. *Bioorg Chem* **131**, (2023).
217. Kaul, R., Risinger, A. L. & Mooberry, S. L. Microtubule-Targeting Drugs: More than Antimitotics. *J Nat Prod* **82**, 680–685 (2019).
218. Walker, S. R., Chaudhury, M., Nelson, E. A. & Frank, D. A. Microtubule-targeted chemotherapeutic agents inhibit signal transducer and activator of transcription 3 (STAT3) signaling. *Mol Pharmacol* **78**, 903–908 (2010).
219. Zou, S. *et al.* Targeting STAT3 in Cancer Immunotherapy. *Molecular Cancer* **19**:1 **19**, 1–19 (2020).

220. Fagard, R., Metelev, V., Souissi, I. & Baran-Marszak, F. STAT3 inhibitors for cancer therapy: Have all roads been explored? *JAKSTAT* **2**, e22882 (2013).
221. Meissner, M. *et al.* Microtubule-Targeted Drugs Inhibit VEGF Receptor-2 Expression by both Transcriptional and Post-Transcriptional Mechanisms. *Journal of Investigative Dermatology* **128**, 2084–2091 (2008).
222. Zhang, Y. *et al.* Hyperphosphorylation of microtubule-associated tau protein plays dual role in neurodegeneration and neuroprotection. *Pathophysiology* **16**, 311–316 (2009).
223. Hernández, F. & Avila, J. Tauopathies. *Cellular and Molecular Life Sciences* **64**, 2219–2233 (2007).
224. Williams, D. R. Tauopathies: classification and clinical update on neurodegenerative diseases associated with microtubule-associated protein tau. *Intern Med J* **36**, 652–660 (2006).
225. Tan, M. S. *et al.* Associations of Alzheimer’s disease risk variants with gene expression, amyloidosis, tauopathy, and neurodegeneration. *Alzheimers Res Ther* **13**, 1–11 (2021).
226. Fiock, K. L., Smalley, M. E., Crary, J. F., Pasca, A. M. & Hefti, M. M. Increased Tau Expression Correlates with Neuronal Maturation in the Developing Human Cerebral Cortex. *eNeuro* **7**, (2020).
227. Sjölin, K. *et al.* Distribution of five clinically important neuroglial proteins in the human brain. *Mol Brain* **15**, (2022).
228. Corsi, A., Bombieri, C., Valenti, M. T. & Romanelli, M. G. Tau Isoforms: Gaining Insight into MAPT Alternative Splicing. *Int J Mol Sci* **23**, (2022).
229. Bachmann, S., Bell, M., Klimek, J. & Zempel, H. Differential Effects of the Six Human TAU Isoforms: Somatic Retention of 2N-TAU and Increased Microtubule Number Induced by 4R-TAU. *Front Neurosci* **15**, 643115 (2021).
230. Falcon, B. *et al.* Structures of filaments from Pick’s disease reveal a novel tau protein fold. *Nature* **561**, 137 (2018).
231. Fyfe, I. Tau folds differently between diseases. *Nature Reviews Neurology* **14**:11 **14**, 633–633 (2018).
232. Martínez-Maldonado, A. *et al.* Molecular Processing of Tau Protein in Progressive Supranuclear Palsy: Neuronal and Glial Degeneration. *J Alzheimers Dis* **79**, 1517–1531 (2021).
233. Aizawa, H. *et al.* Microtubule-binding domain of tau proteins. *Journal of Biological Chemistry* **263**, 7703–7707 (1988).
234. Paglini, G., Peris, L., Mascotti, F., Quiroga, S. & Caceres, A. Tau Protein Function in Axonal Formation\*. *Neurochem Res* **25**, 37–42 (2000).
235. Metaxas, A. & Kempf, S. J. Neurofibrillary tangles in Alzheimer’s disease: elucidation of the molecular mechanism by immunohistochemistry and tau protein phospho-proteomics. *Neural Regen Res* **11**, 1579 (2016).
236. Iqbal, K. *et al.* Tau pathology in Alzheimer disease and other tauopathies. *Biochim Biophys Acta* **1739**, 198–210 (2005).

237. Ando, K. *et al.* Tau phosphorylation at Alzheimer's disease-related Ser356 contributes to tau stabilization when PAR-1/MARK activity is elevated. *Biochem Biophys Res Commun* **478**, 929–934 (2016).
238. Biernat, J., Gustke, N., Drewes, G., Mandelkow, E. & Mandelkow, E. Phosphorylation of Ser262 strongly reduces binding of tau to microtubules: Distinction between PHF-like immunoreactivity and microtubule binding. *Neuron* **11**, 153–163 (1993).
239. Carlomagno, Y. *et al.* An acetylation–phosphorylation switch that regulates tau aggregation propensity and function. *Journal of Biological Chemistry* **292**, 15277–15286 (2017).
240. Lund, H. *et al.* MARK4 and MARK3 associate with early tau phosphorylation in Alzheimer's disease granulovacuolar degeneration bodies. *Acta Neuropathol Commun* **2**, (2014).
241. Toral-Rios, D., Pichardo-Rojas, P. S., Alonso-Vanegas, M. & Campos-Peña, V. GSK3 $\beta$  and Tau Protein in Alzheimer's Disease and Epilepsy. *Front Cell Neurosci* **14**, (2020).
242. Drewes, G., Ebnet, A., Preuss, U., Mandelkow, E. M. & Mandelkow, E. MARK, a Novel Family of Protein Kinases That Phosphorylate Microtubule-Associated Proteins and Trigger Microtubule Disruption. *Cell* **89**, 297–308 (1997).
243. Natalia, M.-A., Alejandro, G.-T., Virginia, T.-V. J. & Alvarez-Salas, L. M. MARK1 is a Novel Target for miR-125a-5p: Implications for Cell Migration in Cervical Tumor Cells. *MicroRNA* **7**, 54–61 (2018).
244. Gu, G. J. *et al.* Role of individual MARK isoforms in phosphorylation of tau at Ser<sup>262</sup> in Alzheimer's disease. *Neuromolecular Med* **15**, 458–469 (2013).
245. Gu, G. J. *et al.* Elevated MARK2-dependent phosphorylation of Tau in Alzheimer's disease. *J Alzheimers Dis* **33**, 699–713 (2013).
246. Ando, K. *et al.* Stabilization of Microtubule-Unbound Tau via Tau Phosphorylation at Ser262/356 by Par-1/MARK Contributes to Augmentation of AD-Related Phosphorylation and A $\beta$ 42-Induced Tau Toxicity. *PLoS Genet* **12**, (2016).
247. Oba, T. *et al.* Microtubule affinity-regulating kinase 4 with an Alzheimer's disease-related mutation promotes tau accumulation and exacerbates neurodegeneration. *J Biol Chem* **295**, 17138–17147 (2020).
248. Chin, J. Y. *et al.* Microtubule-Affinity Regulating Kinase (MARK) Is Tightly Associated with Neurofibrillary Tangles in Alzheimer Brain: A Fluorescence Resonance Energy Transfer Study. *J Neuropathol Exp Neurol* **59**, 966–971 (2000).
249. Saito, T. *et al.* Cdk5 increases MARK4 activity and augments pathological tau accumulation and toxicity through tau phosphorylation at Ser262. *Hum Mol Genet* **28**, 3062–3071 (2019).
250. Lizcano, J. M. *et al.* LKB1 is a master kinase that activates 13 kinases of the AMPK subfamily, including MARK/PAR-1. *EMBO J* **23**, 833–843 (2004).
251. Chatterjee, S., Sang, T. K., Lawless, G. M. & Jackson, G. R. Dissociation of tau toxicity and phosphorylation: role of GSK-3 $\beta$ , MARK and Cdk5 in a *Drosophila* model. *Hum Mol Genet* **18**, 164–177 (2009).



252. Hernández, F., Gómez de Barreda, E., Fuster-Matanzo, A., Lucas, J. J. & Avila, J. GSK3: A possible link between beta amyloid peptide and tau protein. *Exp Neurol* **223**, 322–325 (2010).
253. Hou, H. *et al.* Synaptic NMDA receptor stimulation activates PP1 by inhibiting its phosphorylation by Cdk5. *J Cell Biol* **203**, 521 (2013).
254. Zhan, F., Phiel, C. J., Spece, L., Gurvich, N. & Klein, P. S. Inhibitory Phosphorylation of Glycogen Synthase Kinase-3 (GSK-3) in Response to Lithium: EVIDENCE FOR AUTOREGULATION OF GSK-3. *Journal of Biological Chemistry* **278**, 33067–33077 (2003).
255. Cho, J. H. & Johnson, G. V. W. Primed phosphorylation of tau at Thr231 by glycogen synthase kinase 3beta (GSK3beta) plays a critical role in regulating tau's ability to bind and stabilize microtubules. *J Neurochem* **88**, 349–358 (2004).
256. Kosuga, S. *et al.* GSK-3beta directly phosphorylates and activates MARK2/PAR-1. *J Biol Chem* **280**, 42715–42722 (2005).
257. Timm, T. *et al.* Glycogen Synthase Kinase (GSK) 3 $\beta$  Directly Phosphorylates Serine 212 in the Regulatory Loop and Inhibits Microtubule Affinity-regulating Kinase (MARK) 2. *Journal of Biological Chemistry* **283**, 18873–18882 (2008).
258. Annunziata, M. C. *et al.* Phosphorylation Sites in Protein Kinases and Phosphatases Regulated by Formyl Peptide Receptor 2 Signaling. *International Journal of Molecular Sciences* 2020, Vol. 21, Page 3818 **21**, 3818 (2020).
259. Guise, S., Braguer, D., Carles, G., Delacourte, A. & Briand, C. Hyperphosphorylation of tau is mediated by ERK activation during anticancer drug-induced apoptosis in neuroblastoma cells. *J Neurosci Res* **63**, 257–267 (2001).
260. Voura, M. *et al.* Probing the Inhibition of Microtubule Affinity Regulating Kinase 4 by N-Substituted Acridones. *Scientific Reports* 2019 9:1 **9**, 1–17 (2019).
261. Peerzada, M. N. *et al.* Identification of morpholine based hydroxylamine analogues: selective inhibitors of MARK4/Par-1d causing cancer cell death through apoptosis. *New Journal of Chemistry* **44**, 16626–16637 (2020).
262. Aneja, B. *et al.* Design and development of Isatin-triazole hydrazones as potential inhibitors of microtubule affinity-regulating kinase 4 for the therapeutic management of cell proliferation and metastasis. *Eur J Med Chem* **163**, 840–852 (2019).
263. Shamsi, A. *et al.* Inhibition of MARK4 by serotonin as an attractive therapeutic approach to combat Alzheimer's disease and neuroinflammation. *RSC Med Chem* **13**, 737–745 (2022).
264. Naqvi, A. A. T. *et al.* Evaluation of pyrazolopyrimidine derivatives as microtubule affinity regulating kinase 4 inhibitors: Towards therapeutic management of Alzheimer's disease. *J Biomol Struct Dyn* **38**, 3892–3907 (2020).
265. Shamsi, A. *et al.* MARK4 Inhibited by AChE Inhibitors, Donepezil and Rivastigmine Tartrate: Insights into Alzheimer's Disease Therapy. *Biomolecules* 2020, Vol. 10, Page 789 **10**, 789 (2020).
266. Hrubá, L., Polishchuk, P., Das, V., Hajduch, M. & Dzubak, P. An identification of MARK inhibitors using high throughput MALDI-TOF mass spectrometry. *Biomedicine & Pharmacotherapy* **146**, 112549 (2022).

267. Shupp, A., Casimiro, M. C. & Pestell, R. G. Biological functions of CDK5 and potential CDK5 targeted clinical treatments. *Oncotarget* **8**, 17373 (2017).
268. Pozo, K. & Bibb, J. A. The Emerging Role of Cdk5 in Cancer. *Trends Cancer* **2**, 606–618 (2016).
269. Umfress, A. *et al.* Systemic Administration of a Brain Permeable Cdk5 Inhibitor Alters Neurobehavior. *Front Pharmacol* **13**, (2022).
270. Umfress, A. *et al.* Systemic Administration of a Brain Permeable Cdk5 Inhibitor Alters Neurobehavior. *Front Pharmacol* **13**, 863762 (2022).
271. Tomov, N., Surchev, L., Wiedenmann, C., Döbrössy, M. & Nikkhah, G. Roscovitine, an experimental CDK5 inhibitor, causes delayed suppression of microglial, but not astroglial recruitment around intracerebral dopaminergic grafts. *Exp Neurol* **318**, 135–144 (2019).
272. Daniels, M. H. *et al.* Discovery and Optimization of Highly Selective Inhibitors of CDK5. *J Med Chem* **65**, 3575–3596 (2022).
273. Zhao, R.-X. & Xu, Z.-X. Targeting the LKB1 Tumor Suppressor. *Curr Drug Targets* **15**, 32 (2014).
274. Borzi, C. *et al.* Beyond LKB1 Mutations in Non-Small Cell Lung Cancer: Defining LKB1less Phenotype to Optimize Patient Selection and Treatment. *Pharmaceuticals* **13**, 1–12 (2020).
275. Wingo, S. N. *et al.* Somatic LKB1 mutations promote cervical cancer progression. *PLoS One* **4**, (2009).
276. Guldberg, P. *et al.* Somatic mutation of the Peutz-Jeghers syndrome gene, LKB1/STK11, in malignant melanoma. *Oncogene* **18**, 1777–1780 (1999).
277. Huang, E. & Li, S. Liver Kinase B1 Functions as a Regulator for Neural Development and a Therapeutic Target for Neural Repair. *Cells* **11**, (2022).
278. Ji, J. *et al.* Antagonizing peroxisome proliferator-activated receptor  $\gamma$  facilitates M1-to-M2 shift of microglia by enhancing autophagy via the LKB1-AMPK signaling pathway. *Aging Cell* **17**, (2018).
279. Shin, S. *et al.* Glycogen synthase kinase-3 $\beta$  positively regulates protein synthesis and cell proliferation through the regulation of translation initiation factor 4E-binding protein 1. *Oncogene* **33**, 1690–1699 (2014).
280. Domoto, T. *et al.* Glycogen synthase kinase-3 $\beta$  is a pivotal mediator of cancer invasion and resistance to therapy. *Cancer Sci* **107**, 1363 (2016).
281. Augello, G. *et al.* The Role of GSK-3 in Cancer Immunotherapy: GSK-3 Inhibitors as a New Frontier in Cancer Treatment. *Cells* **9**, (2020).
282. Griebel, G. *et al.* The selective GSK3 inhibitor, SAR502250, displays neuroprotective activity and attenuates behavioral impairments in models of neuropsychiatric symptoms of Alzheimer's disease in rodents. *Scientific Reports* **9**, 1–15 (2019).
283. Noh, M. Y. *et al.* Neuroprotective effects of donepezil through inhibition of GSK-3 activity in amyloid- $\beta$ -induced neuronal cell death. *J Neurochem* **108**, 1116–1125 (2009).

284. Snitow, M. E., Bhansali, R. S. & Klein, P. S. Lithium and Therapeutic Targeting of GSK-3. *Cells* **10**, 1–24 (2021).
285. Culbert, A. A. *et al.* GSK-3 inhibition by adenoviral FRAT1 overexpression is neuroprotective and induces Tau dephosphorylation and  $\beta$ -catenin stabilisation without elevation of glycogen synthase activity. *FEBS Lett* **507**, 288–294 (2001).
286. Silva, M. A., Kiametis, A. S. & Treptow, W. Donepezil Inhibits Acetylcholinesterase via Multiple Binding Modes at Room Temperature. *J Chem Inf Model* **60**, 3463–3471 (2020).
287. Markar, H. R. & Mander, A. J. Efficacy of Lithium Prophylaxis in Clinical Practice. *The British Journal of Psychiatry* **155**, 496–500 (1989).
288. Gawesh, E. H. E. *et al.* Clinical, laboratory and neurological assessment of lithium toxicity in patients with bipolar disorders. *Journal of Population Therapeutics and Clinical Pharmacology* **30**, 379–391 (2023).
289. Ugolkov, A. *et al.* GSK-3 inhibition overcomes chemoresistance in human breast cancer. *Cancer Lett* **380**, 384–392 (2016).
290. Park, E. J. *et al.* Suppression of Src/ERK and GSK-3/ $\beta$ -catenin signaling by pinosylvin inhibits the growth of human colorectal cancer cells. *Food and Chemical Toxicology* **55**, 424–433 (2013).
291. Kadry, H., Noorani, B. & Cucullo, L. A blood–brain barrier overview on structure, function, impairment, and biomarkers of integrity. *Fluids and Barriers of the CNS* **2020** *17:1* **17**, 1–24 (2020).
292. Abbott, N. J. Comparative Physiology of the Blood-Brain Barrier. in 371–396 (Springer, Berlin, Heidelberg, 1992). doi:10.1007/978-3-642-76894-1\_15.
293. Löscher, W. & Potschka, H. Blood-Brain Barrier Active Efflux Transporters: ATP-Binding Cassette Gene Family. *NeuroRx* **2**, 86 (2005).
294. Rankovic, Z. CNS Drug Design: Balancing Physicochemical Properties for Optimal Brain Exposure. *J Med Chem* **58**, 2584–2608 (2015).
295. Lipinski, C. A. Drug-like properties and the causes of poor solubility and poor permeability. *J Pharmacol Toxicol Methods* **44**, 235–249 (2000).
296. Ghose, A. K., Herbertz, T., Hudkins, R. L., Dorsey, B. D. & Mallamo, J. P. Knowledge-based, central nervous system (CNS) lead selection and lead optimization for CNS drug discovery. *ACS Chem Neurosci* **3**, 50–68 (2012).
297. Pajouhesh, H. & Lenz, G. R. Medicinal chemical properties of successful central nervous system drugs. *NeuroRx* **2**, 541–553 (2005).
298. Pardridge, W. M. Drug transport across the blood–brain barrier. *Journal of Cerebral Blood Flow & Metabolism* **32**, 1959 (2012).
299. Mikitsh, J. L. & Chacko, A. M. Pathways for Small Molecule Delivery to the Central Nervous System Across the Blood-Brain Barrier. *Perspect Medicin Chem* **6**, 11 (2014).
300. Clark, D. E. What has polar surface area ever done for drug discovery? *Future Med Chem* **3**, 469–484 (2011).

301. Suenderhauf, C., Hammann, F. & Huwyler, J. Computational Prediction of Blood-Brain Barrier Permeability Using Decision Tree Induction. *Molecules* **17**, 10429 (2012).
302. Sleire, L. *et al.* Drug repurposing in cancer. *Pharmacol Res* **124**, 74–91 (2017).
303. Teml, A. *et al.* A prospective, open-label trial of 6-thioguanine in patients with ulcerative or indeterminate colitis. *Scand J Gastroenterol* **40**, 1205–1213 (2005).
304. Chaiyawat, P. *et al.* IMPDH2 and HPRT expression and a prognostic significance in preoperative and postoperative patients with osteosarcoma. *Sci Rep* **11**, 10887 (2021).
305. Pieters, R. *et al.* Prognostic Value of Hypoxanthine-Guanine Phosphoribosyl-Transferase in Childhood Leukemia. 405–409 (1994) doi:10.1007/978-3-642-78350-0\_73.
306. Li, Y. *et al.* Relationship between ATM and ribosomal protein S6 revealed by the chemical inhibition of Ser/Thr protein phosphatase type 1. *jstage.jst.go.jp* Y Li, S Mitsuhashi, M Ikejo, N Miura, T Kawamura, T Hamakubo, M Ubukata *Bioscience, biotechnology, and biochemistry, 2012*•*jstage.jst.go.jp* doi:10.1271/bbb.110774.
307. Ruvinsky, I. & Meyuhos, O. Ribosomal protein S6 phosphorylation: from protein synthesis to cell size. *Trends Biochem Sci* **31**, 342–348 (2006).
308. Ruvinsky, I. *et al.* Ribosomal protein S6 phosphorylation is a determinant of cell size and glucose homeostasis. *Genes Dev* **19**, 2199–2211 (2005).
309. Wettenhall, R. E. H., Erikson, E. & Maller, J. L. Ordered multisite phosphorylation of *Xenopus* ribosomal protein S6 by S6 kinase II. *Journal of Biological Chemistry* **267**, 9021–9027 (1992).
310. Sun, C. K. *et al.* Phosphorylation of ribosomal protein S6 confers PARP inhibitor resistance in BRCA1-deficient cancers. *Oncotarget* **5**, 3375 (2014).
311. Pokorný, J. *et al.* Substituted dienes prepared from betulonic acid – Synthesis, cytotoxicity, mechanism of action, and pharmacological parameters. *Eur J Med Chem* **224**, (2021).
312. Borková, L. *et al.* Synthesis and biological evaluation of triterpenoid thiazoles derived from betulonic acid, dihydrobetulonic acid, and ursonic acid. *Eur J Med Chem* **185**, (2020).
313. Hoover, B. R. *et al.* Tau mislocalization to dendritic spines mediates synaptic dysfunction independently of neurodegeneration. *Neuron* **68**, 1067–1081 (2010).
314. Di, L., Kerns, E. H., Hong, Y. & Chen, H. Development and application of high throughput plasma stability assay for drug discovery. *Int J Pharm* **297**, 110–119 (2005).
315. Rovelet-Lecrux, A. *et al.* De novo deleterious genetic variations target a biological network centered on A $\beta$  peptide in early-onset Alzheimer disease. *Molecular Psychiatry* **20**, 1046–1056 (2015).
316. Sun, W. *et al.* Attenuation of synaptic toxicity and MARK4/PAR1-mediated Tau phosphorylation by methylene blue for Alzheimer’s disease treatment. *Scientific Reports* **6**, 1–10 (2016).
317. Hübinger, G. *et al.* Inhibition of PHF-like tau hyperphosphorylation in SH-SY5Y cells and rat brain slices by K252a. *J Alzheimers Dis* **13**, 281–294 (2008).

318. Hu, L., Jiang, G., Xu, S., Pan, C. & Zou, H. Monitoring enzyme reaction and screening enzyme inhibitor based on MALDI-TOF-MS platform with a matrix of oxidized carbon nanotubes. *Journal of The American Society for Mass Spectrometry* 2006 17:11 **17**, 1616–1619 (2006).
319. Sanchez-Ruiz, A., Serna, S., Ruiz, N., Martin-Lomas, M. & Reichardt, N.-C. MALDI-TOF Mass Spectrometric Analysis of Enzyme Activity and Lectin Trapping on an Array of N-Glycans. *Angewandte Chemie* **123**, 1841–1844 (2011).
320. Ritorto, M. S. *et al.* Screening of DUB activity and specificity by MALDI-TOF mass spectrometry. *Nature Communications* 2014 5:1 **5**, 1–11 (2014).
321. Mirande, C. *et al.* Rapid detection of carbapenemase activity: benefits and weaknesses of MALDI-TOF MS. *European Journal of Clinical Microbiology and Infectious Diseases* **34**, 2225–2234 (2015).
322. Khan, N. S. *et al.* Thienopyrimidine-Chalcone Hybrid Molecules Inhibit Fas-Activated Serine/Threonine Kinase: An Approach To Ameliorate Antiproliferation in Human Breast Cancer Cells. *Mol Pharm* **15**, 4173–4189 (2018).
323. Advani, D. *et al.* Protective role of anticancer drugs in neurodegenerative disorders: A drug repurposing approach. *Neurochem Int* **140**, 104841 (2020).
324. Longley, D. B., Harkin, D. P. & Johnston, P. G. 5-Fluorouracil: mechanisms of action and clinical strategies. *Nature Reviews Cancer* 2003 3:5 **3**, 330–338 (2003).
325. Rando, A. *et al.* Chemotherapeutic agent 5-fluorouracil increases survival of SOD1 mouse model of ALS. *PLoS One* **14**, (2019).
326. De Stefano, N. *et al.* Reduced brain atrophy rates are associated with lower risk of disability progression in patients with relapsing multiple sclerosis treated with cladribine tablets. *Mult Scler* **24**, 222–226 (2018).
327. Montillo, M. *et al.* Phase II study of cladribine and cyclophosphamide in patients with chronic lymphocytic leukemia and prolymphocytic leukemia. *Cancer* **97**, 114–120 (2003).
328. Ruggieri, M. *et al.* Effect of Cladribine on Neuronal Apoptosis: New Insight of In Vitro Study in Multiple Sclerosis Therapy. *Brain Sciences* 2020, Vol. 10, Page 548 **10**, 548 (2020).
329. Faulds, D., Balfour, J. A., Chrisp, P. & Langtry, H. D. Mitoxantrone. *Drugs* 1991 41:3 **41**, 400–449 (2012).
330. Bleich, H. L. *et al.* New Approaches to Cancer Chemotherapy with Methotrexate. <http://dx.doi.org/10.1056/NEJM197504172921607> **292**, 846–851 (2010).
331. Dickey, A. S. *et al.* PPAR $\Delta$  activation by bexarotene promotes neuroprotection by restoring bioenergetic and quality control homeostasis. *Sci Transl Med* **9**, (2017).
332. Fewer, D., Wilson, C. B., Boldrey, E. B., Enot, K. J. & Powell, M. R. The Chemotherapy of Brain Tumors: Clinical Experience With Carmustine (BCNU) and Vincristine. *JAMA* **222**, 549–552 (1972).
333. Bellozi, P. M. Q. *et al.* Neuroprotective effects of the anticancer drug NVP-BEZ235 (dactolisib) on amyloid- $\beta$  1–42 induced neurotoxicity and memory impairment. *Scientific Reports* 2016 6:1 **6**, 1–12 (2016).

334. Ramachandran, V., Arun Nair, T. & Vadivelan, R. BEHAVIORAL STUDIES OF DASATINIB AND RESVERATROL IN ROTENONE INDUCED PARKINSON'S RAT MODEL. *Int J Pharm Sci Res* **10**, 2004–2011 (2019).
335. Shemesh, O. A. & Spira, M. E. Rescue of neurons from undergoing hallmark tau-induced Alzheimer's disease cell pathologies by the antimetabolic drug paclitaxel. *Neurobiol Dis* **43**, 163–175 (2011).

## 8 Bibliography

Articles and works related to Ph.D. thesis are labelled\*

### 8.1 Original articles and reviews

\***L. HRUBÁ**, V. DAS, M. HAJDÚCH, P. DŽUBÁK. Nucleoside-based anticancer drugs: Mechanism of action and drug resistance, *Biochem Pharmacol*, 2023, 215: 115741, IF: 6.1, DOI: 10.1016/j.bcp.2023.115741

\***M. JURÁŠEK**, J. ŘEHULKA, **L. HRUBÁ**, A. IVANOVA (NIKONENKO), S. GURSKÁ, O. MOKSHYNA, P. TROUSIL, K. HUML, P. POLISHCHUK, M. HAJDÚCH, P. DRAŠAR, P. DŽUBÁK, Triazole-based estradiol dimers prepared via CuAAC from 17 $\alpha$ -ethinyl estradiol with five-atom linkers causing G2/M arrest and tubulin inhibition, *Bioorganic Chemistry*, 2023, 131, 106334, 0045-2068, IF: 5.307, PMID: 36592487.

\***L. HRUBÁ**, P. POLISHCHUK, V. DAS, M. HAJDÚCH, P. DŽUBÁK, An identification of MARK inhibitors using high throughput MALDI-TOF mass spectrometry, *Biomedicine & Pharmacotherapy*, 2022, 146, 112549, 0753-3322, IF: 6.530, PMID: 34923338.

### 8.2 Book chapters

\***L. HRUBÁ**. Chapter 30: Functional test of MDR transporters. In J. DRÁBEK, P. DŽUBÁK, M. HAJDÚCH, M. MISTRÍK *et al.* Laboratory techniques in cellular and molecular medicine, Book, 2021

### 8.3 Oral and poster presentations

\***L. HRUBÁ**, K. JEČMEŇOVÁ, M. HAJDÚCH, P. DŽUBÁK. In vitro cellular models or nucleoside-based drugs resistance. In: Czech Annual Cancer Research Meeting, Abstract book, 2022

\***L. HRUBÁ**, V. DAS, P. POLISHCHUK, M. HAJDÚCH, P. DŽUBÁK. A high throughput screening of MARK inhibitors using MALDI-TOF/TOF mass. In: OL4PERMED, Abstract book, 2021

\***L. HRUBÁ**, K. JEČMEŇOVÁ, P. DŽUBÁK. Development and characterization of resistant cell lines to nucleoside based cytostatics. IMTM Reactor Conference, 2021

P. DŽUBÁK, M. HOCEK, D. HOLUB, **L. HRUBÁ**, K. JEČMEŇOVÁ, J. KOTULOVÁ, B. LIŠKOVÁ, M. POPPER, M. TICHÝ, J. VÁCLAVKOVÁ, J. VRBKOVÁ, P. ŽIŽKOVIČOVÁ, M. HAJDÚCH. Highly active anticancer drug, PNH173, mechanism of action. In: OL4PERMED, Abstract book, 2021

\***L. ŘEHÁČKOVÁ**. Mark inhibitors. IMTM Reactor Conference, Abstract book, 2020

\***L. ŘEHÁČKOVÁ**, K. JEČMEŇOVÁ, M. HAJDÚCH, P. DŽUBÁK. Development of resistant cell lines to nucleoside based cytostatics. XV. Diagnostic, Predictive and Experimental Oncology Days, Abstract book, 2019

\***L. ŘEHÁČKOVÁ**. Enzymatic reactions and their application in screening of MARK4 inhibitors. IMTM Reactor Conference, Abstract book, 2019

\***L. ŘEHÁČKOVÁ**. Screening of potential inhibitors of MARK4. IMTM Reactor Conference, Abstract book, 2018



## **9 Appendix – Full text publications related to the thesis**

### **9.1 Nucleoside-based anticancer drugs: Mechanism of action and drug resistance**

**L. HRUBÁ**, V. DAS, M. HAJDÚCH, P. DŽUBÁK. Nucleoside-based anticancer drugs: Mechanism of action and drug resistance, *Biochem Pharmacol*, 2023, 215: 115741, IF: 6.1, DOI: 10.1016/j.bcp.2023.115741

Personal contribution: conceptualization, literature review and writing, text edition, creation of graphic schemes



Contents lists available at ScienceDirect

Biochemical Pharmacology

journal homepage: [www.elsevier.com/locate/biochempharm](http://www.elsevier.com/locate/biochempharm)

Review

## Nucleoside-based anticancer drugs: Mechanism of action and drug resistance

Lenka Hrubá<sup>a</sup>, Viswanath Das<sup>a</sup>, Marian Hajdúch<sup>a,b</sup>, Petr Dzubak<sup>a,b,\*</sup>

<sup>a</sup> Institute of Molecular and Translational Medicine, Faculty of Medicine and Dentistry, Palacký University in Olomouc, Olomouc, Czech Republic  
<sup>b</sup> Laboratory of Experimental Medicine, University Hospital, Olomouc 779 00, Czech Republic

## ARTICLE INFO

## Keywords:

Drug resistance  
 Cancer  
 Nucleosides  
 ABC transporters  
 SLC transporters  
 Cancer therapy  
 Metabolism

## ABSTRACT

Nucleoside-based drugs, recognized as purine or pyrimidine analogs, have been potent therapeutic agents since their introduction in 1950, deployed widely in the treatment of diverse diseases such as cancers, myelodysplastic syndromes, multiple sclerosis, and viral infections. These antimetabolites establish complex interactions with cellular molecular constituents, primarily via activation of phosphorylation cascades leading to consequential interactions with nucleic acids. However, the therapeutic efficacy of these agents is frequently compromised by the development of drug resistance, a continually emerging challenge in their clinical application. This comprehensive review explores the mechanisms of resistance to nucleoside-based drugs, encompassing a wide spectrum of phenomena from alterations in membrane transporters and activating kinases to changes in drug elimination strategies and DNA damage repair mechanisms. The critical analysis in this review underlines complex interactions of drug and cell and also guides towards novel therapeutic strategies to counteract resistance. The development of targeted therapies, novel nucleoside analogs, and synergistic drug combinations are promising approaches to restore tumor sensitivity and improve patient outcomes.

## 1. Introduction

Cancer is a complex disease that affects millions of people around the world. Despite the availability of numerous treatments, curing and eradicating cancer proves challenging, largely due to the development of resistance by cancer cells to treatments. Mechanisms of chemoresistance (MOC) include several cellular alterations that significantly enhance cell survival. The first mechanism represents reduced drug uptake, particularly in the case of nucleoside-based drugs, facilitated by Concentrative Nucleoside Transporters (CNTs/*SLC28s*) and/or Equilibrative Nucleoside Transporters (ENTs/*SLC29s*). MOC-1b refers to an increased drug efflux, which can be often mediated by MDR (multidrug resistance) proteins such as P-glycoprotein (Pgp), Multidrug Resistance-related Proteins (MRPs) or Breast Cancer Resistance Protein (BCRP). MOC-2 is characterized by a decrease in the concentration of active metabolites due to the reduction of pro-drug activation or higher active metabolite elimination. Other mechanisms include cellular changes in drug targets (MOC-3), enhanced DNA-repair mechanisms (MOC-4), decreased activity of pro-apoptotic factors (MOC-5a), and/or increase of anti-apoptotic factors (MOC-5b), alterations in the tumor cells microenvironment (MOC-6), and activation

of epithelial-mesenchymal transition (EMT) (MOC-7) [1,2]. Historically, nucleosides, compounds comprising a ribose or 2-deoxyribose sugar ring and purine (adenine and guanine) or pyrimidine (cytosine, thymine, and uracil) bases, were among the first widely used anticancer and antiviral therapeutics [3,4]. As anticancer drugs, nucleosides belong to a class of antimetabolites, a category that encompasses purine or pyrimidine analogs (nucleosides), folic acid and amino acid analogs, and ribonucleotide reductase inhibitors.[5] In 1948, the first antimetabolite, aminopterin (4-aminopteroyl-glutamic acid), was used to treat acute leukemia in children, where it was shown to induce temporary remission.[6] Nucleosides compete with physiological nucleosides and interact with a plethora of intracellular targets involved in nucleoside metabolism and signaling. The nucleoside 6-mercaptopurine (6-MP), which was synthesized in 1950 for the treatment of acute leukemia, was one of the first nucleosides to be used clinically. A few years later, structurally similar 6-thioguanine (6-TG) was synthesized, which was gradually followed by other compounds such as gemcitabine.[7,8] While the first nucleosides targeted hematological malignancies, later-developed compounds like 5-fluorouracil and gemcitabine demonstrated high efficacy in solid tumors (Fig. 1) [9].

Currently, the primary obstacles in chemotherapy include tumor cell

\* Corresponding author.

E-mail address: [petr.dzubak@upol.cz](mailto:petr.dzubak@upol.cz) (P. Dzubak).<https://doi.org/10.1016/j.bcp.2023.115741>

Received 8 June 2023; Received in revised form 6 August 2023; Accepted 8 August 2023

Available online 9 August 2023

0006-2952/© 2023 The Authors. Published by Elsevier Inc. This is an open access article under the CC BY license (<http://creativecommons.org/licenses/by/4.0/>).

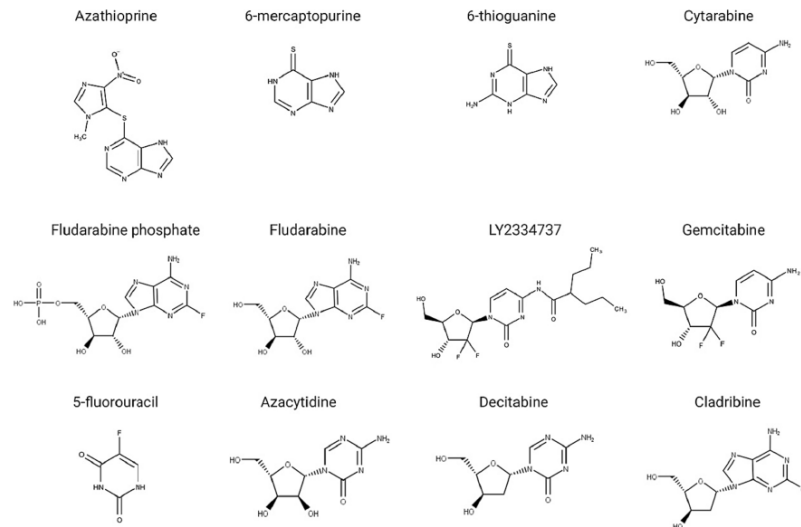


Fig. 1. Chemical structures of the most commonly used nucleoside-based anticancer drugs.

selectivity, systemic side effects, and the development of multidrug resistance due to recurrent treatment cycles, which reduce overall treatment efficacy.[10] This review summarizes the mechanisms underlying resistance of the most prevalently used nucleoside-based drugs, with a focus on drug transporters and clinically relevant resistance mechanisms, and potential strategies to overcome them.

1.1. 6-Mercaptopurine (6-MP)

6-mercaptopurine is a purine analog widely used for the treatment of acute leukemia. Its immunosuppressive properties also make it a suitable treatment option to treat autoimmune diseases and inflammatory conditions such as rheumatoid arthritis, Crohn’s disease, and ulcerative colitis.[11] In clinics, 6-MP is typically administered as a pro-drug

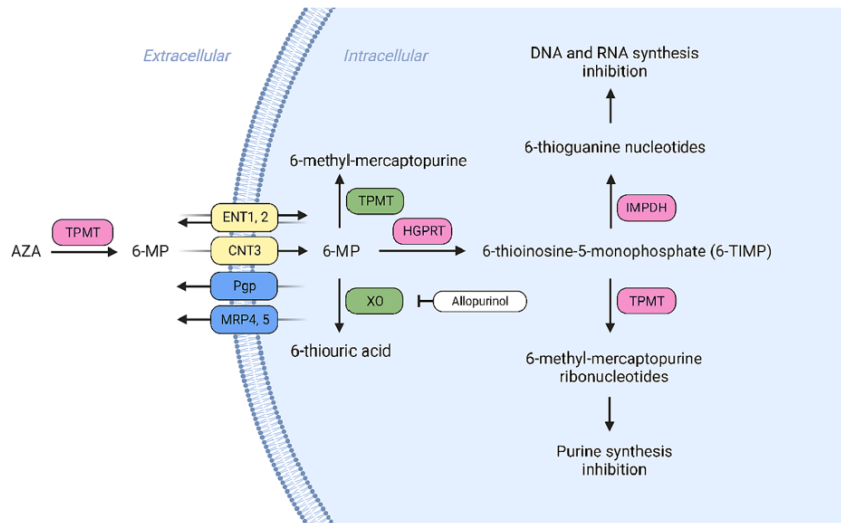


Fig. 2. Transport and metabolism of 6-mercaptopurine (6-MP). AZA: azathioprine, TPMT: Thiopurine S-methyl transferase, XO: Xanthine oxidase, HGPRT: Hypoxanthine-guanine phosphoribosyltransferase, IMPDH: Inosine-5'-monophosphate dehydrogenase.

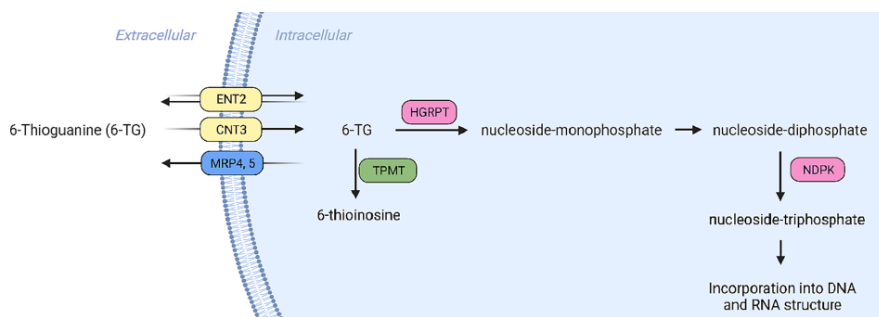


Fig. 3. Membrane transport and metabolism of 6-thioguanine (6-TG). HGRPT: Hypoxanthine-guanine phosphoribosyltransferase, TPMT: Thiopurine S-methyl transferase, NDPK: Nucleoside diphosphate kinase.

(azathioprine, AZA, Fig. 1), and both compounds are relatively slow acting, limiting their usage in monotherapy.[12] For pediatric patients with acute leukemia, 6-MP is recommended to be combined with methotrexate, resulting in a higher remission rate.[13] Recent research indicates that the addition of a low dose of 6-thioguanine (6-TG) to a 6-MP/methotrexate regimen improves disease-free survival in pediatric and adult patients newly diagnosed with acute lymphoblastic leukemia.[14] Furthermore, this combination therapy can be complemented by prednisone, which induces remission in patients with steroid-dependent inflammatory bowel disease (IBD) and Crohn's disease.[15].

The oral absorption of 6-MP is variable and incomplete, with approximately 50% of the dose entering the systemic circulation and a half-life ranging from 60 to 120 min.[16] In the case of intravenous administration, plasma half-disappearance varies from 21 min in pediatric patients to 47 min in adults. The primary catabolic pathways of 6-MP are methylation and oxidation. Other drugs, such as allopurinol, can inhibit the oxidative degradation of 6-MP by inhibition of xanthine oxidase (XO), which mediates 6-MP oxidation. However, this inhibition leads to an accumulation of 6-MP, resulting in increased toxicity without enhancing therapeutic effects.[17] Despite this, the combined therapy of allopurinol (or alternative XO inhibitor infliximab) and a low dose of thiopurines (AZA and 6-MP) has been suggested as a potential immunosuppressive strategy for treating adult patients with inflammatory bowel disease.[18] The combination of AZA/6-MP and allopurinol was initially considered controversial due to its side effects. Nonetheless, recent studies show that monitoring thiopurine metabolite levels can help adjust the dosage and reduce the adverse effects of the treatment.[19,20].

Azathioprine, the pro-drug of 6-MP,[12] is extracellularly metabolized to 6-MP by thiopurine S-methyl transferase (TPMT), and then transported into cells by nucleoside transporters.[21] Intracellularly 6-MP is converted to 6-methylmercaptopurine (6-MMP) by TPMT, and subsequently to 6-thiouric acid by xanthine oxidase, or alternatively, to 6-thioinosine 5-monophosphate (6-TIMP) via hypoxanthine-guanine phosphoribosyltransferase (HGPRT). 6-TIMP undergoes two potential metabolic pathways: 1) it can be converted into 6-methylmercaptopurine ribonucleotides (6-MMPR), which inhibits purine synthesis; or 2) it can be metabolized by inosine-5'-monophosphate dehydrogenase (IMPDH) into 6-thioguanine nucleotides, which inhibit DNA and RNA synthesis (Fig. 2) [22].

Resistance to 6-MP can develop through various mechanisms, including alterations in the expression of membrane transporters. Notably, 6-MP acts as a substrate for efflux pumps such as MDR1/P-glycoprotein (Pgp/ABCB1) and multidrug resistance-related proteins 4 and 5 (MRP4/ABCC4; MRP5/ABCC5). Overexpression of these efflux pumps can reduce 6-MP activity and lead to the development of a resistant phenotype.[23–26] Typically, a decrease in intracellular 6-MP

concentration is associated with alterations in the expression of influx/uptake transporters, such as equilibrative nucleoside transporters (ENTs/*SLC29s*) and concentrative nucleoside transporters (CNTs/*SLC28s*). Approximately half of 6-MP transport is carried out via a sodium-dependent mechanism.[27] Moreover, 6-MP has been identified as a substrate for ENT1/*SLC29A1*, ENT2/*SLC29A2*, and CNT3/*SLC28A3*. [27] Historically, sensitivity to 6-MP has often been associated with a decrease or loss in the activity of enzymes such as inosinic or guanylic acid pyrophosphorylase. These enzymes facilitate the formation of mercaptopurine ribonucleotides in human cancer cells.[28].

An activating mutation in *NT5C2* (cytosolic 5'-nucleotidase II) has been recently discovered in approximately 20% of patients diagnosed with acute lymphoblastic leukemia (ALL). *NT5C2*, as a nucleotidase, dephosphorylates and inactivates HGPRT, effectively inhibiting conversion of 6-MP into its active form and reducing its therapeutic effectiveness.[29] Consequently, leukemia cells with *NT5C2* mutations develop resistance to 6-MP. Overcoming this resistance can be achieved either through direct targeting of *NT5C2* or by the inhibition of compensatory pathways, which are notably active in cells with *NT5C2* mutations. One such pathway involves the enhanced purine biosynthesis due to the excess export of purine nucleosides in cells with *NT5C2* mutations. This leads to the activation of allosteric feedback loops, which in turn increases the sensitivity of these cells to the inhibition of IMPDH, a crucial enzyme in purine biosynthesis. By inhibiting IMPDH it's possible to partially compensate for the purine nucleotide depletion caused by the *NT5C2* mutation, thereby reducing the resistance of these cells to 6-MP. This approach offers a promising alternative strategy for the treatment of ALL in patients with *NT5C2* mutations [30].

Several studies have also identified a relationship between the inhibition of the mTOR pathway, particularly mTOR complex 1, and resistance to 6-MP in cases of B-cell acute lymphoblastic leukemia (B-ALL).[31] Another mechanism contributing to resistance involves the preferential metabolism of AZA into 6-MMP, particularly in patients with inflammatory bowel disease who exhibit a lower response to 6-MP. This effect appears to be dose-dependent; an increase in 6-MP results in a significant elevation in 6-MMP levels and minor changes in 6-thioguanine nucleotide concentrations [32].

Recent research has explored the genes *TPMT*, *NUDT15*, *ITPA*, and *APEX1* as potential predictive markers of 6-MP treatment efficacy in pediatric patients diagnosed with ALL. However, these markers have yet to find application in clinical settings.[33,34] Notably, variants of the *NUDT15* have been associated with the onset of thiopurine-induced leukopenia in Asian patients suffering from Crohn's disease. In particular, the homozygous T/T variant has been linked to the development of early leukopenia in nearly all observed cases. Consequently, the administration of 6-MP and 6-TG treatments is strongly discouraged in these cases [35,36].

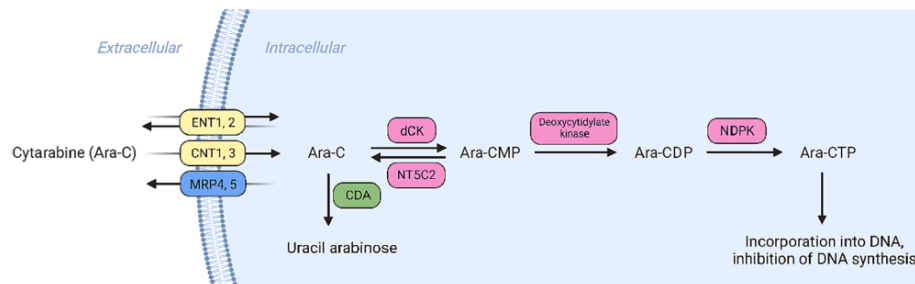


Fig. 4. Membrane transport and metabolism of cytarabine (Ara-C). Ara-CMP: Cytarabine-monophosphate, Ara-CDP: Cytarabine-diphosphate, Ara-CTP: Cytarabine-triphosphate, CDA: Cytidine deaminase, dCK: Deoxycytidine kinase, NDPK: Nucleoside diphosphate kinase.

### 1.2. 6-Thioguanine (6-TG)

6-Thioguanine, a metabolite structurally akin to 6-MP, can often induce cross-resistance due to its similarities. Despite this resemblance, both 6-TG and 6-MP have distinct metabolic pathways and modes of action. In instances where patients with inflammatory bowel disease (IBD) experience adverse effects from 6-MP therapy, 6-TG is often used as an alternative therapeutic agent.[37] In haemato-oncology, 6-TG, when combined with cytarabine, serves to induce remission in patients suffering from acute and chronic myeloid leukemia (ALL, CML). Preclinical studies also suggest its efficacy against prostate and pancreatic cancers.[39–41] Recent research has explored the potential of a 6-TG and disulfiram/Cu combination in inhibiting the cellular proliferation of triple-negative breast cancer. This combination seemingly disrupts DNA damage checkpoints and enhances DNA damage.[42] Furthermore, this drug combination appears to synergistically inhibit tumor-associated deubiquitinases, ubiquitin-specific protease 2 and 21 (USP2 and USP21). The activity of these enzymes is related to breast and prostate cancers, as well as hepatocellular carcinomas, making them potential targets in cancer therapy [43].

Once orally administered, 6-TG is converted into nucleoside-monophosphate by hypoxanthine-guanine phosphoribosyltransferase (HGPRT) and then phosphorylated into di- (TGDP) and tri-phosphate (TGTP) forms by nucleoside diphosphate kinase (NDPK).[44,45] Subsequently, TGTP is incorporated into the nucleic acid structure, inhibiting DNA and RNA synthesis, and leading to cellular death (Fig. 3).[46] The absorption of 6-TG by patients varies, with an average bioavailability of approximately 30% and a median half-life of 90 min. Unlike 6-MP, 6-TG metabolism does not rely on xanthine oxidase (XO), implying that a combination therapy with XO inhibitors, such as allopurinol, does not impact the activity or toxicity of the drug. 6-TG is metabolized into its inactive form, 6-thioinosine, via TPMT.[47] Pancreatic ductal adenocarcinoma cells (PDACs) exhibit low levels of TPMT, which makes 6-TG an ideal candidate for the treatment of this cancer type. The reduced inactivation via TPMT increases the efficacy of 6-TG therapy in such cases [41].

Resistance to 6-TG is often correlated with mutations in *HGPRT*, as shown in mismatch repair-deficient cell lines. These cell lines exhibit greater resistance compared to those with a fully functional DNA-repair system.[48] Mutations and inactivation of *HGPRT* impede the metabolism of 6-TG into its active form. Interestingly, such mutations have been detected in circulating human lymphocytes, with the frequency of mutated cells increasing with patient age, indicating a potential relationship between aging and mutagenesis.[49] *In vitro* experiments with melanoma cells have demonstrated that 6-TG resistant cells express approximately three times more methylguanine-DNA methyltransferase (MGMT), a DNA repair enzyme. Administration of MGMT inhibitors has been shown to enhance the sensitivity of resistant cell lines to 6-TG,

suggesting a correlation between MGMT activity and resistance to 6-TG.[50] Resistance to 6-TG can also be linked to variations in the expression levels of membrane transporters. For instance, leukemia cells (MOLT-4) displaying reduced levels of ENT2 and CNT3, transporters critical to drug influx, demonstrate resistance to 6-TG.[51] It is important to note that 6-TG is also a substrate of efflux pumps, such as MRP4 and 5.[52] The relationship between MRP4 levels and 6-TG sensitivity has been observed in Japanese patients with IBD.[53] Since 6-TG is not a substrate of P-glycoprotein (Pgp), it has the potential to be used in tumors with elevated Pgp levels, such as breast and ovarian cancers with BRCA1 mutations. This could potentially overcome resistance to Poly (ADP-ribose) polymerase (PARP) inhibitors [54].

### 1.3. Cytarabine (Ara-C, cytosine arabinose)

Cytarabine, a cytosine analog, is a cornerstone in the treatment of ALL, Acute Non-Lymphocytic Leukemia (ANLL), the blast phase of CML, and Acute Myeloid Leukemia (AML).[55–57] The Food and Drug Administration (FDA) gave its approval to cytarabine for cancer treatment in 1969, and it has been administered in combination with other anticancer drugs to augment its efficacy since the 1990s. For example, in AML patients over 60 years, cytarabine is often used in combination with clofarabine.[58] An estimated 20–35% of AML patients harbor a mutation in the *DNMT3A* gene (DNA methyltransferase 3A), predisposing them to drug resistance (mainly to anthracyclines), a higher incidence of minimal residual disease and an increased risk of clinical relapse, particularly in an advanced-aged cohort. Yet, those carrying the *DNMT3A* R882 mutation exhibit heightened sensitivity to the replication stress induced by cytarabine. For patients with a wild-type variant of the *DNMT3A* gene, a combination of cytarabine and PARP inhibitors can enhance treatment efficacy [59].

Furthermore, cytarabine can be co-administered with decitabine, a combination that has shown improved prognosis in elderly patients with high-risk AML.[60] Younger and adult AML patients have also demonstrated favorable responses to the combined regimen of cytarabine, sorafenib, and idarubicin.[61,62] Recently, a combination of venetoclax with low-dose cytarabine has emerged as an effective treatment for adult AML patients who cannot undergo standard intensive chemotherapy (IC). This combined therapy can induce complete remission in 60–80 % of patients aged 16–60 years [63].

While the standard dose of cytarabine is 100–200 mg/m<sup>2</sup> body surface area, a higher dose (3 g/m<sup>2</sup> body surface area) with an elimination half-life of 3–4 h has demonstrated superior efficacy in AML treatment, although the underlying mechanism responsible for this difference remains elusive.[64,65] This high-dose cytarabine therapy is also administered to children and adolescents with ALL, ANLL, CML, and Burkitt's lymphoma. Despite serious side effects, including bone marrow suppression, nausea, vomiting, fever, and diarrhea, the increased

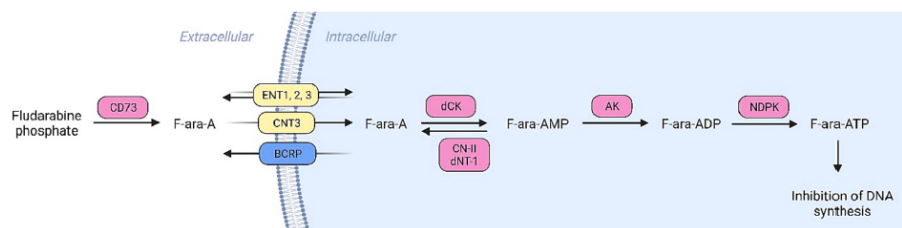


Fig. 5. Membrane transport and metabolism of fludarabine (F-ara-A). F-ara-A: Fludarabine, F-ara-AMP: Fludarabine monophosphate, F-ara-ADP: Fludarabine diphosphate, F-ara-ATP: Fludarabine triphosphate, CD73: Ecto-5'-nucleotidase, dCK: Deoxycytidine kinase, CN-II: 5'nucleotidase, dNT-1: Deoxynucleotidase-1, AK: Adenylate kinase, NDPK: Nucleoside diphosphate kinase.

cytarabine dose has proven effective in inducing remission in patients with lymphoma resistant to the standard dose [66].

Oral administration of cytarabine is less effective due to its high first-pass metabolism, with less than 20% of the drug being absorbed from the gastrointestinal tract (GIT). The primary metabolism of cytarabine into its inactive form, uracil arabinose (Ara-U), is facilitated by cytidine deaminase (CDA). Overexpression of CDA has been implicated in the development of cytarabine resistance, and it is also recognized as a valuable predictive marker of toxicity in cytarabine treatment.[67,68] Notably, lower CDA activity has been observed in adult patients suffering from severe or lethal toxicity [67].

Cytarabine is typically administered intravenously, intrathecally, or subcutaneously due to its limited absorption through the GIT. Primarily transported into cells via the ENT1 transporter, cytarabine also serves as a substrate for ENT2 CNT1 and CNT3.[69] The efflux of cytarabine is facilitated by MRP4 and 5, and the overexpression of these proteins can contribute to the development of cytarabine resistance [70,71].

Following its transport into cells, mainly via the ENT1 transporter [72], cytarabine is phosphorylated into its active form, cytarabine triphosphate (Ara-CTP). This conversion is facilitated by deoxycytidine kinase (dCK), deoxycytidylate kinase, and nucleoside diphosphate kinase (NDPK) (Fig. 4). The efficacy of cytarabine is directly related to the expression of these proteins.[64] Once activated, Ara-CTP incorporates into the nascent DNA, leading to the induction of single-strand breaks, replication fork stalling, and eventually, cell death [73].

Resistance to cytarabine can primarily emerge due to: a) rapid elimination by CDA, b) restricted intracellular transport associated with reduced ENT1 expression or c) limited activation due to inhibition or reduced expression of activating kinases, notably dCK.[39] Levin et al. (2019) documented the loss of dCK function in cytarabine-resistant acute myeloblastic cells, which exhibited hypersensitivity to a combination of hydroxyurea (HU) and azidothymidine (AZT), an approach that could potentially overcome cytarabine resistance.[74] Recent *in vitro* studies have highlighted the role of CD157 (ADP-ribosyl cyclase 2) in cytarabine sensitivity in AML. CD157 induces the expression of anti-apoptotic proteins, particularly Mcl-1, while its inhibition has been shown to enhance the efficacy of cytarabine treatment in CD157-high AML cells [75].

Cytarabine resistance is also correlated with the expression of cytosolic 5-nucleotidase II (NT5C2), which inactivates cytarabine by dephosphorylating cytarabine monophosphate into cytarabine.[76] Furthermore, SAMHD1 (SAM and HD domain-containing protein 1), a deoxynucleotide triphosphate triphosphorylase, has been identified as a predictive marker of cytarabine treatment efficacy. SAMHD1 hydrolyzes Ara-CTP, leading to a significant reduction in cytarabine activity.[77] Inhibitors of SAMHD1, such as hydroxyurea, can suppress Ara-CTP hydrolysis and enhance the efficacy of cytarabine [78,79].

An analysis of AML primary cells resistant to cytarabine treatment has revealed a link between high mitochondrial oxidation based on Bcl2 and cytarabine resistance. Consequently, these cells exhibited high

sensitivity to the combined therapy of venetoclax and cytarabine. However, adaptive resistance can occur due to changes in oxidative phosphorylation, electron transport chain complex and/or the p53 pathway. Using electron transport chain inhibitors, mitochondrial ClpP protease agonists, or pyruvate dehydrogenase inhibitors could potentially offer ways to overcome this adaptive cytarabine/venetoclax resistance [80].

Recent findings suggest a role for glucose transporters (GLUTs) in determining the sensitivity of AML cells to cytarabine. Specifically, heightened glycolysis appears to diminish the sensitivity of these cells to chemotherapy in AML. Consequently, the inhibiting of glucose uptake may enhance the cells' sensitivity to cytarabine treatment [81].

#### 1.4. Fludarabine (F-ara-A)

Fludarabine is a purine analog primarily employed in the treatment of lymphoproliferative malignancies, notably chronic lymphocytic leukemia (CLL). It has also proven to be useful in managing AML.[82,83] Fludarabine can be used alone or in combination with other anticancer drugs, including cytarabine, ibrutinib, bortezomib, cyclophosphamide, rituximab, clofarabine, and idarubicin.[84–86] Recent research has revealed fludarabine's potential as an inhibitor of DNA-dependent RNA polymerase in the treating of monkeypox virus [87].

Fludarabine is typically administered as the 5-O-phosphorylated pro-drug, fludarabine phosphate, and it is converted into the active form, F-ara-A, by the ectoenzyme CD73 (ecto-5'-nucleotidase, 5-NT). The drug has an elimination half-life of approximately 20 h.[88] The drug enters cells mainly via ENT1, ENT2, ENT3 and CNT3, after which it is phosphorylated into mono-, di-, and active triphosphate forms F-ara-AMP, F-ara-DTP, and F-ara-ATP by deoxycytidine kinase (dCK), adenylate kinase (AK), and nucleoside diphosphate kinase (NDPK), respectively (Fig. 5).[88,89] For patients with CML, fludarabine is often used in tandem with cytarabine, as fludarabine elevates the intracellular concentration of cytarabine triphosphate and augments its activity [90].

In adults, CML is frequently associated with the overexpression of MDR proteins, such as Pgp, breast cancer resistance protein (BCRP/ABCG2), multidrug resistance-related proteins (MRPs), and lung resistance-related protein (LRP). Higher expression of these proteins is viewed as a negative prognostic marker. Fludarabine, which is not typically associated with MDR, has shown resistance in cases with heightened expression of Pgp, MRP1, and LRP.[91] As fludarabine is a substrate for BCRP, its treatment efficacy decreases in patients with BCRP-positive CML, which also heightens the risk of relapse [92].

Fludarabine resistance primarily presents in adult patients with CLL. A study of peripheral blood mononuclear cells (PBMCs) from fludarabine-sensitive and resistant CLL patients revealed a significant increase in the expression of Pgp, glucosylceramide synthase (GSC), and CD34, a marker of leukemic stem cells. Higher GSC expression leads to the accumulation of glucosylceramide, which fosters cell proliferation, and survival, inhibits apoptosis, and stimulates resistance development.

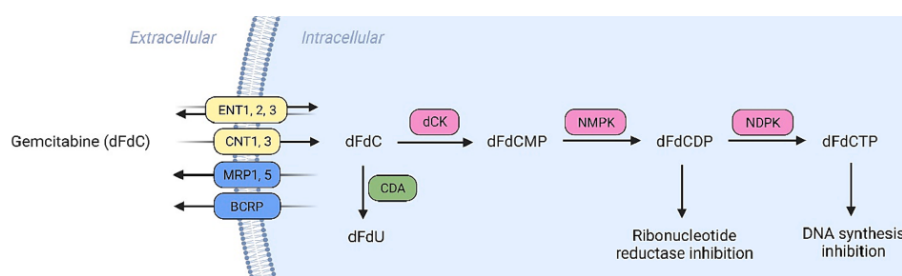


Fig. 6. Membrane transport and metabolism of gemcitabine (dFdC). dCK: Deoxycytidine kinase, CDA: Cytidine deaminase, dFdU: 2,2-difluoro-2-deoxyuridine, dFdCMP: Gemcitabine-monophosphate, dFdCDP: Gemcitabine-diphosphate, dFdCTP: Gemcitabine-triphosphate, NMPK: Nucleotide monophosphate kinase, NDPK: Nucleotide diphosphate kinase.

This fludarabine resistance can be counteracted by inhibiting GSC with 1-phenyl-2-decanoylamino-3-morpholino-1-propanol (PDMP) [93].

In CLL, mitochondrial metabolism plays a key role in fludarabine sensitivity. Beyond the effect of enhanced oxidative phosphorylation and reactive oxygen species (ROS) production, recent studies have drawn a link between mitochondrial abnormalities (such as mtDNA mutations, aberrant mitochondrial biogenesis, respiration, and increased superoxide production) and a negative impact on apoptosis, which results in the development of fludarabine resistance. Moreover, malignancies showing reduced sensitivity to fludarabine seem to rely heavily on ER-Golgi protein transport. Therefore, targeting this process could present a promising therapeutic strategy that may also influence fludarabine efficacy [94–96].

CLL cell lines exhibit a more robust endoplasmic reticulum network compared to normal B-lymphocytes. Brefeldin A, an anticancer compound targeting the ER, has demonstrated its ability to induce apoptosis in fludarabine-resistant CLL cells.[94] Additionally, fludarabine resistance in CLL cell lines is linked with increased phosphorylation of ribosomal protein S6 kinase (phospho-p70S6K), activated by the mTORC1 complex implicated in translation. This mTORC1 activation is relatively prevalent across a wide range of cancers. However, mTORC1 inhibitors, including rapamycin and its analogs (rapalogs), often fail to produce the anticipated clinical effect as they only inhibit phosphatidylinositol-3-kinase (PI3K) and don't affect Akt. A compensatory surge in Akt activity has been observed, leading to a pro-survival effect. Nevertheless, in fludarabine-resistant and primary CLL cells, rapalogs succeeded in triggering cell death and inhibiting oxidative phosphorylation and glycolysis, both of which are elevated in these fludarabine-resistant cells. Thus, the inhibition of mitochondrial respiration and down-regulation of mTORC1 may prove selectively cytotoxic to fludarabine-resistant CLL cells, presenting a potential therapeutic target to counteract drug resistance [95].

CLL cells are also found to have higher levels of ROS compared to normal lymphocytes. Trachootham et al. (2008) explored a strategy to eliminate fludarabine-resistant cells using ROS and discovered that fludarabine-sensitive/resistant CLL cell lines were five times more sensitive to the anticancer and chemopreventive agent  $\beta$ -phenethyl isothiocyanate (PEITC) than normal lymphocytes. The exposure of fludarabine-resistant CLL cells to PEITC resulted in ROS accumulation, glutathione depletion, and the oxidation of mitochondrial cardiolipin, causing cellular death [96].

### 1.5. Gemcitabine (GEM, dFdC)

Gemcitabine, a deoxycytidine nucleoside analog, is deployed in the treatment of solid tumors, including breast, non-small cell lung, pancreatic, bladder, and ovarian cancers.[97–99] Its more efficient phosphorylation and activation, along with slower elimination

compared to other nucleoside drugs, make gemcitabine one of the most effective nucleoside-based anticancer drugs. The half-life of gemcitabine after a brief infusion ranges from 32 to 94 min and is extended to 4 to 10 h with a longer infusion. Innovative strategies are being explored, utilizing gemcitabine in the form of a pro-drug, LY2334737, as its valproic ester [100,101].

Gemcitabine is actively transported into cells, primarily via ENT1 (SLC29A1) and CNT3 (SLC28A3). Once inside the cell, gemcitabine is phosphorylated into gemcitabine-monophosphate (dFdCMP) by deoxycytidine kinase (dCK), gemcitabine-diphosphate (dFdCDP) by nucleotide monophosphate kinase (NMPK), and gemcitabine-triphosphate (dFdCTP), the active metabolite accountable for the cytotoxic effect of gemcitabine, by nucleotide diphosphate kinase (NDPK).[102] Gemcitabine-diphosphate inhibits ribonucleotide reductase (RR), which is responsible for deoxyribonucleotide synthesis. In contrast, gemcitabine-triphosphate disrupts DNA synthesis (Fig. 6).[103,104] A portion of the incorporated triphosphate nucleosides is eliminated by the 3-5exonuclease. As detailed by Yang et al. (2020), gemcitabine mono/di/triphosphates can inhibit the 3-5exonuclease and increase the incorporation of gemcitabine-triphosphates [105].

The conversion of gemcitabine into 2,2-difluoro-2-deoxyuridine (dFdU) is mediated by cytidine deaminase, which also plays a crucial role in the clearance of gemcitabine [106].

Though gemcitabine often prompts an excellent initial response, drug resistance tends to develop over time. This resistance is primarily associated with factors such as increased efflux/reduced influx (primarily via ENT1), alterations in drug metabolism, inhibition of apoptosis, changes in micro-RNA levels, and the presence of cancer stem cells (CSCs) with heightened expression of efflux pumps.[107] CDA is a protein involved in the metabolic deactivation of cytidine analogs, encompassing not only gemcitabine but also cytarabine, azacytidine, and decitabine. The expression level of CDA could serve as a reliable marker for predicting the efficacy of these analog treatments, alongside the expression level of ENT1, the primary transporter for gemcitabine influx and dCK, which mediates gemcitabine activation [108,109].

Various transporters, predominantly ENTs that function as both influx and efflux pumps, as well as ABC transporters, especially MRP5, are involved in gemcitabine efflux. The latter is associated with multi-drug resistance.[110] Although the relationship between Pgp expression and gemcitabine resistance remains unclear, over-expression of Pgp seems to heighten the cells' sensitivity to gemcitabine.[111].

Recent studies have suggested an association between alterations in the Erk/Akt/Stat3, Hedgehog (Hh), Wnt and Notch pathways and the development of gemcitabine resistance.[112] Specifically, the Erk/Akt/Stat3 pathway, activated by cyclin L1 (CCNL1), promotes cell survival, thereby facilitating the development of gemcitabine resistance [113].

Gemcitabine resistance has also been linked to the Hedgehog pathway (Hh), particularly in patients with urothelial carcinoma. In

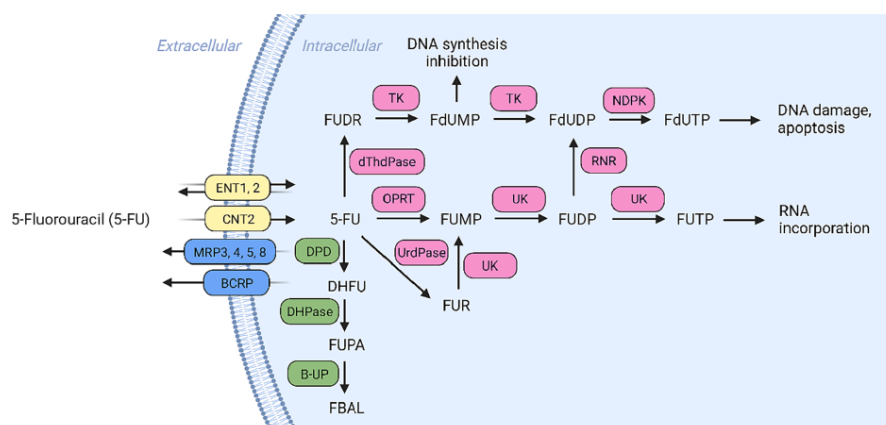


Fig. 7. Membrane transport and metabolism of 5-fluorouracil (5-FU). FBAL:  $\alpha$ -fluoro- $\beta$ -alanine,  $\beta$ -UP:  $\beta$ -ureidopropionase, FUPA:  $\alpha$ -fluoro- $\beta$ -ureido propionic acid, DHPase: Dihydropyrimidinase, DHFU: 5,6-dihydro-5-fluorouracil, DPD: Dihydropyrimidine dehydrogenase, UrdPase: Uridine phosphorylase, FUR: Fluorouridine, UK: Uridine kinase, OPRT: Orotate phosphoribosyltransferase, FUMP: Fluorouridine monophosphate, FUDP: Fluorouridine diphosphate, FUTP: Fluorouridine triphosphate, dThdPase: Thymidine phosphorylase, FUDR: Fluorodeoxyuridine, TK: Thymidine kinase, FdUMP: Fluorodeoxyuridine monophosphate, FdUDP: Fluorodeoxyuridine diphosphate, NDPK: Nucleoside diphosphate kinase, FdUTP: Fluorouridine triphosphate.

these cases, gemcitabine induces a Gli2-dependent activation of the Hh pathway, which in turn fosters cell migration and invasion, enhancing the resistant phenotype. Consequently, a potential strategy to reduce gemcitabine resistance in these patients could involve targeting the Gli2 pathway.[114] The Hh pathway also plays a significant role in the tumorigenesis of pancreatic adenocarcinoma (PC). However, clinical trials involving patients with PC treated with vismodegib, an Hh pathway inhibitor, alongside gemcitabine, have not demonstrated any significant differences in treatment efficacy when compared to a control group.[115].

The Wnt pathway, featuring  $\beta$ -catenin as a crucial protein in its signaling cascade, also contributes to gemcitabine resistance. Studies focused on the correlation between  $\beta$ -catenin expression and the efficacy of gemcitabine treatment in pancreatic carcinoma have shown that patients with lower  $\beta$ -catenin expression demonstrated enhanced sensitivity to gemcitabine and significantly longer disease-free and overall survival compared to those presenting high  $\beta$ -catenin expression [116].

Gemcitabine resistance has also been associated with dysregulation of the Notch pathway, frequently upregulated in pancreatic and ovarian cancer.[117,118] An increased expression of Notch3 is associated with reduced sensitivity to gemcitabine, which is mediated by the activation of the PI3K/Akt pathway. Consequently, a decrease in Notch3 expression reduces PI3K/Akt activity, thereby inducing apoptosis in resistant cells.[119].

Research has indicated that pancreatic cancer is not only associated with alterations in the Hh, Wnt, and Notch pathways but that gemcitabine-resistant cells also demonstrate an increase in tumor stemness.[107] While the exact mechanism remains somewhat unclear, the induction of pancreatic cell stemness seems to result from the activation of the AKT/Notch1 pathway. Hypoxia further augments the activation of this pathway, thereby promoting the development of a resistant phenotype [120].

#### 1.6. 5-Fluorouracil (5-FU)

5-fluorouracil ranks among the earliest nucleoside-based anticancer drugs, together with 6-MP and 6-TG. First synthesized in 1957, it has since been employed in the treatment of patients with breast, colon, or head and neck cancers [121] 5-FU, an analog of uracil, is used both as a

monotherapy and in combination with other anticancer drugs, such as methotrexate, leucovorin, baicalin, and oxaliplatin in order to enhance treatment efficacy [122–124] The combined use of 5-FU and curcumin has also demonstrated promising results in sensitizing 5-FU-resistant tumor cells.[125] Both *in vitro* and *in vivo* studies have provided evidence that tazemetostad (an inhibitor of the histone methyltransferase EZH2) can increase sensitivity to 5-FU treatment in cases of colorectal cancer [126].

5-FU is administered intravenously, and approximately 80%–85% of the given dosage is rapidly catabolized and deactivated (with an elimination time between 8 and 20 min) by dihydropyrimidine dehydrogenase (DPD) into 5,6-dihydro-5-fluorouracil (DHFU). Subsequently, it is processed by dihydropyrimidinase (DHPase) into  $\alpha$ -fluoro- $\beta$ -ureido propionic acid (FUPA), and then by  $\beta$ -ureidopropionase ( $\beta$ -UP) into  $\alpha$ -fluoro- $\beta$ -alanine (FBAL). The remaining molecules are mainly metabolized into fluorouridine monophosphate (FUMP) by orotate phosphoribosyltransferase (OPRT), with phosphoribosyl pyrophosphate acting as a cofactor. FUMP can also be indirectly synthesized from fluorouridine (FUR) by uridine kinase (UK).[127].

FUMP is phosphorylated by UK into fluorouridine diphosphate (FUDP), which can then be phosphorylated by UK into fluorouridine triphosphate (FUTP) and subsequently incorporated into the RNA structure. Alternatively, FUDP can be converted by ribonucleotide reductase (RNR) into fluorodeoxyuridine diphosphate (FdUDP) [128,129].

Additionally, 5-FU can be activated by thymidine phosphorylase (dThdPase) into fluorodeoxyuridine (FUDR).[127] FUDR is phosphorylated by thymidine kinase (TK) into fluorodeoxyuridine monophosphate (FdUMP), which inhibits thymidylate synthase (TS), a key enzyme in the synthesis of 2-deoxythymidine-5-monophosphate (dTMP). Enhancing or prolonging TS inhibition could potentially improve 5-FU treatment efficacy.[129–131] FdUMP also contributes to 5-FU myelotoxicity and cytotoxicity in the GIT.[127] FdUMP can be further phosphorylated by TK into FdUDP, which is then phosphorylated by nucleoside diphosphate kinase (NDPK) into FdUTP, another active metabolite of 5-FU that can cause DNA damage and apoptosis (Fig. 7). [132].

The limitations of 5-FU therapy include dose-dependent toxicity and the development of multidrug resistance. Several mechanisms have been



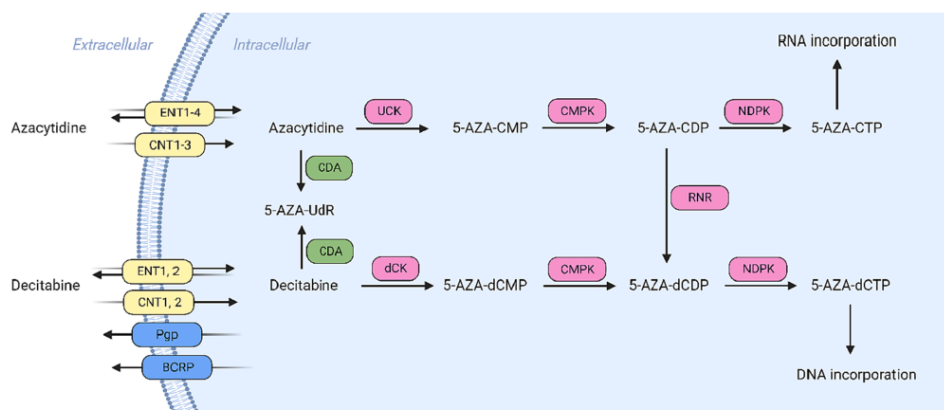


Fig. 8. Membrane transport and metabolism of azacytidine and decitabine. 5-AZA-Udr: 5-AZA-2-deoxyuridine, CDA: Cytidine deaminase, UCK: Uridine-cytidine kinase, dCK: Deoxycytidine kinase, 5-AZA-CMP: 5-azacytidine-monophosphate, CMPK: Cytosine monophosphate kinase, 5-AZA-CDP: 5-azacytidine-diphosphate, NDPK: Nucleoside diphosphate kinase, 5-AZA-CTP: 5-azacytidine-triphosphate, 5-AZA-dCMP: 5-AZA-2-deoxycytidine-monophosphate, 5-AZA-dCDP: 5-AZA-2-deoxycytidine-diphosphate, 5-AZA-dCTP: 5-AZA-2-deoxycytidine-triphosphate.

identified that contribute to altered sensitivity to 5-FU treatment. These include modifications of drug influx/efflux pumps, accelerated degradation or limited activation, and a deficiency in dihydropyrimidine dehydrogenase which can cause fatal 5-FU toxicity and alterations in various genes and molecules. These include the insulin-like growth factor-1 receptor, epidermal growth factor receptor, nuclear factor kappa B, cyclooxygenase-2, activator of transcription 3, the anti-apoptotic Bcl-2, and pro-apoptotic Bax proteins. [123,125,133] The expression of thymidylate synthase (TS) has also been recognized as one of the most important predictive markers of 5-FU sensitivity in cancer treatment. Higher TS expression is known to decrease 5-FU sensitivity. [131,134].

The overexpression of Nrf3 (nuclear factor erythroid 2-like 3) and Bcl-2 has been observed in 5-FU-resistant tissues, with Nrf3 found to promote Bcl-2 expression. [135] Another factor contributing to 5-FU resistance is the hypermethylation of the *MLH1* gene promoter. This hypermethylation inhibits *MLH1* expression, which is involved in DNA mismatch repair (MMR). Cells with hypermethylated *MLH1* resist various anticancer drugs, including 5-FU. *In vitro* experiments have shown that this resistance can be overcome by the re-expression of *MLH1* via the demethylation of the promoter region by decitabine. [136].

FOXM1 is another transcription factor involved in 5-FU resistance. FOXM1 is essential for DNA repair, angiogenesis, and metastasis, and the knockout of FOXM1 results in increased sensitivity to 5-FU treatment. [137,138] These studies have also highlighted an association between cancer stem cells (CSCs) and alterations in anticancer drug

sensitivity. CSCs, being quiescent and poorly differentiated populations, may evade 5-FU treatment targeting cell proliferation. [137].

The disruption of the p53 pathway is a predictive marker of the efficacy of combination therapy with 5-FU and oxaliplatin in patients with gastric cancer. Defects in this pathway are associated with a poorer response to treatment. [139].

The transport of 5-FU across the cell membrane is mediated by various transporters, including ABC transporters and nucleoside transporters. A study investigating 5-FU-resistant pancreatic carcinoma cells revealed a significant increase in the expression of MRP3, 4, and 5. Furthermore, the silencing of MRP5 was found to increase sensitivity to 5-FU. [140] An association between MRP5 overexpression and 5-FU resistance has been reported in both colon and breast cancers. [141,142] An analysis of small-cell lung cancer cells resistant to 5-FU demonstrated an approximately 25-fold increase in MRP3 expression. Interestingly, the alteration in MRP3 expression was induced by 5-FU treatment. The expression level of MRP3 is directly correlated with active 5-FU efflux and resistance development. [143] Overexpression of both MRP5 and MRP3 has been observed in colorectal cancer patients. [142].

While Pgp does not transport 5-FU, *in vitro* studies using 5-FU-resistant gastric cancer cell lines have shown that increased Pgp expression can lead to cross-resistance to taxanes such as paclitaxel and docetaxel. [144].

5-FU is a substrate of the breast cancer resistance protein (BCRP), which is primarily associated with drug resistance in breast cancer. Therefore, BCRP expression could potentially serve as another

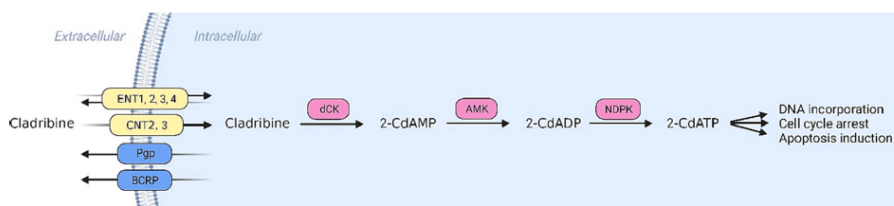


Fig. 9. Membrane transport and metabolism of cladribine. 2-CdAMP: Cladribine-monophosphate, dCK: Deoxycytidine kinase, 2-CdADP: Cladribine-diphosphate, AMK: Adenosine-monophosphate kinase, 2-CdATP: Cladribine-triphosphate, NDPK: Nucleoside diphosphate kinase.

**Table 1**  
Nucleoside-based drugs and their predictive markers.

Drug	Disease	Predictive markers	Clinical relevance	References
5-fluorouracil	Colon cancer	ERCC1, PARP-1, AQP1	ERCC1 positivity, high expressions of PARP-1, and negative expression of AQP1 are associated with tumor progression	[203]
	Gastric cancers	p53	A defective p53 signalling pathway is associated with a worse response to combined 5-FU and oxaliplatin treatment	[139]
	Solid tumors	DPD	A DPD deficiency can cause fatal 5-FU toxicity	[133]
6-mercaptopurine	ALL	TS	Lower expression/activity of TS increases 5-FU treatment efficacy	[131]
		TPMT, NUD15, ITPA, and APEX1	Currently studied candidates for predictive markers of 6-MP therapy	[33]
6-thioguanine	IBD	NUD15	T/T homozygous variant of <i>NUD15</i> is strongly associated with thiopurine-induced leukopenia in Asian patients	[35,36]
	IBD	HGPRT	A mutation or inactivation of <i>HGPRT</i> blocks the activating metabolism of 6-TG	[49]
		MRP4	Overexpression of the MRP4 efflux pump is associated with decreased 6-TG efficacy	[53]
Azacitidine	Melanoma	NUD15	T/T homozygous variant of <i>NUD15</i> is strongly associated with thiopurine-induced leukopenia in Asian patients	[35,36]
	Hematologic malignancies	MGMT	DNA repair enzyme, which is overexpressed in 6-TG resistant cells	[56]
Cladribine	Hematologic malignancies, MS	CDA	Lower expression is associated with higher treatment efficacy	[157]
		UCK	Lower expression leads to lower azacytidine activation	[157]
Cytarabine	AML	dCK	Cladribine activating kinase; lower expression decreases treatment efficacy	[176]
		CDA	Overexpression causes cytarabine resistance, and lower activity is associated with severe/lethal toxicity	[67]
		dCK	Ara-C activating kinase; loss of dCK function leads to Ara-C resistance	[56]
Decitabine	Hematologic malignancies	ENT1	Lower expression decreases the concentration of intracellular cytarabine	[72]
		NTSC2	It inactivates Ara-C by dephosphorylating Ara-C monophosphate to Ara-C and decreases cytarabine treatment efficacy	[76]
		SAMHD1	Deoxynucleotide triphosphate triphosphorylase, which hydrolyses Ara-CTP and decreases Ara-C treatment efficacy	[77]
Fludarabine	CLL	CDA	Higher expression leads to faster elimination of decitabine	[157]
		dCK	dCK phosphorylates decitabine into its active form; lower expression decreases decitabine treatment efficacy	[157]
Gemcitabine	CML	GSC	GSC overexpression leads to the accumulation of glucosylceramide, promoting proliferation, cell survival, apoptosis inhibition, and development of fludarabine resistance	[93]
		BCRP	There is a decrease in fludarabine treatment efficacy in patients with BCRP-positive CML, and higher relapse risk	[92]
		CDA	This protein is involved in gemcitabine inactivation; a lower expression can lead to toxicity	[169]
Solid tumors	dCK	The gemcitabine activating kinase; the inhibition/lower expression of which decreases treatment efficacy	[109]	
	ENT1	The primary gemcitabine influx transporter; a higher expression is associated with increased sensitivity to gemcitabine	[109]	

Table 2

Nucleoside-based drugs as binding partners of MDR proteins and substrates for transporters: P-glycoprotein (Pgp), multidrug resistance-associated proteins (MRPs), lung resistance-related protein (LRP), breast cancer resistance protein (BCRP), and nucleoside transporters: equilibrative nucleoside transporters (ENTs) and concentrative nucleoside transporters (CNTs).

Nucleoside-based drug	Pgp	MRPs	LRP	BCRP	ENTs	CNTs	Ref.
5-fluorouracil	No	MRP3, 4, 5, 6	Yes	Yes	ENT1, 2	CNT2	[140,141,143-148]
6-mercaptopurine	Yes	MRP4, 5	Nd	Yes	ENT1, 2	CNT3	[23-27,196]
6-thioguanine	No	MRP4, 5	Nd	Nd	ENT2	CNT3	[51,52]
Azacytidine	Nd	Nd	Nd	Nd	ENT 1, 2, 3, 4	CNT1, 2, 3	[158]
Cladribine	Yes	No	Nd	Yes	ENT1, 2, 3, 4	CNT3	[64,173,177]
Cytarabine	No	MRP4, 5	Nd	No	ENT1, 2	CNT1, 3	[69-72,147,199]
Decitabine	Yes	Nd	Nd	Yes	ENT1, 2	CNT1, 2	[158,167,168]
Fludarabine	No	Nd	Nd	Yes	ENT1, 2, 3	CNT3	[198,200]
Gemcitabine	No	MRP1, 5	Nd	Yes	ENT1, 2, 3	CNT1, 3	[102,110,202,202]

Nd: Not described.

prognostic marker of 5-FU treatment efficacy.[145] Research has shown that the lung resistance protein (LRP), also known as the human major vault protein (MVP), is involved in the development of resistance to 5-FU.[146] 5-FU uptake is mediated mainly via nucleoside transporters, specifically ENT1, ENT2, and CNT2. The expression levels of these transporters could potentially help predict the efficacy of 5-FU treatment. However, resistance to 5-FU is typically associated with low expression or inhibition of these transporters.[147-149].

### 1.7. 5-Azacytidine

5-Azacytidine, a pyrimidine analog of cytidine, was firstly synthesized in 1963. Since then, azacytidine has primarily been used in the treatment of AML, chronic myelomonocytic leukemia, and myelodysplastic syndrome (MDS), which transforms into leukemia in approximately 30% of patients.[150,151].

Azacytidine can be administered both as a monotherapy and in combination therapy. In adult patients, azacytidine, when combined with venetoclax, has shown promising results for the treatment of AML.[152] This therapeutic combination also appears to be effective in managing high-risk MDS or chronic myelomonocytic leukemia.[153] The bioactivation process of azacytidine begins with its phosphorylation by the uridine-cytidine kinase (UCK) into 5-azacytidine-monophosphate (5-AZA-CMP). This compound is then phosphorylated by the cytosine nucleoside monophosphate kinase (CMPK) into 5-azacytidine-diphosphate (5-AZA-CDP). Subsequently, the nucleoside diphosphate kinase (NDPK) phosphorylates this diphosphate into 5-azacytidine-triphosphate (5-AZA-CTP), which is incorporated into RNA.[154] Azacytidine exhibits a relatively short elimination half-life, approximately 41 min, and its metabolism is similar to that of decitabine.[151] 5-AZA-CDP can be further metabolized by the ribonucleotide reductase (RNR) into 5-AZA-dCDP, which represents a phosphorylated form of decitabine (Fig. 8).[155] The inactivation of azacytidine can occur either by spontaneous hydrolysis or by the action of the cytidine deaminase (CDA), which metabolizes azacytidine into 5-AZA-2-deoxyuridine (5-AZA-UdR).[154].

Resistance to azacytidine can arise from various factors, such as the decreased activation of kinases (particularly uridine-cytidine kinase 2 [UCK2]), diminished expression levels of CDA, alterations in the pyrimidine metabolism pathway, or the expression of specific membrane transporters.[156,157] Although azacytidine is transported by ENT1-4 and CNT1-3, CNT3 seems to play a pivotal role.[158] Consequently, a reduction in expression or inhibition of these transporters may diminish the efficacy of azacytidine. While no direct correlation has been reported between azacytidine resistance and Pgp over-expression, cell-based experiments have revealed an enhancement in azacytidine efficacy following the inhibition of ABC transporters (Pgp and MRPs) by erlotinib.[159,160].

Next-generation sequencing of patients with AML and MDS treated with azacytidine has uncovered numerous genetic mutations. However,

none of these were significantly associated with treatment response. The only clinical marker linked with shorter survival was a platelet count of less than 50,000/ $\mu$ l.[161] The expression of UCK, which phosphorylates azacytidine into its active form, and CDA, which is responsible for the deactivation and elimination of azacytidine, could potentially serve as predictive markers for azacytidine treatment efficacy.[157].

### 1.8. Decitabine (5-AZA-2-deoxycytidine, 5-AZA-CdR)

Decitabine is a compound structurally similar to azacytidine, synthesized a year later in 1964. Like azacytidine, decitabine is indicated for the treatment of adult patients diagnosed with AML and MDS.[151,162] Decitabine is used as a monotherapy or in combination with talacotuzumab for AML patients, and with cedazuridine for patients suffering from MDS or CMML.[163].

Decitabine is administered intravenously and transported into cells primarily via ENT1 and CNT1, and to a lesser extent, via ENT2 and CNT2.[158] Within the cell, decitabine is phosphorylated into 5-AZA-2-deoxycytidine-monophosphate (5-AZA-dCMP) by deoxycytidine kinase (dCK). Following this, 5-AZA-dCMP undergoes phosphorylation by cytosine monophosphate kinase (CMPK) to form diphosphate (5-AZA-dCDP) and subsequently into triphosphate (5-AZA-dCTP) by nucleoside diphosphate kinase (Fig. 8).[155] The 5-AZA-2-deoxycytidine triphosphate (5-AZA-dCTP) is incorporated into DNA, thereby inhibiting DNA methylation.[164] The half-life of decitabine ranges between 37 and 47 min.[151].

Our understanding of the mechanism behind decitabine resistance remains incomplete. However, in cases of MDS, non-responders have been observed to exhibit higher expression of CDA compared to responders, leading to increased elimination of decitabine.[165] Decitabine treatment efficacy is also related to the expression of dCK, which plays a role in its activating phosphorylation. Lower expression levels of this kinase may contribute to reduced efficacy of decitabine treatment.[166] Both decitabine and azacytidine resistance have been linked with alterations in the pyrimidine metabolism pathway.[157] Although decitabine is a substrate for BCRP protein, over-expression of this protein has not been reported in decitabine-resistant cell lines.[159,167] Decitabine is a poor Pgp substrate, and *in vitro* studies show, that decitabine treatment decreases Pgp expression leading to increasing sensitivity to drugs, which are Pgp substrates.[168].

### 1.9. Cladribine (2-CdA)

Cladribine, an analog of deoxyadenosine, is used to treat multiple sclerosis (MS) and hairy cell leukemia.[169,170] Cladribine is a pro-drug and is metabolized into its active form, cladribine-triphosphate. The oral bioavailability of cladribine varies from 37% to 51%, but reaches 100% when administered subcutaneously.[171] The drug has an elimination half-life of approximately 10 h.[172] Cladribine enters cells via ENT1, 2, 3, 4, CNT2, and 3,[173] and is subsequently

phosphorylated by deoxycytidine kinase (dCK) into cladribine-monophosphate (2-CdAMP). Following this, 2-CdAMP is phosphorylated by adenosine-monophosphate kinase (AMK) into cladribine-diphosphate (2-CdADP), and then by nucleoside diphosphate kinase (NDPK) into cladribine-triphosphate (2-CdATP) (Fig. 9).[174] Upon integration into DNA, 2-CdATP inhibits ribonuclease reductase and arrests the cell cycle. Cladribine also induces apoptosis in non-dividing cells.[169].

The resistance to cladribine is multifaceted, attributed to factors such as increased activity of 5'-nucleotidase, which dephosphorylates cladribine-monophosphate into its inactive form, decreased activity of the activating dCK, or alterations in the apoptotic pathway.[175,176] Cladribine is a substrate of Pgp and BCRP but not MRPs, and elevated expression of these efflux pumps may adversely impact cladribine's efficacy.[172,173,177].

## 2. Current strategies to overcome nucleoside-based drug resistance

The development of drug resistance is a multifactorial process, including cellular changes improving cancer cell viability and proliferation.[10] Drug resistance can be connected with the altered expression of enzymes involved in the metabolic pathways, which activate or eliminate drugs. This is called cross-resistance, which arise among drugs with similar structure or mechanism of action. This kind of resistance is typical, for example, between 6-mercaptopurine and 6-thioguanine, [178] or among cytarabine, gemcitabine, and fludarabine, which are intracellularly activated by the same kinase (dCK).[179] Therapeutic strategy how to overcome this resistance can be choosing a drug with a different structure, and/or mechanism of action or to employ combinatory therapy, which can enhance treatment efficacy.

Multidrug resistance (MDR) rising between drugs with completely different chemical structures and mechanisms of action is typically associated with altered expression of ABC-transporters (Pgp, MRPs, BCRP).[180,181] Since these proteins were identified as risk factors for MDR development, they became potential therapeutic targets. Until now, four generations of Pgp inhibitors were synthesized, but clinical trials did not demonstrate significantly improved therapeutic effects. [182] Reason for this failure can be the fact that ABC-transporters are very often co-expressed, and their substrate specificity is overlapping, so inhibition of one of them can be compensated by the others. Recently dual Pgp/BCRP inhibitors, such as flavonoids, their precursors and derivatives, curcumin, chalcone, and quinazoline derivatives etc., have been investigated with promising results.[183–186] In contrast, some MRP inhibitors show clinical relevance by themselves. For example, Ibrutinib, an MRP1 inhibitor, is improving the cytotoxicity of drugs that are substrates of this transporter.[187].

Other cellular mechanisms of chemoresistance are not connected only with the expression of membrane transporters or with the activity of metabolic enzymes. These therapeutic targets include changes at the genomic or proteomic level, which can be heterogeneous among patients. Identifying biomarkers is important in finding new therapeutic approaches based on synthesizing small drug molecules, antibiotics, and monoclonal antibodies, which are the main focus of current research. [188] please in this position insert (te'In addition to direct binding to a cellular target and eliciting an immune response, monoclonal antibodies can also be applied as conjugates with anticancer drugs leading to the accumulation of drugs in the tumor tissue or with radionuclides enabling focus cytotoxic effect of radiation only at a specific location.[189,190] Specific binding and reducing the side effect caused by the off-target interactions is the biggest advantage of using monoclonal antibodies in cancer treatment.

The first antibody-drug conjugate (ADC), vindesine-anti-CEA, was successfully prepared in 1983, and many others followed.[191] However, finding the optimal combination of drug and antibody is

challenging, and not all ADCs have successfully passed the clinical trial. Currently, more than 11 FDA-approved ADCs are utilized in clinical settings, for example, gemtuzumab ozogamicin, which is used in the treatment of acute myeloid leukemia, brentuximab vedotin used in the treatment of Hodgkin lymphoma or ado-trastuzumab emtansine for breast cancer treatment.[192–193].

Nucleoside-based drugs are also being studied in their conjugated form. In this case, aptamer-drug conjugates (ApDCs) are being developed, which utilize nucleic acids instead of monoclonal antibodies.[195] Aptamers have been constructed for many nucleoside drugs. For example, the RNA aptamer (P19) was developed for gemcitabine and 5-fluorouracil, and these ApDCs significantly inhibited the proliferation of gemcitabine-resistant pancreatic cells.[196] In 2022, a new class of drug-constituted DNA-like oligomers, known as "drugtamers", were developed for clofarabine, gemcitabine, floxuridine and ara-guanosine. Compared to ApDCs drugtamers are expected to have a higher loading ratio, active targeting capability, and enzymatically controlled release of active compounds. This represents a promising advancement in the field of drug conjugates.[197].

The ultimate goal of current research is to advance personalized medicine, which can identify the optimal treatment for each individual patient. The identification of predictive markers is a useful tool, enabling the prediction of treatment efficacy and the implementation of the most effective cancer therapy.

## 3. Conclusion

Nucleosides, as delineated in Table 1, represent a versatile group of antimetabolites that have been successfully applied in the treatment of a broad spectrum of conditions, including diverse forms of cancer, myelodysplastic syndromes (MDSs), multiple sclerosis, and viral infections. The mechanism of action of this class of drugs typically involves the activation of a phosphorylation cascade, culminating in the formation of triphosphate forms that interact with nucleic acids. However, as these drugs take effect, cancer cells can evolve strategies to resist their impacts. While the pathways leading to resistance are diverse and multifactorial, several common pathways emerge, including a) alterations in membrane transporters, which can be characterized by reduced expression or activity of ENTs, CNTs, and/or overexpression of efflux pumps such as Pgp, MRPs, and BCRP (refer to Table 2); b) reduced activity of activating kinases, which may result in decreased phosphorylation of the drug and its capacity to interact with nucleic acids; and c) accelerated drug elimination through the activation of metabolic processes or increased renal clearance (see Table 1). Alongside these mechanisms, cancer cells may also develop resistance to nucleoside drugs by activating DNA repair mechanisms. This approach enables cancer cells to repair the damage caused by nucleoside drugs, thereby reducing their effectiveness.

Given these complex resistance mechanisms, several strategies for countermeasures have been proposed. These include targeted therapies, the development of innovative nucleoside drugs, and the formulation of unique drug combinations yielding synergistic effects. Such strategies hold the potential to prevent and overcome the resistant phenotype, thereby restoring tumor sensitivity and ultimately enhancing patient survival rates. The development of new strategies to combat resistance to nucleoside drugs continues to be a vibrant area of research, promising further breakthroughs in the future.

## Declaration of Competing Interest

The authors declare that they have no known competing financial interests or personal relationships that could have appeared to influence the work reported in this paper.

## Acknowledgments

This work was supported in parts from infrastructural projects (CZ-OPENSREEN – LM2023052; EATRIS-CZ – LM2023053) and the project National Institute for Cancer Research (Program EXCELES, ID Project No. LX22NPO5102), and by project nr. LX22NPO5107 (MEYS): Financed by EU – Next Generation EU, and by the IGA\_LF\_2023\_025.

## References

- [1] J.J.G. Marin, et al., Molecular bases of drug resistance in hepatocellular carcinoma, *Cancers (Basel)* 12 (2020) 1–26.
- [2] H.C. Zheng, The molecular mechanisms of chemoresistance in cancers, *Oncotarget* 8 (2017) 59950.
- [3] K.L. Seley-Radtke, J.E. Thames, C.D. Waters, Broad spectrum antiviral nucleosides—Our best hope for the future, *Annu. Rev. Med. Chem.* 57 (2021) 109–132.
- [4] M. Guinan, C. Benckendorff, M. Smith, G.J. Miller, Recent advances in the chemical synthesis and evaluation of anticancer nucleoside analogues, *Molecules* 25 (2020).
- [5] S.J. Clarke, A.L. Jackman, K.R. Harrap, Antimetabolites in cancer chemotherapy, *Adv. Exp. Med. Biol.* 309 (1991) 7–13.
- [6] S. Farber, L.K. Diamond, R.D. Mercer, R.F. Sylvester, J.A. Wolff, Temporary remissions in acute leukemia in children produced by folic acid antagonist, 4-aminopterin-glutamic acid, *N. Engl. J. Med.* 238 (1948) 787–793.
- [7] M. Pannico, P. Musto, SERS spectroscopy for the therapeutic drug monitoring of the anticancer drug 6-Mercaptopurine: Molecular and kinetic studies, *Appl. Surf. Sci.* 539 (2021), 148225.
- [8] M. Tu, A. Zhang, L. Hu, F. Wang, A retrospective cohort study of the efficacy, safety, and clinical value of 6-TG versus 6-MP maintenance therapy in children with acute lymphoblastic leukemia, *Biomol. Res. Int.* 2022 (2022).
- [9] C.M. Galmarni, J.R. Mackey, C. Dumontet, Nucleoside analogues and nucleobases in cancer treatment, *Lancet Oncol.* 3 (2002) 415–424.
- [10] A.F. Read, T. Day, S. Huijben, The evolution of drug resistance and the curious orthodoxy of aggressive chemotherapy, *Proc. Natl. Acad. Sci.* 108 (2011) 10871–10877.
- [11] Mercaptopurine. *LiverTox: Clinical and Research Information on Drug-Induced Liver Injury* (2017).
- [12] N.K. Ye, W.J. Park, D.W. Eom, M.Y. Oh, J.H. Lee, Effects of azathioprine and its metabolites on inflammatory cytokines in human nasal polyp organ cultures, *Int Forum Allergy Rhinol* 9 (2019) 648–655.
- [13] E. Frei, et al., Studies of sequential and combination antimetabolite therapy in acute leukemia: 6-mercaptopurine and methotrexate, *Blood* 18 (1961) 431–454.
- [14] L.N. Toksvang, et al., Thiopurine Enhanced ALL Maintenance (TEAM): study protocol for a randomized study to evaluate the improvement in disease-free survival by adding very low dose 6-thioguanine to 6-mercaptopurine/methotrexate-based maintenance therapy in pediatric and adult patients (0–45 years) with newly diagnosed B-cell precursor or T-cell acute lymphoblastic leukemia treated according to the intermediate risk-high group of the ALLTogether1 protocol, *BMC Cancer* 22 (2022).
- [15] J. Maté-Jiménez, C. Hermida, 6-mercaptopurine or methotrexate added to prednisone induces and maintains remission in steroid-dependent inflammatory bowel disease, *Eur. J. Gastroenterol. Hepatol.* 12 (2000) 1227–1233.
- [16] van Laar, J. M. Immunosuppressive Drugs. *Kelley and Firestein's Textbook of Rheumatology* 983-998.e4 (2017) doi:10.1016/B978-0-323-31696-5.00062-0.
- [17] S.E. Conneely, S.L. Cooper, R.E. Rau, Use of allopurinol to mitigate 6-mercaptopurine associated gastrointestinal toxicity in acute lymphoblastic leukemia, *Front. Oncol.* 10 (2020) 1129.
- [18] M.L. Seinen, K.h. De Boer, A.A. Van Bodegraven, S.B. Hanauer, F. Hoentjen, Allopurinol-thiopurine combination therapy in inflammatory bowel disease, *Clin. Investig.* (2014) 873–879, <https://doi.org/10.4155/CLI.14.81>.
- [19] J. Amin, B. Huang, J. Yoon, D.Q. Shih, Update 2014: advances to optimize 6-mercaptopurine and azathioprine to reduce toxicity and improve efficacy in the management of IBD, *Inflamm. Bowel Dis.* 21 (2015) 445–452.
- [20] E.L.S.A. van Lier, et al., Azathioprine with allopurinol is a promising first-line therapy for inflammatory bowel diseases, *Dig. Dis. Sci.* 67 (2022) 4008–4019.
- [21] C. Cuffari, A Physician's guide to azathioprine metabolite testing, *Gastroenterol. Hepatol. (N Y)* 2 (2006) 58.
- [22] G.L.C. Chan, G.R. Erdmann, S.A. Gruber, A.J. Matas, D.M. Canafax, Azathioprine metabolism: pharmacokinetics of 6-mercaptopurine, 6-thiouric acid and 6-thioguanine nucleotides in renal transplant patients, *J. Clin. Pharmacol.* 30 (1990) 358–363.
- [23] X.X. Peng, et al., Up-regulation of P-glycoprotein confers acquired resistance to 6-mercaptopurine in human chronic myeloid leukemia cells, *Oncol. Lett.* 2 (2011) 549.
- [24] Y. Chen, et al., Discovery of novel multidrug resistance protein 4 (MRP4) inhibitors as active agents reducing resistance to anticancer drug 6-Mercaptopurine (6-MP) by structure and ligand-based virtual screening, *PLoS One* 13 (2018) e0205175.
- [25] J. Wijnholds, et al., Multidrug-resistance protein 5 is a multispecific organic anion transporter able to transport nucleotide analogs, *Proc. Natl. Acad. Sci.* 97 (2000) 7476–7481.
- [26] H. Zeng, Z.P. Lin, A.C. Sartorelli, Resistance to purine and pyrimidine nucleoside and nucleobase analogs by the human MDR1 transfected murine leukemia cell line L1210/VMDRC.06, *Biochem. Pharmacol.* 66 (2004) 911–921.
- [27] L.S. Conklin, et al., 6-mercaptopurine transport in human lymphocytes: Correlation with drug-induced cytotoxicity, *J. Dig. Dis.* 13 (2012) 82.
- [28] R.W. Brockman, Biochemical aspects of mercaptopurine inhibition and resistance - PubMed, *Cancer Res.* 23 (1963) 1191–1201.
- [29] G. Tzoneva, et al., Activating mutations in the NT5C2 nucleotidase gene drive chemotherapy resistance in relapsed ALL, *Nat. Med.* 19 (2013) 368–371.
- [30] C.L. Dieck, A. Ferrando, Genetics and mechanisms of NT5C2-driven chemotherapy resistance in relapsed ALL, *Blood* 133 (2019) 2263–2268.
- [31] T.T.T. Vo, et al., mTORC1 Inhibition Induces resistance to methotrexate and 6-mercaptopurine in Ph + and Ph-like B-ALL, *Mol. Cancer Ther.* 16 (2017) 1942–1953.
- [32] M.C. Dubinsky, et al., 6-MP metabolite profiles provide a biochemical explanation for 6-MP resistance in patients with inflammatory bowel disease, *Gastroenterology* 122 (2002) 904–915.
- [33] Lee, J. M., Shim, Y. J., Kim, D. H., Jung, N. & Ha, J. S. The Effect of NUDT15, TPMT, APEX1, and ITPA genetic variations on mercaptopurine treatment of pediatric acute lymphoblastic leukemia. *Children* 2021, Vol. 8, Page 224 8, 224 (2021).
- [34] T.W. Kouwenberg, et al., Dosage of 6-mercaptopurine in relation to genetic TPMT and ITPA variants: toward individualized pediatric acute lymphoblastic leukemia maintenance treatment, *J. Pediatr. Hematol. Oncol.* 42 (2020) e94–e97.
- [35] J.H. Lee, et al., Measurements of 6-thioguanine nucleotide levels with TPMT and NUDT15 genotyping in patients with Crohn's disease, *PLoS One* 12 (2017) e0189925.
- [36] K. Matsuoka, NUDT15 gene variants and thiopurine-induced leukopenia in patients with inflammatory bowel disease, *Intest. Res* 18 (2020) 275.
- [37] B. Jharap, et al., Biotransformation of 6-thioguanine in inflammatory bowel disease patients: a comparison of oral and intravenous administration of 6-thioguanine, *Br. J. Pharmacol.* 163 (2011) 722.
- [38] L. Chen, H.X. Yan, X.W. Liu, W.X. Chen, Clinical efficacy and safety of 6-thioguanine in the treatment of childhood acute lymphoblastic leukemia: A protocol for systematic review and meta-analysis, *Medicine* 99 (2020) e20082.
- [39] C. Arthur, et al., Prolonged administration of low-dose cytarabine and thioguanine in elderly patients with acute myeloid leukemia (AML) achieves high complete remission rates and prolonged survival, *Leuk. Lymphoma* 61 (2020) 831–839.
- [40] Laera, L., Guaragnella, N., Giannattasio, S. & Moro, L. 6-Thioguanine and its analogs promote apoptosis of castration-resistant prostate cancer cells in a BRCA2-dependent manner. *Cancers* 2019, Vol. 11, Page 945 11, 945 (2019).
- [41] I. Kim, et al., A drug-repositioning screen for primary pancreatic ductal adenocarcinoma cells identifies 6-thioguanine as an effective therapeutic agent for TPMT-low cancer cells, *Mol. Oncol.* 12 (2018) 1526–1539.
- [42] M. Chu, et al., Combination of the 6-thioguanine and disulfiram/Cu synergistically inhibits proliferation of triple-negative breast cancer cells by enhancing DNA damage and disrupting DNA damage checkpoint. *Biochimica et Biophysica Acta (BBA) - Molecular, Cell Res.* 1869 (2022), 119169.
- [43] H.C. Lin, et al., Disulfiram and 6-thioguanine synergistically inhibit the enzymatic activities of USP2 and USP21, *Int. J. Biol. Macromol.* 176 (2021) 490–497.
- [44] S. Karner, et al., Determination of 6-thioguanosine diphosphate and triphosphate and nucleoside diphosphate kinase activity in erythrocytes: novel targets for thiopurine therapy? *Ther. Drug Monit.* 32 (2010) 119–128.
- [45] L. Zhang, D.J. Hinz, G.S.M. Kiruba, X. Ding, J.K. Lee, Gas-phase experimental and computational studies of human hypoxanthine-guanine phosphoribosyltransferase substrates: Intrinsic properties and biological implications, *J. Phys. Org. Chem.* 35 (2022) e4343.
- [46] L. Ding, et al., Hypoxanthine guanine phosphoribosyltransferase activity is related to 6-thioguanine nucleotide concentrations and thiopurine-induced leukopenia in the treatment of inflammatory bowel disease, *Inflamm. Bowel Dis.* 18 (2012) 63–73.
- [47] L. Dean, Thiopurine therapy and TPMT and NUDT15 genotype, *Medical Genetics Summaries* (2020).
- [48] W.E. Glaab, et al., Resistance to 6-thioguanine in mismatch repair-deficient human cancer cell lines correlates with an increase in induced mutations at the HPRT locus, *Carcinogenesis* 19 (1998) 1931–1937.
- [49] A.A. Morley, S. Cox, R. Holluday, Human lymphocytes resistant to 6-thioguanine increase with age, *Mech. Ageing Dev.* 19 (1982) 21–26.
- [50] N. Gefen, et al., Acquired resistance to 6-thioguanine in melanoma cells involves the repair enzyme O 6-methylguanine-DNA methyltransferase (MGMT), *Cancer Biol. Ther.* 49 (2010) 49–55.
- [51] A.K. Fotoohi, M. Lindqvist, C. Peterson, F. Albertoni, Involvement of the concentrative nucleoside transporter 3 and equilibrative nucleoside transporter 2 in the resistance of T-lymphoblastic cell lines to thiopurines, *Biochem. Biophys. Res. Commun.* 343 (2006) 208–215.
- [52] P.R. Wieling, et al., Thiopurine metabolism and identification of the thiopurine metabolites transported by MRP4 and MRP5 overexpressed in human embryonic kidney cells, *Mol. Pharmacol.* 62 (2002) 1321–1331.
- [53] H. Ban, et al., The multidrug-resistance protein 4 polymorphism is a new factor accounting for thiopurine sensitivity in Japanese patients with inflammatory bowel disease, *J. Gastroenterol.* 45 (2010) 1014–1021.
- [54] N. Issaeva, et al., 6-thioguanine selectively kills BRCA2-defective tumors and overcomes PARP inhibitor resistance, *Cancer Res.* 70 (2010) 6268–6276.

- [55] L. Möllgård, et al., High single dose of mitoxantrone and cytarabine in acute non-lymphocytic leukemia: A pharmacokinetic and clinical study, *Theor. Drug Monit.* 20 (1998) 640–645.
- [56] J.E. Cortes, et al., Glasdegib in combination with cytarabine and daunorubicin in patients with AML or high-risk MDS: Phase 2 study results, *Am. J. Hematol.* 93 (2018) 1301–1310.
- [57] R. Hehlmann, et al., Assessment of imatinib as first-line treatment of chronic myeloid leukemia: 10-year survival results of the randomized CML study IV and impact of non-CML determinants, *Leukemia* 2017 31:11 31, 2398–2406 (2017).
- [58] S. Faderl, et al., Clofarabine and cytarabine combination as induction therapy for acute myeloid leukemia (AML) in patients 50 years of age or older, *Blood* 108 (2006) 45–51.
- [59] K. Venugopal, et al., DNMT3A Harboring Leukemia-Associated Mutations Directs Sensitivity to DNA Damage at Replication Forks, *Clin. Cancer Res.* 28 (2022) 756–769.
- [60] M. Hong, et al., Decitabine in combination with low-dose cytarabine, aclarubicin and G-CSF tends to improve prognosis in elderly patients with high-risk AML, *Aging (Albany NY)* 12 (2020) 5792.
- [61] A.B. Halpern, et al., Addition of sorafenib to cladribine, high-dose cytarabine, G-CSF, and mitoxantrone (CLAG-M) in adults with newly-diagnosed acute myeloid leukemia (AML) and high-grade myeloid neoplasms independent of FLT3-mutation status: final results of a phase 1/2 study, *Blood* 140 (2022) 8999–9001.
- [62] F. Ravandi, et al., Final report of phase II study of sorafenib, cytarabine, and idarubicin for initial therapy in younger patients with acute myeloid leukemia, *Leukemia* 28 (2014) 1543.
- [63] R. Dillon, et al., Venetoclax combined with low dose cytarabine compared to standard of care intensive chemotherapy for the treatment of favourable risk adult acute myeloid leukaemia (VICTOR): Study protocol for an international, open-label, multicentre, molecularly-guided randomised, phase II trial, *BMC Cancer* 22 (2022) 1–13.
- [64] Z. Li, et al., Exploring the antitumor mechanism of high-dose cytarabine through the metabolic perturbations of ribonucleotide and deoxyribonucleotide in human promyelocytic Leukemia HL-60 Cells, *Molecules* 22 (2017).
- [65] J.F. Zeidner, et al., Final clinical results of a phase II study of high dose cytarabine followed by pembrolizumab in relapsed/refractory AML, *Blood* 134 (2019) 831.
- [66] N.J. Barrios, C.K. Tebbi, A.I. Freeman, M.L. Brecher, Toxicity of high dose Ara-C in children and adolescents, *Cancer* 60 (1987) 165–169.
- [67] R. Fanciullino, et al., CDA as a predictive marker for life-threatening toxicities in patients with AML treated with cytarabine, *Blood Adv.* 2 (2018) 462–469.
- [68] D. Malani, et al., Enhanced sensitivity to glucocorticoids in cytarabine-resistant AML, *Leukemia* 2017 31:5 31, 1187–1195 (2016).
- [69] J.H. Gray, R.P. Owen, K.M. Giacomini, The concentrative nucleoside transporter family, SLC28, *PLoS One* 4:7 (2009) 728–734.
- [70] A.D. Adema, et al., Overexpression of MRP4 (ABCC4) and MRP5 (ABCC5) confer resistance to the nucleoside analogs cytarabine and troxacitabine, but not gemcitabine, *Springerplus* 3 (2014) 1–11.
- [71] A.C. Jaramillo, et al., Ex vivo resistance in childhood acute lymphoblastic leukemia: Correlations between BCRP, MRP1, MRP4 and MRP5 ABC transporter expression and intracellular methotrexate polyglutamate accumulation, *Leuk. Res.* 79 (2019) 45–51.
- [72] P. Macanas-Pirard, et al., Resistance of leukemia cells to cytarabine chemotherapy is mediated by bone marrow stroma, involves cell-surface equilibrative nucleoside transporter-1 removal and correlates with patient outcome, *Oncotarget* 8 (2017) 23073.
- [73] W. Qi, et al., The effects of cytarabine combined with ginsenoside compound K synergistically induce DNA damage in acute myeloid leukemia cells, *Biomed. Pharmacother.* 132 (2020), 110812.
- [74] M. Levin, M. Stark, B. Berman, Y.G. Assaraf, Surmounting Cytarabine-resistance in acute myeloblastic leukemia cells and specimens with a synergistic combination of hydroxyurea and azidothymidine, *Cell Death & Disease* 2019 10:6 10, 1–14 (2019).
- [75] Y. Yakymiv, et al., CD157 signaling promotes survival of acute myeloid leukemia cells and modulates sensitivity to cytarabine through regulation of anti-apoptotic Mcl-1, *Sci. Rep.* 2021 11:1 11, 1–16 (2021).
- [76] A.K. Mitra, et al., Genetic variants in cytosolic 5'-nucleotidase II are associated with its expression and cytarabine sensitivity in HapMap cell lines and in patients with acute myeloid leukemia, *J. Pharmacol. Exp. Ther.* 339 (2011) 9–23.
- [77] C. Schneider et al., SAMHD1 is a biomarker for cytarabine response and a therapeutic target in acute myeloid leukemia, *Nature Medicine* 2016 23:2 23, 250–255 (2016).
- [78] S.G. Rudd, et al., Ribonucleotide reductase inhibitors suppress SAMHD1 ara-CITase activity enhancing cytarabine efficacy, *EMBO Mol. Med.* 12 (2020) e10419.
- [79] M. Jädersten, et al., Targeting SAMHD1 with hydroxyurea in first-line cytarabine-based therapy of newly diagnosed acute myeloid leukaemia: results from the HEAT-AML trial, *J. Intern. Med.* 292 (2022) 925–940.
- [80] C. Boss et al., Mitochondrial inhibitors circumvent adaptive resistance to venetoclax and cytarabine combination therapy in acute myeloid leukemia, *Nature Cancer* 2021 2:11 2, 1204–1223 (2021).
- [81] H. Åbacka, et al., Targeting GLUT1 in acute myeloid leukemia to overcome cytarabine resistance, *Haematologica* 106 (2021) 1163.
- [82] M.J. Keating, et al., Fludarabine: A new agent with marked cytoreductive activity in untreated chronic lymphocytic leukemia, *J. Clin. Oncol.* 9 (1991) 44–49.
- [83] G. Borthakur, et al., Retrospective comparison of survival and responses to Fludarabine, Cytarabine, G-CSF (FLAG) in combination with gemtuzumab ozogamicin (GO) or idarubicin (IDA) in patients with newly diagnosed core binding factor (CBF) acute myelogenous leukemia: MD Anderson experience in 174 patients, *Am. J. Hematol.* 97 (2022) 1427–1434.
- [84] M.S. Davids, et al., Ibrutinib plus fludarabine, cyclophosphamide, and rituximab as initial treatment for younger patients with chronic lymphocytic leukaemia: a single-arm, multicentre, phase 2 trial, *Lancet Haematol.* 1 6 (2019) e419–e428.
- [85] L. Smolej, et al., Low-dose fludarabine and cyclophosphamide combined with rituximab in the first-line treatment of elderly/comorbid patients with chronic lymphocytic leukaemia/small lymphocytic lymphoma (CLL/SLL): long-term results of project Q-lite by the Czech CLL Study Group, *Br. J. Haematol.* 193 (2021) 769–773.
- [86] X.X. Wang, et al., Bortezomib in combination with fludarabine plus cyclophosphamide for patients with relapsed or refractory mantle-cell lymphoma: results of the LYM-4003 study, *Ann. Hematol.* 100 (2021) 2961–2968.
- [87] H.N. Altayb, Fludarabine, a potential DNA-dependent RNA polymerase inhibitor, as a prospective drug against monkeypox virus: a computational approach, *Pharmaceuticals* 15 (2022) 93–103.
- [88] V. Gandhi, W. Plunkett, Cellular and clinical pharmacology of fludarabine, *Clin. Pharmacokinet.* 41 (2002) 93–103.
- [89] M. Gorzkiewicz, et al., Glycodendrimer nanocarriers for direct delivery of fludarabine triphosphate to leukemic cells: improved pharmacokinetics and pharmacodynamics of fludarabine, *Biomacromolecules* 19 (2018) 531–543.
- [90] A. Michelutti, et al., Effect of fludarabine and arabinosylcytosine on multidrug resistant cells - PubMed, *Haematologica* 82 (1997) 143–147.
- [91] A. Candoni, et al., Flai (fludarabine, cytarabine, idarubicin) plus low-dose Gemtuzumab Ozogamicin as induction therapy in CD33-positive AML: Final results and long term outcome of a phase II multicenter clinical trial, *Am. J. Hematol.* 93 (2018) 655–663.
- [92] D. Damiani, et al., Fludarabine-based induction therapy does not overcome the negative effect of ABCG2 (BCRP) over-expression in adult acute myeloid leukemia patients, *Leuk. Res.* 34 (2010) 942–945.
- [93] C. Huang, Y. Tu, C.E. Preter, Fludarabine-resistance associates with ceramide metabolism and leukemia stem cell development in chronic lymphocytic leukemia, *Oncotarget* 9 (2018) 33124.
- [94] J.S. Carew, et al., Targeting endoplasmic reticulum protein transport: a novel strategy to kill malignant B cells and overcome fludarabine resistance in CLL, *Blood* 107 (2006) 222–231.
- [95] A. Sharma, et al., Targeting mTORC1-mediated metabolic addiction overcomes fludarabine resistance in malignant B cells, *Mol. Cancer Res.* 12 (2014) 1205–1215.
- [96] D. Trachootham, et al., Effective elimination of fludarabine-resistant CLL cells by PEITC through a redox-mediated mechanism, *Blood* 112 (2008) 1912–1922.
- [97] L. Toschi, G. Finocchiaro, S. Bartolini, V. Gioia, F. Cappuzzo, Role of gemcitabine in cancer therapy, *Future Oncol.* 1 (2005) 7–17.
- [98] T. Conroy, et al., FOLFIRINOX or Gemcitabine as Adjuvant Therapy for Pancreatic Cancer, *N. Engl. J. Med.* 379 (2018) 2395–2406.
- [99] D.A. Yardley, et al., nab-Paclitaxel plus carboplatin or gemcitabine versus gemcitabine plus carboplatin as first-line treatment of patients with triple-negative metastatic breast cancer: results from the tAcity trial, *Ann. Oncol.* 29 (2018) 1763–1770.
- [100] S. Gesto, M.F.S.A. Cerqueira, N.A.P. Fernandes, J.M. Ramos, Gemcitabine: a critical nucleoside for cancer therapy, *Curr. Med. Chem.* 19 (2012) 1076–1087.
- [101] E.J.B. Derissen, A.D.R. Huitema, H. Rosing, J.H.M. Schellens, J.H. Beijnen, Intracellular pharmacokinetics of gemcitabine, its deaminated metabolite 2',2'-difluorodeoxyuridine and their nucleotides, *Br. J. Clin. Pharmacol.* 84 (2018) 1279–1289.
- [102] J. Ciccolini, C. Serdjebi, G.J. Peters, E. Giovannetti, Pharmacokinetics and pharmacogenetics of Gemcitabine as a mainstay in adult and pediatric oncology: an EORTC-PAMM perspective, *Cancer Chemother. Pharmacol.* 78 (2016) 1.
- [103] H. Xu, C. Faber, T. Uchiki, J. Racca, C. Dealwis, Structures of eukaryotic ribonucleotide reductase I define gemcitabine diphosphate binding and subunit assembly, *PNAS* 103 (2006) 4028–4033.
- [104] W. Plunkett, P. Huang, V. Gandhi, Preclinical characteristics of gemcitabine, *Anticancer Drugs* 6 (Suppl 6) (1995) 7–13.
- [105] S. Yang, et al., New mechanism of gemcitabine and its phosphates: DNA polymerization disruption via 3'-5' exonuclease inhibition, *Biochemistry* 59 (2020) 4344–4352.
- [106] T.K. Bjånes, et al., Intracellular cytidine deaminase regulates gemcitabine metabolism in pancreatic cancer cell lines, *Drug Metab. Dispos.* 48 (2020) 153–158.
- [107] J.Y. Lee, S.Y. Song, J.Y. Park, Notch pathway activation is associated with pancreatic cancer treatment failure, *Pancreatology* 14 (2014) 48–53.
- [108] G.J. Peters, E. Giovannetti, R.J. Honeywell, J. Ciccolini, Can cytidine deaminase be used as predictive biomarker for gemcitabine toxicity and response? *Br. J. Clin. Pharmacol.* 85 (2019) 1213.
- [109] M. Yamamoto, et al., Roles for hENT1 and dCK in gemcitabine sensitivity and malignancy of meningioma, *Neuro Oncol.* 23 (2021) 945–954.
- [110] W. Hagnmann, R. Jesnowski, J.M. Lohr, Interdependence of gemcitabine treatment, transporter expression, and resistance in human pancreatic carcinoma cells, *Neoplasia* 12 (2010) 740.
- [111] A.M. Bergman, et al., Increased sensitivity to gemcitabine of P-glycoprotein and multidrug resistance-associated protein-overexpressing human cancer cell lines, *Br. J. Cancer* 88 (2003) 1963.
- [112] Y. Jia, J. Xie, Promising molecular mechanisms responsible for gemcitabine resistance in cancer, *Genes Dis* 2 (2015) 299–306.

- [113] H. Yang, et al., Genome-wide CRISPR screening identifies DCK and CNL1 as genes that contribute to gemcitabine resistance in pancreatic cancer, *Cancers (Basel)* 14 (2022).
- [114] Y.H. Chang, H.L. Tam, M.C. Lu, H.S. Huang, Gemcitabine-induced Gii-dependent activation of hedgehog pathway resists to the treatment of urothelial carcinoma cells, *PLoS One* 16 (2021).
- [115] D.V.T. Catenacci, et al., Randomized phase Ib/II study of gemcitabine plus placebo or vismodegib, a hedgehog pathway inhibitor, in patients with metastatic pancreatic cancer, *J. Clin. Oncol.* 33 (2015) 4284–4292.
- [116] Q. Zhang, et al., The Wnt/ $\beta$ -catenin signaling pathway mechanism for pancreatic cancer chemoresistance in a three-dimensional cancer microenvironment, *Am. J. Transl. Res.* 9 (2016) 4490.
- [117] V. Kumar, et al., The role of notch, hedgehog, and wnt signaling pathways in the resistance of tumors to anticancer therapies, *Front. Cell Dev. Biol.* 9 (2021) 857.
- [118] M.T. Rahman, et al., Notch3 overexpression as potential therapeutic target in advanced stage chemoresistant ovarian cancer, *Am. J. Clin. Pathol.* 133 (2012) 535–544.
- [119] J. Yao, C. Qian, Inhibition of Notch3 enhances sensitivity to gemcitabine in pancreatic cancer through an inactivation of PI3K/Akt-dependent pathway, *Med. Oncol.* 27 (2010) 1017–1022.
- [120] Z. Zhang, et al., Hypoxia potentiates gemcitabine-induced stemness in pancreatic cancer cells through AKT/Notch1 signaling, *J. Exp. Clin. Cancer Res.* 37 (2018) 1–13.
- [121] L.M.P. Verissimo, et al., Transport properties of aqueous solutions of the oncologic drug 5-fluorouracil: A fundamental complement to therapeutics, *J. Chem. Thermodyn.* 161 (2021), 106533.
- [122] H. Blomstrand, U. Scheibling, C. Brattahl, H. Green, N.O. Elander, Real world evidence on gemcitabine and nab-paclitaxel combination chemotherapy in advanced pancreatic cancer, *BMC Cancer* 19 (2019) 1–9.
- [123] N.H. Shehata, T.M. Okda, G.A. Omran, M.M. Abd-Alhaseeb, Baicalin; a promising chemopreventive agent, enhances the antitumor effect of 5-FU against breast cancer and inhibits tumor growth and angiogenesis in Ehrlich solid tumor, *Biomed. Pharmacother.* 146 (2022), 112599.
- [124] S. Chakrabarti, et al., Bolus 5-fluorouracil (5-FU) In Combination With Oxaliplatin Is Safe and Well Tolerated in Patients Who Experienced Coronary Vasospasm With Infusional 5-FU or Capecitabine, *Clin. Colorectal Cancer* 18 (2019) 52–57.
- [125] S. A. Hosseini, H. Zand, M. Cheraghpour, The Influence of Curcumin on the Downregulation of MYC, Insulin and IGF-1 Receptors: A Possible Mechanism Underlying the Anti-Growth and Anti-Migration in Chemoresistant Colorectal Cancer Cells, *Medicine* 2019, Vol. 55, Page 99 55, 90 (2019).
- [126] X. Tan, et al., Inhibition of EZH2 enhances the therapeutic effect of 5-FU via PUMA upregulation in colorectal cancer, *Cell Death & Disease* 2020 11:12 11, 1–13 (2020).
- [127] K. Mitra, et al., 5-FU metabolism in cancer and orally-administrable 5-FU drugs, *Cancers (Basel)* 2 (2010) 1717.
- [128] T.J. Wigle, E. Tsvetkova, S.A. Welch, R.B. Kim, DPYD and fluorouracil-based chemotherapy: Mini review and case report, *Pharmaceutics* 11 (2019).
- [129] W.W. Ma, et al., Emergency use of uridine triacetate for the prevention and treatment of life-threatening 5-fluorouracil and capecitabine toxicity, *Cancer* 123 (2017) 345–356.
- [130] W.B. Parker, Y.C. Cheng, Metabolism and mechanism of action of 5-fluorouracil, *Pharmacol. Ther.* 48 (1990) 381–395.
- [131] G.J. Peters, et al., Induction of thymidylate synthase as a 5-fluorouracil resistance mechanism, *Biochim. Biophys. Acta (BBA) - Mol. Basis Dis.* 1587 (2002) 194–205.
- [132] S. Blondy, et al., 5-Fluorouracil resistance mechanisms in colorectal cancer: From classical pathways to promising processes, *Cancer Sci.* 111 (2020) 3142–3154.
- [133] S.S. Fidayi, A.E. Sharma, D.N. Johnson, J.P. Segal, R.R. Lastra, Dihydropyrimidine dehydrogenase deficiency as a cause of fatal 5-Fluorouracil toxicity, *Autops. Case Rep.* 8 (2018).
- [134] S.L. Showalter, et al., Evaluating the drug-target relationship between thymidylate synthase expression and tumor response to 5-fluorouracil: Is it time to move forward? *Cancer Biol. Ther.* 7 (2008) 966.
- [135] B.Q. Cai, W.M. Chen, J. Zhao, W. Hou, J.C. Tang, Nrf3 promotes 5-FU resistance in colorectal cancer cells via the NF- $\kappa$ B/BCL-2 signaling pathway in vitro and in vivo, *J. Oncol.* 2021 (2021).
- [136] C.N. Arnold, A. Goel, C.R. Boland, Role of hMLH1 promoter hypermethylation in drug resistance to 5-fluorouracil in colorectal cancer cell lines, *Int. J. Cancer* 106 (2003) 66–73.
- [137] C. Sethy, C.N. Kundu, 5-Fluorouracil (5-FU) resistance and the new strategy to enhance the sensitivity against cancer: Implication of DNA repair inhibition, *Biomed. Pharmacother.* 137 (2021), 111285.
- [138] V. Varghese, et al., FOXM1 modulates 5-FU resistance in colorectal cancer through regulating TYMS expression, *Sci. Rep.* 9 (2019).
- [139] D. Na, et al., Predictive biomarkers for 5-fluorouracil and oxaliplatin-based chemotherapy in gastric cancers via profiling of patient-derived xenografts, *Nat. Commun.* 12 (2021).
- [140] W. Hagemann, R. Jenowski, R. Faisner, C. Guo, J.M. Löhr, ATP-binding cassette C transporters in human pancreatic carcinoma cell lines: upregulation in 5-fluorouracil-resistant cells, *Pancreatology* 9 (2009) 136–144.
- [141] Y.D. Kartika, I. Astuti, W.R. Pratiwi, The expression of multidrug resistance protein 5 and thymidylate synthase on fluorouracil resistance WiDr colon cancer cell line, *J. Kedokteran Kesehatan Indonesia* 7 (2015) 59–64.
- [142] S. Pratt, et al., The multidrug resistance protein 5 (ABCC5) confers resistance to 5-fluorouracil and transports its monophosphorylated metabolites, *Mol. Cancer Ther.* 4 (2005) 855–863.
- [143] T. Oguri, et al., MRP6/ABCC11 directly confers resistance to 5-fluorouracil, *Mol. Cancer Ther.* 6 (2007) 122–127.
- [144] R. Mori, et al., P-glycoprotein plays an important role in the cross-resistance to taxanes in SFU-resistant gastric cancer cells, *Transl. Gastrointest. Cancer* 4, 12390–12130 (2015).
- [145] J. Yuan, et al., Role of BCRP as a biomarker for predicting resistance to 5-fluorouracil in breast cancer, *Cancer Chemother. Pharmacol.* 63 (2009) 1103–1110.
- [146] U. Stein, et al., YB-1 facilitates basal and 5-fluorouracil-inducible expression of the human major vault protein (MVP) gene, *Oncogene* 24 (2005) 3606–3618.
- [147] S.M. Naes, S. Ab-Rahim, M. Mazlan, A.A. Rahman, Equilibrative nucleoside transporter 2: properties and physiological roles, *Biomol. Res. Int.* 2020 (2020).
- [148] M. Tsujie, et al., Human equilibrative nucleoside transporter 1, as a predictor of 5-fluorouracil resistance in human pancreatic cancer, *Anticancer Res* 27 (2007) 2241–2249.
- [149] C.E. Cass, S.A. Baldwin, J. Young, CNT2, concentrative nucleoside transporter 2, *xPharm: The Comprehensive Pharmacology Reference* 1–4 (2007) doi:10.1016/B979-008055232-3.60462-3.
- [150] K. Raj, G.J. Mufti, Azacitidine (Vidaza®) in the treatment of myelodysplastic syndromes, *Ther. Clin. Risk Manag.* 2 (2006) 377.
- [151] E.J.B. Derissen, J.H. Beijnen, J.H.M. Schellens, Concise drug review: azacitidine and decitabine, *Oncologist* 18 (2013) 619.
- [152] C.D. DiNardo, et al., Azacitidine and venetoclax in previously untreated acute myeloid leukemia, *N. Engl. J. Med.* 383 (2020) 617–629.
- [153] A. Bazinet, et al., Azacitidine plus venetoclax in patients with high-risk myelodysplastic syndromes or chronic myelomonocytic leukaemia: phase 1 results of a single-centre, dose-escalation, dose-expansion, phase 1–2 study, *Lancet Haematol* 9 (2022) e756–e765.
- [154] G. Leone, F. D'Alo, G. Zardo, M. Voso, C. Nervi, Epigenetic treatment of myelodysplastic syndromes and acute myeloid leukemias, *Curr. Med. Chem.* 15 (2008) 1274–1287.
- [155] R. L. Momparler, A Perspective on the Comparative Antileukemic Activity of 5-Aza-2'-deoxycytidine (Decitabine) and 5-Azacitidine (Vidaza), *Pharmaceutics* 2012, Vol. 5, Pages 875-881 5, 875–881 (2012).
- [156] P. Sriyapay, et al., Mechanisms of resistance to azacitidine in human leukemia cell lines, *Exp. Hematol.* 42 (2014).
- [157] X. Gu, et al., Decitabine- and 5-azacytidine resistance emerges from adaptive responses of the pyrimidine metabolism network, *Leukemia* 2020 35:4 35, 1023–1036 (2020).
- [158] V.L. Damaraju, et al., Role of human nucleoside transporters in the uptake and cytotoxicity of azacitidine and decitabine, *Nucleosides Nucleotides Nucleic Acids* 31 (2012) 236–255.
- [159] E.-H. Hun, et al., Establishment and characterization of hypomethylating agent-resistant cell lines, MOLM/AZA-1 and MOLM/DEC-5, *Oncotarget* 8 (2016) 11748–11762.
- [160] E. Lainey, et al., Erlotinib increases efficacy of 5-azacitidine (AZA) by inhibiting drug efflux via ABC-transporters, *Blood* 116 (2010) 974.
- [161] A. Kuendgen, et al., Efficacy of azacitidine is independent of molecular and clinical characteristics - an analysis of 128 patients with myelodysplastic syndromes or acute myeloid leukemia and a review of the literature, *Oncotarget* 9 (2018) 27882.
- [162] S. Dhillon, Decitabine/Cedazuridine: First Approval, *Drugs* 2020 80:13 80, 1373–1378 (2021).
- [163] P. Montesinos, et al., Safety and efficacy of talocatumzumab plus decitabine or decitabine alone in patients with acute myeloid leukemia not eligible for chemotherapy: results from a multicenter, randomized, phase 2/3 study, *Leukemia* 2020 35:1 35, 62–74 (2020).
- [164] J. Bouchard, R.L. Momparler, Incorporation of 5-Aza-2'-deoxycytidine-5'-triphosphate into DNA. Interactions with mammalian DNA polymerase alpha and DNA methylase - PubMed, *Mol. Pharmacol.* 24 (1983) 109–114.
- [165] T. Qin, et al., Mechanisms of resistance to decitabine in the myelodysplastic syndrome, *PLoS One* 6 (2011).
- [166] X. Gu, et al., Decitabine- and 5-azacytidine resistance emerges from adaptive responses of the pyrimidine metabolism network, *Leukemia* 35 (2021) 1023.
- [167] C. Säll, C. Fogt Hjorth, In vitro drug-drug interactions of decitabine and tetrahydrouridine involving drug transporters and drug metabolising enzymes, *Xenobiotica* 52 (2022) 1–15.
- [168] T. Ando, M. Nishimura, Y. Oka, Decitabine (5-Aza-2'-deoxycytidine) decreased DNA methylation and expression of MDR-1 gene in K562/ADM cells, *Leukemia* 14 (2000) 1915–1920.
- [169] H. M. Bryson, E.M. Sorkin Cladribine, *Drugs* 1993 46:5 46, 872–894 (2012).
- [170] G. Giovannoni, et al., Safety and efficacy of cladribine tablets in patients with relapsing-remitting multiple sclerosis: Results from the randomized extension trial of the CLARITY study, *Mult. Scler.* 24 (2018) 1594–1604.
- [171] J. Lillemark, The clinical pharmacokinetics of cladribine, *Clin. Pharmacokinet.* 32 (1997) 120–131.
- [172] R. Hermann, et al., The clinical pharmacology of cladribine tablets for the treatment of relapsing multiple sclerosis, *Clin. Pharmacokinet.* 58 (2019) 283–297.
- [173] R. Hermann, et al., Review of transporter substrate, inhibitor, and inducer characteristics of cladribine, *Clin. Pharmacokinet.* 60 (2021) 1509.
- [174] K.W. Rammohan, J. Shoemaker, J. Emerging multiple sclerosis oral therapies, *undefined* 74, (2010).
- [175] K. Lotfi, G. Juliusson, F. Albertoni, Pharmacological basis for cladribine resistance, *Leuk. Lymphoma* 44 (2003) 1705–1712.

- [176] F. Aybar, et al., 2-Chlorodeoxyadenosine (Cladribine) preferentially inhibits the biological activity of microglial cells, *Int. Immunopharmacol.* 105 (2022), 108571.
- [177] N. Chen, et al., Xenobiotics the fate of foreign compounds in biological systems in vitro drug-drug interactions of budesonide: inhibition and induction of transporters and cytochrome P450 enzymes In vitro drug-drug interactions of budesonide: inhibition and induction of transporters and cytochrome P450 enzymes, *Xenobiotica* 48 (2018) 637–646.
- [178] A.C. Sartorelli, G.A. LePage, E.C. Moore, Metabolic effects of 6-thioguanine: I. studies on thioguanine-resistant and sensitive ehrlich ascites cells, *Cancer Res.* 18 (1958) 1232–1239.
- [179] M. Klanova, et al., Downregulation of deoxycytidine kinase in cytarabine-resistant mantle cell lymphoma cells confers cross-resistance to nucleoside analogs gemcitabine, fludarabine and cladribine, but not to other classes of anti-lymphoma agents, *Mol. Cancer* 13 (2014) 1–14.
- [180] S. Dei, L. Braconi, M.N. Romanelli, E. Teodori, Recent advances in the search of BCRP- and dual P-gp/BCRP-based multidrug resistance modulators, *Cancer Drug Resistance* 2 (2019) 710.
- [181] K. Sodani, A. Patel, R.J. Kathawala, Z.S. Chen, Multidrug resistance associated proteins in multidrug resistance, *Chin. J. Cancer* 31 (2012) 58.
- [182] J. Dong, et al., Medicinal chemistry strategies to discover P-glycoprotein inhibitors: An update, *Drug Resist. Updat.* 49 (2020), 100631.
- [183] J. Lee, et al., Dual inhibition of P-gp and BCRP improves oral topotecan bioavailability in rodents, *Pharmaceutics* 13 (2021).
- [184] S. Zhang, X. Yang, M.E. Morris, Flavonoids are inhibitors of breast cancer resistance protein (ABCG2)-mediated transport, *Mol. Pharmacol.* 65 (2004) 1208–1216.
- [185] A. Pick, M. Wiese, Tyrosine kinase inhibitors influence ABCG2 expression in EGFR-positive MDCK BCRP cells via the PI3K/Akt signaling pathway, *ChemMedChem* 7 (2012) 650–662.
- [186] C.Y. Gai, et al., Biological evaluation of non-basic chalcone CYB-2 as a dual ABCG2/ABCB1 inhibitor, *Biochem. Pharmacol.* 175 (2020), 113848.
- [187] H. Zhang, et al., In vitro, in vivo and ex vivo characterization of ibrutinib: a potent inhibitor of the efflux function of the transporter MRP1, *Br. J. Pharmacol.* 171 (2014) 5845–5857.
- [188] K. Sechidis, et al., Distinguishing prognostic and predictive biomarkers: an information theoretic approach, *Bioinformatics* 34 (2018) 3365–3376.
- [189] J.M. Lambert, Drug-conjugated antibodies for the treatment of cancer, *Br. J. Clin. Pharmacol.* 76 (2013) 248.
- [190] F. Buchegger, et al., Radiolabeled fragments of monoclonal antibodies against carcinoembryonic antigen for localization of human colon carcinoma grafted into nude mice, *J. Exp. Med.* 158 (1983) 413–427.
- [191] C.H.J. Ford, et al., Localisation and toxicity study of a vindesine-anti-CEA conjugate in patients with advanced cancer, *Br. J. Cancer* 47 (1983) 35–42.
- [192] J. Hitzler, E. Estey, Gemtuzumab ozogamicin in acute myeloid leukemia: act 2, with perhaps more to come, *Haematologica* 104 (2019) 7.
- [193] N.W.C.J. Van De Donk, E. Dhimolea, Brentuximab vedotin, *MAbs* 4 (2012) 458.
- [194] P.F. Peddi, S.A. Hurvitz, Ado-trastuzumab emtansine (T-DM1) in human epidermal growth factor receptor 2 (HER2)-positive metastatic breast cancer: latest evidence and clinical potential, *Ther Adv Med Oncol* 6 (2014) 202.
- [195] M.R. Dunn, Jimenez, R. M., Chaput, J. C. Analysis of aptamer discovery and technology, *Nat. Rev. Chem.* 2017 1:10 1, 1–16 (2017).
- [196] S. Yoon, et al., Aptamer-drug conjugates of active metabolites of nucleoside analogs and cytotoxic agents inhibit pancreatic tumor cell growth, *Mol. Ther. Nucleic Acids* 6 (2017) 80–88.
- [197] L. Zhu, J. Yang, Y. Ma, X. Zhu, C. Zhang, Aptamers entirely built from therapeutic nucleoside analogues for targeted cancer therapy, *J. Am. Chem. Soc.* 144 (2022) 1493–1497.
- [198] K. Natarajan, Y. Xie, M.R. Baer, D.D. Ross, Role of breast cancer resistance protein (BCRP/ABCG2) in cancer drug resistance, *Biochem. Pharmacol.* 83 (2012) 1084.
- [199] E. Yagüe, et al., P-glycoprotein (MDR1) expression in leukemic cells is regulated at two distinct steps, mRNA stabilization and translational initiation, *J. Biol. Chem.* 278 (2003) 10344–10352.
- [200] E.L. Woodahl, J. Wang, S. Heinfield, A.G. Ren, J.S. McCune, Imatinib inhibition of fludarabine uptake in T-lymphocytes, *Cancer Chemother. Pharmacol.* 62 (2008) 735–739.
- [201] M. Pastor-Anglada et al. Nucleoside transporters in chronic lymphocytic leukaemia, *Leukemia* 2004 18:3 18, 385–393 (2004).
- [202] J. Gu, et al., Hsa-miR-3178/RhoB/PI3K/Akt, a novel signaling pathway regulates ABC transporters to reverse gemcitabine resistance in pancreatic cancer, *Mol. Cancer* 21 (2022).
- [203] A.E. Abdelrahman, D.A. Ibrahim, A. El-Azomy, A.A. Alnagar, A. Ibrahim, ERCC1, PARP-1, and AQP1 as predictive biomarkers in colon cancer patients receiving adjuvant chemotherapy, *Cancer Biomark.* 27 (2020) 251–264.



## **9.2 Triazole-based estradiol dimers prepared via CuAAC from 17 $\alpha$ -ethinyl estradiol with five-atom linkers causing G2/M arrest and tubulin inhibition**

M. JURÁŠEK, J. ŘEHULKA, L. HRUBÁ, A. IVANOVA (NIKONENKO), S. GURSKÁ, O. MOKSHYNA, P. TROUSIL, K. HUML, P. POLISHCHUK, M. HAJDÚCH, P. DRAŠAR, P. DŽUBÁK, Triazole-based estradiol dimers prepared via CuAAC from 17 $\alpha$ -ethinyl estradiol with five-atom linkers causing G2/M arrest and tubulin inhibition, *Bioorganic Chemistry*, 2023, 131, 106334, 0045-2068, IF: 5.307, PMID: 36592487.

Personal contribution: cytotoxicity assays, flow cytometry analyses



Contents lists available at ScienceDirect

Bioorganic Chemistry

journal homepage: [www.elsevier.com/locate/bioorg](http://www.elsevier.com/locate/bioorg)

## Triazole-based estradiol dimers prepared via CuAAC from 17 $\alpha$ -ethinyl estradiol with five-atom linkers causing G<sub>2</sub>/M arrest and tubulin inhibition

Michal Jurášek<sup>a</sup>, Jiří Řehulka<sup>b</sup>, Lenka Hrubá<sup>b</sup>, Aleksandra Ivanová<sup>b</sup>, Soňa Gurská<sup>b</sup>, Olena Mokshyna<sup>b</sup>, Pavel Trousil<sup>a</sup>, Lukáš Huml<sup>a</sup>, Pavel Polishchuk<sup>b</sup>, Marián Hajdúch<sup>b</sup>, Pavel B. Drašar<sup>a</sup>, Petr Džubák<sup>b,\*</sup>

<sup>a</sup> Department of Chemistry of Natural Compounds, University of Chemistry and Technology Prague, Technická 5, 166 28 Prague 6, Czech Republic

<sup>b</sup> Institute of Molecular and Translational Medicine, Faculty of Medicine and Dentistry, Palacký University and University Hospital in Olomouc, Hněvotínská 1333/5, 779 00 Olomouc, Czech Republic

### ARTICLE INFO

**Keywords:**  
Steroid dimer  
Estradiol  
Chemistry  
CuAAC reaction  
Cytotoxicity  
Cell cycle  
G<sub>2</sub>/M arrest  
Microtubules  
Antimitotic activity  
Tubulin assembly  
*In silico* simulations

### ABSTRACT

Microtubule dynamic is exceptionally sensitive to modulation by small-molecule ligands. Our previous work presented the preparation of microtubule-targeting estradiol dimer (ED) with anticancer activity. In the present study, we explore the effect of selected linkers on the biological activity of the dimer. The linkers were designed as five-atom chains with carbon, nitrogen or oxygen in their centre. In addition, the central nitrogen was modified by a benzyl group with hydroxy or methoxy substituents and one derivative possessed an extended linker length. Thirteen new dimers were subjected to cytotoxicity assay and cell cycle profiling. Dimers containing linker with benzyl moiety substituted with one or more methoxy groups and longer branched ones were found inactive, whereas other structures had comparable efficacy as the original ED (e.g. D1 with IC<sub>50</sub> = 1.53  $\mu$ M). Cell cycle analysis and immunofluorescence proved the interference of dimers with microtubule assembly and mitosis. The proposed *in silico* model and calculated binding free energy by the MM-PBSA method were closely correlated with *in vitro* tubulin assembly assay.

### 1. Introduction

Steroids are an important group of lipophilic biologically active substances. They play several key roles in the biological environment, in particular, they are components of biological membranes or act as signalling molecules. Any change in the chemical structure of steroids can lead to change or loss of efficacy, enhancement or alteration of the mechanism of action. Chemical modifications of steroids are a popular discipline of medical chemists dealing with the discovery of new potential drugs or their transport to the target tissue.

Steroid dimers are a group of substances containing two steroid skeletons in a molecule. Such structures can also be found in nature, but most of them come from a chemical laboratory [1–3] (reviewed by Nahar et al. [4]). In our recent work, we have described the preparation and biological properties of the estradiol homodimer (ED, Fig. 1) linked via a heterocyclic bridge at the C-17 position [5]. ED was prepared by a CuAAC [6] reaction of 17 $\alpha$ -ethinylestradiol (EE) and a heterocyclic diazide [1]. In this work, we described the cytotoxic properties and

investigated the mechanism of ED action.

Cell cycle studies have shown an increase in cells in the G<sub>2</sub>/M phase and polyploid cells accompanied by a decrease in DNA/RNA synthesis in CCRF-CEM cells. Further experimental work led to the conclusion that ED acts at the cytoskeletal level by inhibiting tubulin polymerization. ED has been shown to be more effective compared to the well-studied steroidal microtubule polymerization inhibitor 2-methoxyestradiol (ME, Fig. 1) and equipotent to nocodazole (Noc). Both ED and Noc completely and reversibly depolymerized microtubules in U2OS cells. Although several dimeric structures containing estradiol in the molecule can be found in the literature [7–11] (Supplementary Figure S1, compounds s1–s8) only dimer s8 based on ME published by Cushman et al. [11] has shown significant activity at the cytoskeletal level. Thus, the structural motif of ED was found as a new type of steroid-based inhibitor of microtubule polymerization and dynamics.

In the current work, we focused on the study of dimeric structures of estradiol with a variable connecting bridge. The length of the bridge contained in twelve cases 5 atoms (L1–L12, Fig. 2) and one PEG<sub>3</sub> (L13,

\* Corresponding author.

E-mail address: [petr.dzubak@upol.cz](mailto:petr.dzubak@upol.cz) (P. Džubák).

<https://doi.org/10.1016/j.bioorg.2022.106334>

Received 27 September 2022; Received in revised form 9 December 2022; Accepted 19 December 2022

Available online 23 December 2022

0045-2068/© 2022 The Authors. Published by Elsevier Inc. This is an open access article under the CC BY license (<http://creativecommons.org/licenses/by/4.0/>).

Fig. 2) linker was used. This five-atom length was derived from the structure of ED. The new dimers (D1-D12, Fig. 3) contained atoms such as carbon, nitrogen or oxygen in the centre of the linker. Other structures were modified with hydroxy or methoxy-substituted benzyl pendant on the central nitrogen atom in the linker. The implementation of such substituted benzyls was motivated by the structure of natural and synthetic mitotic poisons containing precisely these groups in the molecule (reviewed by Skubník et al. [12]).

## 2. Results and discussion

### 2.1. Chemistry

The design of the new estradiol dimers was inspired by results recently published by our group [5]. A new series of steroid dimers were prepared by CuAAC from diazide linkers L1-L12 and EE. The preparation of azide-terminated bridges (L1-L12) was performed by nucleophilic substitution of corresponding alkyl halides by sodium azide in DMF at elevated temperatures (L1-L3, Fig. 2). The *N*-benzyl substituted linkers were prepared by reductive amination from the linker L3 and variously substituted benzaldehyde derivatives containing hydroxy, methoxy or a combination of such groups. Sodium cyanoborohydride in the presence of acetic acid was used as a reducing agent (Fig. 2). These tertiary amine diazides were isolated in rather moderate yields (Fig. 2).

Estradiol dimers D1-D12 were prepared via CuAAC from diazides L1-L12 and EE by microwave-assisted synthesis (MW) using an optimized catalyst system operating on the principle of *in situ* reduction of Cu(II) to Cu(I) by sodium ascorbate (Fig. 3). The dimers were prepared without problems and the substances were isolated in good to excellent yields (61–94 %). Images of NMR and HRMS spectra and results from HPLC analyzes of dimers are documented as Supplementary material (Figures S2-S53).

### 2.2. Cytotoxicity

The prepared estradiol dimers D1-D13 were tested for their cytotoxic activity against the cell line panel under *in vitro* conditions. Table 1 shows that compound D1 possess significant cytotoxic activity against human cell lines derived from both leukaemias and solid tumours. The IC<sub>50</sub> values were highly comparable with 2-methoxyestradiol (ME), nevertheless previously published ED was slightly more effective [5]. Dimers D2-D4 and D9-D10 exhibited a strong cytotoxic effect in leukaemia cell lines, however in some solid tumor-derived cell lines was observed lower cytotoxicity. Structures D6 and D8 showed weak cytotoxicity only against leukaemia cell lines, whereas D5, D7, D11, D12

and D13 showed no cytotoxic activity against all cell lines included in the panel at 50 μM concentration. A common feature of these inactive dimers is the presence of one, two or three methoxy groups at the *N*-benzyl aromatic ring. Interestingly, when a hydroxy group was introduced to the skeleton with one methoxy group, the cytotoxic activity was restored as visible from a comparison of D5 and D10 or D6 and D9. Extension of the bridge as in the case of D13 led to a loss of cytotoxic activity.

To monitor cytotoxicity in non-malignant cells, the panel involved cell lines MRC-5 and BJ derived from normal lung or foreskin tissue. MRC-5 cells displayed generally low sensitivity except for D2, D9 and D10, whereas the BJ cell line was not sensitive toward the compounds. Compound D1 exerted medium cytotoxic effect in both non-malignant cell lines. To assess the influence of drug-efflux transporters on the activity of compounds, we exploited sublines expressing proteins associated with multi-drug resistance. CEM-DNR subline overexpressing P-glycoprotein and LRP was resistant to all tested compounds in comparison with parental cell line CCRF-CEM. The IC<sub>50</sub> values determined in the K562-TAX cell line expressing P-glycoprotein were also above 50 μM except for structure D1. D1 displayed comparable cytotoxicity against subline K562-TAX and parental cell line K562 and the overall results suggest that it can be a substrate of LRP but not P-glycoprotein similarly to ED [5].

### 2.3. Cell cycle analysis

Cytotoxic compounds D1-D4 and D9-D10 were tested for their effect on CCRF-CEM proliferation and cell cycle (Fig. 4, Supplementary Table S1). Following 24-hour incubation with compounds, the cell population was examined using flow cytometry methods for DNA content and the presence of mitotic and proliferation markers. All tested compounds at high concentration induced DNA fragmentation (sub-G<sub>1</sub> population). The major effect of all tested compounds was mitotic arrest accompanied by the increased percentage of the polyploid cells. Treatment with compounds increased the percentage of the pH3<sup>Ser10</sup> positive cells as well as a fraction of cells in the G<sub>2</sub>/M phase. In addition, all tested structures inhibited CCRF-CEM proliferation as monitored by 5-bromo-2-deoxyuridine (BrdU) incorporation into replicating DNA. A similar trend was observed by labelling with complementary marker 5-bromouridine (BrdU), which reflects the rate of RNA synthesis.

### 2.4. Tubulin assay

We performed *in vitro* tubulin polymerization assay to examine the effect of dimers on tubulin assembly (Fig. 5). All tested active estradiol

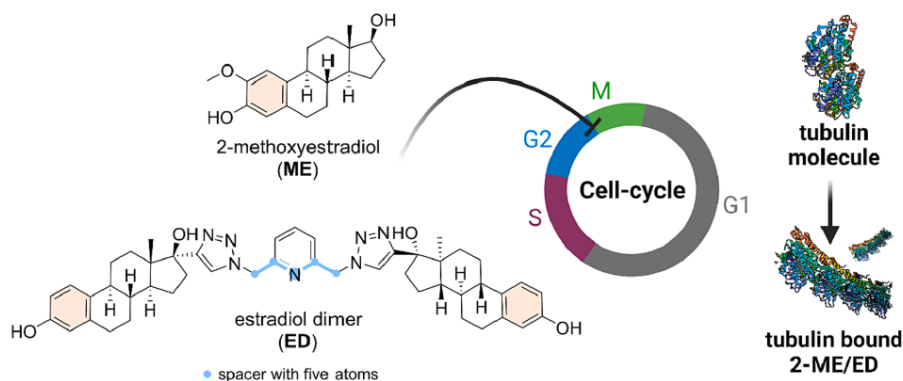


Fig. 1. Molecular structures of estradiol-based antimicrotubules.

dimers inhibited tubulin polymerization in comparison to the control reaction containing DMSO (Fig. 5A). The most potent compounds D2 and D1 flattened the polymerization curve in a similar manner as tubulin assembly inhibitor colchicine. Maximal velocity of polymerization values ( $V_{max}$ ) indicates that D2 and D1 exerted at equimolar concentration stronger inhibition than ED, ME and nocodazole, however weaker than colchicine (Fig. 5B). Structures with *N*-benzyl aromatic ring D3, D4, D9 and D10 displayed comparable or better effects than nocodazole. The results suggest that ED activity can be improved by structural changes within the linker and simple linkers might be more suitable than the more complex ones.

### 2.5. Fluorescence microscopy

Immunofluorescence images revealed disruption of microtubules in U-2 OS cells following 24-hour treatment with compounds D1, D2, D4, D9 and D10 (Fig. 6; image of control is shown in Supplementary Figure S55A). All of the aforementioned substances showed an  $IC_{50} < 2 \mu M$  on U-2 OS cells (Table 1). Incubation led to complete microtubule disorganization with free unpolymerized  $\alpha$ -tubulin in the cytoplasm. To determine whether the effect of compounds on microtubule dynamics is reversible, we observed the microtubular network after the cell washout procedure. Following the complete removal of compounds from the media the microtubular network was reestablished. Interestingly, D3 also showed activity at the cytoskeletal level (see Supplementary Figure S55B), although its  $IC_{50}$  in U-2 OS was determined above  $50 \mu M$ . The probable reason could be a differential sensitivity of leukaemia and epithelial cell lines to antimicrotubule agents.  $IC_{50}$  values of D3 estimated for the leukaemia lines CCRF-CEM and K562 were  $1.41 \mu M$  and  $1.31 \mu M$ . In contrast, U2OS cell line or other epithelial cell lines such as HCT116 or A549 can for some period tolerate polyploidization and had  $IC_{50}$  values above  $50 \mu M$  due to metabolization of MTS in the viability assay.

In summary, cell-based data as well as *in vitro* data demonstrate that newly developed estradiol dimers behave similarly to ED [5]. They inhibit tubulin polymerization, reversibly affect microtubule distribution in interphase cells and suppress microtubule dynamics effectively than ME or nocodazole (Fig. 5B).

### 2.6. In silico modelling

All compounds were docked in a tubulin structure which was complexed with colchicine (4O2B), as was demonstrated previously it fits this kind of structure better than other tubulin structures [5]. All compounds have the same binding mode. One estradiol residue is buried deep inside the colchicine binding site, whereas the other binds on the interface between  $\alpha$ - and  $\beta$ -chains (Fig. 7).

We performed 150 ns molecular dynamic (MD) simulations for compounds D1, D2, D3 and D9. Compounds D1, D2 and D3 have a variable effect on tubulin polymerization speed and their comparison should allow evaluation of the effect of replacement of a methylene group in the spacer with oxygen or nitrogen. Compound D9 was chosen as one of the most active compounds in this series which has a

phenylamino group within the spacer. The ligand poses found in docking did not fluctuate much in MD simulations that supported their validity (Figure S56). The majority of contacts for all ligands identified by ProLIF [13] were hydrophobic, which was expected due to the hydrophobic nature of molecules (Fig. 8, Figure S57). D1 formed stable H-bonds with backbone carbonyl groups of Val236B and Thr179A, which were observed during the whole simulation. Both these contacts were created by two hydroxyl groups of the inner estradiol moiety. The outer estradiol was bound to the hydroxyl group of Tyr210A for most of the time, but closer to the end of the simulation the estradiol moiety was slightly shifted and the contact was broken. The spacer is surrounded by water molecules but also participates in hydrophobic contacts with suitable amino acid residues (Fig. 8A). The inner estradiol moiety of D2 contacted with Val236B and Thr179A similar to D1, but the former bond was quickly broken because the moiety was shifted outside. The hydroxyl group of the outer estradiol moiety formed stable contacts with the backbone carbonyl of Gln176A and a hydroxyl group of Tyr210A. The oxygen in the spacer was not involved in H-bonding with tubulin for most of the time, occasionally forming H-bonds with a hydroxyl group of Thr178A (Fig. 8B). The hydroxyl group of the inner estradiol moiety of D3 formed stable H-bonds with Val236B, while the hydroxyl group of the outer moiety with Gln176A. This is similar to D1 and D2. The protonated amino group in the spacer created a stable H-bond with the hydroxyl group of Ser178A, which was observed for the whole simulation, and occasionally contacted with Asp327B (Fig. 8C). D9 created several contacts stable in the course of the whole simulation – the hydroxyl group of the outer estradiol moiety formed H-bond with the hydroxyl group of Thr178A, the hydroxyl group of the 4-hydroxy-3-methoxyphenylamino group created H-bond with the hydroxyl of Tyr210A, the protonated nitrogen atom formed H-bond with the backbone carbonyl of Gln176A and an ion interaction with Asp327B (Fig. 8D). The outer estradiol moiety of D9 was directed outside of the cavity and was not tightly bound to the protein surface, unlike the other three ligands.

The calculated binding free energy by the MM-PBSA method was in good agreement with the observed polymerization speed caused by these inhibitors, compounds with stronger inhibiting polymerization speed had lower binding free energy (Table 2).

Only the binding energy of D1 was overestimated. We hypothesize that the observed difference in the inhibitory activity of these compounds can be explained by the entropy factor. Ligands comprising a protonated nitrogen within their flexible spacers (D3 and D9) formed charged H-bonds and ionic interactions with the protein. Thus, they should lose more degrees of freedom upon binding which may result in less favourable binding entropy than in the case of compounds D1 and D2. The spacer of compound D1 does not form any specific interactions with the protein and the spacer of D2 comprising an oxygen atom forms H-bonds occasionally, therefore movement of these ligands is less restricted. This hypothesis is indirectly confirmed by the calculated interaction entropy, which was the largest for D3 and D9 (Table 2).

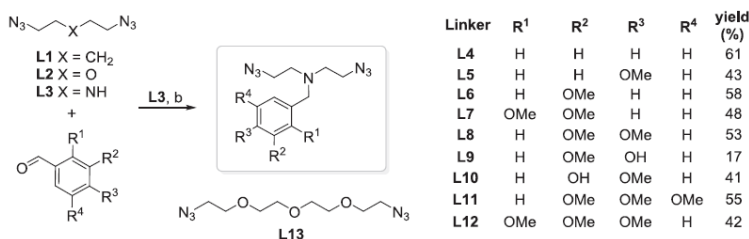


Fig. 2. Synthesis of benzyl substituted diazides. Reagents and conditions: NaCNBH<sub>3</sub>, HOAc, MeOH, 90 min, RT.

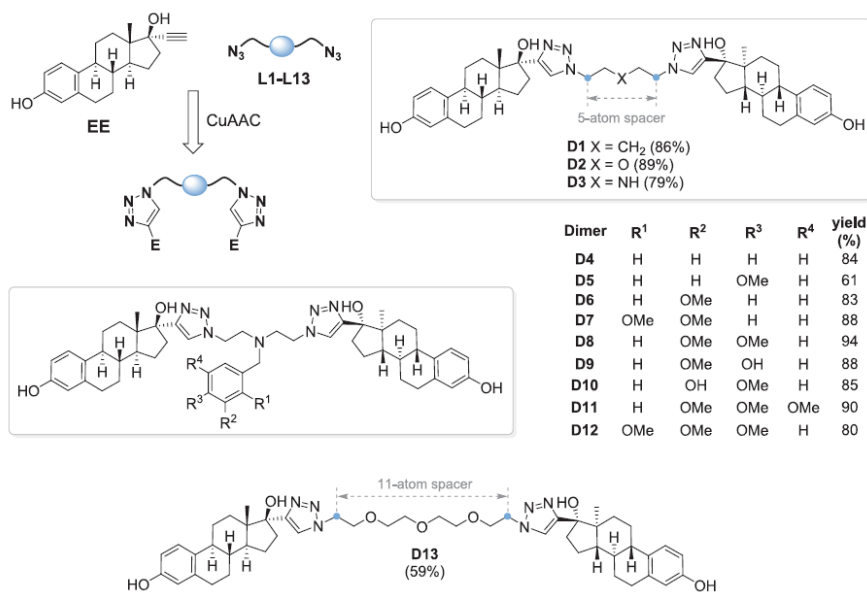


Fig. 3. Structures of synthesized estradiol dimers. CuAAC: CuSO<sub>4</sub>·5H<sub>2</sub>O, sodium ascorbate, DMF, MW-80 °C, 2 h.

Table 1

Cytotoxic activity was determined using an MTS assay following 3-day incubation. Values represent the means of IC<sub>50</sub> from 3 independent experiments with SD ranging from 10 to 25 % of the average values. \*Tested cell lines: CCRF-CEM (childhood T acute lymphoblastic leukaemia), CEM-DNR (CCRF-CEM daunorubicin resistant), K562 (chronic myelogenous leukaemia), K562-Tax (K562 paclitaxel-resistant), A549 (lung adenocarcinoma), HCT116 (colorectal cancer), HCT116p53<sup>-/-</sup> (null p53 gene), U2OS (osteosarcoma). Normal human cell lines: MRC-5 and BJ (normal cycling fibroblasts). EE = 17 $\alpha$ -ethinylestradiol, ME = 2-methoxyestradiol, ED = estradiol dimer [5]. Data show the average from three independent replicates and the standard deviation in cytotoxicity assays is typically up to 15 % of the average value.

Compd. Cell line <sup>a</sup>	EE	ME	ED	D1	D2	D3	D4	D6	D8	D9	D10
IC <sub>50</sub> [ $\mu$ M]											
CCRF-CEM	22.58	1.55	0.48	1.53	1.49	1.43	1.21	16.04	12.08	1.22	1.39
CEM-DNR	21.79	1.67	>50	>50	>50	>50	>50	>50	>50	>50	>50
K562	8.43	1.66	0.58	1.25	1.21	1.31	1.31	12.38	9.59	1.11	1.08
K562-TAX	14.89	1.18	3.54	1.65	>50	>50	>50	>50	>50	>50	>50
A549	33.20	2.25	1.12	1.55	>50	>50	>50	>50	>50	>50	>50
HCT116	31.31	1.68	0.95	1.48	2.12	>50	2.50	>50	>50	1.71	1.70
HCT116p53 <sup>-/-</sup>	29.88	1.79	0.90	1.45	1.83	>50	2.26	>50	>50	1.60	1.70
U2OS	22.77	1.98	6.28	1.96	3.04	>50	1.96	>50	>50	7.35	2.68
MRC-5	>50	>50	1.15	30.32	3.00	>50	>50	>50	>50	10.64	2.76
BJ	>50	>50	>50	13.91	>50	>50	>50	>50	>50	>50	>50

### 3. Conclusions

On the newly synthesized thirteen estradiol dimers (D1-D13), we have shown that structural changes in the bridge are very important for the activity of estradiol dimers at the cytoskeletal level. Introduction of a bulky group into the linker (benzyl pendants) usually reduces the activity of dimers. Likewise, extending the bridge leads to a loss of activity (D13). We have confirmed that all of the active dimers behave similarly to ED by reversible inhibition of tubulin polymerization which is favorable, and in such cases, less toxicity, compared to irreversible inhibitor colchicine, is expected in the therapeutic use in humans [14]. The results indicate that the activity of the originally discovered ED [5] can be further modulated by structural changes in the linker, and for targeting tubulin, simple linkers seem more suitable than more complex ones.

### 4. Experimental

#### 4.1. Chemistry

##### 4.1.1. General methods and materials

For thin-layer chromatography (TLC), aluminium silica gel sheets for detection in UV light (TLC silica gel 60 F254, Merck) were used. For TLC visualization, a diluted solution of H<sub>2</sub>SO<sub>4</sub> in MeOH was used and plates were heated. For column chromatography, 30–60  $\mu$ m silica gel (ICN Biomedicals, Costa Mesa, USA) was used. NMR spectra were recorded by Agilent-MR DDR2 and Varian Gemini 300 (Varian, Palo Alto, CA, USA). The Quadrupole LC/MS (ESI ionization) with an Infinity III LC system (Agilent Technologies, Santa Clara, USA) was used for LR-MS and HPLC analyses (C18 column: 100 mm; UV detection). The method for HPLC was as follows (A – 50 % MeOH, B – 100 % MeOH): 0 min 100 % A; 2 min 100 % B; 2 – 16 min 100 %; 13 min 50 % A; 20 min 100 % A. HRMS

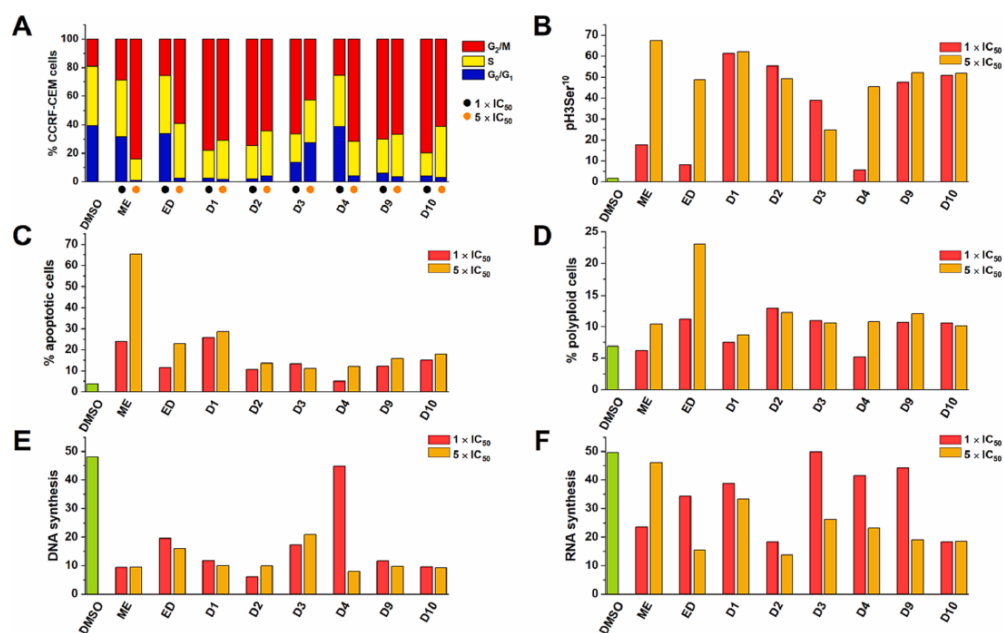


Fig. 4. Effect of cytotoxic compounds on the cell cycle (A), mitosis (B), apoptosis (C), induction of polyploidy (D) and DNA/RNA synthesis (E, F, resp.) in CCRF-CEM lymphoblasts (% of positive cells). Flow cytometry analysis was used for the quantification of cell cycle distribution and apoptotic cells with a concentration of compounds equal to  $1 \times IC_{50}$  and  $5 \times IC_{50}$  values. The DNA fragmentation was assessed using the logarithmic model expressing the percentage of the particles with the propidium iodide content lower than cells in the G<sub>0</sub>/G<sub>1</sub> phase ( $<G_1$ ) of the cell cycle. The table with values is available in Suppl. Mat. as Table S1 and raw data are depicted in Figure S54.

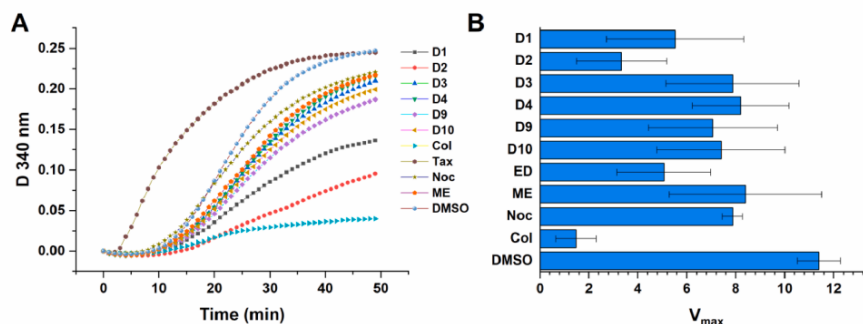


Fig. 5. Inhibition of tubulin assembly by dimers in a turbidometric tubulin polymerization assay (A).  $10 \mu\text{mol/L}$  of dimers D1, D2, D3, D4, D9, D10, 2-methoxyestradiol (ME), taxol (Tax), nocodazole (Noc), colchicine (Col) or corresponding volume of DMSO were used. Polymerization curves are mean values from three independent experiments. The maximal velocity of polymerization values ( $V_{\text{max}}$ ) was calculated from tubulin polymerization curves in the growth phase (B).

spectra were measured by Micro Q-TOF with ESI ionization (Thermo Scientific, Waltham, USA). Optical rotations were measured with an Autopol VI polarimeter (Rudolph Research Analytical, Hackettstown, NJ, USA). For microwave synthesis (MW), an Initiator Classic 355,301 (Biotage, Uppsala, Sweden) was used. Chemicals were purchased from

TCI Europe (Zwijndrecht, Belgium): sodium ascorbate ( $>99\%$ ), ethinylestradiol – EE ( $>98\%$ ); and from Sigma-Aldrich (St. Louis, MO, USA): copper(II) sulfate pentahydrate –  $\text{CuSO}_4 \cdot 5\text{H}_2\text{O}$  ( $\geq 98\%$ ), benzaldehyde ( $\geq 99\%$ ), 4-methoxybenzaldehyde (98%), 3-methoxybenzaldehyde (97%), 2,3-dimethoxybenzaldehyde (98%), 3,4-

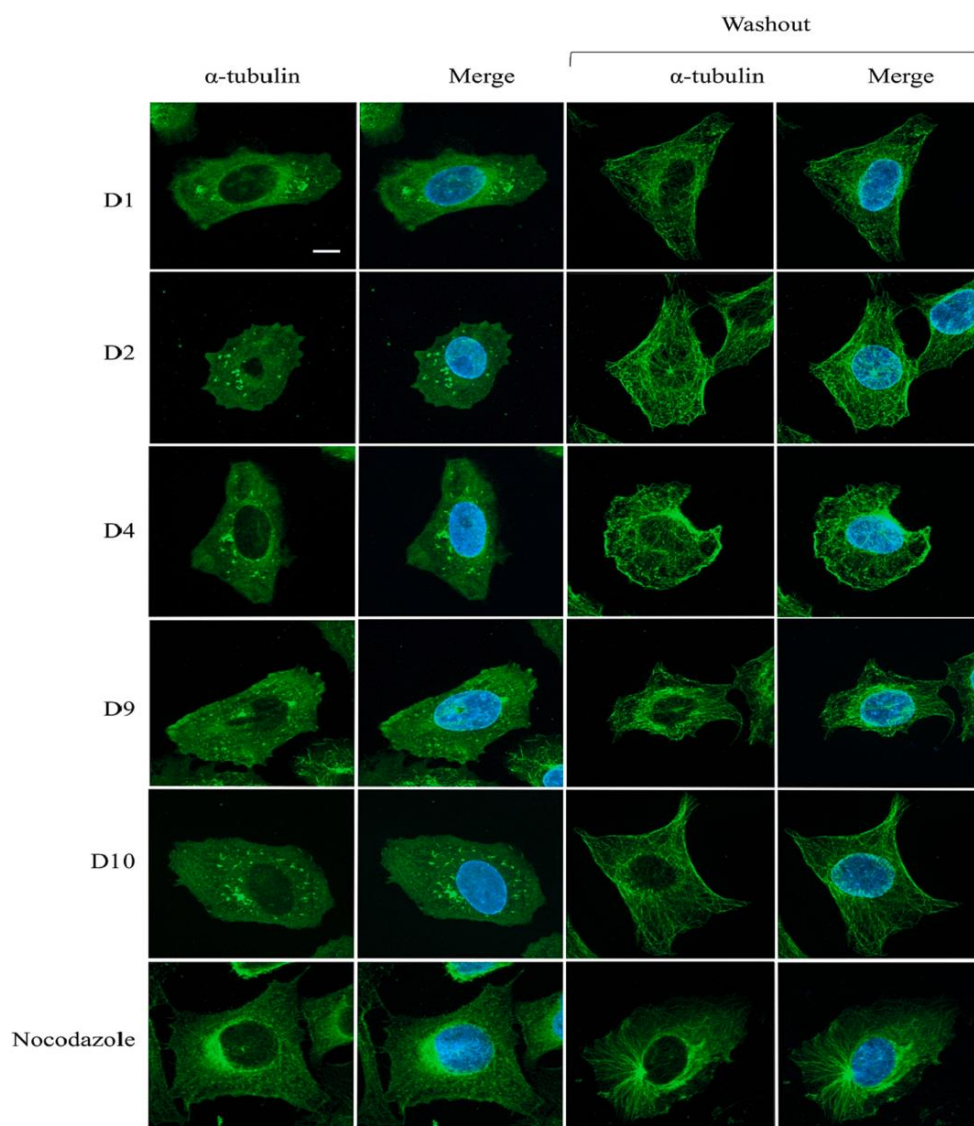


Fig. 6. Immunofluorescent images of U2OS cells treated for 24 h with 10  $\mu\text{M}$  concentration of dimers or 0.75  $\mu\text{M}$  nocodazole. For the purpose of the washout experiment the media with compounds were aspirated, coverslips with cells washed 3 times and incubated for an additional 30 min in the incubator in cultivation media. Nuclei were stained using Hoechst 33,342 (blue) and  $\alpha$ -tubulin with primary antibody and secondary Alexa Fluor 488-conjugated antibody (green). Scale bar 10  $\mu\text{m}$ . (For interpretation of the references to colour in this figure legend, the reader is referred to the web version of this article.)

dimethoxybenzaldehyde (99 %), vanillin (99 %), isovanillin (99 %), 3,4,5-trimethoxybenzaldehyde (98 %), 2,3,4-trimethoxybenzaldehyde (99 %), 1,11-diaziido-3,6,9-trioxaundecane (L13). Solvents for column chromatography and reactions supplied by PENTA (Praha, Czech Republic) were used as delivered. Synthesis of some diazides was

previously described, namely: 1,5-diazidopentane (L1) [15], bis(2-azidoethyl)ether (L2) [15] and *N,N*-bis(2-azidoethyl)amine (L3) [16].

#### 4.1.2. Synthesis of diazides

General procedure: To L3 (250 mg, 1.61 mmol, 1 equiv.) and

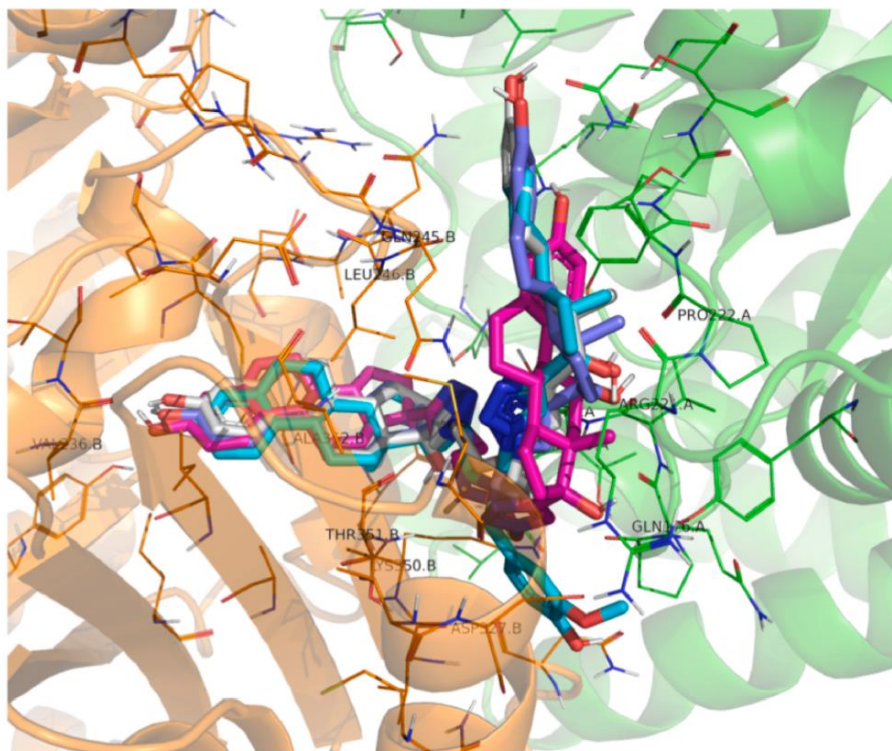


Fig. 7. Docking poses of compounds D1 (blue), D2 (grey), D3 (magenta) and D9 (cyan). (For interpretation of the references to colour in this figure legend, the reader is referred to the web version of this article.)

aldehyde (1 equiv.) in MeOH (15 mL) HOAc (193 mg, 3.2 mmol, 2 equiv.) and NaCNBH<sub>3</sub> (202 mg, 3.2 mmol, 2 equiv.) were added at RT. The mixture was stirred for 90 min after which the solvents were evaporated under reduced pressure. Chloroform (25 mL) was added and the solids were filtered off. The solvent was evaporated and the crude product was purified by silica gel column chromatography.

**2-Azido-*N*-(2-azidoethyl)-*N*-benzylethan-1-amine (L4).**

Reaction with benzaldehyde (171 mg, 1.61 mmol). Chromatography using hexanes-AcOEt 5:1 (v/v). L4 (240 mg, 0.98 mmol) was isolated as a slightly yellowish oil in 61 % yield.  $R_F = 0.8$  in hexanes-AcOEt 5:1 (v/v). <sup>1</sup>H NMR (300 MHz, CDCl<sub>3</sub>)  $\delta$  ppm: 2.78 (t,  $J = 6.1$  Hz, 4H), 3.31 (t,  $J = 6.1$  Hz, 4H), 3.73 (s, 2H), 7.26–7.33 (m, 1H), 7.34–7.45 (m, 4H). <sup>13</sup>C NMR (75 MHz, CDCl<sub>3</sub>)  $\delta$  ppm: 49.45, 53.68, 59.34, 127.40, 128.50, 128.76, 138.59. LRMS-ESI: calcd 245.1 Da, found  $m/z$  246.2 [M + H]<sup>+</sup>.

**2-Azido-*N*-(2-azidoethyl)-*N*-(4-methoxybenzyl)ethan-1-amine (L5).**

Reaction with 4-methoxybenzaldehyde (219 mg, 1.61 mmol). Chromatography using hexanes-AcOEt 4:1 (v/v). L5 (190 mg, 0.69 mmol) was isolated as a colorless oil in 43 % yield.  $R_F = 0.7$  in hexanes-AcOEt 4:1 (v/v). <sup>1</sup>H NMR (300 MHz, CDCl<sub>3</sub>)  $\delta$  ppm: 2.74 (t,  $J = 6.2$  Hz, 4H), 3.28 (t,  $J = 6.2$  Hz, 4H), 3.64 (s, 2H), 3.80 (s, 3H), 6.84–6.91 (m, 2H), 7.23–7.30 (m, 2H). <sup>13</sup>C NMR (75 MHz, CDCl<sub>3</sub>)  $\delta$  ppm: 49.43, 53.54, 55.22, 58.68, 113.81, 129.90, 130.44, 158.91. LRMS-ESI: calcd 275.1 Da, found  $m/z$  276.2 [M + H]<sup>+</sup>.

**2-Azido-*N*-(2-azidoethyl)-*N*-(3-methoxybenzyl)ethan-1-amine (L6).**

Reaction with 3-methoxybenzaldehyde (219 mg, 1.61 mmol).

Chromatography using hexanes-AcOEt 4:1 (v/v). L6 (260 mg, 0.94 mmol) was isolated as a yellowish oil in 58 % yield.  $R_F = 0.8$  in hexanes-AcOEt 4:1 (v/v). <sup>1</sup>H NMR (300 MHz, CDCl<sub>3</sub>)  $\delta$  ppm: 2.76 (t,  $J = 5.9$  Hz, 4H), 3.30 (t,  $J = 5.9$  Hz, 4H), 3.68 (s, 2H), 3.81 (s, 3H), 6.83 (dd,  $J = 7.9, 2.1$  Hz, 1H), 6.92 (d,  $J = 7.0$  Hz, 1H), 6.97–7.02 (m, 1H), 7.20–7.28 (m, 1H). <sup>13</sup>C NMR (75 MHz, CDCl<sub>3</sub>)  $\delta$  ppm: 49.40, 53.75, 55.16, 59.31, 113.28, 113.64, 120.90, 129.37, 140.32, 159.87. LRMS-ESI: calcd 275.2 Da, found  $m/z$  276.2 [M + H]<sup>+</sup>.

**2-Azido-*N*-(2-azidoethyl)-*N*-(2,3-dimethoxybenzyl)ethan-1-amine (L7).**

Reaction with 2,3-dimethoxybenzaldehyde (268 mg, 1.61 mmol). Chromatography using hexanes-AcOEt 4:1 (v/v). L7 (239 mg, 0.78 mmol) was obtained as a slightly yellowish oil in 48 % yield.  $R_F = 0.7$  in hexanes-AcOEt 3:1 (v/v). <sup>1</sup>H NMR (300 MHz, CDCl<sub>3</sub>)  $\delta$  ppm: 2.74 (t,  $J = 6.2$  Hz, 4H), 3.30 (t,  $J = 6.4$  Hz, 4H), 3.73 (s, 2H), 3.81 (s, 3H), 3.84 (s, 3H), 6.93 (dd,  $J = 7.3, 2.6$  Hz, 1H), 6.97–7.07 (m, 2H). <sup>13</sup>C NMR (75 MHz, CDCl<sub>3</sub>)  $\delta$  ppm: 49.45, 52.30, 53.52, 55.66, 60.71, 111.35, 122.18, 123.93, 131.87, 147.54, 152.68. LRMS-ESI: calcd 305.2 Da, found  $m/z$  306.2 [M + H]<sup>+</sup>.

**2-Azido-*N*-(2-azidoethyl)-*N*-(3,4-dimethoxybenzyl)ethan-1-amine (L8).**

Reaction with 3,4-dimethoxybenzaldehyde (268 mg, 1.61 mmol). Chromatography using hexanes-AcOEt 4:1 (v/v). L8 (263 mg, 0.86 mmol) was obtained as a slightly colorless oil in 53 % yield.  $R_F = 0.6$  in hexanes-AcOEt 3:1 (v/v). <sup>1</sup>H NMR (300 MHz, CDCl<sub>3</sub>)  $\delta$  ppm: 2.68 (t,  $J =$



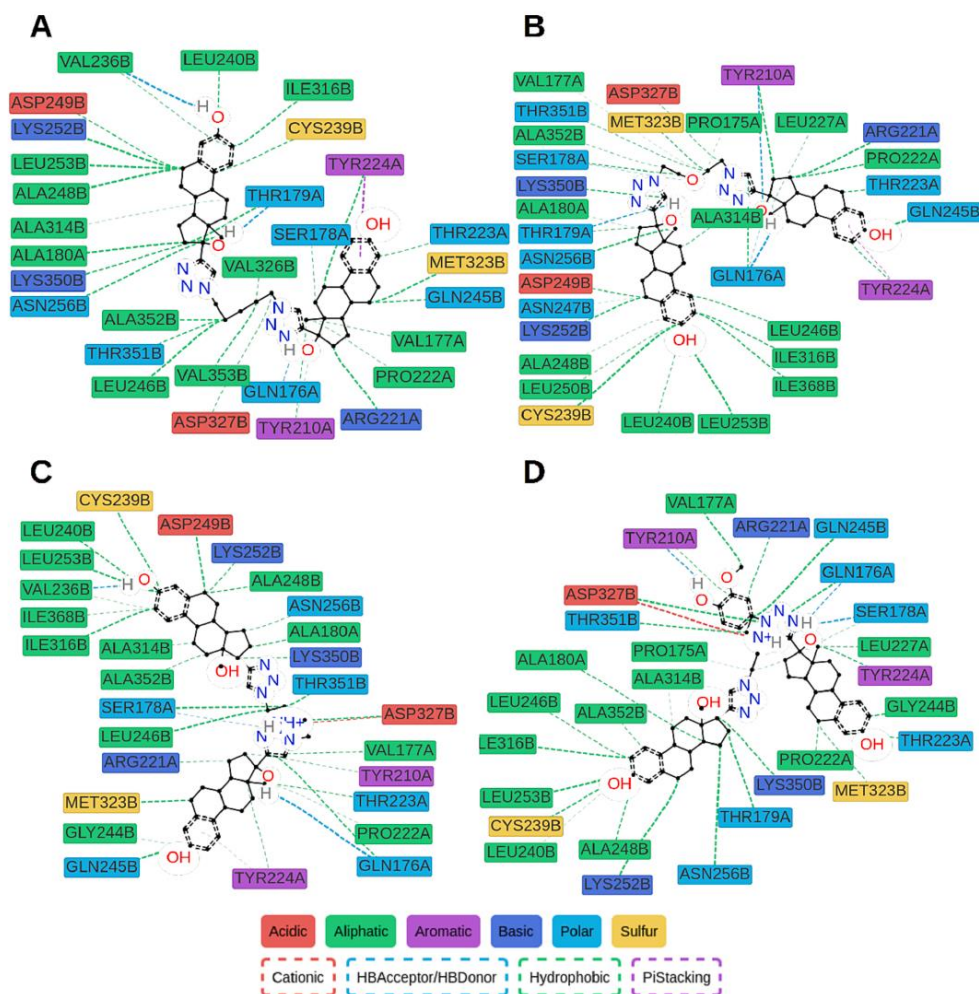


Fig. 8. Protein-ligand contacts were observed in at least 10 % of MD trajectories for D1 (A), D2 (B), D3 (C) and D9 (D). Contacts were analyzed only for the stable part of trajectories, 50–150 ns.

Table 2  
Calculated binding free energy by MM-PBSA method, interaction entropy and maximal velocity of polymerization.

Dimer	$\Delta G$ [kcal mol <sup>-1</sup> ]	$-T\Delta S$ [kcal mol <sup>-1</sup> ]	$v_{max}$
D1	-22.6	16.8	4.1
D2	-19.4	13.0	2.0
D3	-2.9	28.8	7.4
D9	-5.6	35.6*	5.9

\*Calculated interaction entropy for compound D9 had a large standard deviation (6.5) whereas for other ligands it did not exceed 0.05.

5.9 Hz, 4H), 3.22 (t,  $J = 6.2$  Hz, 4H), 3.57 (s, 2H), 3.80 (s, 3H), 3.82 (s, 3H), 6.70–6.81 (m, 2H), 6.95 (s, 1H). <sup>13</sup>C NMR (75 MHz, CDCl<sub>3</sub>)  $\delta$  ppm: 49.31, 53.72, 55.74, 55.80, 59.13, 110.68, 111.48, 120.64, 131.13, 140.22, 149.11. LRMS-ESI: calcd 305.2 Da, found  $m/z$  306.2 [M + H]<sup>+</sup>.

4-((Bis(2-azidoethyl)amino)methyl)-2-methoxyphenol (L9).

Reaction with vanillin (245 mg, 1.61 mmol). Chromatography using hexanes-AcOEt 4:1 (v/v). L9 (78 mg, 0.27 mmol) was obtained as an oil in 17 % yield.  $R_f = 0.7$  in hexanes-AcOEt 3:1 (v/v).

<sup>1</sup>H NMR (300 MHz, CDCl<sub>3</sub>)  $\delta$  ppm: 2.76 (t,  $J = 5.9$  Hz, 4H), 3.30 (t,  $J = 5.9$  Hz, 4H), 3.62 (s, 2H), 3.89 (s, 3H), 5.73 (br. s., 1H), 6.73–6.79 (m, 1H), 6.83–6.88 (m, 1H), 7.01 (s, 1H). <sup>13</sup>C NMR (75 MHz, CDCl<sub>3</sub>)  $\delta$  ppm: 49.37, 53.74, 55.90, 59.29, 110.96, 113.89, 121.38, 130.47, 144.90, 146.83. LRMS-ESI: calcd 291.1 Da, found  $m/z$  292.1 [M + H]<sup>+</sup>.

5-((Bis(2-azidoethyl)amino)methyl)-2-methoxyphenol (L10).

Reaction with isovanillin (245 mg, 1.61 mmol). Chromatography using hexanes-AcOEt 4:1 (v/v). **L10** (191 mg, 0.66 mmol) was obtained as an oil in 41 % yield.  $R_f = 0.6$  in hexanes-AcOEt 3:1 (v/v).  $^1\text{H NMR}$  (300 MHz,  $\text{CDCl}_3$ )  $\delta$  ppm: 2.73 (t,  $J = 5.9$  Hz, 4H), 3.28 (t,  $J = 5.9$  Hz, 4H), 3.59 (s, 2H), 3.86 (s, 3H), 5.84 (br. s., 1H), 6.77–6.84 (m, 2H), 6.87–6.93 (m, 1H).  $^{13}\text{C NMR}$  (75 MHz,  $\text{CDCl}_3$ )  $\delta$  ppm: 49.42, 53.49, 55.98, 58.76, 110.59, 115.05, 120.27, 131.63, 145.57, 145.92. LRMS-ESI: calcd 291.1 Da, found  $m/z$  292.2  $[\text{M} + \text{H}]^+$ .

2-Azido-*N*-(2-azidoethyl)-*N*-(3,4,5-trimethoxybenzyl)ethanamine (**L11**).

Reaction with 3,4,5-trimethoxybenzaldehyde (316 mg, 1.61 mmol). Chromatography using hexanes-AcOEt 2:1 (v/v). **L11** (298 mg, 0.89 mmol) was obtained as a colorless gel in 55 % yield.  $R_f = 0.7$  in hexanes-AcOEt 2:1 (v/v).  $^1\text{H NMR}$  (400 MHz,  $\text{CDCl}_3$ )  $\delta$  ppm: 2.75 (t,  $J = 6.1$  Hz, 4H), 3.30 (t,  $J = 5.9$  Hz, 4H), 3.63 (s, 2H), 3.83 (s, 3H), 3.84 (s, 6H), 6.61 (s, 2H).  $^{13}\text{C NMR}$  (101 MHz,  $\text{CDCl}_3$ )  $\delta$  ppm: 49.34, 53.83, 56.03, 59.67, 60.82, 105.05, 134.37, 136.91, 153.23. LRMS-ESI: calcd 335.2 Da, found  $m/z$  336.2  $[\text{M} + \text{H}]^+$ .

2-Azido-*N*-(2-azidoethyl)-*N*-(2,3,4-trimethoxybenzyl)ethanamine (**L12**).

Reaction with 2,3,4-trimethoxybenzaldehyde (316 mg, 1.61 mmol). Chromatography using hexanes-AcOEt 3:1 (v/v). **L12** (226 mg, 0.67 mmol) was obtained as a colorless gel in 42 % yield.  $R_f = 0.7$  in hexanes-AcOEt 2:1 (v/v).  $^1\text{H NMR}$  (400 MHz,  $\text{CDCl}_3$ )  $\delta$  ppm: 2.74 (t,  $J = 6.3$  Hz, 4H), 3.31 (t,  $J = 6.3$  Hz, 4H), 3.65 (s, 2H), 3.85 (s, 3H), 3.86 (s, 3H), 3.88 (s, 3H), 6.66 (d,  $J = 8.6$  Hz, 1H), 7.04 (d,  $J = 8.6$  Hz, 1H).  $^{13}\text{C NMR}$  (101 MHz,  $\text{CDCl}_3$ )  $\delta$  ppm: 49.42, 52.50, 53.41, 55.93, 60.75, 61.02, 107.14, 123.84, 124.71, 142.12, 152.31, 153.03. LRMS-ESI: calcd 335.2 Da, found  $m/z$  336.2  $[\text{M} + \text{H}]^+$ .

#### 4.1.3. Synthesis of dimers

General procedure: To a solution of diazide (**L1**–**L13**, 1 equiv.) and 17 $\alpha$ -ethynylestradiol (**EE**, 2.2 equiv.) in dry DMF aqueous solutions (250  $\mu\text{L}$ ) of  $\text{CuSO}_4 \cdot 5\text{H}_2\text{O}$  (0.1 equiv.) and sodium ascorbate (0.15 equiv.) were added. The mixture was placed in a microwave reactor and heated to 80 °C for 2 h. Solvents were evaporated under reduced pressure and the crude product was purified by column chromatography on silica gel. The product thus obtained was precipitated, filtered, washed with ether and dried *in vacuo*.

(17 $\beta$ ,17 $\beta'$ )-17,17'-[Pentane-1,5-diylbis(1*H*-1,2,3-triazole-1,4-diyl)]bisestra-1,3,5(10)-triene-3,17-diol (**D1**).

In reaction: **L1** (50 mg, 0.32 mmol), **EE** (210 mg, 0.71 mmol),  $\text{CuSO}_4 \cdot 5\text{H}_2\text{O}$  (18 mg, 0.071 mmol), sodium ascorbate (21 mg, 0.1 mmol), DMF (6 mL). Chromatography with  $\text{CHCl}_3$ -MeOH 20:1  $\rightarrow$  10:1  $\rightarrow$  5:1 (v/v). Compound **D1** (209 mg, 0.28 mmol) was obtained as a white solid in 86 % yield.  $R_f = 0.2$  in DCM-MeOH 10:1 (v/v).  $^1\text{H NMR}$  (400 MHz,  $\text{DMSO}-d_6$ )  $\delta$  ppm: 0.58 (td,  $J = 12.7$ , 3.1 Hz, 2H), 0.92 (s, 6 H), 1.13–1.53 (m, 12H), 1.58–1.69 (m, 2 H), 1.72–2.00 (m, 11H), 2.04–2.15 (m, 2 H), 2.28–2.43 (m, 2 H), 2.63–2.78 (m, 4 H), 4.31 (t,  $J = 7$  Hz, 4 H), 5.08 (s, 2 H), 6.41 (d,  $J = 2.4$  Hz, 2 H), 6.46 (dd,  $J = 8.6$ , 2.4 Hz, 2 H), 6.96 (d,  $J = 8.6$  Hz, 2 H), 7.84 (s, 2 H), 8.96 (s, 2 H); Fig. S2.  $^{13}\text{C NMR}$  (101 MHz,  $\text{DMSO}-d_6$ )  $\delta$  ppm: 14.83, 23.29, 24.01, 26.52, 27.64, 29.54, 29.72, 33.12, 37.66, 43.63, 47.12, 47.95, 49.32, 81.52, 113.08, 115.31, 122.94, 126.45, 130.85, 137.59, 154.51, 155.30; Fig. S3. HRMS-ESI: (calcd 746.45195 Da), found  $m/z$  769.44140  $[\text{M} + \text{Na}]^+$ ; Fig. S4.  $[\alpha]_D^{20} = +60.8$  ( $c = 0.25$ , DMF- $\text{CHCl}_3$ , 1:1). HPLC:  $R_T = 7.425$  min; Fig. S5.

17,17'-{(Oxybis[(ethane-2,1-diyl)-1*H*-1,2,3-triazole-1,4-diyl])diestra-1,3,5(10)-triene-3,17 $\beta$ -diol} (**D2**).

In reaction: **L2** (50 mg, 0.32 mmol), **EE** (210 mg, 0.71 mmol),  $\text{CuSO}_4 \cdot 5\text{H}_2\text{O}$  (18 mg, 0.071 mmol), sodium ascorbate (21 mg, 0.1 mmol), DMF (6 mL). Chromatography with DCM-MeOH 15:1  $\rightarrow$  10:1  $\rightarrow$  5:1 (v/v). Compound **D2** (217 mg, 0.29 mmol) was obtained as a white solid in 89 % yield.  $R_f = 0.2$  in DCM-MeOH 10:1 (v/v).  $^1\text{H NMR}$  (400 MHz,  $\text{DMSO}-d_6$ )  $\delta$  ppm: 0.58 (td,  $J = 12.7$ , 3.5 Hz, 2H), 0.92 (s, 6H), 1.12–1.52 (m, 10H), 1.54–1.69 (m, 2H), 1.70–1.88 (m, 6H), 1.89–2.00

(m, 2H), 2.01–2.14 (m, 2H), 2.31–2.43 (m, 2H), 2.60–2.78 (m, 4H), 3.81 (t,  $J = 5.5$  Hz, 4H), 4.48 (td,  $J = 5.3$ , 2.0 Hz, 4H), 5.12 (s, 2H), 6.40 (d, 2H), 6.45 (dd,  $J = 8.4$ , 2.5 Hz, 2H), 6.95 (d,  $J = 8.2$  Hz, 2H), 7.81 (s, 2H), 8.95 (s, 2H); Fig. S6.  $^{13}\text{C NMR}$  (101 MHz,  $\text{DMSO}-d_6$ )  $\delta$  ppm: 14.83, 24.02, 26.52, 27.64, 29.71, 33.08, 37.58, 43.62, 47.14, 47.96, 49.49, 69.13, 81.54, 113.07, 115.30, 120.41, 123.46, 126.45, 130.86, 137.59, 154.48, 155.30; Fig. S7. HRMS-ESI: calcd 748.43122 Da, found  $m/z$  749.43843  $[\text{M} + \text{H}]^+$ , 771.42062  $[\text{M} + \text{Na}]^+$  and 787.39343  $[\text{M} + \text{K}]^+$ ; Fig. S8.  $[\alpha]_D^{28} = +70.4$  ( $c = 0.25$ , DMF- $\text{CHCl}_3$ , 1:1). HPLC:  $R_T = 7.573$  min; Fig. S9.

(17 $\beta$ ,17 $\beta'$ )-17,17'-[iminobis(ethane-2,1-diyl)-1*H*-1,2,3-triazole-1,4-diyl]bisestra-1,3,5(10)-triene-3,17-diol (**D3**).

In reaction: **L3** (50 mg, 0.32 mmol), **EE** (210 mg, 0.71 mmol),  $\text{CuSO}_4 \cdot 5\text{H}_2\text{O}$  (18 mg, 0.071 mmol), sodium ascorbate (21 mg, 0.1 mmol), DMF (6 mL). Chromatography with  $\text{CHCl}_3$ -MeOH 10:1 (v/v). Compound **D3** (189 mg, 0.25 mmol) was obtained as a white solid in 79 % yield.  $R_f = 0.15$  in DCM-MeOH 10:1 (v/v).  $^1\text{H NMR}$  (400 MHz,  $\text{DMSO}-d_6$ )  $\delta$  ppm: 0.60 (td,  $J = 12.8$ , 3.7 Hz, 2H), 0.92 (s, 6H), 1.12–1.52 (m, 10H), 1.58–2.15 (m, 13H), 2.30–2.40 (m, 2H), 2.61–2.77 (m, 4H), 2.97 (br t,  $J = 6.5$  Hz, 4H), 4.35 (t,  $J = 6.5$  Hz, 3 H), 5.08 (s, 2H), 6.41 (d,  $J = 2.4$  Hz, 2H), 6.46 (dd,  $J = 8.4$ , 2.5 Hz, 2H), 6.95 (d,  $J = 8.6$  Hz, 2H), 7.80–7.91 (s, 2H), 8.88–9.01 (s, 2H); Fig. S10.  $^{13}\text{C NMR}$  (101 MHz,  $\text{DMSO}-d_6$ )  $\delta$  ppm: 14.8, 24.0, 26.5, 27.6, 29.7, 33.1, 37.6, 43.6, 47.1, 47.9, 48.3, 49.8, 81.6, 113.1, 115.3, 123.4, 126.4, 130.9, 137.6, 154.3, 155.3; Fig. S11. HRMS-ESI: calcd 747.44720 Da, found  $m/z$  748.45435  $[\text{M} + \text{H}]^+$ , 770.43622  $[\text{M} + \text{Na}]^+$  and 786.40954  $[\text{M} + \text{K}]^+$ ; Fig. S12.  $[\alpha]_D^{28} = +66.5$  ( $c = 0.26$ , DMF- $\text{CHCl}_3$ , 1:1). HPLC:  $R_T = 7.587$  min; Fig. S13.

17 $\beta$ ,17 $\beta'$ )-17,17'-[(Benzylimino)bis(ethane-2,1-diyl)-1*H*-1,2,3-triazole-1,4-diyl]bisestra-1,3,5(10)-triene-3,17-diol (**D4**).

In reaction: **L4** (100 mg, 0.41 mmol), **EE** (266 mg, 0.9 mmol),  $\text{CuSO}_4 \cdot 5\text{H}_2\text{O}$  (22 mg, 0.09 mmol), sodium ascorbate (27 mg, 0.14 mmol), DMF (8 mL). Chromatography with DCM-MeOH 10:1 (v/v). Compound **D4** (287 mg, 0.34 mmol) was obtained as a white solid in 84 % yield.  $R_f = 0.2$  in DCM-MeOH 10:1 (v/v).  $^1\text{H NMR}$  (400 MHz,  $\text{DMSO}-d_6$ )  $\delta$  ppm: 0.60 (td,  $J = 12.9$ , 3.5 Hz, 2H), 0.90 (s, 6H), 1.02–1.52 (m, 11H), 1.54–2.08 (m, 13H), 2.26–2.39 (m, 2H), 2.58–2.76 (m, 4H), 2.92 (br t,  $J = 6.3$  Hz, 4H), 3.62 (s, 2H), 4.36 (br t,  $J = 6.3$  Hz, 4H), 5.05 (s, 2H), 6.38 (d,  $J = 2.4$  Hz, 2H), 6.44 (dd,  $J = 8.2$ , 2.4 Hz, 2H), 6.89 (d,  $J = 8.6$  Hz, 2H), 7.08–7.23 (m, 5H), 7.84 (s, 2H), 8.93 (s, 2H); Fig. S14.  $^{13}\text{C NMR}$  (101 MHz,  $\text{DMSO}-d_6$ )  $\delta$  ppm: 14.8, 24.0, 26.5, 27.6, 29.7, 33.1, 37.7, 43.6, 47.1, 47.7, 48.0, 53.3, 57.3, 81.6, 113.1, 115.3, 123.4, 126.4, 127.3, 128.5, 128.8, 130.8, 137.6, 139.2, 154.4, 155.3; Fig. S15. HRMS-ESI: calcd 837.49415 Da, found  $m/z$  838.50126  $[\text{M} + \text{H}]^+$  and 860.48328  $[\text{M} + \text{Na}]^+$ ; Fig. S16.  $[\alpha]_D^{28} = +46.8$  ( $c = 0.25$ , DMF- $\text{CHCl}_3$ , 1:1). HPLC:  $R_T = 7.855$  min; Fig. S17.

(17 $\beta$ ,17 $\beta'$ )-17,17'-[[4-Methoxybenzyl]imino]bis(ethane-2,1-diyl)-1*H*-1,2,3-triazole-1,4-diyl]bisestra-1,3,5(10)-triene-3,17-diol (**D5**).

In reaction: **L5** (100 mg, 0.36 mmol), **EE** (234 mg, 0.79 mmol),  $\text{CuSO}_4 \cdot 5\text{H}_2\text{O}$  (20 mg, 0.08 mmol), sodium ascorbate (24 mg, 0.12 mmol), DMF (8 mL). Chromatography with  $\text{CHCl}_3$ -MeOH 10:1 (v/v). Compound **D5** (190 mg, 0.22 mmol) was obtained as a white solid in 61 % yield.  $R_f = 0.2$  in DCM-MeOH 10:1 (v/v).  $^1\text{H NMR}$  (400 MHz,  $\text{DMSO}-d_6$ )  $\delta$  ppm: 0.61 (td,  $J = 12.8$ , 3.7 Hz, 2H), 0.92 (s, 6 H), 1.10–1.52 (m, 11H), 1.54–2.07 (m, 12H), 2.28–2.40 (m, 2 H), 2.59–2.77 (m, 4 H), 2.92 (br t,  $J = 6.3$  Hz, 4 H), 3.49–3.59 (m, 2 H), 3.62 (s, 3 H), 4.36 (br t,  $J = 6.5$  Hz, 4 H), 5.07 (s, 2 H), 6.40 (d,  $J = 2.4$  Hz, 2 H), 6.45 (dd,  $J = 8.2$ , 2.4 Hz, 2 H), 6.75 (d,  $J = 8.6$  Hz, 2 H), 6.90 (d,  $J = 8.6$  Hz, 2 H), 7.03 (d,  $J = 8.6$  Hz, 1 H), 7.85 (s, 2 H), 8.95 (s, 2 H); Fig. S18.  $^{13}\text{C NMR}$  (101 MHz,  $\text{DMSO}-d_6$ )  $\delta$  ppm: 14.8, 24.0, 26.5, 27.6, 29.7, 33.1, 37.7, 43.6, 47.1, 47.7, 48.0, 53.1, 55.2, 57.2, 81.6, 113.1, 113.9, 115.3, 123.3, 126.4, 130.0, 130.8, 130.9, 137.6, 154.4, 155.3, 158.6; Fig. S19. HRMS-ESI: calcd 867.50472 Da, found  $m/z$  868.51186  $[\text{M} + \text{H}]^+$ , 890.49345  $[\text{M} + \text{Na}]^+$  and 906.46701  $[\text{M} + \text{K}]^+$ ; Fig. S20.  $[\alpha]_D^{28} = +43.6$  ( $c = 0.25$ , DMF- $\text{CHCl}_3$ , 1:1). HPLC:  $R_T = 7.797$  min; Fig. S21.

(17 $\beta$ ,17 $\beta'$ )-17,17'-[[3-Methoxybenzyl]imino]bis(ethane-2,1-diyl-

1*H*-1,2,3-triazole-1,4-diyl))bisestra-1,3,5(10)-triene-3,17-diol (D6).

In reaction: L6 (100 mg, 0.36 mmol), EE (234 mg, 0.79 mmol), CuSO<sub>4</sub>·5H<sub>2</sub>O (20 mg, 0.09 mmol), sodium ascorbate (24 mg, 0.12 mmol), DMF (8 mL). Chromatography with CHCl<sub>3</sub>-MeOH 10:1 (v/v). Compound D6 (260 mg, 0.3 mmol) was obtained as a white solid in 83 % yield. R<sub>F</sub> = 0.2 in DCM-MeOH 10:1 (v/v). <sup>1</sup>H NMR (400 MHz, DMSO-*d*<sub>6</sub>) δ ppm: 0.60 (td, *J* = 12.7, 3.5 Hz, 2H), 0.91 (s, 6H), 1.11–1.50 (m, 10H), 1.56–2.07 (m, 10H), 2.28–2.40 (m, 2H), 2.59–2.77 (m, 4H), 2.94 (br t, *J* = 6.7 Hz, 4H), 3.55–3.65 (m, 2H), 3.68 (s, 3H), 4.36 (br t, *J* = 6.5 Hz, 4H), 5.05 (s, 2H), 6.40 (d, *J* = 2.4 Hz, 2H), 6.45 (dd, *J* = 8.4, 2.5 Hz, 2H), 6.69–6.76 (m, 2H), 6.78 (s, 1H), 6.90 (d, *J* = 8.2 Hz, 2H), 7.12 (t, *J* = 7.8 Hz, 1H), 7.36 (s, 2H), 8.95 (s, 2H); Fig. S22. <sup>13</sup>C NMR (101 MHz, DMSO-*d*<sub>6</sub>) δ ppm: 14.8, 24.0, 26.5, 27.6, 29.7, 33.1, 37.7, 43.6, 47.1, 47.8, 48.0, 53.4, 55.3, 57.8, 81.6, 112.9, 113.1, 114.3, 115.3, 121.0, 123.2, 126.4, 129.5, 130.8, 137.6, 140.9, 154.5, 155.3, 159.6; Fig. S23. HRMS-ESI: calcd 867.50472 Da, found *m/z* 868.51199 [M + H]<sup>+</sup>, 890.49372 [M + Na]<sup>+</sup> and 906.46604 [M + K]<sup>+</sup>; Fig. S24. [α]<sub>D</sub><sup>25</sup> = +48.8 (c = 0.25, DMF-CHCl<sub>3</sub>, 1:1). HPLC: R<sub>T</sub> = 7.858 min; Fig. S25.

(17β,17′β)-17,17′-((2,3-dimethoxybenzyl)imino)bis(ethane-2,1-diyl-1*H*-1,2,3-triazole-1,4-diyl))bisestra-1,3,5(10)-triene-3,17-diol (D7).

In reaction: L7 (100 mg, 0.33 mmol), EE (213 mg, 0.72 mmol), CuSO<sub>4</sub>·5H<sub>2</sub>O (17 mg, 0.07 mmol), sodium ascorbate (21 mg, 0.11 mmol), DMF (8 mL). Chromatography with CHCl<sub>3</sub>-MeOH 10:1 (v/v). Compound D7 (264 mg, 0.29 mmol) was obtained as a white solid in 88 % yield. R<sub>F</sub> = 0.2 in DCM-MeOH 10:1 (v/v). <sup>1</sup>H NMR (400 MHz, DMSO-*d*<sub>6</sub>) δ ppm: 0.91 (s, 6H), 1.08–1.51 (m, 12H), 1.55–2.06 (m, 14H), 2.28–2.38 (m, 2H), 2.60–2.72 (m, 4H), 2.94 (br t, *J* = 6.5 Hz, 4H), 3.64 (s, 3H), 3.66 (s, 2H), 3.73 (s, 3H), 4.37 (br t, *J* = 6.5 Hz, 4H), 5.05 (s, 2H), 6.39 (d, *J* = 2.4 Hz, 2H), 6.45 (dd, *J* = 8.4, 2.5 Hz, 2H), 6.68 (dd, *J* = 7.2, 1.8 Hz, 1H), 6.85–6.93 (m, 4H), 7.85 (s, 2H), 8.95 (s, 2H); Fig. S26. <sup>13</sup>C NMR (101 MHz, DMSO-*d*<sub>6</sub>) δ ppm: 14.8, 24.0, 26.5, 27.6, 29.7, 33.1, 37.7, 43.6, 47.1, 47.9, 48.0, 51.7, 53.6, 55.9, 60.6, 81.6, 111.9, 113.1, 115.3, 121.9, 123.3, 124.1, 126.4, 130.8, 132.3, 137.6, 147.4, 152.7, 154.4, 155.3; Fig. S27. HRMS-ESI: calcd 897.51528 Da, found *m/z* 898.52256 [M + H]<sup>+</sup>, 920.50447 [M + Na]<sup>+</sup> and 936.47639 [M + K]<sup>+</sup>; Fig. S28. [α]<sub>D</sub><sup>27</sup> = +47.4 (c = 0.27, DMF-CHCl<sub>3</sub>, 1:1). HPLC: R<sub>T</sub> = 7.809 min; Fig. S29.

(17β,17′β)-17,17′-((3,4-Dimethoxybenzyl)imino)bis(ethane-2,1-diyl-1*H*-1,2,3-triazole-1,4-diyl))bisestra-1,3,5(10)-triene-3,17-diol (D8).

In reaction: L8 (100 mg, 0.33 mmol), EE (213 mg, 0.72 mmol), CuSO<sub>4</sub>·5H<sub>2</sub>O (17 mg, 0.07 mmol), sodium ascorbate (21 mg, 0.11 mmol), DMF (8 mL). Chromatography with CHCl<sub>3</sub>-MeOH 10:1 (v/v). Compound D8 (281 mg, 0.31 mmol) was obtained as a white solid in 94 % yield. R<sub>F</sub> = 0.2 in DCM-MeOH 10:1 (v/v). <sup>1</sup>H NMR (400 MHz, DMSO-*d*<sub>6</sub>) δ ppm: 0.58 (td, *J* = 12.8, 3.7 Hz, 2H), 0.90 (s, 6 H), 1.08–1.51 (m, 12H), 1.54–2.04 (m, 13H), 2.29–2.39 (m, 2 H), 2.60–2.77 (m, 4 H), 2.93 (br t, *J* = 6.7 Hz, 4 H), 3.60 (s, 3 H), 3.73 (s, 3 H), 4.35 (br t, *J* = 6.3 Hz, 4 H), 5.06 (s, 2 H), 6.39 (d, *J* = 2.4 Hz, 2 H), 6.44 (dd, *J* = 8.6, 2.4 Hz, 2 H), 6.64 (dd, *J* = 8.0, 1.4 Hz, 1 H), 6.70–6.74 (m, 1 H), 6.82 (d, *J* = 1.57 Hz, 1 H), 6.88 (d, *J* = 8.6 Hz, 2 H), 7.87 (s, 2 H), 8.95 (s, 2 H); Fig. S30. <sup>13</sup>C NMR (101 MHz, DMSO-*d*<sub>6</sub>) δ ppm: 14.8, 22.5, 24.0, 26.5, 27.6, 29.7, 31.4, 33.1, 37.6, 43.5, 47.1, 47.9, 47.9, 53.3, 55.6, 55.8, 57.6, 81.6, 111.5, 112.6, 113.0, 115.3, 120.8, 123.2, 126.4, 130.8, 131.5, 137.6, 148.1, 149.0, 154.5, 155.3; Fig. S31. HRMS-ESI: calcd 897.51528 Da, found *m/z* 898.52251 [M + H]<sup>+</sup>, 920.50437 [M + Na]<sup>+</sup> and 936.47709 [M + K]<sup>+</sup>; Fig. S32. [α]<sub>D</sub><sup>27</sup> = +41.5 (c = 0.26, DMF-CHCl<sub>3</sub>, 1:1). HPLC: R<sub>T</sub> = 7.652 min; Fig. S33.

(17β,17′β)-17,17′-((3,4-Dimethoxybenzyl)imino)bis(ethane-2,1-diyl-1*H*-1,2,3-triazole-1,4-diyl))bisestra-1,3,5(10)-triene-3,17-diol (D9).

In reaction: L9 (100 mg, 0.34 mmol), EE (223 mg, 0.76 mmol), CuSO<sub>4</sub>·5H<sub>2</sub>O (17 mg, 0.07 mmol), sodium ascorbate (21 mg, 0.11 mmol), DMF (8 mL). Chromatography with CHCl<sub>3</sub>-MeOH 40:1 → 20:1 → 15:1 (v/v). Compound D9 (266 mg, 0.3 mmol) was obtained as a

white solid in 88 % yield. R<sub>F</sub> = 0.6 in DCM-MeOH 10:1 (v/v). <sup>1</sup>H NMR (400 MHz, DMSO-*d*<sub>6</sub>) δ ppm: 0.61 (td, *J* = 12.7, 3.1 Hz, 2H), 0.91 (s, 6 H), 1.11–1.52 (m, 12H), 1.54–2.08 (m, 13H), 2.28–2.40 (m, 2 H), 2.60–2.76 (m, 4 H), 2.91 (br t, *J* = 6.5 Hz, 4 H), 3.51 (s, 2 H), 3.65 (s, 3 H), 4.34 (br t, *J* = 6.5 Hz, 4 H), 5.07 (s, 2 H), 6.39 (d, *J* = 2.4 Hz, 2 H), 6.45 (dd, *J* = 8.4, 2.5 Hz, 2 H), 6.52 (dd, *J* = 8.2, 2.0 Hz, 1 H), 6.66 (d, *J* = 1.6 Hz, 1 H), 6.72 (d, *J* = 8.2 Hz, 1 H), 6.91 (d, *J* = 8.61 Hz, 2 H), 7.85 (s, 2 H), 8.80 (s, 1 H), 8.95 (s, 2 H); Fig. S34. <sup>13</sup>C NMR (101 MHz, DMSO-*d*<sub>6</sub>) δ ppm: 14.8, 24.0, 26.5, 27.6, 29.7, 33.1, 37.7, 43.6, 47.1, 47.8, 48.0, 53.3, 55.9, 81.6, 112.2, 113.1, 115.3, 116.5, 119.6, 123.3, 126.4, 130.9, 131.4, 137.6, 146.6, 147.0, 154.4, 155.3; Fig. S35. HRMS-ESI: calcd 883.49963 Da, found *m/z* 884.50653 [M + H]<sup>+</sup>, 906.48840 [M + Na]<sup>+</sup> and 922.46112 [M + K]<sup>+</sup>; Fig. S36. [α]<sub>D</sub><sup>27</sup> = +50.0 (c = 0.26, DMF-CHCl<sub>3</sub>, 1:1). HPLC: R<sub>T</sub> = 7.576 min; Fig. S37.

(17β,17′β)-17,17′-((3-Hydroxy-4-methoxybenzyl)imino)bis(ethane-2,1-diyl-1*H*-1,2,3-triazole-1,4-diyl))bisestra-1,3,5(10)-triene-3,17-diol (D10).

In reaction: L10 (100 mg, 0.34 mmol), EE (223 mg, 0.76 mmol), CuSO<sub>4</sub>·5H<sub>2</sub>O (17 mg, 0.07 mmol), sodium ascorbate (21 mg, 0.11 mmol), DMF (8 mL). Chromatography with CHCl<sub>3</sub>-MeOH 20:1 → 10:1 (v/v). Compound D10 (253 mg, 0.29 mmol) was obtained as a white solid in 85 % yield. R<sub>F</sub> = 0.5 in DCM-MeOH 10:1 (v/v). <sup>1</sup>H NMR (400 MHz, DMSO-*d*<sub>6</sub>) δ ppm: 0.60 (td, *J* = 12.6, 3.3 Hz, 2H), 0.91 (s, 6 H), 1.07–1.53 (m, 12H), 1.55–2.11 (m, 13H), 2.28–2.39 (m, 2 H), 2.58–2.78 (m, 4 H), 2.91 (br t, *J* = 6.5 Hz, 4 H), 3.54 (br s, 2 H), 3.73 (s, 3 H), 4.33 (br t, *J* = 6.3 Hz, 4 H), 5.05 (s, 2 H), 6.39 (d, *J* = 2.4 Hz, 2 H), 6.45 (dd, *J* = 8.4, 2.5 Hz, 2 H), 6.55 (br dd, *J* = 8.0, 1.4 Hz, 1 H), 6.60–6.65 (m, 1 H), 6.79 (d, *J* = 1.2 Hz, 1 H), 6.91 (br d, *J* = 8.6 Hz, 2 H), 7.83–7.88 (m, 2 H), 8.79 (s, 1 H), 8.94 (s, 2 H); Fig. S38. <sup>13</sup>C NMR (101 MHz, DMSO-*d*<sub>6</sub>) δ ppm: 14.8, 24.0, 26.5, 27.6, 29.7, 33.1, 37.7, 43.6, 47.1, 47.8, 48.0, 53.3, 56.0, 81.6, 113.1, 115.3, 121.3, 123.2, 126.4, 129.8, 130.8, 137.6, 145.9, 147.8, 154.5, 155.3; Fig. S39. HRMS-ESI: calcd 883.49963 Da, found *m/z* 884.50654 [M + H]<sup>+</sup>, 906.48847 [M + Na]<sup>+</sup> and 922.46096 [M + K]<sup>+</sup>; Fig. S40. [α]<sub>D</sub><sup>28</sup> = +33.2 (c = 0.25, DMF-CHCl<sub>3</sub>, 1:1). HPLC: R<sub>T</sub> = 7.504 min; Fig. S41.

(17β,17′β)-17,17′-((3,4,5-Trimethoxybenzyl)imino)bis(ethane-2,1-diyl-1*H*-1,2,3-triazole-1,4-diyl))bisestra-1,3,5(10)-triene-3,17-diol (D11).

In reaction: L11 (100 mg, 0.3 mmol), EE (194 mg, 0.66 mmol), CuSO<sub>4</sub>·5H<sub>2</sub>O (17 mg, 0.07 mmol), sodium ascorbate (21 mg, 0.11 mmol), DMF (8 mL). Chromatography with CHCl<sub>3</sub>-MeOH 25:1 (v/v). Compound D11 (250 mg, 0.27 mmol) was obtained as a white solid in 90 % yield. R<sub>F</sub> = 0.5 in DCM-MeOH 10:1 (v/v). <sup>1</sup>H NMR (400 MHz, DMSO-*d*<sub>6</sub>) δ ppm: 0.57 (td, *J* = 12.8, 3.3 Hz, 2H), 0.90 (s, 6 H), 1.10–1.48 (m, 12H), 1.55–2.02 (m, 13H), 2.27–2.38 (m, 2 H), 2.61–2.75 (m, 4 H), 2.94 (br t, *J* = 5.7 Hz, 4 H), 3.53 (s, 3 H), 3.73 (s, 6 H), 4.36 (br t, *J* = 6.7 Hz, 3 H), 5.05 (s, 2 H), 6.39 (d, *J* = 2.4 Hz, 2 H), 6.44 (dd, *J* = 8.4, 2.5 Hz, 2 H), 6.53 (s, 2 H), 6.87 (d, *J* = 8.6 Hz, 2 H), 7.88 (s, 2 H), 8.94 (s, 2 H); Fig. S42. <sup>13</sup>C NMR (101 MHz, DMSO-*d*<sub>6</sub>) δ ppm: 14.8, 24.0, 26.5, 27.6, 29.7, 33.1, 37.6, 43.5, 47.1, 47.9, 53.5, 56.2, 60.2, 81.6, 105.9, 113.0, 115.3, 123.1, 126.4, 130.8, 134.9, 136.6, 137.5, 153.1, 154.6, 155.3; Fig. S43. HRMS-ESI: calcd 927.52585 Da, found *m/z* 928.53309 [M + H]<sup>+</sup>, 950.51508 [M + Na]<sup>+</sup> and 966.48715 [M + K]<sup>+</sup>; Fig. S44. [α]<sub>D</sub><sup>28</sup> = +38.1 (c = 0.26, DMF-CHCl<sub>3</sub>, 1:1). HPLC: R<sub>T</sub> = 7.782 min; Fig. S45.

(17β,17′β)-17,17′-((2,3,4-Trimethoxybenzyl)imino)bis(ethane-2,1-diyl-1*H*-1,2,3-triazole-1,4-diyl))bisestra-1,3,5(10)-triene-3,17-diol (D12).

In reaction: L12 (100 mg, 0.3 mmol), EE (194 mg, 0.66 mmol), CuSO<sub>4</sub>·5H<sub>2</sub>O (17 mg, 0.07 mmol), sodium ascorbate (21 mg, 0.11 mmol), DMF (8 mL). Chromatography with CHCl<sub>3</sub>-MeOH 25:1 (v/v). Compound D12 (220 mg, 0.24 mmol) was obtained as a white solid in 80 % yield. R<sub>F</sub> = 0.4 in DCM-MeOH 10:1 (v/v). <sup>1</sup>H NMR (400 MHz, DMSO-*d*<sub>6</sub>) δ ppm: 0.60 (td, *J* = 12.9, 3.9 Hz, 2H), 0.91 (s, 6 H), 1.10–1.52 (m, 12H), 1.55–2.09 (m, 10H), 2.25–2.41 (m, 2 H), 2.56–2.77 (m, 4 H), 2.93 (br t, *J* = 6.7 Hz, 4 H), 3.55–3.63 (s, 2 H), 3.67 (s, 3 H),

3.68 (s, 3 H), 3.70 (s, 3 H), 4.36 (br t,  $J = 6.7$  Hz, 4 H), 5.05 (s, 2 H), 6.39 (d,  $J = 2.4$  Hz, 2 H), 6.44 (dd,  $J = 3.2, 2.4$  Hz, 2 H), 6.61 (d,  $J = 3.6$  Hz, 1 H), 6.76 (d,  $J = 3.6$  Hz, 1 H), 6.91 (d,  $J = 3.61$  Hz, 2 H), 7.35 (s, 2 H), 8.95 (s, 2 H); Fig. S46.  $^{13}\text{C}$  NMR (101 MHz, DMSO- $d_6$ )  $\delta$  ppm: 14.8, 24.0, 26.5, 27.6, 29.7, 33.1, 37.6, 43.6, 47.1, 47.8, 48.0, 51.7, 53.5, 56.0, 60.7, 61.3, 81.6, 107.9, 113.1, 115.3, 123.3, 124.2, 124.7, 126.4, 130.8, 137.6, 142.0, 152.2, 152.8, 154.4, 155.3; Fig. S47. HRMS-ESI: calcd 927.52585 Da, found  $m/z$  928.53317  $[\text{M} + \text{H}]^+$ , 950.51524  $[\text{M} + \text{Na}]^+$  and 966.48676  $[\text{M} + \text{K}]^+$ ; Fig. S48.  $[\alpha]_D^{25} = +41.9$  ( $c = 0.26$ , DMF- $\text{CHCl}_3$ , 1:1). HPLC:  $R_T = 7.647$  min; Fig. S49.

(17 $\beta$ ,17 $\beta$ )-17,17'-[Oxybis(ethane-2,1-diyloxyethane-2,1-diyl)-1*H*-1,2,3-triazole-1,4-diyl]bisestra-1,3,5(10)-triene-3,17-diol (D13).

In reaction: L13 (50 mg, 0.2 mmol), EE (133 mg, 0.45 mmol),  $\text{CuSO}_4 \cdot 5\text{H}_2\text{O}$  (11.2 mg, 0.045 mmol), sodium ascorbate (13 mg, 0.068 mmol), DMF (3 mL). Chromatography with  $\text{CHCl}_3$ -MeOH 25:1  $\rightarrow$  10:1 (v/v). Compound D13 (99 mg, 0.12 mmol) was obtained as a white solid in 59 % yield.  $R_F = 0.43$  in DCM-MeOH 10:1 (v/v).  $^1\text{H}$  NMR (400 MHz, DMSO- $d_6$ )  $\delta$  ppm: 0.59 (td,  $J = 12.6, 3.3$  Hz, 2H), 0.91 (s, 6 H), 1.14–2.10 (m, 22H), 2.30–2.41 (m, 4 H), 2.62–2.72 (m, 4 H), 3.43–3.53 (m, 8 H), 3.79 (t,  $J = 5.3$  Hz, 4 H), 4.49 (t,  $J = 5.3$  Hz, 4 H), 5.10 (s, 2 H), 6.41 (d,  $J = 2.4$  Hz, 2 H), 6.46 (dd,  $J = 3.2, 2.4$  Hz, 2 H), 6.93 (d,  $J = 3.6$  Hz, 2 H), 7.82 (s, 2 H), 8.98 (s, 2 H); Fig. S50.  $^{13}\text{C}$  NMR (101 MHz, DMSO- $d_6$ )  $\delta$  ppm: 14.83, 24.00, 26.51, 27.64, 29.70, 33.05, 37.57, 43.62, 47.10, 47.94, 49.62, 69.31, 69.97, 70.14, 81.51, 113.08, 115.31, 123.43, 126.40, 130.80, 137.57, 154.37, 155.31; Fig. S51. HRMS-ESI: calcd 836.48365 Da, found  $m/z$  837.49030  $[\text{M} + \text{H}]^+$ , 859.47229  $[\text{M} + \text{Na}]^+$  and 875.44519  $[\text{M} + \text{K}]^+$ ; Fig. S52.  $[\alpha]_D^{20} = +56.8$  ( $c = 0.25$ , DMF- $\text{CHCl}_3$ , 1:1). HPLC:  $R_T = 9.109$  min; Fig. S53.

#### 4.2. Biochemistry

##### 4.2.1. Cell lines

CCRF-CEM, K562, U2OS, A549, MRC-5 and BJ cell lines were purchased from American Tissue Culture Collection (ATCC) HCT116 and HCT116p53 $^-$ /cell lines were obtained from Horizon Discovery. Resistant CEM-DNR bulk cell line overexpressing MRP-1 and P-glycoprotein and K562-TAX subline expressing P-glycoprotein were selected by increasing doses of daunorubicin or paclitaxel [17]. Cells were cultured in the humidified incubator under the atmosphere of 95 % air and 5 %  $\text{CO}_2$  at 37 °C according to the suppliers' recommendations. The cell culture medium DMEM/RPMI 1640 (Lonza) was supplemented with 100 U/mL penicillin, 100 mg/mL streptomycin and 10 % fetal bovine serum (Gibco).

##### 4.2.2. MTS assay

Cells were seeded into 384-well microtiter plates and incubated overnight. The next day, the treatment in dose-response was performed using Echo550 acoustic liquid handler (Labcyte). The plates were incubated for 72 h in a humidified  $\text{CO}_2$  incubator and then treated with 3-(4,5-dimethylthiazol-2-yl)-5-(3-carboxymethoxyphenyl)-2-(4-sulfophenyl)-2*H*-tetrazolium (MTS) and phenazine methosulfate solution. The absorbance of the reduced substrate was measured at 490 nm using EnVision multilabel plate reader (PerkinElmer) after an additional 2-hour incubation. The  $\text{IC}_{50}$  value was calculated from the appropriate dose-response curves using Dotmatics Studies software.

##### 4.2.3. FACS analysis

The cell cycle analysis and immunolabeling of cell cycle markers were described previously [18]. Briefly, CCRF-CEM were incubated with compounds for 24 h, then harvested, washed with cold phosphate-buffered saline (PBS), fixed in cold 70 % ethanol, treated with RNase (0.5 mg/mL) and stained with propidium iodide (PI) (0.1 mg/mL). The data were acquired using FACSCalibur (Becton Dickinson) and analyzed in the program ModFitLT (Verity). Apoptosis was measured in logarithmic mode as a percentage of the particles with PI content lower than cells in G0/G1 phase ( $<G0/G1$ ) of the cell cycle and polyploidy was

measured in linear mode as a percentage of particles with PI content higher than cells in G2/M phase of the cell cycle. To assess the rate of DNA and RNA synthesis the cells were incubated with compounds for 24 h and pulse-labelled with 5-bromo-2-deoxyuridine (BrdU) or 5-bromouridine (BrU) for 30 min. BrdU, as well as BrU, are recognized by anti-BrdU antibody clone MoBu-1 (Exbio). As a mitotic marker was used anti-phospho-Histone H3 (Ser10) antibody (Merck Millipore). All above-mentioned primary antibodies were diluted in blocking buffer and used with secondary anti-mouse-FITC-conjugated antibody (Sigma-Aldrich). Following the labelling, cells were washed with PBS and incubated with 0.1 mg/mL propidium iodide and 0.5 mg/mL RNase A for 1 h and analyzed by flow cytometry using a 488 nm single beam laser (FACS-Calibur, Becton Dickinson). Data analysis was performed using CellQuest software.

##### 4.2.4. Tubulin polymerization assay

Tubulin polymerization assay (Cytoskeleton) was performed according to the manufacturer's protocol. The assay is based on the analysis of light scattering by polymerized tubulin (>99 % purity) in the reaction. The absorbance of polymerized porcine brain tubulin was measured using EnVision Multilabel Plate Reader (PerkinElmer) at 37 °C in the presence of 10  $\mu\text{mol/L}$  compounds or DMSO. Polymerization curves were used for the calculation of the maximal velocity of polymerization values ( $V_{\text{max}}$ ).

##### 4.2.5. Immunofluorescence

U2OS cells were seeded onto coverslips and after overnight incubation with compounds were washed in PBS and fixed in 3 % paraformaldehyde and 10 mM MES, 150 mM NaCl, 5 mM EGTA, 5 mM  $\text{MgCl}_2$ , 5 mM glucose (pH 6.1). Alternatively, the compounds were removed from the cells by three PBS washouts, then incubated in a fresh cultivation medium for 30 min at 37 °C, washed in PBS and fixed in 3 % paraformaldehyde. Cell permeabilization was performed using 0.3 % Triton X-100 in PBS and nuclei were visualized using Hoechst 33342. Following the 1-hour blocking with 1 % bovine serum albumin in PBS (Sigma-Aldrich) samples were incubated for 60 min with  $\alpha$ -tubulin mouse monoclonal antibody (Sigma-Aldrich) in PBS containing 1 % BSA and 0.3 % Triton X-100. For visualization were used Alexa Fluor-488 conjugated anti-mouse antibodies were (Life Technologies). The samples were washed three times in PBS for 5 min and mounted with Vectashield Mounting Medium. Images were acquired using a spinning disk confocal microscope (Zeiss) with a CSU-X1 unit (Yokogawa).

#### 5. In silico modelling

For this study, the 3D complex (4O2B) of bovine tubulin alpha 1B (P81947) and beta-2B (Q6B856) chains with the known inhibitor colchicine were considered. We removed water molecules and native inhibitors from the structures. 3D structure of the unresolved residues was rebuilt by Modeller Tool [19] built-in Chimera [20]. Remodelling of incomplete side chains and protonation of the protein structure was performed by Chimera Dock Prep tool [20]. GTP molecule and  $\text{Mg}^{2+}$  ion nearby the active site are reported to be important for the regulation of the polymerization thereby these crucial cofactors were kept.

##### 5.1. Molecular docking

All compounds were docked using Autodock Vina [21]. Due to the large size of estradiol dimer molecules, we used a large docking box with a size of  $28 \times 28 \times 28$  Å centred around the active site. To provide reasonable accuracy and efficiency the exhaustiveness value was set to 32. Initial conformers were obtained by RDKit 2018.09.1.0 version [22]. Ligand protonation was performed by Marvin cxcalc utility for pH 7.4 (ref. [23]).

## 5.2. Molecular dynamics

We used GROMACS software version 2021.4-plumed-2.7.3 (ref. [24,25]). For target preparation, we used the Amber 99SB-ILDN force field [26] and the TIP3P water model. Na and Cl ions were added to neutralize the system. Ligand topologies were prepared by AmberTools version 20.9 (ref. [27]). Energy minimization for every simulation took 50,000 steps, followed by NVT and then NPT equilibrations for 1000 ps. Production simulations were conducted for 150 ns in an NPT ensemble at 300 K. For the visualization and analysis of the protein–ligand interaction we used ProLIF package [13] using only frames extracted from the last 100 ns.

## 5.3. Calculation of binding free energy with MM-PBSA

MM/PBSA models were generated using gmx\_MMPBSA [28,29]. The Amber99SB-ILDN force field was used to calculate the internal term ( $\Delta E_{\text{int}}$ ) as well as van der Waals ( $\Delta E_{\text{vdw}}$ ) and electrostatic ( $\Delta E$ ) energies. The last 10 ns (1001 frames) from the full 150 ns simulations were used for the binding free energy estimation. The entropic term was calculated by the Interaction Entropy (IE) method [30]. The temperature for IE analysis was set to 293.00 K. IE was calculated using the last quartile ( $\text{seg} = 25$ ) of the last 10 ns (251 frames). The ion strength option (istrg) was set to 150 mM, a typical value for a physiological environment. Atomic radii from the topology files were used (radiopt = 0). Considering charged environment of the active site the internal dielectric constant value (indf) was set to 4 ref. [31]. Other variables of the MM/PBSA method were set by practical examples provided by gmx\_MMPBSA or by the default. The full setup is provided in supplementary materials.

## CRediT authorship contribution statement

Michal Jurásek: Conceptualization, Methodology, Writing – original draft. Jiří Řehulka: Formal analysis, Methodology, Writing – original draft. Lenka Hrubá: synthesis, analytical characterizations. Aleksandra Ivanová: *in silico* modelling. Soňa Gurská: biological experiments. Olena Mokshyna: *in silico* modelling. Pavel Trousil: synthesis, analytical characterizations. Lukáš Huml: synthesis, analytical characterizations. Pavel Polishchuk: Formal analysis, Software, Writing – original draft. Marián Hajdúch: Supervision, Conceptualization, Writing – review & editing. Pavel B. Drašar: Supervision, Writing – review & editing, designed molecules. Petr Dzubák: Supervision, Writing – review & editing, designed biological experiments, biological experiments.

## Declaration of Competing Interest

The authors declare that they have no known competing financial interests or personal relationships that could have appeared to influence the work reported in this paper.

## Data availability

Data will be made available on request.

## Acknowledgement

This work is dedicated to the memory of Ing. Pavel Trousil, who was a highly talented young scientist and who participated in the creation of this work within his master thesis. This work was supported by CEREBIT (Project No. CZ.02.1.01/0.0/0.0/16\_025/0007397), an internal grant of the UCT Prague No. A1\_FPB\_T\_2022\_007 and by the Ministry of Education, Youth and Sports of the Czech Republic through the e-INFRA CZ (ID:90140), infrastructural projects (CZ-OPENSURE – LM2018130; EATRIS-CZ – LM2018133) and National Institute for Cancer Research (Programme EXCELES, ID Project No. LX22NPO5102) - Funded by the

European Union - Next Generation EU.

## Appendix A. Supplementary data

Supplementary data to this article can be found online at <https://doi.org/10.1016/j.bioorg.2022.106334>.

## References

- [1] M. Jurásek, P. Dzubák, D. Sedláč, H. Dvořáková, M. Hajdúch, P. Bartůnek, P. Drašar, Preparation, preliminary screening of new types of steroid conjugates and their activities on steroid receptors, *Steroids* 78 (3) (2013) 356–361.
- [2] K. Battiston, I. Parrag, M. Statham, D. Louka, H. Fischer, G. Mackey, A. Daley, F. Gu, E. Baldwin, B. Yang, B. Muirhead, E.A. Hicks, H. Sheardown, L. Kalachev, C. Crean, J. Edelman, J.P. Santerre, W. Naimark, Polymer-free corticosteroid dimer implants for controlled and sustained drug delivery, *Nat. Commun.* 12 (1) (2021) 2875.
- [3] D. Xu, C. Peng, F. Gao, Z. Guo, R. Zhuang, X. Su, X. Zhang, Radioiodinated estradiol dimer for estrogen receptor targeted breast cancer imaging, *Chem. Biol. Drug. Des.* 96 (6) (2020) 1332–1340.
- [4] L. Nahar, S.D. Sarker, A review on steroid dimers: 2011–2019, *Steroids* 164 (2020), 108736.
- [5] M. Jurásek, M. Černohorská, J. Řehulka, V. Spiwok, T. Sulimkeno, E. Dráberová, M. Darmostuk, S. Gurská, I. Frydrych, R. Burianová, T. Ruml, M. Hajdúch, P. Bartůnek, P. Dráber, P. Dzubák, P.B. Drašar, D. Sedláč, Estradiol dimer inhibits tubulin polymerization and microtubule dynamics, *J. Steroid. Biochem. Mol. Biol.* 183 (2018) 68–79.
- [6] R. Hüsgen, Kinetics and mechanism of 1,3-dipolar cycloadditions, *Angew. Chem. Int. Ed.* 2 (11) (1963) 633–645.
- [7] J.J. Fairlamb, P.S. Bäuerlein, L.R. Morrison, J.M. Dickinson, Pd-catalysed cross coupling of terminal alkynes to diynes in the absence of a stoichiometric additive, *Chem. Commun.* 5 (2003) 632–633.
- [8] N. Aguilar-Valdez, M. Maldonado-Domínguez, R. Arcos-Ramos, M. Romero-Ávila, R. Santillan, N. Farfán, Synthesis of steroidal molecular compasses: exploration of the controlled assembly of solid organic materials, *CrystEngComm* 19 (13) (2017) 1771–1777.
- [9] D. Fournier, D. Poirier, Estradiol dimers as a new class of steroid sulfatase reversible inhibitors, *Bioorg. Med. Chem. Lett.* 19 (3) (2009) 693–696.
- [10] D. Rabouin, V. Perron, B. N'Zemba, R. C.-Gaudreault, G. Bérubé, A facile synthesis of C2-symmetric 17 $\beta$ -estradiol dimers, *Bioorg. Med. Chem. Lett.* 13(3) (2003) 557–560.
- [11] M. Cushman, H.M. He, J.A. Katzenellenbogen, R.K. Varma, E. Hamel, C.M. Lin, S. Ram, Y.P. Sachdeva, Synthesis of analogs of 2-methoxyestradiol with enhanced inhibitory effects on tubulin polymerization and cancer cell growth, *J. Med. Chem.* 40 (15) (1997) 2323–2334.
- [12] J. Skubník, M. Jurásek, T. Ruml, S. Rimpelová, Mitotic poisons in research and medicine, *Molecules* 25 (20) (2020).
- [13] C. Bouysset, S. Fiorucci, ProLIF: a library to encode molecular interactions as fingerprints, *J. Cheminform.* 13 (2021).
- [14] L. Niu, J. Yang, W. Yan, Y. Yu, Y. Zheng, H. Ye, Q. Chen, L. Chen, Reversible binding of the anticancer drug KX01 (tiributin) to the colchicine-binding site of  $\beta$ -tubulin explains KX01's low clinical toxicity, *J. Biol. Chem.* 294 (48) (2019) 18099–18108.
- [15] J.R. Thomas, X.J. Liu, P.J. Hergenrother, Size-specific ligands for RNA hairpin loops, *J. Am. Chem. Soc.* 127 (36) (2005) 12434–12435.
- [16] Y. Song, H. Zong, E.R. Trivedi, B.J. Vesper, E.A. Waters, A.G.M. Barrett, J. A. Radosevich, B.M. Hoffman, T.J. Meade, Synthesis and Characterization of New Porphyrazine-Gd(III) Conjugates as Multimodal MR Contrast Agents, *Bioconjugate Chem.* 21 (12) (2010) 2267–2275.
- [17] V. Nosková, P. Dzubák, G. Kuzmina, A. Ludková, D. Stehlík, R. Trojanec, A. Janostáková, G. Kofírková, V. Mihal, M. Hajdúch, In vitro chemoresistance profile and expression/function of MDR associated proteins in resistant cell lines derived from CCRF-CEM, K562, A549 and MDA MB 231 parental cells, *Neoplasma* 49 (6) (2002) 418–425.
- [18] A. Bourderioux, P. Nauš, P. Perlíková, R. Pohl, I. Pichová, I. Votruba, P. Dzubák, P. Konečný, M. Hajdúch, K.M. Stray, T. Wang, A.S. Ray, J.Y. Feng, G. Birkus, T. Čihlár, M. Hoček, Synthesis and significant cytostatic activity of 7-hetaryl-7-deazaadenosines, *J. Med. Chem.* 54 (15) (2011) 5498–5507.
- [19] A. Sali, T.L. Blundell, Comparative protein modelling by satisfaction of spatial restraints, *J. Mol. Biol.* 234 (3) (1993) 779–815.
- [20] E.F. Pettersen, T.D. Goddard, C.C. Huang, G.S. Couch, D.M. Greenblatt, E.C. Meng, T.E. Ferrin, UCSF Chimera—a visualization system for exploratory research and analysis, *J. Comput. Chem.* 25 (13) (2004) 1605–1612.
- [21] O. Trott, A.J. Olson, AutoDock Vina: improving the speed and accuracy of docking with a new scoring function, efficient optimization, and multithreading, *J. Comput. Chem.* 31 (2) (2010) 455–461.
- [22] G. Landrum, RDKit, Open-Source Cheminformatics Software, 2021.
- [23] Cxcalc utility was used for ligand protonation, Cxcalc version 19.22.0, ChemAxon (<https://www.chemaxon.com>).
- [24] B. Hess, C. Kutzner, D. van der Spoel, E. Lindahl, GROMACS 4: Algorithms for highly efficient, load-balanced, and scalable molecular simulation, *J. Chem. Theory. Comput.* 4 (3) (2008) 435–447.

- [25] S. Pronk, S. Pall, R. Schulz, P. Larsson, P. Bjelkmar, R. Apostolov, M.R. Shirts, J. C. Smith, P.M. Kasson, D. van der Spoel, B. Hess, E. Lindahl, GROMACS 4.5: a high-throughput and highly parallel open source molecular simulation toolkit, *Bioinformatics* 29 (7) (2013) 845–854.
- [26] K. Lindorff-Larsen, S. Piana, K. Palmo, P. Maragakis, J.L. Klepeis, R.O. Dror, D. E. Shaw, Improved side-chain torsion potentials for the Amber ff99SB protein force field, *Proteins* 78 (8) (2010) 1950–1958.
- [27] D.A. Case, T.E. Cheatham 3rd, T. Darden, H. Gohlke, R. Luo, K.M. Merz Jr., A. Onufriev, C. Simmerling, B. Wang, R.J. Woods, The Amber biomolecular simulation programs, *J. Comput. Chem.* 26 (16) (2005) 1668–1688.
- [28] M.S. Valdes-Tresanco, M.E. Valdes-Tresanco, P.A. Valiente, E. Moreno, gmx\_MMPBSA: A New Tool to Perform End-State Free Energy Calculations with GROMACS, *J. Chem. Theory. Comput.* 17 (10) (2021) 6281–6291.
- [29] B.R. Miller 3rd, T.D. McGee Jr., J.M. Swails, N. Homeyer, H. Gohlke, A.E. Roitberg, MMPBSA.py: An Efficient Program for End-State Free Energy Calculations, *J. Chem. Theory. Comput.* 8 (9) (2012) 3314–3321.
- [30] L. Duan, X. Liu, J.Z. Zhang, Interaction entropy: A new paradigm for highly efficient and reliable computation of protein-ligand binding free energy, *J. Am. Chem. Soc.* 138 (17) (2016) 5722–5728.
- [31] T. Hou, J. Wang, Y. Li, W. Wang, Assessing the performance of the MM/PBSA and MM/GBSA methods. 1. The accuracy of binding free energy calculations based on molecular dynamics simulations, *J. Chem. Inf. Model.* 51 (1) (2011) 69–82.

### **9.3 An identification of MARK inhibitors using high throughput MALDI-TOF mass spectrometry**

L. HRUBÁ, P. POLISHCHUK, V. DAS, M. HAJDÚCH, P. DŽUBÁK, An identification of MARK inhibitors using high throughput MALDI-TOF mass spectrometry, *Biomedicine & Pharmacotherapy*, 2022, 146, 112549, 0753-3322, IF: 6.530, PMID: 34923338.

Personal contribution: methods development, drug screening, kinase assays, data analyses, conceptualization, writing and editing of manuscript



## An identification of MARK inhibitors using high throughput MALDI-TOF mass spectrometry

Lenka Hruba, Pavel Polishchuk, Viswanath Das, Marian Hajduch, Petr Dzubak<sup>\*</sup>

*Institute of Molecular and Translational Medicine, Faculty of Medicine and Dentistry, Palacký University in Olomouc, Olomouc, Czech Republic*

### ARTICLE INFO

**Keywords:**  
MALDI-TOF  
MARK kinases  
Alzheimer's disease  
Tau-peptide phosphorylation  
Drug repositioning  
LOPAC 1280

### ABSTRACT

MAP/microtubule affinity-regulating kinases (MARKs) were recently identified as potential drug targets for Alzheimer's disease (AD) due to their role in pathological hyperphosphorylation of tau protein. Hyperphosphorylated tau has decreased affinity for microtubule binding, impairing their stability and associated functions. Destabilization of microtubules in neuronal cells leads to neurodegeneration, and microtubule-unbound tau forms neurofibrillary tangles, one of the primary hallmarks of AD. Many phosphorylation sites of tau protein have been identified, but phosphorylation at Ser<sup>262</sup>, which occurs in early stages of AD, plays a vital role in the pathological hyperphosphorylation of tau. It has been found that Ser<sup>262</sup> is phosphorylated by MARK4, which is currently an intensively studied target for treating Alzheimer's disease and other neurodegenerative diseases. Our present study aimed to develop a high throughput compatible assay to directly detect MARK enzymatic activity using echoacoustic transfer and MALDI-TOF mass spectrometer. We optimized the assay for all four isoforms of MARK and validated its use for identifying potential inhibitors by the screening of 1280 compounds from the LOPAC1280 International (Library Of Pharmacologically Active Compounds). Six MARK4 inhibitors with IC<sub>50</sub> < 1 μM were identified. To demonstrate their therapeutic potential, active compounds were further tested for MARK4 selectivity and ability to cross the blood-brain barrier. Lastly, the molecular docking with the most active inhibitors to predict their interaction with MARK4 was performed.

### 1. Introduction

MAP/microtubule affinity-regulating kinases (MARKs) are a family of protein kinases consisting of four members (MARK1–4) [1,2]. MARK kinases phosphorylate the tau protein repeat domain and reduce its affinity to microtubules. Because tau protein is necessary for microtubule stabilization, they become destabilized and unbound hyperphosphorylated tau protein forms aggregates leading to the formation of neurofibrillary tangles typical of Alzheimer's disease (AD) brains [2,3]. More than 45 phosphorylated sites of tau protein have been identified [3–5], with MARK kinases phosphorylating tau protein on Ser<sup>262</sup> and Ser<sup>356</sup> [6]. In terms of the formation of neurofibrillary tangles and AD pathology phosphorylation of Ser<sup>262</sup> seems to be most important [6]. This site is phosphorylated by MARK4 and to some extent by MARK3 which was shown as anticancer target [7–9]. Thus MARK4 remains a potential target for developing new drugs that can help in the therapy of neurodegenerative diseases.

Several molecules that act as MARK4 inhibitors have recently been published. For example, donepezil (DP) and rivastigmine tartrate (RT), which are acetylcholinesterase (AChE) inhibitors used in the treatment of mild to moderate Alzheimer's disease, have also been identified as MARK4 inhibitors with IC<sub>50</sub> values of 5.3 μM (DP) and 6.7 μM (RT) in *in vitro* experiments. MARK4 activity has been tested by an ATPase enzyme assay using standard malachite green (BIOMOL® reagent, Enzo Life Sciences) for quantification, with the color intensity measured spectrophotometrically at 620 nm [10–12]. Another study, based on *in silico* screening of the affinity to MARK4 and molecular docking analysis, identified five pyrazolopyrimidine derivatives (PubChem IDs: 90794095, 91145515, 91895673, 91895692, 91895679) as potential MARK4 inhibitors [13].

MARK4 has also been studied as a target to treat obesity [14] and other associated disorders (cardiovascular diseases, type 2 diabetes mellitus) [15–17] and cancer treatment [18]. It was found that apart from its function in tau protein phosphorylation, MARK4 is also

<sup>\*</sup> Correspondence to: Institute of Molecular and Translational Medicine, Faculty of Medicine and Dentistry, Palacký University Olomouc, Hnevotinska 1333/5, Olomouc 77900, Czech Republic.

E-mail addresses: [lenka.hruba@upol.cz](mailto:lenka.hruba@upol.cz) (L. Hruba), [pavlo.polishchuk@upol.cz](mailto:pavlo.polishchuk@upol.cz) (P. Polishchuk), [viswanath.das@upol.cz](mailto:viswanath.das@upol.cz) (V. Das), [marian.hajduch@upol.cz](mailto:marian.hajduch@upol.cz) (M. Hajduch), [petr.dzubak@upol.cz](mailto:petr.dzubak@upol.cz) (P. Dzubak).

<https://doi.org/10.1016/j.bioph.2021.112549>

Received 27 September 2021; Received in revised form 8 December 2021; Accepted 13 December 2021

0753-3322/© 2021 The Author(s). Published by Elsevier Masson SAS. This is an open access article under the CC BY-NC-ND license

<https://creativecommons.org/licenses/by-nc-nd/4.0/>



connected with adipogenesis, cell polarity, progression through the cell cycle, transduction of cellular signals and organelle positioning in cells [15,17–19]. MARK4 inhibitors for cancer treatment are currently being searched. Screening of isatin-triazole hydrazones revealed a MARK4 inhibitor with an  $IC_{50}$  value of 1.54  $\mu$ M. This compound inhibited cancer cell proliferation, metastasis and also induced apoptosis. In this screening, MARK4 activity was tested by radioactive ATPase assay [20]. A study of acridone derivatives identified three compounds as selective MARK4 inhibitors (MARK4 activity was detected by the ATPase inhibition assay using standard malachite green) which inhibited cancer cell proliferation, induced apoptosis, and decreased tau protein phosphorylation [18]. These findings suggest that MARK4 may be a promising target in drug design to treat a wide range of diseases.

As we have focused on detecting MARK4 activity and screening its potential inhibitors for possible use in AD therapy, CNS permeability of the compounds was considered. The central nervous system (CNS) is protected by, among other things, a system of biological membranes, including the blood-brain barrier (BBB), which potential CNS drugs have to overcome to gain access to the CNS. The structure of the BBB (presence of tight junctions, absence of fenestrations, low activity of transport vesicles, limited pinocytosis and close contact between astrocyte protrusions) affects the active transport of molecules between the blood and brain, and only certain of compounds can pass through it [21]. Lipophilic compounds, usually small, uncharged molecules, e.g., oxygen, water, and  $CO_2$  can passively cross the BBB [22]. Water is also transported by aquaporins [23]. Molecules with higher molecular weight, e.g., glucose or charged molecules, e.g.,  $K^+$  or  $Na^+$  ions, are actively transported [21,24].

Numerous sets of physicochemical parameters have been proposed for the estimation of the permeability of compounds through the BBB [25]. Most frequently they comprise the lipophilicity, number of H-bond donors and acceptors, number of rotatable bonds and polar surface area of molecules. There is a general agreement that the lipophilicity should not be very high ( $\log < 3-5$ ), the number of H-bond donors should be  $< 3$  and the topological polar surface area should be  $< 60-90 \text{ \AA}^2$  [26–30]. An elegant way to estimate permeability through the BBB was proposed by Egan et al. by the evaluation of lipophilicity and polar surface area and discrimination of well-absorbed compounds from poorly absorbed ones by an ellipse [31]. Later, this approach was optimized and more rigorously validated by Daina and Zoete [32].

In this study, we present the development of an assay for the direct detection of the enzymatic activity of MARK using a MALDI-TOF technology. Furthermore, we validated the potential use of this assay by identifying six MARK4 inhibitors with  $IC_{50}$  values  $< 1 \mu$ M by screening 1290 compounds from the Library Of Pharmacologically Active Compounds (LOPAC®1290 International). Such a set of medicinally used drugs or failed clinical candidates is valuable tool to speed-up the usually very slow process of new therapeutics development by the reprofiling strategy [33]. LOPAC compounds were studied in the past and information about their use and targets is well known. To compare the activity against described targets, the active compounds were tested for MARK 1–4 isoform selectivity and ability to cross the BBB to elucidate their potential as antineurodegenerative drugs.

## 2. Materials and methods

Enzymes MARK 1 – 4 were purchased from Carna Biosciences, Inc. All enzymes were stored at  $-80 \text{ }^\circ\text{C}$  and diluted in the assay buffer on the day of analysis. The peptide substrate (CHKtide) was obtained from SignalChem and was diluted in deionized water (concentration of the peptide solution was 5 mg/ml) and stored at  $-20 \text{ }^\circ\text{C}$ . The matrix for MALDI-TOF ( $\alpha$ -cyano-4-hydroxycinnamic acid, HCCA) and the calibration standard for MS (peptide calibration standard II) were purchased from Bruker. HCCA was dissolved in a solution consisting of 2% TFA (trifluoroacetic acid), 18% deionized water and 80% acetonitrile (10 mg of the matrix in 1 ml of solution). The assay buffer contained 1 mM

HEPES (pH 7.5), 1 mM  $MgCl_2$ , 2 mM DTT and 0.01% Brij-35 and was stored at  $4 \text{ }^\circ\text{C}$  for 1 week. Chemicals for the assay buffer and matrix solution were purchased from Sigma-Aldrich. 384-well LDV (low dead volume) and 1536-well LDV plates were obtained from Labcyte. Kinase inhibitor staurosporine was purchased from Sigma-Aldrich. We used LOPAC®1290 for screening MARK4 inhibitors. This library consisted of 1290 compounds dissolved in dimethyl sulfoxide (DMSO) at 10 mM concentration and was purchased from Sigma-Aldrich.

### 2.1. MALDI-TOF mass spectrometry assay

The assay was based on direct detection of the peptide substrate (CHKtide) and its phosphorylated form by MALDI-TOF mass spectrometry (ultrafleXtreme, Bruker Daltonik GmbH). The voltage of ion source 1 was 25.11 kV, ion source 2 22.46 kV, reflector 1 26.5 kV, reflector 2 13.7 kV and the lens 0.02 kV. Ion detection was carried out in the positive mode.

We used a known kinase inhibitor, staurosporine, as a control of enzyme activity inhibition. Inhibition was detected as a decrease in the conversion of CHKtide to the phospho-CHKtide form. The ratio of conversion following treatment with inhibitor was compared to the ratio of control reaction without inhibitor. Control samples were treated with DMSO (final concentration 0.5%) in which all chemicals used in the screening were diluted.

The primary assay had a reaction volume of 7.5  $\mu$ l and comprised of 2.01  $\mu$ l reaction buffer, 0.19  $\mu$ l MARK4 (547  $\mu$ g/ml in the storage buffer), 1  $\mu$ l of CHKtide (1 mg/ml in deionized water) and 3.5 ATP (214  $\mu$ M in the reaction buffer). The reaction was incubated at room temperature for 60 min and then mixed with MALDI matrix (HCAA) in a ratio 1:1. The mixture of sample and matrix was applied to a MALDI 384-well plate (0.5  $\mu$ l) and analyzed. Mass spectra were detected in the range 2660–2820 Da.

To speed up the methodology, it was necessary to optimize it and make it more automated. The assay was optimized for incubation in 1536-well plates, and the reaction volume was 2.593  $\mu$ l. Reaction buffer (1.5  $\mu$ l) and ATP (1  $\mu$ l, Sigma-Aldrich) were applied by a Multidrop Combi Dispenser (Thermo Scientific). The enzyme (20 nL, concentration 136.75  $\mu$ g/ml diluted in the reaction buffer), peptide substrate (60 nL, concentration 5 mg/ml diluted in the deionized water) and inhibitors (12.5 nL, concentration depended on the type of screening) were transferred by an Echo 550 acoustic dispenser (Labcyte Inc.). The reaction plates were briefly shaken by a Variomag Teleshake 1536-8 (Thermo Scientific), centrifuged at 1200 rpm for 1 min and incubated for 1 h at room temperature. An aliquot of the MALDI matrix (2  $\mu$ l, concentration 10 mg/ml) was added using the Multidrop Combi Dispenser. The incubation plate was centrifuged at 1200 rpm, and the mixture of sample-matrix was transferred to a MALDI plate by the Echo 550 (150 nL). We designed and 3D printed a holder for the 1536-well MALDI plates (Fig. 1), inspired by standard source plates for the Echo 550 but significantly lighter than usual metal MALDI holders. Owing to its compatibility with Echo, we were able to automatically transfer samples with matrix to the 1536-well MALDI plates, speeding up the process considerably. We also used Echo 550 to transfer the MALDI calibration standard, which was mixed with the MALDI matrix in the same way as the samples (ratio 1:1). The positions of calibration spots were defined by Bruker Daltonics software. After the samples and calibration standard crystallized with the matrix, they were analyzed by MALDI-TOF.

Assay development included optimization of the ATP, enzyme and substrate concentrations. The assay was optimized for the MARK4 enzyme and was used for the primary screening of the LOPAC library. The compounds were tested at a single concentration of 20  $\mu$ M in duplicates across two independent 1536-well plates. Compounds with inhibition activity higher than 50% were selected for secondary dose-dependent analysis (in three replicates) at concentrations of 50  $\mu$ M – 2.44 nM (dose range at 2-fold dilution) for  $IC_{50}$  calculation. Compounds with  $IC_{50} < 1 \mu$ M were analyzed for inhibition of MARK1–3 (in three

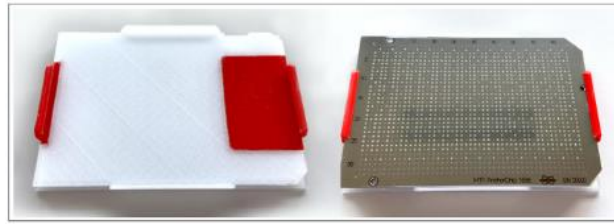


Fig. 1. MALDI plate holder fabricated by 3D printing.

replicates). Thus, we additionally optimized the conditions of the assay (concentration of enzyme and ATP) for MARK1 – 3.

## 2.2. Data analysis

Data from MALDI-TOF were processed by flexAnalysis 3.4 software (Bruker Daltonik GmbH). We analyzed the substrate's intensity signal (2701  $m/z$ ) and phosphorylated product peak (2781  $m/z$ ). Peak intensities were exported by the flexAnalysis Batch Process and analyzed by Microsoft Excel and GraphPad Prism Software (version 9). The enzyme activity in percentage was calculated as a ratio of the product peak intensity ( $I_P$ ) to the substrate peak intensity ( $I_S$ ), as described below.

$$\text{Enzyme activity}[\% \text{ of conversion}] = 100 \times (I_P / I_S)$$

The percentage of inhibition was calculated as the conversion of the substrate to the product in the presence of inhibitor compared to control reaction without inhibitor.  $IC_{50}$  (half-maximal inhibitory concentration) values were calculated by GraphPad Prism 9.

$$\text{Inhibition} [\%] = 100 - [(I_P / I_S) / (I_{Pc} / I_{Sc}) \times 100]$$

$I_P$  is the product's peak intensity and  $I_S$  is the intensity of the substrate peak in the reaction with inhibitor present.  $I_{Pc}$  is the intensity of the product peak and  $I_{Sc}$  is the intensity of the substrate peak in the control reaction without inhibitor.

## 3. Results and discussion

### 3.1. Assay development

Our assay was based on the direct detection of enzyme-substrate CHKtide peptide with a molecular mass of 2701 Da and its phosphorylated form as a product of this reaction. Phospho-CHKtide has a molecular mass of 2781 Da (Fig. 2A, B). The detection of both molecules was performed using an ultrafleXtreme MALDI-TOF mass spectrometer in the positive reflector mode.

Assay development was divided into three steps: optimization of enzyme, ATP and substrate concentration. Initially, we determined the optimal conditions for the MARK4 enzyme and then optimized the conditions for the other three isoforms, MARK1 – 3. All steps were performed in at least three replicates and standard deviation was

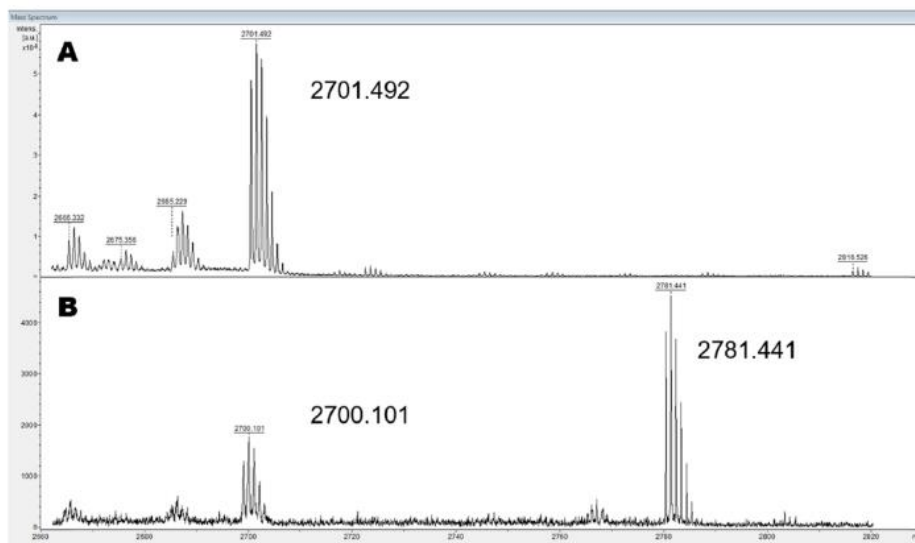


Fig. 2. Detection of CHKtide peptide ( $m/z$  2701.492) by MALDI-TOF mass spectrometry. Mass spectra were analyzed by flexAnalysis software (Bruker Daltonik GmbH). (A) Detection of CHKtide peptide and (B) its phosphorylated form ( $m/z$  2781.441) in the presence of the MARK4 enzyme.

calculated.

The enzyme concentration was tested in the range 0.05 – 2.95  $\mu\text{g/ml}$  for initial concentrations of 100  $\mu\text{M}$  of ATP and 0.13 mg/ml of CHKtide peptide (Fig. 3A). For another analysis, we chose an enzyme concentration of 2.25  $\mu\text{g/ml}$  at which conversion of the substrate (CHKtide) to product (phosphor-CHKtide) was in the ratio 1:2. The ATP concentration was tested in the range 1.85–200  $\mu\text{M}$  with initial concentrations of 2.25  $\mu\text{g/ml}$  of MARK4 and 0.13 mg/ml of CHKtide peptide (Fig. 3B). The optimal concentration of ATP was found to be 46.4  $\mu\text{M}$ . We then tested MARK4 concentration again under the optimized ATP concentration (Fig. 3C). The final selected concentration of MARK4 was 1.19  $\mu\text{g/ml}$ . In the last step, we also optimized the concentration of CHKtide peptide, which served as the substrate in our reaction. CHKtide peptide was tested at concentrations of 0.020 – 0.267 mg/ml and  $K_M$  was calculated (Fig. 3D). We selected a substrate concentration of 0.12  $\mu\text{g/ml}$  for our screening corresponding to  $K_M$ . The final conditions chosen for the MARK4 assay were 1.19  $\mu\text{g/ml}$  of MARK4, 46.4  $\mu\text{M}$  ATP and 0.12 mg/ml of CHKtide.

Optimization of conditions for MARK1, 2 and 3 consisted of two steps. In the first step we tested the conversion of the substrate to the product at different concentrations of the enzyme (0.05 – 2.92  $\mu\text{g/ml}$ ) and initial concentrations of ATP (46.4  $\mu\text{M}$ ) and CHKtide (0.12  $\mu\text{g/ml}$ ) (Fig. 4A). As in the MARK4 optimization procedure, we selected the concentration of enzyme at which the substrate to product ratio was 1:2. We selected a concentration of 0.31  $\mu\text{g/ml}$  for MARK1, 0.55  $\mu\text{g/ml}$  for MARK2 and 0.40  $\mu\text{g/ml}$  for MARK3. The ATP concentration was then optimized in the range 3.21 – 205  $\mu\text{M}$  with the concentration of enzyme determined from the previous step and 0.12  $\mu\text{g/ml}$  of CHKtide (Fig. 4B). The optimal concentration value appeared to be the same as the MARK4 enzyme and was similar for all three isoforms. The selected concentration of ATP was 46.4  $\mu\text{M}$ .

When optimization was completed, we tested whether we could

detect inhibition of enzyme activity using our assay. We used staurosporine, a general kinase inhibitor and evaluated its dose-dependent (0.1 nM – 0.8  $\mu\text{M}$ ) anti-MARK activity (Fig. 5). Staurosporine inhibited all four MARK isoforms with  $\text{IC}_{50}$  values of 9.46 nM  $\pm$  0.13 (MARK1), 5.82 nM  $\pm$  0.12 (MARK2), 3.79 nM  $\pm$  0.12 (MARK3) and 4.6 nM  $\pm$  0.12 (MARK4).

### 3.2. LOPAC screening

To determine the potential use of our MALDI-TOF mass spectrometry-based method for compound screening, we analyzed the potential anti-MARK4 activity of 1280 compounds from the LOPAC1280. Inhibition was tested at single concentration of 20  $\mu\text{M}$ . We identified 108 compounds showing inhibition of MARK4 activity higher than 50%, and these compounds were tested in secondary screening. The percentage of inhibition and  $\text{IC}_{50}$  values are provided in the Supplementary Information Table 1 and Table 2. All compounds were tested in 6 replicates across two independent 1536-well plates. We identified six compounds with  $\text{IC}_{50}$  for MARK4 < 1  $\mu\text{M}$ : PD173952 ( $\text{IC}_{50}$  = 0.0033  $\mu\text{M}$   $\pm$  0.00016), PD-166285 hydrate ( $\text{IC}_{50}$  = 0.0035  $\mu\text{M}$   $\pm$  0.00012), PF-431396 hydrate ( $\text{IC}_{50}$  = 0.011  $\mu\text{M}$   $\pm$  0.0011), sunitinib malate ( $\text{IC}_{50}$  = 0.038  $\mu\text{M}$   $\pm$  0.0015), DMH4 ( $\text{IC}_{50}$  = 0.27  $\mu\text{M}$   $\pm$  0.013) and PHA 767491 hydrochloride ( $\text{IC}_{50}$  = 0.80  $\mu\text{M}$   $\pm$  0.01) (Fig. 6).

All of these compounds were previously tested for anticancer activities and belongs to the class of the kinase inhibitors, as discussed below. In the scientific literature there is ongoing debate with new evidence about the reduction of incidence of AD and neurodegenerative disorders in cancer survivors. Direct mechanism is not known, but it can be caused by the inhibition of the enzymes and pathways with crosstalk to cancer and neuronal disorders [34–36]. MARK3 and MARK4 was previously published as potential anticancer target, as was mentioned in the introduction. Therefore, we have tested all four MARK isoforms tested to

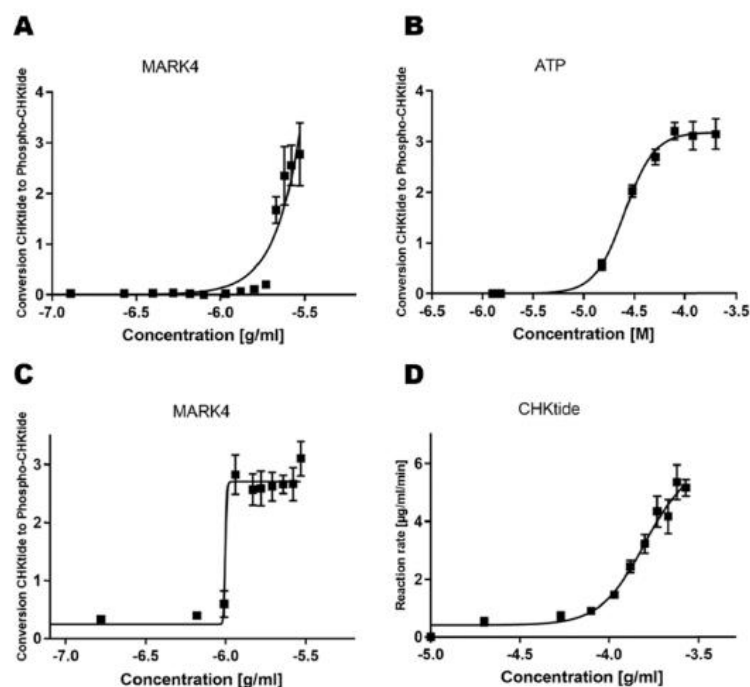


Fig. 3. (A) Optimization of MARK4 concentration at initial concentrations of ATP (100  $\mu\text{M}$ ) and CHKtide (0.13 mg/ml). (B) Dose-response analysis of ATP at the optimized concentrations of MARK4 of 2.25  $\mu\text{g/ml}$  and CHKtide of 0.13 mg/ml. (C) Reevaluation of MARK4 concentration under optimized conditions (46.4  $\mu\text{M}$  ATP and 0.13 mg/ml CHKtide). (D) Optimization of CHKtide concentration under optimized conditions (1.19  $\mu\text{g/ml}$  MARK4, 46.5  $\mu\text{M}$ , 0.13 mg/ml CHKtide). The reaction rate was calculated as the conversion of substrate to the product over time. Data are mean  $\pm$  SD, n = 3.

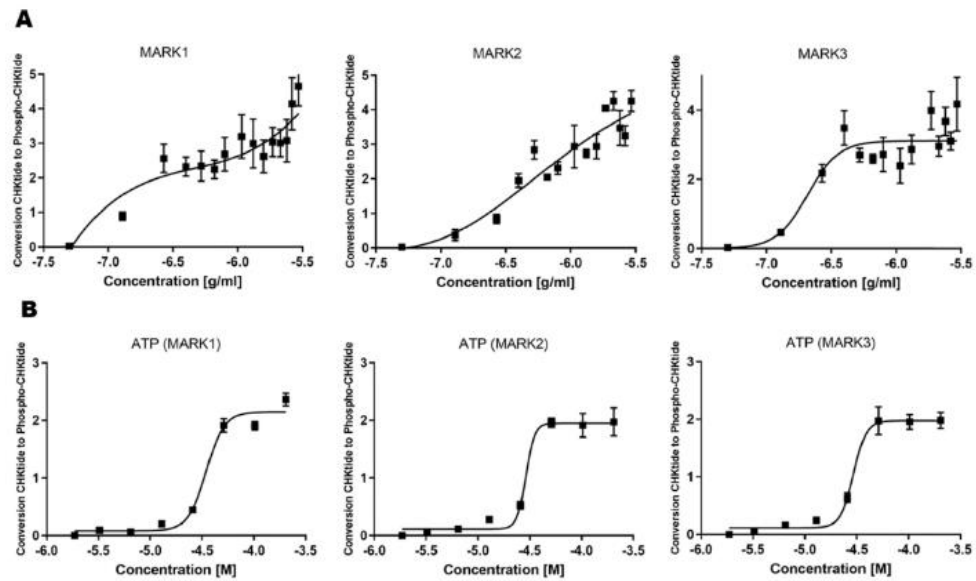


Fig. 4. (A) Optimization of enzyme concentration with initial concentration of ATP (46.4  $\mu$ M) and substrate (0.12 mg/ml CHKtide). (B) ATP optimization using optimized enzyme concentrations (0.31 mg/ml for MARK1, 0.5 mg/ml for MARK2 and 0.55 mg/ml for MARK3).

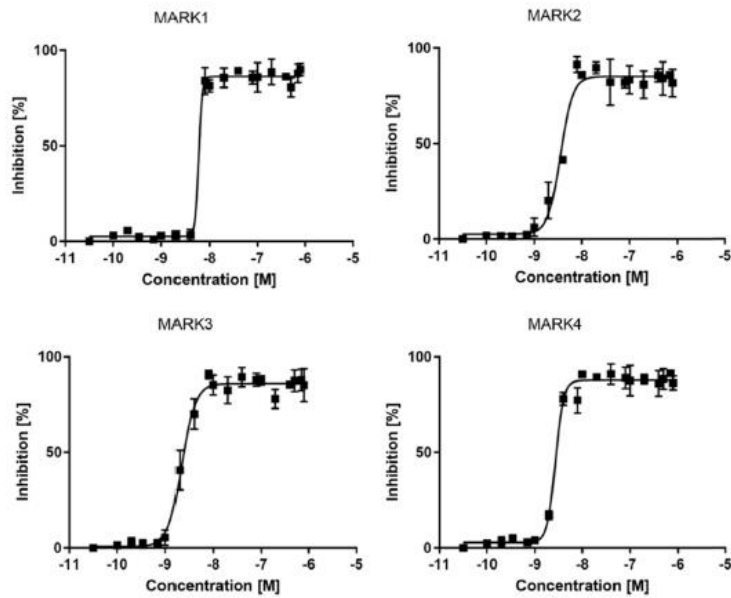


Fig. 5. Inhibition of MARK1–4 by non-selective kinase inhibitor staurosporine under optimized conditions. Data are mean  $\pm$  SD,  $n = 3$ .

evaluate the compounds selectivity (Table 1).

PD173952 is a Bcr-Abl tyrosine kinase inhibitor, a member of the Src protein family [37]. As a Bcr-Abl inhibitor, it could be possibly used in

the treatment of chronic myelogenous leukemia [38]. In our assay, PD173952 was the most active MARK4 inhibitor among all the identified compounds from the LOPAC library ( $IC_{50} = 3.30$  nM). It was

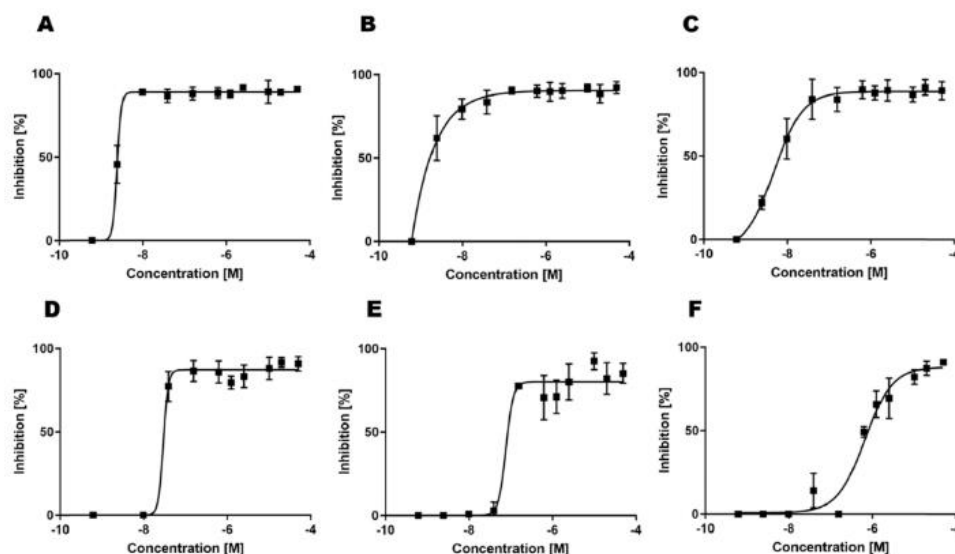


Fig. 6. The most active MARK4 inhibitors ( $IC_{50} < 1 \mu M$ ) from the LOPAC library. (A) PD173952, (B) PD-166285 hydrate, (C) PF-431396 hydrate, (D) sunitinib malate, (E) DMH4 and (F) PHA 767491 hydrochloride. Data are mean  $\pm$  SD,  $n = 3$ .

Table 1

Inhibition of MARK1–3 by the most active MARK4 inhibitors. Inhibition was tested under optimized conditions for each MARK isoform and an initial concentration of CHKtide substrate of 0.12 mg/ml. The table shows the mean  $IC_{50}$  values and standard deviations (SD) of the most active MARK inhibitors against MARK1–3,  $n = 4$ .

Compound	MARK1 $IC_{50}$ [ $\mu M$ ]	SD	MARK2 $IC_{50}$ [ $\mu M$ ]	SD	MARK3 $IC_{50}$ [ $\mu M$ ]	SD	MARK4 $IC_{50}$ [ $\mu M$ ]	SD
PD173952	0.010	0.002	0.052	0.001	0.10	0.01	0.0033	0.0002
PD-166285 hydrate	0.042	0.001	0.0024	0.0002	0.0021	0.0002	0.0035	0.0001
PF-431396 hydrate	0.067	0.001	0.034	0.001	0.16	0.02	0.011	0.001
Sunitinib malate	0.14	0.009	0.013	0.001	0.0027	0.0002	0.038	0.002
DMH4	> 50	0	0.35	0.01	2.08	0.1	0.27	0.01
PHA 767491 hydrochloride	0.33	0.009	0.16	0.01	0.93	0.01	0.80	0.01

3-times less active as an MARK1 ( $IC_{50} = 10$  nM), MARK2 ( $IC_{50} = 52$  nM) and MARK3 ( $IC_{50} = 100$  nM) inhibitor. This data indicates that in the case of PD173952 there was a slight selectivity to MARK4 isoform.

PD-166285 hydrate is a broad-spectrum kinase inhibitor with nanomolar activity. It has been found to inhibit Src nonreceptor tyrosine kinase ( $IC_{50} = 8.4 \pm 2.3$  nM), fibroblast growth factor receptor-1 ( $IC_{50} = 39.3 \pm 2.8$  nM), epidermal growth factor receptor ( $IC_{50} = 37.5 \pm 13.7$  nM) and the platelet-derived growth factor receptor beta subunit ( $IC_{50} = 98.3 \pm 7.9$  nM), which are enzymes involved in cancer signaling pathways [39–43]. It was one of the most active MARK4 inhibitors in our LOPAC screening with an  $IC_{50}$  value of 3.5 nM, which is comparable to the activities against kinases and growth factors mentioned above. PD-166285 hydrate was 12-times less active as an inhibitor of MARK1 than of MARK4. However, it had similar activity toward MARK2, MARK3 and MARK4, suggesting that it is a non-selective, biologically active compound.

PF-431396 hydrate has been identified as a potent proline-rich tyrosine kinase 2 inhibitor ( $IC_{50} = 11$  nM) [44] and a focal adhesion kinase inhibitor ( $IC_{50} = 2$  nM) [45,46]. These enzymes are involved in intracellular processes, such as cell proliferation, migration, differentiation and survival [47,48]. In our assay PF-431396 hydrate had similar inhibitory activity against MARK4 with an  $IC_{50}$  value of 11 nM. However, it was less active in inhibiting the other three MARK isoforms (MARK1–3): with the decrease in inhibition activity being

approximately 3.2–14.5-times less compared to MARK4 inhibition. Therefore, there was a slight selectivity of PD173952 towards MARK4 isoform.

Sunitinib malate is a tyrosine kinase inhibitor with a known inhibitory activity to vascular endothelial growth factor receptor 2 ( $IC_{50} = 60$  nM), platelet-derived growth factor receptor beta (PDGFR $\beta$ ) ( $IC_{50} = 2$  nM) and fibroblast growth factor receptor 1 ( $IC_{50} = 2.9$   $\mu M$ ). It has been approved by the U.S. Food and Drug Administration for treating gastrointestinal stromal tumors, advanced renal cell carcinoma (RCC) and other cancer types [49,50]. Sunitinib malate was highly active toward MARK4 inhibition ( $IC_{50} = 35$  nM) compared to other compounds in the LOPAC library. In the case of MARK2 ( $IC_{50} = 13$  nM) and MARK3 ( $IC_{50} = 2.7$  nM), its activity was higher, similar to its reported PDGFR $\beta$  inhibition. In contrast, MARK1 was inhibited at an  $IC_{50}$  value of 140 nM.

DMH4 has been reported as a selective inhibitor of vascular endothelial growth factor receptor 2 (VEGRF2) ( $IC_{50} = 0.16$   $\mu M$ ) [51] and had similar activity in our assay for MARK4 ( $IC_{50} = 0.27$   $\mu M$ ). However, it was inactive ( $IC_{50} > 50$   $\mu M$ ) against MARK1 and showed 7.7-times lesser activity toward MARK3 than MARK4. Surprisingly this compound seems to be a selective inhibitor not only for VEGRF2 (as already published) but also for MARK4 and MARK2 ( $IC_{50} = 0.35$   $\mu M$ ).<sup>51</sup>

PHA 767491 hydrochloride is a dual ATP-competitive inhibitor of cell division cycle 7-related protein kinase (cdc7) with an  $IC_{50}$  of 10 nM and cyclin-dependent kinase 9 (CDK9) with an  $IC_{50}$  of 34 nM. It also

inhibits glycogen synthase kinase-3 beta (GSK3- $\beta$ ) ( $IC_{50}$  = 0.22  $\mu$ M), cyclin-dependent kinase 2 ( $IC_{50}$  = 0.24  $\mu$ M) and cyclin-dependent kinase 1 ( $IC_{50}$  = 0.25  $\mu$ M) [52]. This compound also showed similar inhibitory activity towards MARK1 and MARK2, but lower activity against MARK4 and MARK3 isoforms in our study.

### 3.3. CNS activity of the most active MARK4 inhibitors

To predict the potential ability to cross the BBB and support its use in CNS, we used the SwissADME service (Swiss Institute of Bioinformatics) [32] to create a BOILED-Egg diagram to evaluate the lipophilicity and topological polar surface area of compounds. According to this diagram, compounds PD173952, DMH4, PHA 767491 and sunitinib were predicted to cross the BBB. PD-166285 hydrate was predicted to be absorbed intestinally but not permeate through the BBB, whereas PF-431396 hydrate was predicted as poorly absorbed (Fig. 7).

DMH4 was described as a potential anti-cancer drug with promising activity against lung cancer [53], but its CNS activity has not yet been published. PHA 767491 hydrochloride, which has been shown to reduce glioblastoma cell viability, induce apoptosis in cancer cells and suppress migration and invasion, which can lead to metastasis development [54]. This compound has also been studied as a potential therapeutic candidate for protein aggregation diseases that affect the CNS and lead to neurodegeneration [55]. PHA 767491 hydrochloride reduced phosphorylation of TDP-43 (TAR DNA-binding protein 43) [55], which is hyperphosphorylated in the brain and spinal cord of patients with motor neuron diseases [56]. It seems that PHA 767491 hydrochloride has broad activity. Its neuroprotective effect may also be connected to its ability to inhibit MARK4 activity, thereby preventing hyperphosphorylation of tau protein and the formation of neurofibrillary tangles, which result in neuronal death [57,58].

Sunitinib malate is another compound with described CNS activity [59]. The FDA approved sunitinib malate in 2006 as a drug to treat gastrointestinal stromal tumors and advanced RCC [60]. Other applications were gradually added, including treatment of progressive, well-differentiated pancreatic neuroendocrine tumors (pNETs) in 2012 [61], and as an adjuvant cure of adult patients with a high risk of recurrent RCC after nephrectomy in 2017 [62]. Its anti-cancer activity is well described, and case studies have shown the suppressive effect of sunitinib malate treatment on brain metastases from RCC and gastrointestinal stromal tumors [63–67]. In 2013, the direct effect of sunitinib malate on neuronal cells was shown in vitro. Primary cortical neurons were used for this experiment, and neuroprotective effects of sunitinib malate were observed [68]. Although sunitinib malate appeared to be an

effective drug for treating both primary tumors and brain metastases, patients treated with sunitinib malate suffered from cognitive impairment via inhibition of VEGFR2. It was found that the VEGFR2 signaling pathway play a fundamental role in cognition, especially memory processing [69]. The in vivo effects of sunitinib malate and its potential use in primary brain tumor treatment is currently being studied in clinical trials [70].

CNS activity of PD173952, PD-166285 hydrate and PF-431396 hydrate has not yet been described. This is in accordance with the predicted poor BBB permeation of PD-166285 hydrate and PF-431396 hydrate.

### 3.4. Molecular docking

We performed molecular docking of the most active compounds into the ATP-binding site of MARK4 (PDB: 5ES1). The protein structure was prepared in Chimera. Missing side chains were added, but they were not inside the binding site. Therefore, their exact positions were not crucial for docking. Compounds were docked using Autodock Vina [71]. All six compounds could fit the binding site and had relatively high docking scores, which estimate the affinity of compounds for their target. Four compounds had a score below – 8.1 kcal/mol, whereas DMH4 had a score of – 7.2 kcal/mol. The latter may be due to the small size of the ligand because the docking frequently underestimates the binding ability of smaller compounds. Hydrophobic interactions had a significant impact on binding. All compounds occupied the hydrophobic pocket formed by side chains of Ile65, Val73, Ala86, Val119, Met135, Ala138, and Leu188. Some compounds formed H-bonds, i.e., PHA 767491 with Lys88, Ala138 and Asp199; PF-431396 with Ala138; Sunitinib with Asp199. All compounds sterically hindered Lys88, which is recognized as a major binding residue of ATP (<https://www.uniprot.org/uniprot/Q96L34>) (Fig. 8). Thus, all these ligands may displace ATP from its binding site.

## 4. Conclusions

We developed an optimized sensitive and fast method for in vitro detecting activity toward MARK4 enzyme and its isoforms MARK1 – 3. Compared to other studies, uniqueness of our study is in the connection between non-contact echo-acoustic liquid handling instrumentation (ECHO 550) for reaction preparation and spotting of the samples on the MALDI plate and MALDI-TOF mass spectrometer which has made our assay more automated and allows us to work with very small volume of enzymes, substrates and analysed compounds (total reaction volume is 2.593  $\mu$ l) with low risk of sample cross-contamination. Advantage of this method was its simplicity of implementation, accuracy in the identification of the substrate and reaction product by specific molecular weight detected by highly sensitive MALDI-TOF mass spectrometry and its suitability for high throughput screening. Samples were mixed automatically with minimal enzyme and substrate consumption and the 1536-well format allowed large numbers of samples to be analyzed quickly (3–4 h for the acquisition of 1536 data points). Unlike other methods, the evaluation of enzymatic activity was based on direct detection of the substrate and the reaction product. Thus, there was no need to use any chromogenic substrates or labeled radionuclides. The reaction mixture consists only of the enzyme, peptide substrate and reaction buffer (optionally, an inhibitor may be present) and therefore the interference with the assay is minimized.

A number of applications of MALDI-TOF mass spectrometry for the detection of enzymatic activity have been described in the literature [72–75] indicating suitability of mass spectrometry for in vitro study of enzyme activity. However, each enzymatic reaction is specific and method needs to be developed and optimized to fit its specific conditions. ATPase enzyme assay (colorimetric assay) was described for detection of MARK4 activity [76,77]. Compared to colorimetric assays, mass spectrometry has lower limit of detection, which makes this

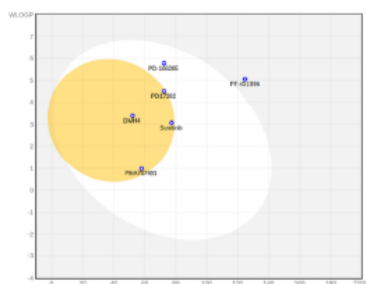


Fig. 7. BOILED-Egg prediction for BBB permeation and intestinal absorption of the most active MARK4 inhibitors ( $IC_{50}$  < 1  $\mu$ M) from LOPAC. The yellow ellipse denotes compounds that pass through the BBB, the white ellipse denotes compounds absorbed through the intestine and the grey zone defines compounds with low bioavailability. The image was produced by the SwissADME service (<http://www.swissadme.ch>). (For interpretation of the references to colour in this figure, the reader is referred to the web version of this article.)

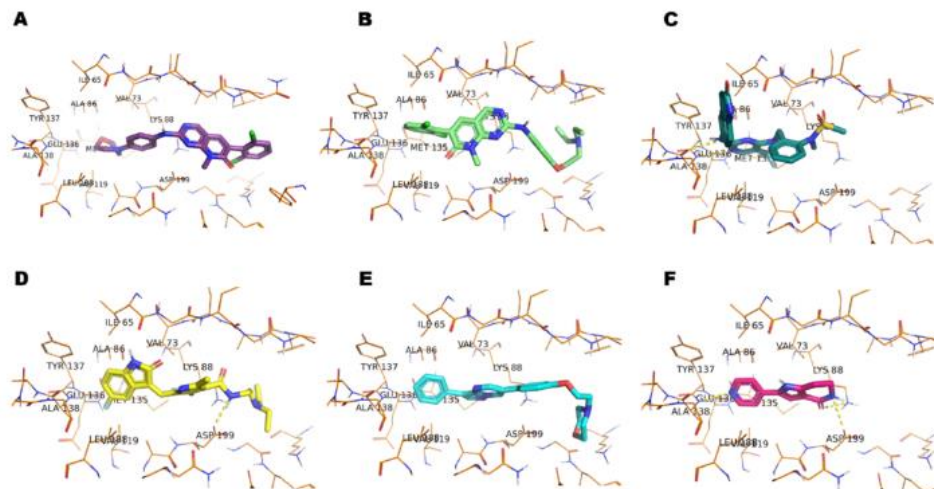


Fig. 8. Molecular docking of (A) PD173952, (B) PD-166285 hydrate, (C) PF-431396 hydrate, (D) sunitinib malate, (E) DMH4 and (F) PHA 767491 hydrochloride to the ATP-binding site of MARK4.

analysis more sensitive [78].

Possible disadvantage of using MALDI-TOF detection could be the limitation that the method is suitable for substrates with a molecular weight higher than 500 Da and with appropriate ionization by the MALDI method. At lower molecular weights, interference with matrix molecules and other reaction buffer adducts may occur.

The optimized MARK4 assay was used for screening against the LOPAC library comprising 1260 pharmacologically active compounds. All compounds were tested for inhibition of MARK4 at a concentration of 20  $\mu$ M. In total, 103 compounds showed inhibition activity higher than 50% and were tested in secondary screening, which included dose-response analysis and determination of  $IC_{50}$ . We identified six compounds with  $IC_{50} < 1 \mu$ M and these compounds were tested for inhibitory activity against MARK1 – 3. Interestingly, the CNS activity has been described for two of these compounds (sunitinib malate and PHA 767491 hydrochloride). Sunitinib malate is an anti-cancer drug with nanomolar inhibitory activity against VEGFR2, PDGFR- $\beta$  and MARK1 – 4. PHA 767491 hydrochloride is an inhibitor of cdc7, CDK9 and GSK-3 $\beta$  and showed similar activity in MARK1–4 inhibition.

Among the tested compounds, the PD173952, the Bcr-Abl kinase inhibitor, showed nanomolar activity and best selectivity against MARK4 isoform and border-line BBB permeability, based on *in silico* modeling. Such a molecule could be considered an interesting structural motive for future development as a tau phosphorylation inhibitor.

#### CRedit authorship contribution statement

**Lenka Hruša:** Methodology, Validation, Investigation, Data curation, Visualisation, Writing – original draft preparation. **Pavel Polishchuk:** Software, Formal analysis, Writing – original draft preparation. **Viswanath Das:** Conceptualization, Writing – review & editing. **Marian Hajduch:** Supervision, Project administration, Funding acquisition. **Petr Dzubak:** Conceptualization, Writing – review & editing, Project administration, Funding acquisition.

#### Conflict of interest statement

The authors declare that they have no known competing financial

interests or personal relationships that could have appeared to influence the work reported in this paper.

#### Acknowledgments

The work was supported by the Czech Ministry of Education, Youth and Sports (CZ-OPENSURE – LM2018130 and EATRIS-CZ – LM2018133), Grant Agency of Czech Republic (19-031245), an internal grant of Palacky University (IGA\_LF\_2021\_030), the European Regional Development Fund - Project ENOCH (No. CZ.02.1.01/0.0/0.0/16\_019/0000063) and the Technology Agency of the Czech Republic: Czech National Centres of Competence, project “PerMed” Personalized Medicine - Diagnostics and Therapy (No. TN01000013).

#### Appendix A. Supporting information

Supplementary data associated with this article can be found in the online version at doi:10.1016/j.biopha.2021.112549.

#### References

- [1] G. Drewes, A. Ebner, U. Preuss, E.M. Mandelkow, E. Mandelkow, MARK, a novel family of protein kinases that phosphorylate microtubule-associated proteins and trigger microtubule disruption, *Cell* 89 (1997) 297–306.
- [2] T. Timm, A. Marx, S. Panneerselvam, E. Mandelkow, E.M. Mandelkow, Structure and regulation of MARK, a kinase involved in abnormal phosphorylation of Tau protein, *BMC Neurosci.* 9 (59) (2008).
- [3] J.C. Augustinack, A. Schneider, E.M. Mandelkow, B.T. Hyman, Specific tau phosphorylation sites correlate with severity of neuronal cytopathology in Alzheimer's disease, *Acta Neuropathol.* 103 (2002) 26–35.
- [4] C.H. Reynolds, J.C. Beets, W.P. Blackstock, A.R. Nebreda, B.H. Anderton, Phosphorylation sites on tau identified by nanoelectrospray mass spectrometry: differences in vitro between the mitogen-activated protein kinases ERK2, c-Jun N-terminal kinase and p38, and glycogen synthase kinase-3 $\beta$ , *J. Neurochem.* 74 (2000) 1587–1595.
- [5] T.J. Singh, T. Zaidi, I. Grundke-Iqbal, K. Iqbal, Non-proline-dependent protein kinases phosphorylate several sites found in tau from Alzheimer disease brain, *Mol. Cell. Biochem.* 154 (1996) 143–151.
- [6] J.Y. Chin, et al., Microtubule-affinity regulating kinase (MARK) is tightly associated with neurofibrillary tangles in Alzheimer brain: a fluorescence resonance energy transfer study, *J. NeuroPathol. Exp. Neurol.* 59 (2000) 966–971.

- [7] H. Lund, et al., MARK4 and MARK3 associate with early tau phosphorylation in Alzheimer's disease granulovacuolar degeneration bodies, *Acta Neuropathol. Commun.* 2 (2014).
- [8] J. Garcia de Araujo Volpini, R. Pereira Rodrigues, L. Bruno Federico, C. Henrique Tomich de Paula da Silva, Structure-based drug design of novel MARK-3 Inhibitors in cancer, *Curr. Bioact. Compd.* 10 (2014) 131–138.
- [9] I. Parsa, Loss of a Mr 78,000 marker in chemically induced transplantable carcinomas and primary carcinoma of human pancreas, *Cancer Res.* 48 (1988).
- [10] A. Shamsi, et al., MARK4 inhibited by AChE inhibitors, donepezil and rivastigmine tartrate: insights into alzheimer's disease therapy, *Biomolecules* 10 (2020) 709.
- [11] P. Khan, et al., Identification of  $\alpha$ -mangrostin as a potential inhibitor of microtubule affinity regulating kinase 4, *J. Nat. Prod.* 82 (2019) 2252–2261.
- [12] S. Anwar, et al., Effect of pH on the structure and function of pyruvate dehydrogenase kinase 3: combined spectroscopic and MD simulation studies, *Int. J. Biol. Macromol.* 147 (2020) 769–777.
- [13] A.A.T. Naqvi, et al., Evaluation of pyrazolopyrimidine derivatives as microtubule affinity regulating kinase 4 inhibitors: towards therapeutic management of alzheimer's disease, *J. Biomol. Struct. Dyn.* 38 (2020) 3092–3097.
- [14] Z. Liu, et al., Mark4 promotes oxidative stress and inflammation via binding to PPAR $\gamma$  and activating NF- $\kappa$ B pathway in mice adipocytes, *Sci. Rep.* 6 (2016).
- [15] L. Li, K.L. Guan, Microtubule-associated protein/microtubule affinity-regulating kinase 4 (MARK4) is a negative regulator of the mammalian target of rapamycin complex 1 (mTORC1), *J. Biol. Chem.* 288 (2013) 703–706.
- [16] C. Sun, et al., Inactivation of MARK4, an AMP-activated protein kinase (AMPK)-related kinase, leads to insulin hypersensitivity and resistance to diet-induced obesity, *J. Biol. Chem.* 287 (2012) 38305–38315.
- [17] E.I. Tang, et al., Microtubule affinity-regulating kinase 4 (MARK4) is a component of the ectoplasmic specialization in the rat testis, *Spermatogenesis* 2 (2012) 117–126.
- [18] M. Voura, et al., Probing the inhibition of microtubule affinity regulating kinase 4 by N-substituted acridones, *Sci. Rep.* 9 (2019) 1676.
- [19] F. Naz, A. Islam, F. Ahmad, M.I. Haesan, Atypical PKC phosphorylates microtubule affinity-regulating kinase 4 in vitro, *Mol. Cell. Biochem.* 410 (2015) 223–229.
- [20] B. Aneja, et al., Design and development of Isatin-triazole hydrazones as potential inhibitors of microtubule affinity-regulating kinase 4 for the therapeutic management of cell proliferation and metastasis, *Eur. J. Med. Chem.* 163 (2019) 840–852.
- [21] N.J. Abbott, *Comparative Physiology of the Blood-Brain Barrier*, Springer, Berlin, Heidelberg, 1992, pp. 371–396, [https://doi.org/10.1007/978-3-642-76094-1\\_15](https://doi.org/10.1007/978-3-642-76094-1_15).
- [22] K.E. Schlager, P. Molnar, G.D. Lapin, D.R. Groothuis, Microvessel organization and structure in experimental brain tumors: microvessel populations with distinctive structural and functional properties, *Microvasc. Res.* 58 (1999) 312–320.
- [23] G.M. Preston, P. Agre, Isolation of the cDNA for erythrocyte integral membrane protein of 28 kilodaltons: member of an ancient channel family, *Proc. Natl. Acad. Sci. USA* 88 (1991) 11110–11114.
- [24] R. Duelli, W. Kuschinsky, Brain glucose transporters: relationship to local energy demand, *Physiology* 16 (2001) 71–76.
- [25] Z. Rankovic, CNS drug design: balancing physicochemical properties for optimal brain exposure, *J. Med. Chem.* 58 (2015) 2504–2600.
- [26] A.K. Ghose, T. Herberich, R.L. Hudkins, B.D. Dorsey, J.P. Mallamo, Knowledge-based, central nervous system (CNS) lead selection and lead optimization for CNS drug discovery, *ACS Chem. Neurosci.* 3 (2012) 50–60.
- [27] S.A. Hitchcock, L.D. Pennington, Structure-brain exposure relationships, *J. Med. Chem.* vol. 49 (2006) 7559–7583.
- [28] H. Pajouhesh, G.R. Lenz, Medicinal chemical properties of successful central nervous system drugs, *NeuroRx* 2 (2005) 541–553.
- [29] J. Kelder, P.D.J. Grootenhuus, D.M. Bayada, L.P.C. Delbressine, J.P. Ploemans, Polar molecular surface as a dominating determinant for oral absorption and brain penetration of drugs, *Pharm. Res.* 16 (1999) 1514–1519.
- [30] H. van de Waterbeemd, G. Camenisch, G. Folkers, J.R. Chretien, O.A. Raevsky, Estimation of blood-brain barrier crossing of drugs using molecular size and shape, and H-bonding descriptors, *J. Drug Target.* 6 (1996) 151–165.
- [31] W.J. Egan, K.M. Merz, J.J. Baldwin, Prediction of drug absorption using multivariate statistics, *J. Med. Chem.* 43 (2000) 3867–3877.
- [32] A. Daina, V. Zoete, A boiled-egg to predict gastrointestinal absorption and brain penetration of small molecules, *ChemMedChem* (2016) 1117–1121, <https://doi.org/10.1002/cmdc.201600102>.
- [33] S. Pushpakom, et al., Drug repurposing: progress, challenges and recommendations, *Nat. Rev. Drug Discov.* 13 (2018) 41–58.
- [34] N. Annadurai, et al., Antitumour drugs targeting tau R3 VQIVYK and Cys322 prevent seeding of endogenous tau aggregates by exogenous seeds, *FEBS J.* (2021), <https://doi.org/10.1111/FEBS.16270>.
- [35] F. Monacelli, M. Gea, R. Borghi, P. Odetti, A. Nencioni, Do cancer drugs counteract neurodegeneration? repurposing for alzheimer's disease, *J. Alzheimer's Dis.* 55 (2017) 1295–1306.
- [36] J.A. Driver, Understanding the link between cancer and neurodegeneration, *J. Geriatr. Oncol.* 3 (2012) 58–67.
- [37] D. Wisniewski, et al., Characterization of potent inhibitors of the Bcr-Abl and the c-Kit receptor tyrosine kinases, *Cancer Res.* 62 (2002) 4244.
- [38] X. An, et al., BCR-ABL tyrosine kinase inhibitors in the treatment of Philadelphia chromosome positive chronic myeloid leukemia: a review, *Leuk. Res.* vol. 34 (2010) 1255–1268.
- [39] R.L. Panek, et al., In vitro pharmacological characterization of PD 166285, a new nanomolar potent and broadly active protein tyrosine kinase inhibitor, *J. Pharmacol. Exp. Ther.* 283 (1997) 1433–1444.
- [40] N. Normanno, et al., Epidermal growth factor receptor (EGFR) signaling in cancer, *Gene* 366 (2006) 2–16.
- [41] A.M. Schultheis, et al., Fibroblast growth factor receptor 1 (FGFR1) amplification is a potential therapeutic target in small-cell lung cancer, *Mod. Pathol.* 27 (2013) 214–221.
- [42] D.L. Wheeler, M. Iida, E.F. Dunn, The role of src in solid tumors, *Oncologist* 14 (2009) 667.
- [43] H. Kumamoto, K. Ooya, Immunohistochemical detection of insulin-like growth factors, platelet-derived growth factor, and their receptors in ameloblastic tumors, *J. Oral. Pathol. Med.* 36 (2007) 196–206.
- [44] S. Han, et al., Structural characterization of proline-rich tyrosine kinase 2 (PYK2) reveals a unique (DFG-out) conformation and enables inhibitor design, *J. Biol. Chem.* 284 (2009) 13193–13201.
- [45] K.W.K. Tse, et al., B cell receptor-induced phosphorylation of Pyk2 and focal adhesion kinase involves Integrins and the rap GTPases and is required for B cell spreading, *J. Biol. Chem.* 284 (2009) 22865–22877.
- [46] L. González-Fernández, B. Macías-García, S.C. Loux, D.D. Varner, K. Hinrichs, Focal adhesion kinases and calcium/calmodulin-dependent protein kinases regulate protein tyrosine phosphorylation in stallion sperm, *Biol. Reprod.* 88 (2013).
- [47] S. Zhang, X. Qiu, Y. Gu, E. Wang, Up-regulation of proline-rich tyrosine kinase 2 in non-small cell lung cancer, *Lung Cancer* 62 (2008) 295–301.
- [48] J.K. Slack-Davis, et al., Cellular characterization of a novel focal adhesion kinase inhibitor, *J. Biol. Chem.* 282 (2007) 14945–14952.
- [49] T.J. Abrams, L.B. Lee, L.J. Murray, N.K. Pryer, J.M. Cherrington, SU11248 inhibits KIT and platelet-derived growth factor receptor  $\beta$  in preclinical models of human small cell lung cancer, *Mol. Cancer Ther.* 2 (2003).
- [50] E.P. Rock, et al., Food and drug administration drug approval summary: sunitinib malate for the treatment of gastrointestinal stromal tumor and advanced renal cell carcinoma, *Oncologist* 12 (2007) 107–113.
- [51] J. Hao, et al., In vivo structure-activity relationship study of dorsomorphin analogues identifies selective VEGF and BMP inhibitors, *ACS Chem. Biol.* 5 (2010) 245–253.
- [52] A. Montagnoli, et al., A Cdc7 kinase inhibitor restricts initiation of DNA replication and has antitumor activity, *Nat. Chem. Biol.* 4 (2008) 357–365.
- [53] H. Li, et al., DMH4, a VEGFR2 inhibitor, effectively suppresses growth and invasion of lung cancer cells, *J. Appl. Biomed.* 16 (2018) 46–50.
- [54] Z. Erbayraktar, B. Altural, R.S. Erbayraktar, E.P. Erkan, Cell division cycle 7-kinase inhibitor PHA-767491 hydrochloride suppresses glioblastoma growth and invasiveness, *Cancer Cell Int.* 16 (2016) 88.
- [55] Y.H. Chung, et al., Targeting inflammation, PHA-767491 shows a broad spectrum in protein aggregation diseases, *J. Mol. Neurosci.* 70 (2020) 1140–1152.
- [56] A. Prasad, V. Bharathi, V. Sivalingam, A. Giridhar, B.K. Patel, Molecular mechanisms of TDP-43 misfolding and pathology in amyotrophic lateral sclerosis, *Front. Mol. Neurosci.* vol. 12 (25) (2019).
- [57] J.G. Wood, S.S. Mirra, N.J. Pollock, L.L. Binder, Neurofibrillary tangles of Alzheimer disease share antigenic determinants with the axonal microtubule-associated protein tau ( $\tau$ ), *Proc. Natl. Acad. Sci. USA* 83 (1986) 4040–4043.
- [58] H. Lund, et al., MARK4 and MARK3 associate with early tau phosphorylation in alzheimer's disease granulovacuolar degeneration bodies, *Acta Neuropathol. Commun.* 2 (2014).
- [59] E. Szalek, et al., The penetration of sunitinib through the blood-brain barrier after the administration of ciprofloxacin, *Acta Pol. Pharm. Drug Res.* 71 (2014) 691–697.
- [60] D. Morse et al. *Carcinoma Treat. Gastrointest. Strom. Tumor Adv. Ren. Cell Food Drug Adm. Drug Approv. Summ.: Sunitinib Mal. Download 2014* doi: 10.1634/theoncologist.12-1-107.
- [61] G.M. Blumenthal, et al., FDA approval summary: sunitinib for the treatment of progressive well-differentiated locally advanced or metastatic pancreatic neuroendocrine tumors, *Oncologist* 17 (2012) 1108–1113.
- [62] FDA approves sunitinib malate for adjuvant treatment of renal cell carcinoma | FDA. (<https://www.fda.gov/drugs/resources-information-approved-drugs/fda-approves-sunitinib-malate-adjuvant-treatment-renal-cell-carcinoma>).
- [63] H. Takeuchi, H. Kolke, T. Fujita, H. Tsujino, Y. Iwamoto, Sunitinib treatment for multiple brain metastases from jejunal gastrointestinal stromal tumor: case report, *Neurol. Med. Chir.* 54 (2014) 664.
- [64] H.H. Helgason, et al., Brain metastases in patients with renal cell cancer receiving new targeted treatment, *J. Clin. Oncol.* 26 (2008) 152–154.
- [65] J. Medioni, O. Cojocaru, J.L. Belcaceres, P. Halimi, S. Oudard, Complete cerebral response with sunitinib for metastatic renal cell carcinoma, *Ann. Oncol.* vol. 18 (2007) 1282–1283.
- [66] Y. Kusuda, et al., Treatment of brain metastases from renal cell carcinoma with sunitinib and radiotherapy: our experience and review of the literature, *Int. J. Urol.* 18 (2011) 326–329.
- [67] H. Zeng, et al., Multifocal brain metastases in clear cell renal cell carcinoma with complete response to sunitinib, *Urol. Int.* 83 (2009) 402–405.
- [68] A. Sanchez, et al., Sunitinib enhances neuronal survival in vitro via NF- $\kappa$ B-mediated signaling and expression of cyclooxygenase-2 and inducible nitric oxide synthase, *J. Neuroinflamm.* 10 (2013) 057.
- [69] A.K. Abdel-Aziz, E.M. Mantawy, R.S. Said, R. Helwa, The tyrosine kinase inhibitor, sunitinib malate, induces cognitive impairment in vivo via dysregulating VEGFR signaling, apoptotic and autophagic machineries, *Exp. Neurol.* 283 (2016) 129–141.
- [70] Sunitinib in Sarcomas of the Central Nervous System - Full Text View - ClinicalTrials.gov. (<https://clinicaltrials.gov/ct2/show/NCT03641326>).



- [71] O. Trott, A.J. Olson, AutoDock Vina: Improving the speed and accuracy of docking with a new scoring function, efficient optimization, and multithreading, *J. Comput. Chem.* 31 (2009).
- [72] L. Hu, G. Jiang, S. Xu, C. Pan, H. Zou, Monitoring enzyme reaction and screening enzyme inhibitor based on MALDI-TOF-MS platform with a matrix of oxidized carbon nanotubes, *J. Am. Soc. Mass Spectrom.* 17 (2006) 1616–1619.
- [73] A. Sanchez-Ruiz, S. Serna, N. Ruiz, M. Martín-Lomas, N.-G. Reichardt, MALDI-TOF mass spectrometric analysis of enzyme activity and lectin trapping on an array of N-Glycans, *Angew. Chem. Int. Ed.* 123 (2011) 1841–1844.
- [74] M.S. Ritorro, et al., Screening of DUB activity and specificity by MALDI-TOF mass spectrometry, *Nat. Commun.* 5 (2014) 1–11.
- [75] C. Mirande, et al., Rapid detection of carbapenemase activity: benefits and weaknesses of MALDI-TOF MS, *Eur. J. Clin. Microbiol. Infect. Dis.* 34 (2015) 2225–2234.
- [76] N.S. Khan, et al., Thienopyrimidine-chalcone hybrid molecules inhibit fos-activated serine/threonine kinase: an approach to ameliorate antiproliferation in human breast cancer cells, *Mol. Pharm.* 15 (2018) 4173–4189.
- [77] M. Voura, et al., Probing the inhibition of microtubule affinity regulating kinase 4 by N-substituted acridones, *Sci. Rep.* 9 (2019) 1–17.
- [78] A. Hamed, P. ben, Táborský, E.M. Peña-Méndez, J. Havel, Matrix-assisted laser desorption/ionization mass spectrometry (MALDI-TOF MS) study of Huperzine A, a natural anti-Alzheimer's disease product, its derivatization and its detection by highly sensitive laser induced fluorescence (LIF), *Talanta* 72 (2007) 760–764.

## **9.4 Laboratory techniques in cellular and molecular medicine**

**L. HRUBÁ.** Chapter 30: Functional test of MDR transporters. In J. DRÁBEK, P. DŽUBÁK, M. HAJDÚCH, M. MISTRÍK *et al.* Laboratory techniques in cellular and molecular medicine, Book, 2021

Personal contribution: methods development, screening of Pgp and MRP inhibitors, data analysis, chapter writing and editing

# LABORATORY TECHNIQUES IN CELLULAR AND MOLECULAR MEDICINE



## EDITORS

Khushboo Agrawal Ph.D., Jan Bouchal Ph.D., Viswanath Das Ph.D., Jiří Drábek Ph.D., Petr Džubák M.D., Ph.D., Marián Hajdúch M.D., Ph.D., Karel Koberna CSc., Anna Ligasová Ph.D., Martin Mistrík Ph.D., Juan Bautista de Sanctis, M.D., Ph.D., Josef Srovnal M.D., Ph.D.

# **LABORATORY TECHNIQUES IN CELLULAR AND MOLECULAR MEDICINE**

## **EDITORS**

Khushboo Agrawal Ph.D., Jan Bouchal Ph.D., Viswanath Das Ph.D., Jiří Drábek Ph.D., Petr Džubák M.D., Ph.D., Marián Hajdúch M.D., Ph.D., Karel Koberna CSc., Anna Ligasová Ph.D., Martin Mistrík Ph.D., Juan Bautista de Sanctis, M.D., Ph.D., Josef Srovnal M.D., Ph.D.

KATALOGIZACE V KNIZE - NÁRODNÍ KNIHOVNA ČR

Laboratory techniques in cellular and molecular medicine / editors Khushboo Agrawal, Jan Bouchal, Viswanath Das, Jiří Drábek, Petr Džubák, Marián Hajdúch, Karel Koberna, Anna Ligasová, Martin Mistrík, Juan Bautista de Sanctis, Josef Srovnal. -- 1st edition. -- Olomouc : Palacký University Olomouc, 2021. -- 1 online zdroj

Obsahuje bibliografie a bibliografické odkazy

ISBN 978-80-244-6049-9 (online ; pdf)

\* 577.2:61 \* 57:61 \* 616-076.5 \* 57.086 \* 616-074/-079 \* 57.082/.089 \* 57.089 \* 57.083.1 \* 577.21 \* (048.8:082)

- molekulární medicína
- biomedicína
- cytodiagnostika
- cytologická technika
- laboratorní diagnostika
- laboratorní technika
- biomedicínské metody
- mikrobiologická technika
- molekulární genetika
- kolektivní monografie

57 - Obecná biologie [2]

Expert reviews:

Dolores Moreno, M.D.

prof. Isaac Blanca, Ph.D.

Unauthorized use of this work is a violation of copyright and may establish civil, administrative, or criminal liability.

1<sup>st</sup> edition

© IMTM Institute of Molecular and Translational Medicine, 2021

© Palacký University Olomouc, 2021

## Contents

<b>Chapter 1: Cultivation and cryopreservation of cell lines</b>	7
<i>Anna Janoščíáková</i>	
<b>Chapter 2: Cell lines and cell culture conditions - 3D cultures</b>	15
<i>Viswanath Das</i>	
<b>Chapter 3: Cell quantification</b>	23
<i>Natálie Kudlová</i>	
<b>Chapter 4: STR profiling for cell line authentication</b>	29
<i>Jana Stránská</i>	
<b>Chapter 5: Detection of mycoplasma contamination in cell lines by PCR</b>	37
<i>Renata Buriánová and Jana Kotulová</i>	
<b>Chapter 6: Eradication of microbial contamination</b>	43
<i>Ermin Schádich</i>	
<b>Chapter 7: Transformation of bacteria by PCR</b>	51
<i>Martin Ondra</i>	
<b>Chapter 8: Transient transfection</b>	57
<i>Agáta Kubičková</i>	
<b>Chapter 9: Stable transduction by lentiviral particles</b>	61
<i>Agáta Kubičková</i>	
<b>Chapter 10: Analysis of cytotoxicity by tetrazolium salt reduction test</b>	67
<i>Soňa Gurská</i>	
<b>Chapter 11: Laser microdissection</b>	73
<i>Pavla Flodrová and Patrik Flodr</i>	
<b>Chapter 12: Immunohistochemistry</b>	77
<i>Daniela Kurfürstová and Gabriela Kořínková</i>	
<b>Chapter 13: Multiplex immunohistochemistry</b>	83
<i>Mariam Gachechiladze</i>	
<b>Chapter 14: Quantitative immunofluorescence microscopy</b>	89
<i>Tereza Buchtová and Martin Mistrík</i>	
<b>Chapter 15: ISH technology, FISH probes for DNA detection</b>	101
<i>Radek Trojanec and Žuzana Šponková</i>	
<b>Chapter 16: Immunofluorescence staining of intracellular protein targets</b>	111
<i>Jiří Řehulka</i>	
<b>Chapter 17: <i>In situ</i> detection of replicated DNA in mammalian cell nuclei</b>	119
<i>Anna Ligasová and Karel Koberna</i>	
<b>Chapter 18: <i>In situ</i> detection of overall and replicated mitochondrial DNA in mammalian cells</b>	129
<i>Anna Ligasová and Karel Koberna</i>	

<b>Chapter 19: Reporters for subcellular localization and image analysis</b> <i>Jarmila Stanková</i>	141
<b>Chapter 20: Reporters based on luminescence or fluorescence detection</b> <i>Ivo Frydrych</i>	147
<b>Chapter 21: Reporter based DNA demethylation detection system</b> <i>Khushboo Agrawal</i>	153
<b>Chapter 22: Identifying senescent cells using microscopy or flowcytometry</b> <i>Matthew Lacey</i>	161
<b>Chapter 23: Methods for detection and induction of proteotoxic stress response in mammalian cells</b> <i>Ždeněk Škrotrl</i>	169
<b>Chapter 24: Multiparametric analysis of spheroid integrity by brightfield high-content microscopy</b> <i>Viswanath Das</i>	177
<b>Chapter 25: Raman imaging of adherent cells</b> <i>Vlastimil Mašek and Martina Medvedíková</i>	183
<b>Chapter 26: Cell cycle analysis by flow cytometry</b> <i>Ivo Frydrych</i>	193
<b>Chapter 27: Detection of apoptosis by flow cytometry</b> <i>Ján Gurský</i>	201
<b>Chapter 28: Detection and quantification of cellular antigens using flow cytometry</b> <i>Petr Džubák</i>	209
<b>Chapter 29: Analysis of mitochondria function by flow cytometry</b> <i>Juan B. De Sanctis</i>	215
<b>Chapter 30: Functional test of MDR transporters</b> <i>Lenka Hrubá</i>	223
<b>Chapter 31: Methods for quantification of oxygen radicals</b> <i>Juan B. De Sanctis</i>	231
<b>Chapter 32: Detection of nitric oxide enzymes and its metabolites</b> <i>Juan B. De Sanctis</i>	243
<b>Chapter 33: Western blot analysis</b> <i>Jana Václavková</i>	253
<b>Chapter 34: Proteomic analysis of complex samples by mass spectrometry</b> <i>Dušan Holub</i>	265
<b>Chapter 35: Sample Preparation of Formalin-Fixed Paraffin-Embedded Tissue for Mass Spectrometry-Based Proteomic Analysis</b> <i>Dušan Holub</i>	269
<b>Chapter 36: Methods of targeted mass spectrometry in proteomics</b> <i>Tomáš Oždian and Martina Jakoubková</i>	275

<b>Chapter 37: Methods of targeted mass spectrometry in the analysis of small molecules</b>	285
<i>Tomáš Oždian</i>	
<b>Chapter 38: <i>In vivo</i> methods for evaluation of radiolabelled compounds</b>	291
<i>Miloš Petřík and Zbyněk Nový</i>	
<b>Chapter 39: Basic <i>in vitro</i> methods for evaluation of radiolabelled compounds</b>	299
<i>Zbyněk Nový and Miloš Petřík</i>	
<b>Chapter 40: GPCR high-throughput screening for ligands of adenosine receptors</b>	307
<i>Jana Kotulová</i>	
<b>Chapter 41: A combination of kinetic fluorometric assay and microscopy for the screening of potential anti-tau aggregating agents</b>	317
<i>Narendran Annadurai and Viswanath Das</i>	
<b>Chapter 42: Study of absorption, distribution, metabolism, and excretion (ADME) properties of a new drug candidates in pre-clinical development</b>	325
<i>Martina Medvedíková, Alejandro Carazo, and Barbora Lišková</i>	
<b>Chapter 43: <i>HER2</i> gene copy number detection by quantitative polymerase chain reaction (qPCR)</b>	343
<i>Vladimíra Koudeláková</i>	
<b>Chapter 44: Site-Directed mutagenesis using PCR</b>	351
<i>Vaishali Uniyal</i>	
<b>Chapter 45: Genetic risk calculation of cystic fibrosis in prenatal testing</b>	357
<i>Jiří Drábek</i>	
<b>Chapter 46: Analysis of RNA by Northern blot</b>	367
<i>Zuzana Macečková</i>	
<b>Chapter 47: MiRNA expression microarray</b>	371
<i>Hanuš Slavík and Josef Srovnal</i>	
<b>Chapter 48: Circulating tumor cells detection</b>	375
<i>Alona Řehulková and Josef Srovnal</i>	
<b>Chapter 49: DNA copy number variants detection using microarray</b>	379
<i>Karolína Bartáková and Josef Srovnal</i>	
<b>Chapter 50: Determination of length of nucleic acid fragments by digital capillary electrophoresis</b>	399
<i>Lucie Kótková</i>	
<b>Chapter 51: Bisulfite amplicon next-generation sequencing for methylation status assessment</b>	409
<i>Rastislav Slavkovský</i>	
<b>Chapter 52: Detection of methylation by pyrosequencing for biological age estimation</b>	423
<i>Karolína Bartáková</i>	



# Functional test of MDR transporters

Lenka Hrubá

### I. Introduction

Cancer is a globally widespread group of diseases that, despite comprehensive treatment options, ends in the death of a patient in many cases. Statistics show that worldwide there were 18.1 million reported new cases of cancer in 2018 (1) and resulted in 9.6 million deaths in the same year (2).

One of the reasons for treatment failure is the ability of cancer cells ability to resist the action of cytostatic agents (3). This resistance in cells can occur at the first administration of the drug (primary resistance) (4, 5) or during treatment (secondary resistance) (4). Moreover, resistance can arise not only due to the currently administered substance but also for the other drug with a similar chemical structure (cross-resistance) or a completely different structure and function (multidrug resistance, MDR) (5).

Fundamental problem in the cancer cell resistance is the intra-tumour heterogeneity (cellular differences within a single neoplasm), which can be caused by a large number of proliferation cycles and by increasing mutation rates. The result is the emergence of tumour

subpopulations that may be variously sensitive to treatment (6).

### Multidrug resistance proteins

Mechanisms of MDR due to altered expression of MDR proteins have been extensively described (8- 10). The best known MDR protein is P-glycoprotein (Pgp), which is an ATP-dependent efflux pump. Its physiological function is to protect the organism against toxic agents, but its overexpression makes cancer cells more resistant to drug therapy (11- 13). Another protein connected with MDR is a member of the multidrug resistant protein (MRP) protein family, which is also a group of ATP-dependent membrane transporters (7). Since 1992 eight members of MRP family have been described (15- 19). Two of the MRP family members, MRP1 and MRP2, are studied particularly in relation to anti-cancer drugs (7).

Another protein connected with MDR phenotype is lung resistance-related protein (LRP), which is the major vault protein (MVP). MVP is one of the three components (MVP,

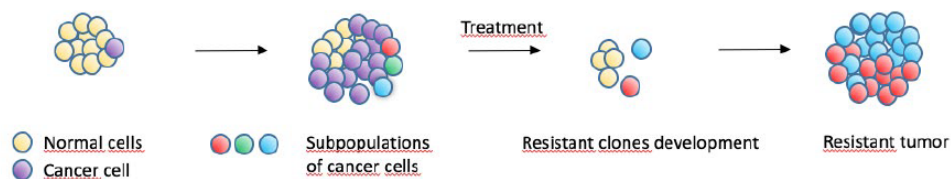
TEP1, VPARP) of vaults that are connected with many physiological functions of cells, especially nucleus-cytoplasm transport (8). LRP is expressed in tissues such as peripheral lung cells and bronchial epithelial cells (9), and overexpressed in many types of multidrug-resistant cancer cell lines (22, 23).

The breast cancer resistance protein (BCRP) is another MDR-associated protein. It was first described in MCF-7/AdrVp human breast carcinoma cells in 1998, and interestingly these cells didn't have altered expression of MDR1 or Pgp (10). BCRP is not only overexpressed in human breast carcinoma cells but also in colon carcinoma, myeloma, gastric carcinoma and fibrosarcoma cells (11). Stem cells frequently BCRP is highly expressed in stem cells (12). BCRP is also expressed in normal tissues, especially in tissues of organs associated with distribution and elimination of drugs or toxic xenobiotics. High expression of BCRP is usually detected in liver, kidney, small intestine and blood-brain and placental barriers, where it works as an efflux pump (24, 26, 27).

### Resistant cancer cell lines as a research model

One of the research targets of Institute of Molecular and Translational Medicine is selection and characterisation cell lines that are resistant to various drugs. In 2002, Noskova et al. published results of *in vitro* analyses of chemoresistance profile of resistance cell lines derived from CCRF-CEM, K562, A549 and MDA MB 231. Expression of MDR proteins was also tested for all lines (resistant and parental).

Combine with the previous paragraph was found that cell line K562-TAX (cell line derived from K562 with resistance to taxol) has high expression levels of Pgp and low expression of MRP1 and LRP. On the other hand, cell line A549-VCR (cell line derived from A549 with resistance to vincristine) expresses high levels of MRP1 and low levels of Pgp and LRP. Therefore, K562-TAX and A549-VCR cell lines were ideal models for testing the activity of MRP1 and Pgp.



**Figure 30.1** Intra-tumour heterogeneity

## II. Materials and instrumentation

### Instrumentation

Multidrop combi (Thermo Scientific), Echo 550 liquid handler (Labcyte), Centrifuge 5810 R (Eppendorf), HERAccl 150i CO2 incubator (Trigon-Plus), EnVision Plate Reader (Perkin-Elmer), FACSCalibur (Becton Dickinson), Scalded analytical scale, Typhoon FLA 9000, Titramax 100 (Heidolph).

### Reagents

Daunorubicine (Cat. No. 23541-50-6), cyclosporine A (Cat. No. 30024-25MG), probenecid (Cat. No. P8761-25G), Triton X-100 (Cat. No. 93443), Nonidet P-40 (Cat. No. 74385-L), sodium deoxycholate (Cat. No. 30970-1006), KCl (Cat. No. P9541-500g), antibiotics (penicillin-streptomycin), fetal bovine serum (Cat. No. FBS-12A), DMEM (Cat. No. D6429, Sigma Aldrich), NaOH (Cat. No. 1310-73-2) from Microchem,

TrisCl (Cat. No. 3718005) from Serva, RPMI cell culture medium (BE12-115F) from Lonza, phenol red-free cell culture medium [Cat. No. 11835063 (RPMI); Cat. No.21041025 (DMEM)] from ThermoFisher Scientific, 1× PBS.

### Material

CellCarrier 384 TC (black, clear bottom) from Perkin Elmer, six-well tissue culture plate from TPP.

### Cell cultures

Cell line K562-TAX cultivated in RPMI medium (supplemented with 10% FCS, 1× penicillin-streptomycin), MDCK1-MDR1 grown in DMEM medium (supplemented with 10 % FCS, and 1× penicillin-streptomycin). A549-VCR cells were cultivated in same medium as MDCK1-MDR1. All cell lines were maintained at 37 °C and 5 % CO<sub>2</sub>.

A549-VCR cell line was selected by growing cells in medium supplement with 10× IC<sub>50</sub> concentration of vincristine. Only the selected cells were used for the experiment.

### Lysis buffers

- Lysis buffer A: 0.2 % Triton X-100/0.01 M NaOH
- Lysis buffer B: 1 % sodium deoxycholate, 40 mM KCl, 20 mM TrisCl
- Lysis buffer C: 1 % Nonidet P-40, 1 % sodium deoxycholate, 40 mM KCl, 20 mM Tris

## III. Procedures

### Detection of MDR transporter activity by flow cytometry

#### Steps:

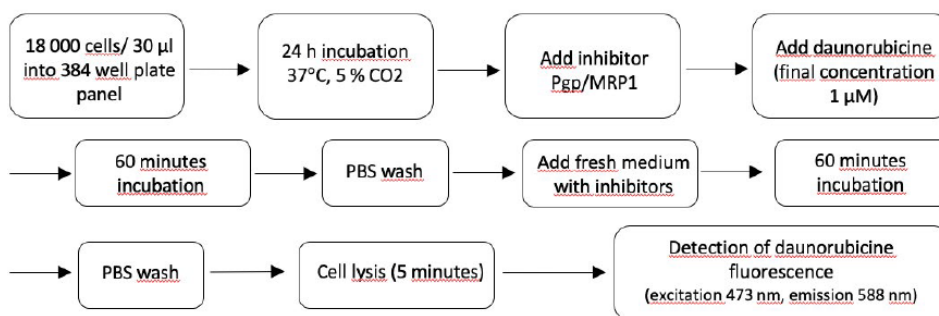
1. Seed 500 000 cells in 2 ml of medium/per well into 6 well plate
2. Incubate overnight at 37 °C, 5 % CO<sub>2</sub>
3. Add inhibitors of MDR transporter at concentrations provided below:
  - Cyclosporine A: 0.39 μM, 1.56 μM, 6.25 μM, 25 μM, 100 μM
  - Probenecid: 1 mM, 1.5 mM, 2 mM, 2.5 mM, 3 mM

- One well is used as control (no inhibitor)
4. Add daunorubicine at a concentration of 1 μM (20 μl from the stock 100 μM solution).
  5. Incubate for 60 minutes in the dark at 37 °C, 5 % CO<sub>2</sub>
  6. Remove media, wash cells twice with 1 ml fresh media
  7. Add 2 ml of fresh media containing cyclosporine or probenecid.
  8. Incubate for 60 minutes in the dark, 37 °C, 5 % CO<sub>2</sub>
  9. Analyze cells using a flow cytometer

### An optimised method for screening of potential inhibitors of MDR transporters

#### Steps

1. Seed 18 000 cells into 30 μl of medium per well in a 384 well plate (black, clear bottom) by multidrop, and centrifuge for 1 minute (1 100 rpm, 21 °C)
2. Incubate cells overnight at 37 °C, 5 % CO<sub>2</sub>
3. Add inhibitors of MDR transporters using ECHO at following concentrations:
  - Cyclosporine A: 0.83 μM, 1.66 μM, 6.25 μM, 12.5 μM, 25 μM, 50 μM, 100 μM, 166 μM
  - Probenecid: 0.125 mM, 0.25 mM, 0.5 mM, 1 mM, 1.5 mM, 2 mM, 2.5 mM, 3 mM
4. Add 1 μM daunorubicine using ECHO, and centrifuge the plate (1 100 rpm, 21 °C)
5. Incubate for 60 minutes in dark, 37 °C, 5 % CO<sub>2</sub>
6. Remove the drug-containing culture media by turning the plate upside down, and wash cells twice with 1× PBS (use a Multidrop to add the PBS)
7. Add 30 μl of fresh medium containing MDR inhibitors and centrifuge for 1 minute (1 100 rpm, 21 °C)
8. Incubate 60 minutes incubation in dark at 37 °C, 5 % CO<sub>2</sub>
9. Remove the culture media, and wash cell as described in Step 6
10. Add 10 μl lysis buffer (1% Nonidet P-40, 1% sodium deoxycholate, 40 mM KCl, 20 mM TRIS), centrifuge for 1 minute (1 100 rpm, 21 °C)
11. Incubate for 5 minutes in dark on Titramax 100
12. Measure daunorubicine fluorescence using a Typhoon FLA 9000



**Scheme 30.1.** Functional test MDR transporters

#### IV. Comments

There are two ways to test the activity of MDR transporters – the first using a 6-well plate and the other in a miniature format using a 384-well plate.

##### Flow cytometry method (6 well plates)

The advantage of this method is the ease of sample preparation and an excellent signal-to-background ratio. The fluorescence of daunorubicin is measured in living cells.

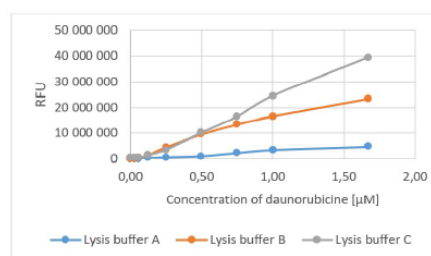
The disadvantage of this method includes the need for a significant volume of the reactant (20 μl of inhibitors/ 20 μl of daunorubicine). This can be an issue when compounds are scarce. Moreover, the longer analysis time (analysis of 1 compound at 5 concentrations takes 3 hours) can be cumbersome. It is possible to analyze only 10 compounds per day by this method, which may not be practical when dealing with a large compound set.

##### Screening method (384-well plates)

For drug screening purposes, the miniaturization of the flow cytometry of this method was needed. We optimised reaction volume and changed manual steps to automated steps. We

miniaturized the assay from 6-well plates to 384-well plates, with the possibility of analysis of more than 10 compounds at different concentrations at a given time. We needed to optimize the method for quantification of daunorubicin fluorescence – new reaction volume was too small for flow cytometry. The easier solution was to scan the fluorescence in the entire panel. In this way, we can detect fluorescence of all 384 wells in a few seconds.

To measure the fluorescence evenly throughout the well, it was necessary to lyse the cells. We tested three different types of lysis buffers (the composition of the solutions is given under the section Material



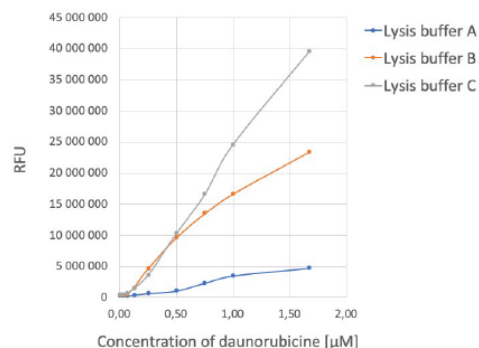
**Figure 30.2** Calibration curve of daunorubicin in lysis buffer A, B, C (transferred by Echo). Fluorescence was detected using a Typhoon FLA 9000.

and Instrumentation, different volumes of lysis buffers and optimal time for cell lysis. Fig. 30.2 shows the fluorescence signal of daunorubicine depending on its concentration in 3 lysis buffer. Lysis buffer A (0.2 % Triton X-100/ 0.01 M NaOH) enhanced the fluorescence. Lysis buffer C seemed to be the best choice for our screening method. The optimal volume of lysis buffer was 10  $\mu$ l and optimal lysis time was 5 minutes. Higher volume of lysis buffer and a longer time of cell lysis reduced the fluorescent signal of daunorubicine.

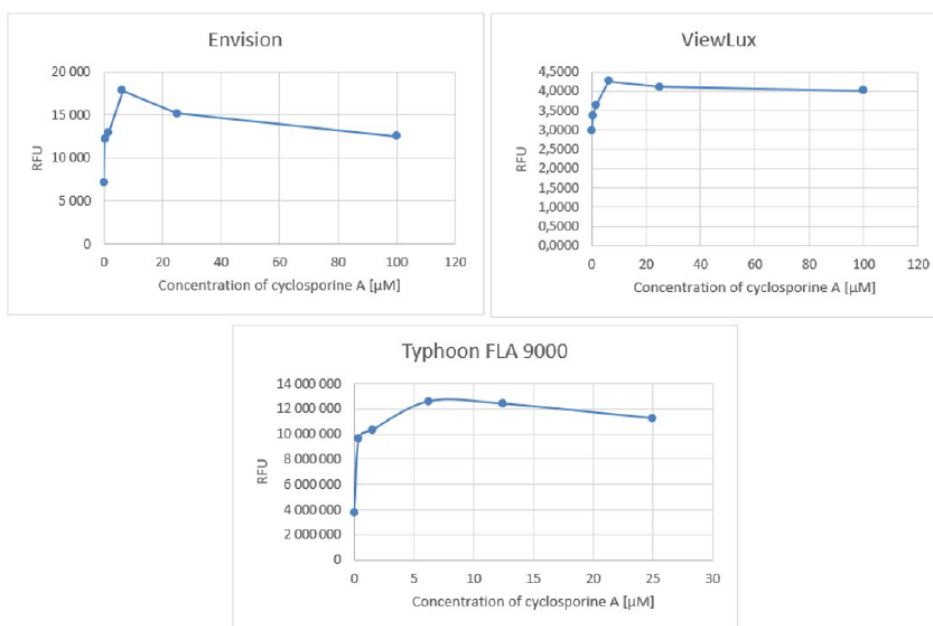
We used phenol red-free cell culture medium to reduce the background signal and prevent the interference of phenol red with daunorubicine fluorescence (Fig. 30.3).

Daunorubicin is transported out of the cell by P-gp. Therefore, we wanted to determine whether inhibition of P-gp by cyclosporine A alters the transportation of daunorubicine in K562-TAX. In the final step of experiment, cells were lysed to release the cellular content and the

fluorescence in the wells determined using an EnVision Plate Reader, Typhoon FLA 9000 and ViewLux™ ultra HTS Microplate Imager.



**Figure 30.3** Fluorescence of RPMI and DMEM medium with and without phenol red measured by Envision (excitation wavelength: 473, emission: 588 nm) in 384 well plates (30  $\mu$ l per well).



**Figure 30.4** Analysis of P-gp inhibition in K562-TAX using cyclosporine A. Detection of daunorubicine fluorescence in cell lysate with lysis buffer C (1% Nomidet P-40, 1% sodium deoxycholate, 40 mM KCl, 20 mM Tris) using an EnVision Plate Reader, Typhoon FLA 9000 and ViewLux™ ultra HTS Microplate Imager.

## V. Pitfalls

Problem	Cause and cure
<b>Too high fluorescence in blank samples</b>	<ul style="list-style-type: none"><li>• Cultivation media contains phenol red and its fluorescence interferes with the fluorescence of daunorubicine.</li><li>• To decrease fluorescence of the background use phenol red-free media and pay attention to washing steps</li></ul>
<b>Uneven fluorescence in the well</b>	<ul style="list-style-type: none"><li>• The non-uniformity of the fluorescence signal is across wells due to incomplete lysis of cells. Extend the lysis time to 10 minutes.</li><li>• Note: When quantifying the fluorescence intensity, TyphoonFLA software selects a few points from well but not the whole area. If cells were not completely lysed in a well, there can be darker and lighter spots in the well that can result in higher standard deviation.</li></ul>
<b>Low fluorescence signal</b>	<ul style="list-style-type: none"><li>• The low signal is probably due to the presence of low number of cells. Gently wash the cells as vigorously washing can result in cell loss.</li><li>• If the plates are left in the light for too long, the signal may be reduced. Perform the experiments in low light.</li></ul>
<b>No increase in fluorescence after the addition of the inhibitor</b>	<ul style="list-style-type: none"><li>• To verify the functionality of the method, you need to add positive control to each plate. Positive control for K562-TAX is cyclosporine A and for A549-VCR probenecid.</li><li>• If you don't detect an increase in the fluorescence according to the concentration of these compounds, there may be a problem in the washing steps. After the first incubation when the media with daunorubicin and inhibitor is removed, wash cells and apply new media with inhibitors as fast as possible. MDR transporters may not stay inactivated for long, and daunorubicine may be transported out of the cells</li></ul>

## VI. Acknowledgement

This work was supported by The Ministry of Education, Youth and Sports, project number L01304 – Support of the sustainability of the Institute of Molecular and Translational Medicine.

## References

1. BRAY, F, FERLAY, J, SOERJOMATARAM, I, SIEGEL, RL, TORRE, LA, JEMAL, A. Global cancer statistics 2018: GLOBOCAN estimates of incidence and mortality worldwide for 36 cancers in 185 countries. *CA Cancer J Clin.* 2018 Nov;68(6):394-424. doi: 10.3322/caac.21492. Epub 2018 Sep 12. Erratum in: *CA Cancer J Clin.* 2020 Jul;70(4):313.
2. World wide cancer statistics. Cancer Research UK [online].: <http://www.cancerresearchuk.org/health-professional/cancer-statistics/worldwide-cancer#heading-Zero>
3. GOTTESMAN, M. Mechanisms of Cancer Drug Resistance. *Annual Review of Medicine.* 2002, 53(1), 615-627
4. ZIGNOL, M., W. VAN GEMERT, D. FALZON, Ch. SISMANIDIS, P. GLAZIOU, K. FLOYD, and M. RAVIGLIONE. Surveillance of anti-tuberculosis drug resistance in the world: an updated analysis, 2007–2010. *Bulletin of the World Health Organization.* 2012, 90(2), 111-119
5. QUINTÁS-CARDAMA, A., H. KANTARJIAN, and J. CORTES. Mechanisms of Primary and Secondary Resistance to Imatinib in Chronic Myeloid Leukemia. *Cancer Control.* 2017, 16(2), 122-131
6. BECK, W. The cell biology of multiple drug resistance. *Biochemical Pharmacology.* 1987, 36(18), 2879-2887
7. FIDLER, IJ. Tumor heterogeneity and the biology of cancer invasion and metastasis. *Cancer Res.* 1978, 38(9), 2651-2660.
8. DOYLE, L., W. YANG, L. ABRUZZO, T. KROGMANN, Y. GAO, A. RISHI, and D. ROSS. A multidrug resistance transporter from human MCF-7 breast cancer cells. *Proceedings of the National Academy of Sciences.* 1998, 95(26), 15665-15670
9. HOPPER-BORGE, E., Z. S. CHEN, I. SHCHAVELEVA, M. BELINSKY, and G. KRUEH. Analysis of the Drug Resistance Profile of Multidrug Resistance Protein 7 (ABCC10). *Cancer Research.* 2004, 64(14), 4927-4930
10. NAKANISHI, T. and D. ROSS. Breast cancer resistance protein (BCRP/ABCG2): its role in multidrug resistance and regulation of its gene expression. *Chinese Journal of Cancer.* 2012, 31(2), 73-99
11. SHAROM, F. Multidrug Resistance Protein: P-Glycoprotein. *Drug Transporters.* 2006, , 223-262.
12. JURANKA, P. F., R. L. ZASTAWNY, and V. LING. P-glycoprotein: multidrug-resistance and a superfamily of membrane-associated transport proteins. *The FASEB Journal.* 1989, 3(14), 2583-2592.
13. LIN, J. and M. YAMAZAKI. Role of P-Glycoprotein in Pharmacokinetics. *Clinical Pharmacokinetics.* 2003, 42(1), 59-98.
14. STAUD, F. and P. PAVEK. Breast cancer resistance protein (BCRP/ABCG2). *The International Journal of Biochemistry & Cell Biology.* 2005, 37(4), 720-725
15. FLENS, M., G. ZAMAN, P. VALK, M. LZQUIERDO, and A. SCHROEIJERS. Tissue Distribution of the Multidrug Resistance Protein. *Am. J. Pathol.* 1996, 148(4), 1237–1247.
16. KOOL, M., M. HAAS, G. SCHEFFER, R. SCHEPPER, and M. EIJK. Analysis of Expression of cMOAT (MRP2), MRP3, MRP4, and MRP5, Homologues of the Multidrug Resistance-associated Protein Gene (MRP1), in Human Cancer Cell Lines. *Cancer Research.* 1997, 57(16), 3537–3547.
17. KOOL, Marcel, Marcel LINDEN, Marcel HAAS, Frank BAAS, and Piet BORST. Expression of Human MRP6, a Homologue of the Multidrug Resistance Protein Gene MRP1, in Tissues and Cancer Cells. *Cancer Research.* 1999, 59(1), 175-182.
18. COLE, S., G BHARDWAJ, and J. GERLACH et al. Overexpression of a transporter gene in a multidrug-resistant human lung cancer cell line. *Science.* 1992, 258(5088), 1650-1654
19. BORST, P., R. EVERS, M. KOOL, and J. WIJNHOLDS. The multidrug resistance protein family. *Biochimica et Biophysica Acta (BBA) - Biomembranes.* 1999, 1461(2), 347-357
20. BERGER, W., E. STEINER, M. GRUSCH,

- 
- L. ELBLING, and M. MICKSCHE. Vaults and the major vault protein: Novel roles in signal pathway regulation and immunity. *Cellular and Molecular Life Sciences*. 2009, 66(1), 43-61
21. LEHMANN, T., A. R. WAGEEH TORKY, E. STEHFEST, S. HOFMANN, and H. FOTH. Expression of lung resistance-related protein, LRP, and multidrug resistance-related protein, MRP1, in normal human lung cells in long-term cultures. *Archives of Toxicology*. 2005, 79(10), 600-609.
22. SCHEPER, R., H. BROXTERMAN, G. SCHEFFER, P. KAAJIK, W. DALTON, and T. VAN HEIJNINGEN. Overexpression of a Mr 110,000 Vesicular Protein in Non-P-Glycoprotein-mediated Multidrug Resistance. *Cancer Research*. 1993, 53(7), 1475-1479.
23. RAIDL, M., W. BERGER, R. SCHULTE-HERMANN, D. KANDIOLER-ECKERSBERGER, S. KAPPEL, F. WRBA, M. MICKSCHE, and B. GRASL-KRAUPP. Expression of the lung resistance-related protein in human and rat hepatocarcinogenesis. *American Journal of Physiology - Gastrointestinal and Liver Physiology*. 2002, 283(5), 1117-1124
24. DOYLE, A. and D. ROSS. Multidrug resistance mediated by the breast cancer resistance protein BCRP (ABCG2). *Oncogene*. 2003, 22, 7340-7358.
25. SARKADI, B., T. ORBÁN, and G. SZAKÁCS et al. Evaluation of ABCG2 Expression in Human Embryonic Stem Cells: Crossing the Same River Twice?. *STEM CELLS*. 2010, 28(1), 174-176
26. COORAY, H., C. BLACKMORE, L. MASKELL, and M. BARRAND. Localisation of breast cancer resistance protein in microvessel endothelium of human brain. *Neuroreport*. 2002, 13(16), 2059-2063.
27. MALIEPAARD, M., G. SCHEFFER, I. FANEYTE, M. VAN GASTELEN, A. PIJNENBORG, and A. SCHINKEL. Subcellular Localization and Distribution of the Breast Cancer Resistance Protein Transporter in Normal Human Tissues. *Cancer Research*. 2001, 61(8), 3458-3464.